Plant community and climatic response to Miocene environmental change in the Pacific Northwest (USA): paleoecological tools and applications

Alexander Lowe

A dissertation

submitted in partial fulfillment of the

requirements for the degree of

Doctor of Philosophy

University of Washington

2024

Reading Committee:

Caroline Strömberg, Chair

Janneke Hill Ris Lambers

Abigail Swann

Program Authorized to Offer Degree:

Biology

University of Washington

Abstract

Plant community and climatic response to Miocene environmental change in the Pacific Northwest (USA): paleoecological tools and applications

Alexander Lowe

Chair of the Supervisory Committee:
Caroline Strömberg
Department of Biology

The Miocene epoch (~23-5 Ma) offers important examples of past ecosystem response to global climatic changes in a relatively modern world and critical perspective to current and future climatic change, and as such, has been referred to as “the future of the past”. The Miocene is marked by two major climatic events: warming of the Miocene Climatic Optimum (MCO; 16.9-14.7 Ma) and cooling of the Middle Miocene Climatic Transition (MMCT; 14.7-13.8 Ma). The U.S. Pacific Northwest (PNW) offers a regional record of plant community and climatic response by hosting a suite of well-preserved fossil floras that span the MCO and MMCT in time. Although a rich history of work exists for these floras, an integrated paleoclimate and paleoecological study utilizing plant macrofossils, palynomorphs, and phytoliths, applying updated methodology, and constrained within a high-resolution radiometrically dated temporal framework is currently lacking. In addition, inferring plant ecological strategy, and its

relationship to climate and disturbance, in these fossil plant records is hindered by limitations in current paleoecological tools.

To refine the use of paleoecological tools, this dissertation presents two "modern analog" studies. In the first (Chapter 1), we refine the reconstruction of leaf economic spectrum (LES) strategies at the community- (i.e., site-) level through a global study of woody non-monocot angiosperm leaf mass per area (LMA) and its morphological correlate, the petiole metric (PM). We find LMA and PM correlate for community mean and variance, but not kurtosis, and provide the necessary equations to reconstruct these community-scale measures and associated uncertainty. This study also highlights the importance of increased temperature seasonality and decreased prevalence of evergreen species in driving low LMA and "fast" LES strategies in temperate climates. However, matching 'absolute' LMA distributions between fossil and modern sites does not allow reliable inference of analogous climate types. In the second modern analog study (Chapter 2), we test for links between leaf economic strategies and leaf morphology across succession in North Carolina. We find, among trees, "faster" leaf economic occur in early succession, as predicted, and highlight the utility of PM, leaf margin, and leaf morphological richness in interpreting successional dynamics and associated ecological strategies from fossil leaf assemblages sourced from temperate deciduous forests.

The last study of this dissertation (Chapter 3) generates a record of plant communities and climate during the MCO and across the MMCT in the PNW. We find the MCO drove warmer-than-modern annual lowland temperatures, and precipitation like the wetter western PNW today but likely lacking summer drought, hosting mixed mesophytic closed canopy forests. Across the MMCT, the interior PNW cooled in annual and winter temperatures, and likely dried, but this climatic change was tempered closer to the coast. Plant community composition also

changed across this interval, with a greater prevalence of deciduous species, and a considerable loss of exotic taxa (those no longer native to the US west coast) and a greater prevalence of open habitats in the PNW interior, which again, was tempered near the coast.

Table of Contents

Acknowledgments 10

Introduction 12

Literature cited 13

Chapter 1. Global patterns in community-scale leaf mass per area distributions of extant woody non-monocot angiosperms and their utility in the fossil record 15

Abstract 16

Introduction 17

Materials and Methods 21

Sites and leaf sampling 21

Leaf trait data 22

Climate data 24

Analyses 24

Results 27

Measured community LMA: correlations with climate and leaf habit 27

Relationship of community-scale LMA and PM 30

Reconstructed LMA: correlations with climate and leaf habit 31

LMA distribution matching 32

Discussion 33

Global patterns in the modern world 33

Application to paleoecology 37

Conclusions 41

Acknowledgements 42

Author contributions 43

Literature Cited 43

Tables and Figures 51

Chapter 2. Links between leaf morphology and ecological strategy across secondary succession in a temperate deciduous forest (North Carolina, USA): implications for the fossil record 64

Abstract 65

Introduction 66

Materials and Methods 70

Study site 71

Plot Census and Leaf Sampling 71

Trait Measurements 72

Analyses 73

Results 75

Species Composition, LMA, C:N, LDMC, and Leaf Thickness 75

Leaf Morphology and $\delta^{13}C$ 76

Climate Reconstructions 77

Discussion 78

LMA and the Role of the LES 78

Leaf morphology and $\delta^{13}C$ as indicators of ecology and succession 80

Application to Reconstructing Successional Dynamics in the Fossil Record 84

The Influence of Disturbance on Paleoclimate Reconstructions 86

Conclusions 87

Acknowledgments 89

Literature Cited 89

Tables and Figures 97

Chapter 3. Pacific Northwest plant community and climate response across global climatic events of the Miocene within a refined temporal framework. 105

Abstract 106

Introduction 108

Hypotheses 113

Geologic and Chronologic Background 114

Review of prior work on Miocene terrestrial ecosystem and climatic response 125

Materials and Methods 128

Field Work and Sampling 128

U-Pb Dating 128

Macrofossils 132

Palynology 135

Phytoliths 136

Analyses 138

Results 144

Stratigraphy and sedimentology 144

Composition of macrofossil and palynomorph records 153

Community ecology and structure (macrofossil, palynomorph, and phytolith assemblages) 156

Paleoclimate 159

Discussion 162

The Miocene Climatic Optimum 162

The Middle Miocene Climatic Transition 168

Conclusions 180

Acknowledgments 181

Literature cited 182

Tables and Figures 205

Conclusions and Outstanding Questions 218

Petiole Metric and Leaf Mass per Area 218

Leaf Traits Across Succession 220

Paleoecology and the Pacific Northwest Neogene 223

Literature cited 227

Acknowledgments

In addition to those funding agencies, institutions, co-authors, and additional people acknowledged and thanked in the individual chapters to follow, I provide more personal acknowledgments here. First, I would like to thank the many undergraduate students I have had the pleasure to work with over the course of this dissertation. Their assistance not only provided critical efforts in data collection and analysis but made the PhD expierence more fun and rewarding. I'd like to thank my committee members Abigail Swann and Janneke Hille Ris Lambers, and past and present GSRs Alexis Licht, Jon Bakker, Frankie Pavia, for their help and support throughout the years taming what turned out to be a fairly unwieldy dissertation. Extreme appreciation and thanks is given to my primary advisor, Caroline Strömberg, for giving me the freedom to explore interdisciplinary research questions, always having my back, and fostering a fun, caring, and supportive lab environment.

Thank you to my close collaborators who have provided me tremendous assistance and who I've learned a lot from, including Mark Schmitz, Rick Dillhoff, Tad Dillhoff, Chris Schiller, Patrick Fields, Bill Rember, Dana Royer, and Daniel Peppe. Thank you to those who have been a part of my academic journey from the start and set me on this path, including Randy Irmis, Carrie Levitt-Bussian, and the late Mike Getty at the Natural History Museum of Utah, Gabe Bowen and Clement Bataille at the University of Utah, and David Greenwood and Christopher West at Brandon University and University of Saskatchewan. A big thank you to staff at the University of Washington Department of Biology and the Burke Museum, including collections managers Katie Anderson, Ron Eng, and, in particular, Paige Wilson-Deibel, for a tremendous amount of on-the-ground technical assistance. Thank you to Biology Department Greenhouse staff, including Katie Sadler, Melissa Lacey, and Nile Kurashige, for your friendship, providing a

home away from home, and giving me the chance to docent with such a diverse array of visitors. Thank you to Liz Van Volkenburg for your mentorship through 3 years of teaching plant physiology, including her last before retirement!

Thank you very much to past and present Strömberg lab graduate students, including Camilla Crifò, Paige Wilson-Deibel, Will Brightly, Elena Stiles, and Ben Lloyd, for your lasting friendship, support, and the good times. Thank you to my father, James Lowe, for instilling a strong work ethic in me and teaching me to be good to people. Thank you to my mother, Regine Dewees, for always giving me the freedom to figure things out on my own and instilling in me an independence and strong work ethic. Thank you greatly to my partner Tia, for the support, love, and incredible patience, and always making sure we get out and have fun. Thank you to the many friends I made in Seattle, including my COVID crew (Elena Stiles, Hayden Davis, and Sarah Guiziou), fossil house crew, and to my musical friends including members of Shelbyville. Lastly, thank you to Lakeside, my longtime friends from back home for being a huge part of who I am today. Rest in peace Brandon Copeland.

Introduction

Our planet is amid significant and anthropogenically-driven environmental changes as accelerated release of greenhouse gas influences atmosphere and ocean systems and land use changes impart disturbances to marine and terrestrial ecosystems (IPCC 2023). Predictions of our future reveal aspects of our planet unlike those occurring today or in our recent history. Like Earth's future, the Earth's deep geological past and its fossil records offer countless examples of conditions unlike those occurring in our recent history and provides critical context in understanding dynamic relationships between global climatic events, disturbance, and ecosystems (e.g., Tierney et al. 2020; Steinthorsdottir et al. 2021). Providing such examples for terrestrial plant communities, which are particularly sensitive to environmental change given their sessile nature, and building tools that enable rich and reliable inference from fossil records, is then a key priority of scientific inquiry.

This dissertation first refined paleoecological tools for reconstructing plant ecological strategies, climate, and disturbance using the plant fossil record. In **Chapter 1**, we refined reconstructions of leaf economic spectrum (LES) strategies at the community-scale through a global study of leaf mass per area and its morphological correlate, the petiole metric (petiole width^2 / leaf area), and identify climatic variables that most strongly influence their variation. In **Chapter 2**, we provided empirical evidence for links between leaf trait variation and ecological strategy across secondary succession in a temperate deciduous forest, allowing reconstruction of disturbance and associated ecology in ancient and analogous forest types.

Lastly, this dissertation applies tools and knowledge gained from the first two chapters, alongside a rich collection of previously published work, and additional novel methods, to provide an example of plant community response to global climatic events in Earth's past. In

Chapter 3, we study a suite of well-preserved fossil plant sites in the Pacific Northwest (USA) by integrating complementary lines of paleobotanical evidence (macrofossils, palynomorphs, phytoliths) to provide a regional record of plant community and climate response to two important climatic events of the Miocene. The first, global warming of the Miocene Climatic Optimum (16.9-14.7 Ma), may represent that most recent period in Earth's history where CO_2 levels were like our predicted near-future (Steinthorsdottir et al. 2021; Hönisch et al. 2023). Second, global cooling of the Middle Miocene Climatic Transition (14.7-13.8 Ma) drove important stages in the modernization of terrestrial ecosystems and climates globally (Flower and Kennett 1994; Steinthorsdottir et al. 2021). Through this work, we also aimed to reinvigorate the study of Neogene fossil floras of the Pacific Northwest and spur future work by diverse sets of researchers by building a macrofossil digital library and by providing comprehensive documentation and justification of our morphotype frameworks.

Literature cited

Flower, B. P., and J. P. Kennett. 1994: The middle Miocene climatic transition: East Antarctic ice sheet development, deep ocean circulation and global carbon cycling. Palaeogeography, Palaeoclimatology, Palaeoecology 108:537–555.

Hönisch, B., D. L. Royer, D. O. Breecker, P. J. Polissar, G. J. Bowen, M. J. Henehan, Y. Cui, M. Steinthorsdottir, J. C. McElwain, M. J. Kohn, A. Pearson, S. R. Phelps, K. T. Uno, A. Ridgwell, E. Anagnostou, J. Austermann, M. P. S. Badger, R. S. Barclay, P. K. Bijl, T. B. Chalk, C. R. Scotese, E. De La Vega, R. M. DeConto, K. A. Dyez, V. Ferrini, P. J. Franks, C. F. Giulivi, M. Gutjahr, D. T. Harper, L. L. Haynes, M. Huber, K. E. Snell, B. A. Keisling, W. Konrad, T. K. Lowenstein, A. Malinverno, M. Guillermic, L. M. Mejía, J. N. Milligan, J. J. Morton, L. Nordt, R. Whiteford, A. Roth-Nebelsick, J. K. C. Rugenstein, M. F. Schaller, N. D. Sheldon, S. Sosdian, E. B. Wilkes, C. R. Witkowski, Y. G. Zhang, L. Anderson, D. J. Beerling, C. Bolton, T. E. Cerling, J. M. Cotton, J. Da, D. D. Ekart, G. L. Foster, D. R. Greenwood, E. G. Hyland, E. A. Jagniecki, J. P. Jasper, J. B. Kowalczyk, L. Kunzmann, C. E. Lawrence, C. H. Lear, M. A. Martínez-Botí, D. P. Maxbauer, P. Montagna, B. D. A. Naafs, J. W. B. Rae, M. Raitzsch, G. J. Retallack, S. J. Ring, O. Seki, J. Sepúlveda, A. Sinha, T. F. Tesfamichael, A. Tripati, J. Van Der Burgh, J. Yu, J. C. Zachos, L. Zhang, and The Cenozoic CO_2 Proxy Integration Project (CenCOPIP) Consortium. 2023: Toward a Cenozoic history of atmospheric CO_2. Science 382:eadi5177.

IPCC. 2023: Summary for Policymakers. Pp.1–34 *in* H. Lee and J. Romero, eds. Climate Change 2023: Synthesis Report. Contribution of Working Groups I, II and III to the Sixth Assessment Report of the Intergovernmental Panel on Climate Change. IPCC, Geneva, Switzerland.

Steinthorsdottir, M., H. K. Coxall, A. M. De Boer, M. Huber, N. Barbolini, C. D. Bradshaw, N. J. Burls, S. J. Feakins, E. Gasson, J. Henderiks, A. E. Holbourn, S. Kiel, M. J. Kohn, G. Knorr, W. M. Kürschner, C. H. Lear, D. Liebrand, D. J. Lunt, T. Mörs, P. N. Pearson, M. J. Pound, H. Stoll, and C. A. E. Strömberg. 2021: The Miocene: The Future of the Past. Paleoceanography and Paleoclimatology 36:e2020PA004037.

Tierney, J. E., C. J. Poulsen, I. P. Montañez, T. Bhattacharya, R. Feng, H. L. Ford, B. Hönisch, G. N. Inglis, S. V. Petersen, N. Sagoo, C. R. Tabor, K. Thirumalai, J. Zhu, N. J. Burls, G. L. Foster, Y. Goddéris, B. T. Huber, L. C. Ivany, S. Kirtland Turner, D. J. Lunt, J. C. McElwain, B. J. W. Mills, B. L. Otto-Bliesner, A. Ridgwell, and Y. G. Zhang. 2020: Past climates inform our future. Science 370:eaay3701.

Chapter 1. Global patterns in community-scale leaf mass per area distributions of extant woody non-monocot angiosperms and their utility in the fossil record

Alexander J. Lowe[1], Dana L. Royer[2], Daniel J. Wieczynski[3], Matthew J. Butrim[4], Tammo Reichgelt[5], Lauren Azevedo-Schmidt[6], Daniel J. Peppe[7], Brian J. Enquist[8,9], Andrew J. Kerkoff[10], Sean T. Michaletz[11], Caroline A.E. Strömberg[1]

[1]Department of Biology, University of Washington, Seattle, WA, USA

[2]Department of Earth and Environmental Sciences, Wesleyan University, Middletown, CT, USA

[3]Department of Biology, Duke University, Durham, NC, USA

[4]Department of Geology and Geophysics, Program in Ecology, University of Wyoming, Laramie, WY, USA

[5]Department of Earth Sciences, University of Connecticut, Storrs, CT, USA

[6]Department of Entomology and Nematology, University of California Davis, Davis, CA, USA

[7]Department of Geosciences, Baylor University, Waco, TX, USA 76798-7354

[8]Department of Ecology and Evolutionary Biology, University of Arizona, AZ, USA

[9]Santa Fe Institute, Santa Fe, NM, USA

[10]Department of Biology, University of Puget Sound, Tacoma, WA, USA

[11]Department of Botany and Biodiversity Research Centre, University of British Columbia, BC, Canada

Abstract

PREMISE: Leaf mass per area (LMA) links leaf economic strategies, community assembly, and climate, and can be reconstructed from woody non-monocot angiosperm (WNMA) fossils using the petiole metric (PM). Reliable interpretation of LMA reconstructed from the fossil record is limited by an incomplete understanding of how PM and LMA correlate at the community scale, and what climatic parameters drive variation of both measured and reconstructed LMA of WNMAs globally.

METHODS: A modern, global, community-scale dataset of in situ WNMA LMA and PM was compiled to test leading hypotheses for environmental drivers of LMA and quantify LMA-PM relationships. Correlations among PM, LMA, climate (Köppen types and continuous data), and leaf habit were assessed and quantified using several uni- and multivariate methods.

RESULTS: Community mean LMA increased under warmer and less seasonal temperatures. Drought-prone communities had the highest LMA variance, likely due to disparity between riparian and non-riparian microhabitats. PM and LMA were correlated for community mean and variance, and their correlations with climate were similar. These patterns indicate that climatic correlatives of modern LMA can inform relative trends in reconstructed fossil LMA. In contrast, matching 'absolute' LMA distributions between fossil and modern sites does not allow reliable inference of analogous climate types.

CONCLUSIONS: This study furthers our understanding of processes influencing the assembly of WNMA leaf economic strategies in plant communities, highlighting the importance of temperature seasonality and habitat heterogeneity. We also provide a method to reconstruct, and refine the framework to interpret, community-scale LMA in the fossil record.

Introduction

The assembly of plant communities is strongly influenced by the interaction of plant functional traits and the environment (Enquist et al., 2015; Keddy and Laughlin, 2021). Consequently, information gleaned from studies of trait-environment interactions are applicable across communities that share few taxa but a common environment—a point particularly pertinent for describing ancient plant communities comprised of extinct species. A trait that has been widely used to describe the prevalence and diversity of ecological strategies in both modern and ancient plant communities is leaf dry mass per area (LMA; abbreviations listed in Table 1) (Royer et al., 2010; Blonder et al. 2014; Enquist et al., 2015; Peppe et al., 2018).

LMA is a constituent of the leaf economics spectrum (LES; Wright et al., 2004; Reich, 2014), which describes physiologically constrained tradeoffs. At one end of the LES, plants emphasize low density and nitrogen-rich photosynthetic enzymes, and invest less in structural compounds, resulting in leaves that are 'cheaper' to construct and have lower LMA and higher within-leaf CO_2 diffusion rates. Thus, plants with low LMA leaves typically have more rapid resource acquisition rates and employ a 'fast' LES strategy (Poorter et al., 2009; Reich, 2014; Onoda et al., 20117). On the other hand, low LMA leaves often have less structural integrity, are less defended against herbivores (Azevedo-Schmidt and Currano 2023), and therefore have short leaf life spans (Wright et al., 2004). In economic terms, fast LES strategies (e.g., deciduous plants) offset a short payback time (short leaf life span) with a higher payback (assimilation) rate and a lower total expenditure (low LMA). At the other end, slow LES strategies (e.g., evergreen plants) with higher expenditure (high LMA) and a slower payback (assimilation) rate require longer payback times (long leaf life span), which they achieve by being more robust and with

better herbivore defenses (Poorter et al., 2009). Additionally, beyond carbon economics, the LES reflects energetic processes that influence thermoregulation (Vogel, 2009; Michaletz et al., 2016).

Several proxies have been developed to reconstruct LMA from fossil plants (Royer et al., 2007; Peppe et al. 2014; Soh et al., 2017; Cheesman et al., 2020) and used to reconstruct plant ecological strategies during extreme environmental change (e.g., Blonder et al., 2014; Butrim et al., 2020, 2022; Carvalho et al., 2021) and to document the functional composition of fossil floras (e.g., Wing et al., 2009; Lowe et al., 2018; Peppe et al., 2018; Flynn and Peppe, 2019; Wagner et al. 2019; Allen et al., 2020; Baumgartner and Peppe 2021; West et al., 2021; Reichgelt et al., 2022). The most widely applied proxy utilizes a species-scale relationship between LMA and the petiole metric (PM = petiole width^2 / leaf area) within woody non-monocot angiosperms (WNMAs; Royer et al. 2007, 2010; Cheesman et al., 2020; Lowe et al. 2024). The relationship is thought to result from biomechanical constraints, whereby a leaf with greater mass requires a petiole with a larger cross-sectional area (approximated by petiole width^2) for support (Niklas, 1994; Royer et al., 2007).

Given the demonstrated relationship between LMA and ecological strategy, the distribution of LMA across entire plant communities should reflect fundamental properties of an environment (Enquist et al., 2015). Using this logic, paleoecological studies have inferred paleoenvironments from fossil assemblages by visually comparing its reconstructed LMA distribution to measured LMA distributions of modern sites to identify a best match and, by extension, an analogous environment (i.e., 'distribution matching'; Royer et al., 2010; Lowe et al., 2018; Peppe et al., 2018; Flynn and Peppe, 2019; Wagner et al., 2019; Allen et al., 2020; Baumgartner and Peppe, 2021; West et al., 2021). However, several assumptions underpinning this distribution matching approach remain untested. For example, reconstructed LMA (from

PM) is assumed to be correlated with measured LMA at the community scale. Royer et al. (2007) showed a significant PM-LMA correlation for community mean using a limited dataset of 25 sites, but correlations for other community central moments (e.g., variance and kurtosis) have not been explored.

The most central set of assumptions in matching LMA distributions is that their position (e.g., mean), influenced by the most prevalent phenotype/LES strategy, and shape (e.g., variance and kurtosis), influenced by LES diversity, vary uniformly and distinctly across abiotic gradients. (Swenson et al., 2012; Enquist et al., 2015; Wieczynski et al., 2019; Maitner et al., 2023). Several hypotheses invoking different ecological processes have been posed to explain such variation. The 'abiotic filtering hypothesis' posits that harsh environments limit available niche space and thus LES diversity (Weiher et al., 1998; Swenson et al., 2012; Wieczynski et al., 2019). The 'favorability hypothesis' posits that the availability of ample resources (i.e., wetter and warmer, more favorable habitats) increases the prevalence of fast LES strategies due to their competitive edge in acquiring resources. When resources are scarce, high rates of resource acquisition are not possible, favoring slow LES strategies (Poorter et al., 2009; Reich, 2014). In contrast, the 'seasonality hypothesis' states that warm environments with low temperature seasonality promote slow LES strategies with evergreen, instead of deciduous, leaf habits (e.g., Adams et al., 2008). The favorability hypothesis emphasizes the importance of payback rate (potential rates of resource acquisition) and the seasonality hypothesis the importance of potential payback time (growing season length).

The abiotic filtering hypothesis has received support in several cases (e.g., Swenson et al., 2012; Wieczynski et al., 2019), but could be dependent on the extent to which heterogenous habitats are sampled, for example, along the strong abiotic gradients that characterize certain

harsh arid environments (Lammerant et al., 2023). Similarly, the relative importance of the favorability and seasonality hypotheses along temperature gradients is generally unresolved. Increased temperature can increase plant physiological rates (e.g., respiration, photosynthesis; Gillooly et al., 2001; Michaletz and Garen, 2024) and favor fast LES strategies, but it is often associated with decreased temperature seasonality which favors slow LES strategies in WNMAs (Adams et al., 2008). Empirical studies, which included plant groups beyond WNMAs, have found conflicting results, reporting positive species-scale relationships between LMA and mean annual temperature (MAT; Wright et al., 2005; Moles et al., 2014; Niinemets, 2001), negative relationships (Swenson et al., 2012; Šímová et al., 2018; Maynard et al., 2022), or no relationship (Ordoñez et al., 2009; Pinho et al., 2021). Community-scale studies show weak negative (Simpson et al., 2016; Bruelheide et al., 2018; Wieczynski et al., 2019) relationships with MAT.

Conflicting results in LMA-MAT relationships may in part be influenced by difficulties in comparing studies with varying inclusion of different plant groups with contrasting stress responses (e.g., stress tolerant evergreen conifers and stress avoidant deciduous WNMAs co-existing in cold climates) and growth forms (e.g., angiosperm herbs vs. WNMAs; Šímová et al., 2018). Thus, focusing on WNMAs might facilitate comparisons among plant communities and provide more reliable perspectives on leaf economic strategies that are also more applicable to the fossil record. Lastly, many of these studies aggregated trait values across broad spatial scales and aligned them with taxonomic lists generated in local vegetation census efforts (e.g., Bruelheide et al., 2018). Instead, locally measured (i.e., in situ) LMA provides a more accurate characterization of the realized traits of local plant communities (Enquist et al., 2015; Maitner et al., 2023).

Here, we employ a global and community-scale dataset of modern in situ LMA and PM data to document patterns and hypothesized drivers of LMA distributions in plant communities, and use the results to refine the use of LMA within paleoecology. We focus on WNMAs as they are the dominant plant group within paleoecological LMA studies. First, we test the favorability and seasonality hypotheses by quantifying relationships among community LMA mean, climatic variables, and the percentage of evergreen species, and the abiotic filtering hypothesis by quantifying relationships of community LMA variance and kurtosis with climatic variables. Second, we hypothesize that reconstructed LMA (from PM) can be reliably related to measured LMA at the community scale by testing for (i) correlations of LMA and PM for community mean, variance, and kurtosis, (ii) similar correlations of both reconstructed and measured LMA to climate and leaf habit, and (iii) distinctiveness of LMA distributions among modern climate types (such that they can be matched reliably with fossil LMA distributions). Our study provides new insights into fundamental plant trait-environment relationships within WNMAs by showing the importance of temperature seasonality and habitat heterogeneity, and contributes to more robust, quantitative approaches in paleoecology.

Materials and Methods

Sites and leaf sampling—We compiled a global dataset of community-scale LMA and PM data for WNMAs using criteria to make them roughly comparable with Late Cretaceous and Cenozoic fossil leaf assemblages (see below). All sites and species assignments are derived from prior work (Fig. 1; Su et al., 2010, 2013; Peppe et al., 2011; Wieczynski et al., 2019; Kattge et al., 2020), totaling 281 sites and 8,409 site-species pairs. Criteria for including sites in this compilation were that (i) leaf trait data represent leaves sampled in situ, (ii) WNMA species of each community were completely or mostly sampled, (iii) sites had minimal human influence

(e.g., planting) or disturbance, (iv) leaf sampling was done, at least in part, from the exposed outer canopy of trees, with no tree saplings sampled, and that (v) species were sampled across a spatial scale that could reasonably be represented in a fossil leaf assemblage (0.1-300 ha). Sites sampled for the development of leaf physiognomy-based paleoclimate proxies fit these criteria well (Su et al., 2010, 2013; Peppe et al., 2011), but other sites were carefully filtered. For example, to ensure the WNMA component of each in situ site from Wieczynski et al. (2019) was well-represented, only sites with ≥ 3 WMNA species and ≥ 50% of WNMA species with reported LMA were included, resulting in the inclusion of 26 of their 66 in situ sites. Additionally, sites from the TRY database (Kattge et al., 2020) were only used if it was clear that they met the above criteria by referencing original data publications (Appendix S1, S2; see Supplemental Data with this article). However, some variation in sampling methodology could not be avoided. For example, some sites included in the dataset exclusively sampled leaves from trees above a defined dbh (i.e., 2-5 cm) whereas others sampled prominent lianas, shrubs, and trees (e.g., CLAMP sites of Peppe et al., 2011). Some sites sampled exclusively riparian (e.g., Kowalski and Dilcher, 2003 sites of Peppe et al., 2011) or non-riparian vegetation, whereas others sampled a mix of both. Two sites contributing PM data, but not LMA data, included leaves sampled from forest floor litter rather than, or in addition to, standing vegetation (Gorgona and Alleghany National Forest, PA).

Leaf trait data—LMA and PM data were compiled from the sites, with some sites having only LMA or PM data. All LMA data in our study were acquired from previous work (Royer et al., 2007, 2012; Wieczynski et al., 2019; Kattge et al., 2011, 2020), and some unpublished or updated data (Appendix S1). PM data for 32 Peppe et al. (2011) sites were compiled from Royer et al. (2007, 2012), and of those, 26 sites were updated to reflect new

morphotype designations and/or to include more taxa. These were supplemented with new measurements at 53 Peppe et al. (2011) sites. In addition, new measurements used to calculate PM were made at 32 of the 50 sites of Su et al. (2010, 2013), which span a gradient from tropical to cold temperate climates in China (Fig. 1).

Leaflets of compound leaves were treated as leaves. PM was calculated by first measuring the petiole width at its junction with the leaf lamina, and leaf area, which included the summed area of the leaf petiole and blade, following Royer et al. (2007) and Lowe et al. (2024) (but see Appendix S4 for special cases). These measurements were performed on digital images using the program ImageJ (Schneider et al., 2012). The following formula was then used: PM = petiole width^2 / leaf area. Leaf area measurements used to calculate LMA and PM were made on either fresh or dry leaves. Area measured on dry leaves do not appear to bias results towards greater LMA or PM due to shrinkage (Appendix S5).

To apply the filtering criteria detailed above, taxonomic names (species or sub-species level) were updated to correct for misspellings and synonymy using the R packages Taxonstand (Cayuela et al., 2021), taxize (Chamberlain and Szocs, 2013), and WorldFlora (Kindt, 2020). Taxa included in the Peppe et al. (2011) and Su et al. (2010) studies were already restricted to WNMA taxa, but those from Wieczynski et al. (2019) and from most sites included from the TRY database were not. To filter for WNMA taxa only, growth form was ascribed using data in Olson et al. (2020) and the 'TRY - Categorical Traits Dataset' (Kattge et al., 2012), and major taxonomic group was assigned by referencing online resources.

To test whether LMA relationships are influenced by patterns of leaf habit, we ascribed habit type (i.e., evergreen, semi-evergreen, or deciduous) to each taxon using the 'TRY - Categorical Traits Dataset' (Kattge et al., 2012), and by searching online databases. The

percentage of evergreen species in a community was calculated for each site by assigning evergreen species a 1, semi-evergreen/semi-deciduous 0.5, and deciduous 0, and then calculating community average from these scores and converting to percentage. To ensure that leaf habit was accurately described for community-scale sites, only those where leaf habit was available for ≥ 50% of WNMA species were included in community-scale leaf habit analyses (214 sites for measured LMA and 72 sites for PM; Appendix S1).

Climate data—Continuous (univariate) and categorical (defined using multiple variables) climate data were obtained for each site to determine the most important climatic variables driving LMA variation (Appendix S3). Continuous climate data were obtained through WorldCLIM 30 second bioclimatic variables (Fick and Hijmans, 2017) and 30 second gridded aridity index and potential evapo-transpiration maps (Zomer et al., 2022). For sites from the TRY database, mean annual temperature and precipitation reported in TRY were preferentially used over the gridded climatic data. For categorical data, each site was assigned a Köppen climate type using distribution maps of Beck et al. (2018). Only the first two Köppen hierarchies were considered, to reduce the total number of categories for greater ease of interpretation (Table 2).

Analyses—All statistical analyses were performed using R (version 4.1.1; R Core Team, 2013).

Abiotic filtering-, favorability-, and seasonality hypotheses—To relate LMA with climatic variables, continuous climate data were first transformed using the bestNormalize package (Peterson, 2021), which determines and applies the most appropriate transformation (among Ordered Quantile, arcsinh, Box-Cox, square-root, and Yeo-Johnson transformations) to force normality in data to permit subsequent parametric statistical tests.

To calculate central moments, species averages were first calculated for PM and LMA data and then used to calculate community mean, variance, and kurtosis, with each species carrying equal weight (i.e., species-weighted). Data typically used to weight central moments by species abundance (e.g., total stem basal area) were not readily available for many of the sites included in this study; in addition, comparable abundance data are difficult to obtain from the fossil record (Burnham et al., 1992). Therefore, modern sites with abundance data (i.e., Wieczynski et al., 2019) were still treated in a consistent manner using species-weighted calculations. Across sites, LMA and PM exhibited right-skewed distributions, so the mean, variance, and kurtosis for each site were $\log_{10}$-transformed. Log_{10} transformation was applied after the calculation of central moments, rather than before (on species averages), because it produced more normal distributions of central moment values across sites and in one case, resulted in increased predictive power (Appendix S6).

We applied ANOVA to test for differences in LMA central moments across categorical climate types, using the aov function (R Core Team, 2013). To test for linear relationships between central moments of LMA and continuous climatic data, and between species and LES diversity, we created linear models using the lm function (R Core Team, 2013). For continuous climate data, we included only a subset of bioclimatic variables (i.e., see Table 1). In assessing the influence of the changing abundance of leaf habit types on trait-climate relationships, the percentage of evergreen species was transformed to force normality by Ordered Quantile (as determined by the bestNormalize package, Peterson, 2021), as it exhibited a bimodal distribution across sites.

Paleoecological hypotheses—To determine if LMA can be reliably inferred from the fossil record at the community scale, relationships in modern sites between PM and measured

LMA central moments were tested and defined using linear models created with log10 transformed values (as described above) using the lm function (R Core Team, 2013). Given that LMA and PM share leaf area as a denominator, the extent of spurious correlation (X/Z vs. Y/Z type; Jackson and Somers, 1991; Brett, 2004) was determined using the bootstrapping approach of Brett (2004) (more details in Appendix 6). To test if climatic drivers of variation in measured LMA similarly drive variation in reconstructed LMA, each modern site with PM data was treated to simulate a fossil assemblage. To do so, LMA central moments were reconstructed from PM using the PM-LMA relationships defined in this study (Fig. 1), and reconstructed LMA was subsequently treated in the same manner described for LMA above: $\log_{10}$ transformed and compared to categorical and continuous climate, and leaf habit data.

A quantitative version of distribution matching was developed to test whether reconstructed LMA of fossil leaf assemblages can be matched to measured LMA distributions of modern sites across distinct climates. Each modern site with PM data was converted into a 'simulated fossil assemblage' ($rLMA_{[site]}$) by reconstructing LMA at the species-scale using an expansion of the Royer et al. (2007) dataset (Appendix S7). Rather than using the LMA distribution of a single site to represent an entire environment type, as done in previous work (e.g., Royer et al., 2010; Lowe et al., 2018), we compiled a 'climate type distribution' for each climate type ($LMA_{[climate\ type]}$), which represents a single probability density function containing all species-averaged LMA data within a given climate type. Each site was then compared to each climate type distribution ($rLMA_{[site]}$ vs. $LMA_{[climate\ type]}$), with the site in question excluded from the calculation of its own $LMA_{[climate\ type]}$ to avoid circularity. Similarities of distributions were quantified using the Kolmogorov-Smirnov (K-S) test, via the ks.test function (R Core Team, 2013). The K-S test produces a test statistic (*D*) describing the similarity of two cumulative

probability distributions in position and shape (example in Fig. 7B), offering an improvement to the visual comparisons done in previous studies. For each climate type, we calculated (i) the 'correct match' rate, that is, the percentage of sites that best matched their true climate type, and (ii) a false match rate, that is, the percentage of sites that best matched a climate type different from their own. To consider if distributions of LMA were more distinct for coarser groupings of temperate climate types, we created four binned climate types: cool temperate with wet summers (i.e., everwet and dry winter climates), warm temperate with wet summers, warm temperate with dry summers, and arid.

Lastly, we tested whether directly comparing PM, instead of reconstructed LMA, would produce better ability to match fossil vs. modern assemblages by avoiding errors introduced when reconstructing LMA from PM (Appendix S7). Thus, in addition to $rLMA_{[site]}$ vs. $LMA_{[climate\ type]}$ comparisons, we also make and quantify $PM_{[site]}$ vs. $PM_{[climate\ type]}$ comparisons in the same manner to assess which method results in more accurate matching between a site and its true climate type.

Results

Table 3 provides an overview of the hypotheses of this study and their key results.

Measured community LMA: correlations with climate and leaf habit

Categorical climate types—Community mean and variance of LMA differs between categorical (Köppen) climate types (ANOVA; $p < 0.001$, Adj-R2 = 0.35 and 0.22, respectively; Fig. 2), but not community kurtosis (ANOVA; $p = 0.63$). However, there is large variability between sites within the same climate type (Fig. 2; Appendix S8).

Temperate climates—With regards to temperature, cool climates have lower LMA mean than warm climate types, so long as there is sufficient growing season precipitation (i.e., everwet

and dry winter types; Fig. 2A). Cool temperate dry winter sites (i.e., monsoonal sites in northern China) have the lowest LMA mean of all climate types, overlapping with cool temperate everwet sites only (Fig. 2A). The three highest LMA values for warm temperate everwet sites include two sites from Tasmania (Mt. Read and Frodsham) and one from New Zealand (Gouland Downs). In addition, the seven warm temperate everwet sites from Australia, Tasmania, and New Zealand are among the 12 highest LMA sites of their climate type.

With regards to precipitation, warm temperate sites with wet summers (everwet and dry winter sites) do not differ significantly in LMA mean from warm temperate dry summer and arid sites (Fig. 2A). Within warm temperate dry summer sites, a southwest Australian site (Margaret River) occurs as a high LMA outlier. No significant differences exist between other temperate climate types (Fig. 2A). The highest median of LMA variance is found in relatively 'unfavorable' arid and warm temperate dry summer sites, significantly higher than cool temperate sites (Fig. 2C). There is statistical overlap of LMA variance within all warm temperate and cool temperate climate types.

Tropical climates—With regards to precipitation, tropical everwet sites have significantly higher LMA mean than seasonally dry sites but overlap with seasonally very dry sites (Fig. 2A). All tropical climate types have significantly higher LMA mean than cool temperate climate types, except that tropical seasonally dry overlaps with cool temperate everwet. Compared to warm temperate sites, the only statistical difference is that tropical everwet sites have higher LMA mean than warm temperate dry winter sites. There are no significant differences in LMA variance between any tropical climate types (Fig. 2C). Tropical everwet and seasonally dry sites have significantly lower LMA variance than arid sites (Fig. 2C).

Continuous climate variables—Combining all climate types together in linear models results in significant correlations for community LMA mean and variance with many climatic variables (Fig. 3), but not for community kurtosis, which has non-significant or very weak correlations with climate (all Adj-R^2 values < 0.07). Relationships are stronger for LMA mean than variance. LMA mean is most strongly correlated with temperature parameters, particularly those relating to temperature seasonality (Fig. 3A).

Temperate climates—Relationships between LMA and temperature are stronger when temperate climate types are considered independently, rather than at the global scale. In temperate climates, mean LMA decreases as temperature seasonality increases and winters get colder. The variance of LMA is most strongly, and negatively, correlated with temperature seasonality variables, and weaker and positively correlated with precipitation and vapor pressure variables (Fig. 3B).

Tropical climates—Relationships of LMA mean and variance with climatic variables within tropical climate types are weak. Precipitation variables are those most correlated (i.e., have the highest R2) to LMA mean, though weakly (Adj-R2 < 0.06; Fig. 3A). Variance of LMA correlates most strongly with temperature seasonality, precipitation, and vapor pressure variables, although also weakly (Adj-R^2 < 0.09; Fig. 3B).

Leaf habit—When all climate types are combined, the percentage of evergreen species in the community ('percent evergreen' hereafter) correlates positively with LMA mean (Adj-R^2 = 0.30). As with continuous climatic variables, the relationship of LMA and percent evergreen is stronger for temperate climate types when they are considered independently (Adj-R^2 = 0.46; Fig. 4A). For tropical climate types, there is no significant correlation between LMA mean and percent evergreen (Fig. 4A). Across all climate types, communities dominated by deciduous

WNMAs (i.e., > 50% deciduous species) have significantly lower measured LMA mean compared to communities dominated by evergreen WNMAs (Fig. 4B).

Because temperature seasonality was the climate variable explaining the greatest proportion of variation in LMA mean in temperate climates, we explored whether increasing LMA mean with decreasing temperature seasonality was mediated by increases in percent evergreen, by increases in the LMA within deciduous and evergreen leaf types, or both. Percent evergreen in temperate climates was most strongly and negatively correlated with measures of temperature seasonality (Adj-R^2 = 0.50 with MART; Appendix S9). Temperate evergreen species have significantly higher LMA than temperate deciduous species (Fig. 5). In addition, there is a modest decrease in LMA within evergreen species with increasing temperature seasonality (Adj-R^2 = 0.14, p = 0.017), but no significant relationship between LMA and temperature seasonality among deciduous taxa (p = 0.992; Fig. 5). Within tropical climates, the strongest relationship with percent evergreen is its negative correlation with temperature seasonality, positive correlation with the aridity index, and negative correlation with potential evapo-transpiration, although all relationships are weaker than in temperate climates (all Adj-R^2 < 0.20; Appendix S9).

Relationship of community-scale LMA and PM—Central moments of WNMA PM distributions were correlated with those of measured LMA for mean and variance (Adj-R^2 = 0.57 and 0.29, respectively; Figs. 6A, 6B), but not for kurtosis (Fig. 6C), for the 70 sites that had both data types. Table 4 provides parameters necessary to calculate 95% prediction intervals using the presented linear models for LMA mean and variance. In contrast, the PM vs. LMA relationship for mean and variance was not significant when considering spurious correlation; that is, the observed correlation coefficient was not higher than those produced by randomized data

(Appendix S10). Thus, PM-LMA relationships presented in this study offer a means of prediction but do not provide evidence that there is a biological significance between the association of LMA and PM (Brett, 2004)—significance which can instead be inferred from additional lines of evidence such as biomechanical principles (see further discussion in Appendix S10).

Reconstructed LMA mean did not consistently over- or under-estimate measured LMA mean (Appendix S11), with a median offset of 0.22 g/m^2 (interquartile range [IQR] = 28.0). However, sites in tropical everwet and tropical seasonally very dry climates were all underestimated, and cool temperate everwet sites were consistently, although only slightly, overestimated (ranging -6.1 to 31.2 g/m^2; Appendix S11). There was no consistent over- or under-estimation of variance, with a median offset of 23.1 ($[g/m^2]^2$; IQR = 2006.4), and there was no strong pattern of offset in different climate types (Appendix S11).

Reconstructed LMA: correlations with climate and leaf habit—Relationships of LMA to climatic variables and leaf habit are similar when reconstructed indirectly via PM as when measured directly (see above). For example, similar trends are seen across temperature regimes in temperate summer wet climates, with cool sites having significantly lower reconstructed mean LMA than warm sites (Fig. 2B). In addition, similar trends are seen across precipitation regimes in temperate climates, with warm temperate summer dry and arid sites overlapping with warm temperate summer wet sites. There are no statistical differences among tropical climate types (Fig. 2B). Although differences in LMA variance between climate types are less pronounced for reconstructed, compared to measured LMA, arid sites have the highest median variance (Fig. 2D) for both. Similarities exist for relationships with continuous climate variables as well. Measures of temperature seasonality most strongly and negatively correlate with mean and variance of reconstructed LMA in temperate climates, although the correlations

are weaker, and less apparent at the global scale (Fig. 3A). Percent evergreen similarly correlates with mean reconstructed LMA across temperate sites only (Adj-R2 = 0.53; Fig. 4C).

LMA distribution matching—Community-scale measured LMA distributions vary substantially in position and shape within climate types (Appendix S8). An example of variation within a climate type is provided by warm temperate everwet (Fig. 7A), highlighting the site Pee Dee, SC, which was used in previous publications to typify this climate type (e.g., Royer et al., 2010; Lowe et al., 2018; Flynn and Peppe, 2019; Allen et al., 2020; West et al., 2021), the LMA distribution of which is similar to the climate type distribution.

When considering all climate categories, reconstructed LMA community distributions in general matched poorly with the measured distribution of the climate type they belonged to, with only 19% of sites best matching with their true climate type (Fig. 7C). Although cool temperate everwet and warm temperate dry winter sites had higher rates of correct matches, they also had high rates of false matches. There was an overall better correct match rate when $PM_{[site]}$ vs. $PM_{[climate\ type]}$ comparisons were made, with 26% of sites having a correct match (Fig. 7E). The PM distributions of both arid and cool temperate dry winter sites show some distinctness, with the former having a long tail of high PM values and the latter lacking a tail with the distribution confined to lower PM values (Appendix S8). Coarser groupings of temperate climate types allowed higher correct match rates, with 29% for reconstructed $LMA_{[site]}$ vs. measured $LMA_{[climate\ type]}$ comparisons (Fig. 7D), and 52% for $PM_{[site]}$ vs. $PM_{[climate\ type]}$ comparisons (Fig. 7F). However, false matches are consistently high across climate types. For example, although 78% of sites in cool wet summer climates best matched with their climate type ($PM_{[site]}$ vs. $PM_{[climate\ type]}$), 43% of all sites that best matched with the cool wet summer distribution belonged to other climate types (Fig. 7F).

Discussion

This study shows, using a global and community-scale dataset of modern in situ LMA data, that climate imparts significant controls on the prevalence and diversity of WNMA LES strategies within plant communities, particularly in temperate climates, which can be explained by leaf economics, trait filtering, and habitat disparity. In addition, we provide evidence and guidelines for how information gleaned from global patterns in the modern world can be applied in a robust framework to interpret reconstructions of community-scale LMA from PM measurements of fossil leaf assemblages.

Global patterns in the modern world

The prevalence of LES strategies—Overall, correlations between LMA community central moments and climate are stronger for mean than variance, consistent with previous work (Fig. 3; Bruelheide et al., 2018; Šímová et al., 2018; Wieczynski et al., 2019; Butrim et al. 2024). We find that as temperatures get warmer and less seasonal, LMA mean increases, reflecting an increased prevalence of slow LES strategies for WNMA components of plant communities (Fig. 3A), supporting the seasonality hypothesis. This result is inconsistent with the favorability hypothesis, which instead predicts that increased temperature favors fast LES strategies by creating more favorable conditions for plant growth. The increase in LMA with lower temperature seasonality is mediated by both relatively more evergreen WNMA species assembled in plant communities (Fig. 4A; Adams et al., 2008), which have higher LMA than deciduous species, and a modest increase in the LMA of evergreen species (Fig. 5). These results suggest that at the global scale, factors like growing season length that influence potential 'payback time' can have more significant influence on the dynamics of LES strategies in WNMA communities than potential resource acquisition rates (i.e., 'payback rates').

LMA-climate relationships were generally stronger than those seen in previous studies (e.g., Bruelheide et al., 2018; Wieczynski et al., 2019; Maynard et al., 2022). Stronger relationships likely reflect the importance of in situ data for characterizing plant community trait distributions (e.g., Maitner et al., 2023) and our focus on WNMAs, which minimizes discordant patterns across plant groups. For example, as the growing season shortens with higher temperature seasonality, WNMA components become increasingly deciduous (lower LMA; Fig. 4A) employing a stress avoidance strategy, alongside an increased contribution of evergreen conifers (higher LMA; Brodribb et al., 2012) that have characteristic traits and physiological mechanisms that confer a frost/stress tolerance strategy (e.g., vessel-less wood, accumulation of soluble sugars, and synthesis of cold-hardy proteins; Chabot and Hicks, 1982; Chang et al., 2021). Herbaceous and woody plants also show discordant trends across gradients of temperature seasonality (Šímová et al., 2018). Thus, combining these plant groups in analyses may obscure patterns relevant for understanding leaf economics within plant groups.

The varying prevalence of LES strategies in tropical climates was poorly explained by the percentage of evergreen species (Fig. 4A) and the climatic variables analyzed in this study (Figs. 2A, 3A). Non-significant percent evergreen-LMA relationships are likely influenced by a weaker dichotomy between evergreen and deciduous habits in the tropics compared to temperate climates, and the fact that deciduous species often occur in seasonally dry climates where low soil water availability may also favor high LMA (Reich, 1995; Russo and Kitajima, 2016; Chakrabarty et al., 2021). Weak LMA-climate relationships were also found in a study across nine neotropical lowland biogeographic regions, where traits conferring leaf hydraulic efficiency were suggested as being more critical (Pinho et al., 2021)—traits that may be unrelated to LMA (Sack et al., 2005; Maréchaux et al., 2020). On the other hand, stronger LMA-climate

relationships consistent with the favorability hypothesis have been found to occur across smaller local–regional scales in the tropics, with LMA increasing alongside increasing elevation and decreasing temperature (e.g., van de Weg et al., 2009; Asner et al., 2016; Neyret et al., 2016; Enquist et al., 2017; Martin et al., 2020), and increasing water table depth (Lourenço et al., 2020).

The diversity of LES strategies—We find significant relationships of climate with variance (Figs. 2C, 3B), but non-significant or very weak correlations with kurtosis. Maitner et al. (2023) found that calculations of kurtosis of community-scale trait distributions are generally more inaccurate (i.e., have weaker correlations with 'true' distributions where all individuals were sampled) than lower central moments such as mean and variance, and that inaccuracy is worse when intraspecific variation is not accounted for (see further discussion in Unexplained variance in LMA-climate relationships). Thus, LMA variance is used, and not kurtosis, to characterize the diversity of LES strategies in plant communities.

We find mixed support for the abiotic filtering hypothesis for explaining variation in the diversity of LES strategies for WNMAs. LMA variance is highest in arid and warm temperate dry summer environments (Fig. 2C), inconsistent with the abiotic filtering hypothesis that instead predicts that arid climates impart strong filtering resulting in low diversity of LES strategies. This result indicates that high habitat disparity across microhabitats (e.g., riparian and non-riparian environments) in water-limiting climates influences high diversity when diverse microhabitats are considered (Lammerant et al., 2023). However, in support of the abiotic filtering hypothesis, LES diversity in temperate climates is most strongly, and negatively, correlated with temperature seasonality (Fig. 3B), such that short yet productive growing seasons (e.g., cool temperate dry winter; Fig. 2C) lead to an apparent selection of consistently fast LES

strategies (e.g., deciduous taxa) at the exclusion of slow LES strategies (e.g., evergreen taxa) in WNMAs. Wieczynski et al. (2019) also found community species-weighted LMA variance to be most strongly, and negatively, correlated with measures of temperature seasonality.

We did not find any differences in LES diversity between tropical climate types (Fig 2C). Previous work has shown significant, though conflicting trends, with functional diversity being either higher (Swenson et al., 2012) or lower (Aguirre-Gutiérrez et al., 2022) in drier tropical forests. These contradicting results suggest that several additional factors (e.g., soil characteristics, biotic interactions) complicate diversity-climate relationships in the tropics (e.g., Fyllas et al., 2009; Asner et al., 2016) (see below).

Unexplained variance in LMA-climate relationships—Although climate imparts important influence on the prevalence and diversity of WNMA LES strategies, each climate type hosts a range of LMA distribution shapes (Figs. 2, 7A), consistent with Butrim et al. (2024). In addition, all climatic variables explained less than 50% of the variation in LMA central moments. Several potential factors may contribute to this unexplained variance including confounding correlation between climatic variables, variation in the spatial scale (0.1 to 300 ha) and incorporation of microhabitats at different sites, differences in whether shrubs and lianas were sampled at sites (Reich et al., 2007; Poorter et al., 2009), regional fire and disturbance regimes (Carreño-Rocabado et al., 2012; Archibald et al., 2018; Fonseca et al., 2018), biotic factors like competition and herbivory (Poorter et al., 2009; HilleRisLambers et al., 2012), and soil characteristics (Fyllas et al., 2009; Ordoñez et al., 2009; Maire et al., 2015; Asner et al., 2016; Joswig et al., 2021). For example, low soil fertility likely explains relatively high LMA mean in Australian and New Zealand sites with warm-temperate everwet climates, as nutrient-poor soils are common in those regions (Beadle, 1966, McGlone et al., 2004).

In addition, incorporating intraspecific variation into the calculation of community-scale central moments via bootstrapping, and weighting those calculations by species abundance, improves how accurately they reflect the 'true' trait distribution of a community (i.e., if all individuals were sampled; Violle et al., 2012; Enquist et al., 2015; Wieczynski et al., 2019; Maitner et al., 2023). Neither approach was taken in this study due to limitations in sampling strategies at most sites, and may contribute additional unexplained variance. However, there is a strong correlation between species- and abundance-weighted LMA mean (Adj-$R^2 = 0.85$) for a subset of sites where data on stem basal area were available (Appendix S12), and trait means were found to be unaffected by whether intraspecific variation is incorporated by bootstrapping (Maitner et al., 2023). In contrast, there is no significant correlation between species- and abundance-weighted LMA variance (Appendix S12), and calculations of trait variance were more accurate when intraspecific variation is incorporated (Maitner et al., 2023). We suggest that confounding effects of intraspecific variation and species abundance may be minimal for calculations of mean but more pronounced for variance; thus, scaling results of species-weighted variance of LMA to ecosystems should be done cautiously.

Application to paleoecology

Reconstructing community-scale LMA from fossil leaf assemblages—We find significant correlations between measured LMA and PM for community mean and variance (Fig. 6); therefore, the prevalence and diversity of LES strategies in ancient plant communities can be inferred via LMA reconstructions from fossil leaves. Reconstructing mean and variance with PM at the site level using the linear regressions presented in this study (Fig. 6), as opposed to reconstructing LMA at the species level and subsequently calculating mean and variance, allows for a simpler estimation of uncertainty. Accurate LMA reconstructions in the paleontological record also rely on minimizing time averaging and habitat mixing, to make sure that fossil leaf

assemblages approximate plant communities. This is best achieved when fossils are pooled across a narrow stratigraphic height and from a single locality (e.g., Lowe et al., 2018).

Although the mean and variance of LMA and PM show a clear correspondence, the community kurtosis of LMA and PM do not (Fig. 6C). We suggest calculating reconstructed LMA variance and associated uncertainty (from PM variance) using the equations of this study (Fig. 6; Table 4), instead of simply assessing the shape of distributions visually, as visually distinguishing between variance (i.e., spread of values from their mean; Sokal and Rohlf, 2012) and kurtosis (i.e., 'tailedness' of a distribution; Balanda and Macgillivray, 1988; Westfall, 2014) may be difficult.

Interpreting reconstructed LMA mean and variance—Reconstructed LMA from fossil leaf assemblages can be assessed using two main approaches: 1) by comparing absolute values of reconstructed LMA to modern measured LMA to identify analogous environments, vegetation, or climates, or 2) by assessing relative trends of reconstructed LMA across fossil assemblages spanning gradients of time and/or space. Below we discuss the utility and reliability of both approaches.

Comparisons of absolute values between fossil and modern assemblages—Previous work inferred paleoenvironmental types by comparing reconstructed LMA distributions to measured LMA distributions of modern sites to find a best match and analogous environment type (Royer et al., 2010; Lowe et al., 2018; Peppe et al., 2018; Flynn and Peppe, 2019; Wanger et al., 2019; Allen et al., 2020; Baumgartner and Peppe, 2021; West et al., 2021). Here, we find that the reconstructed LMA distribution of sites match poorly with the LMA distribution of their true climate type, owing to substantial variation within, and overlap across, climates types (Fig. 7). Substantial overlap of LMA distributions between sites in differing biomes was also found by

Butrim et al. (2024). Higher match rates were achieved for $PM_{[site]}$ vs. $PM_{[climate\ type]}$ comparisons, rather than reconstructed $LMA_{[site]}$ vs. measured $LMA_{[climate\ type]}$, reflecting the error introduced through LMA reconstruction. The best match rate occurred when comparing coarser groupings of temperate climate types for cool wet summer and arid sites, with the former sharing a lack of tail over higher LMA values (> 125 g/m^2), and the latter tending to have a low peak and exaggerated tail over high LMA values. However, sites of other temperate climate types had considerable false match rates with these climate types. This pattern corroborates the results in Butrim et al. (2024) and demonstrates that reconstructed LMA or PM distributions from fossil leaf assemblages cannot be reliably matched with modern community distributions to infer analogous (Köppen) climate types.

In contrast, we do find support for the use of absolute values community mean in some cases. Absolute values of reconstructed LMA have been used by prior work to infer leaf habit (i.e., deciduous vs. evergreen) of fossil species (Royer et al., 2007, 2010). Similarly, we briefly consider if absolute values of reconstructed LMA can be used to distinguish deciduous and evergreen dominated communities. Here, we find that reconstructions of LMA mean <80 g/m^2 have a high probability of being deciduous dominated (i.e., 75% of sites are deciduous dominated below the cutoff), >140 g/m^2 have a high probability of being evergreen dominated (i.e., 80% of sites are evergreen dominated above the cutoff), and values between those are indiscriminate (Appendix S13).

Relative trends of reconstructed LMA across time/space—Most relative trends in measured LMA mean and variance among climate types are mirrored in reconstructed LMA (Figs. 2, 3, 4); hence, relative trends reconstructed from the fossil record can be interpreted in terms of climatic factors in a similar way as with measured LMA today. That said, we argue that

the fundamental interpretation of reconstructed LMA mean and variance should be done at the level of LES strategies rather than climate (see further discussion in Butrim et al., 2024). Nevertheless, paleoecological investigations often aim to provide paleoenvironmental context to plant community dynamics. Our study highlights the importance of habitat disparity in driving high LMA variance. For example, higher LMA variance can be expected to characterize well-sampled fossil assemblages that represent riparian and non-riparian taxa in water-limiting paleoenvironments (e.g., Allen et al., 2020). Within temperate climates, increases in WNMA LMA mean are often associated with increases in the percentage of evergreen species (Fig. 4) and decreased temperature seasonality (Fig. 3), which is highlighted by differences between cool temperate and warm temperate climate types (Fig. 2). In contrast, in tropical climates, we find that climate and the percentage of evergreen species poorly explain variation in the prevalence and diversity of LES strategies (Figs. 2, 3, 4). Paleoecological studies reconstructing community-scale LMA in tropical paleoclimates will benefit from considering additional biotic and abiotic factors influencing LMA (e.g., Fyllas et al., 2009; Asner et al., 2016) and identifying applicable studies addressing LMA-climate relationships across more regional gradients (e.g., van de Weg et al., 2009; Asner et al., 2016; Neyret et al., 2016; Enquist et al., 2017; Martin et al., 2020).

In general, it is important to consider additional abiotic and biotic factors beyond climate when interpreting relative trends in reconstructed LMA of fossil assemblages. For example, it is best to consider likely soil characteristics when possible, as they have important influence on LMA distributions, by, for example, integrating information about potential nutrient-rich volcanic inputs (e.g., Lowe et al., 2018), paleosol chemical weathering proxies (e.g., Beverly et al., 2018), regional bedrock and landscape history (e.g., Carvalho et al., 2018), or taxonomic inferences of taxa with particular soil requirements (e.g., Wing et al., 2012). It is also important

to recognize that an understanding of WNMA leaf economic strategies may be an incomplete perspective on plant communities when herbaceous angiosperms or conifers are also prevalent, with potential to bias interpretations of assembly and interactions across communities and ecosystems. For example, if a fossil assemblage is interpreted as conifer-dominated, WNMAs may occupy a niche space of fast LES strategies, while most of the community biomass is held in conifers with slower LES strategies, and thus community LMA mean and variance may be underestimated (Becker 2000; Brodribb et al., 2012).

Conclusions

This study tested different mechanistic hypotheses for the distribution of leaf economic strategies within WNMA members of plant communities. We found that the favorability hypothesis, which predicts conditions more favorable to plant growth will have a greater prevalence of fast LES strategies, was not supported by this study. Instead, we find that variables describing temperature seasonality and growing season length are more important for explaining the prevalence of LES strategies within communities, in support of the seasonality hypothesis. For example, colder and more seasonal climates have a greater prevalence of fast and deciduous LES strategies and evergreen species with lower LMA. The abiotic filtering hypothesis, which predicts low LES diversity in harsh climates, was partially supported. Cool temperate wet summer sites had the lowest LES diversity, where high temperature seasonality leads to consistently fast LES strategies. In contrast, arid and warm-temperate dry summer sites have the highest LES diversity, where high environmental disparity between riparian and non-riparian environments exists. Climatic variables and the percentage of evergreen species poorly explained variation in LES strategies across tropical climate types, highlighting the importance of additional biotic and abiotic factors.

This study also assessed the extent to which LMA reconstructed from the fossil record reliably reflects measured LMA. We found that the prevalence and diversity of WNMA leaf economic strategies can be assessed in ancient plant communities using fossil leaf assemblages through the correlation of LMA and PM for community-scale mean and variance. However, fossil LMA reconstructions generally cannot be reliably interpreted through direct comparisons with modern assemblages. Instead, we propose that relative differences of reconstructed LMA of fossil assemblages separated in time or space can be explained by potential variation in climatic conditions and the percentage of evergreen vs. deciduous species, particularly in temperate climates. Further, noise in PM and LMA relationships, and in LMA and climate relationships, demonstrates the importance of incorporating independent lines of evidence when drawing strong interpretations from reconstructed LMA distributions. This study thus furthers our understanding of patterns and processes driving the assembly of WNMAs in plant communities and refines our ability to draw important perspectives of community assembly from the geologic past.

Acknowledgements

We thank Tao Su for contributing leaf image sets from sites in China. We also thank the many University of Washington undergraduates part of Team Leaf, for assisting with petiole metric measurements. We thank Brad Boyle and Vanessa Buzzard for their contributions in collecting and curating LMA data from several modern sites included in this study. Funding for this project was provided by NSF EAR-1924390 to C.A.E.S. We thank William Brightly for analytical help and Ellen D. Currano for insightful discussion.

Author contributions

A.J.L, C.A.E.S, D.J.P., D.L.R, D.J.W., T.R., and B.J.E. developed the project, A.J.L, D.J.P., D.L.R, D.J.W., B.J.E., S.T.M, and A.J.K. contributed LMA and PM measurements of modern leaves, M.J.B. acquired and filtered data from TRY, A.J.L lead the analyses and statistical tests. All authors contributed to data interpretation and writing and editing of the manuscript.

Literature Cited

Adams, J. M., W. A. Green, and Y. Zhang. 2008. Leaf margins and temperature in the North American flora: Recalibrating the paleoclimatic thermometer. *Global and Planetary Change* 60: 523–534.

Aguirre-Gutiérrez, J., E. Berenguer, I. Oliveras Menor, D. Bauman, J. J. Corral-Rivas, M. G. Nava-Miranda, S. Both, et al. 2022. Functional susceptibility of tropical forests to climate change. *Nature Ecology & Evolution* 6: 878–889.

Allen, S. E., A. J. Lowe, D. J. Peppe, and H. W. Meyer. 2020. Paleoclimate and paleoecology of the latest Eocene Florissant flora of central Colorado, U.S.A. *Palaeogeography, Palaeoclimatology, Palaeoecology* 551: 109678.

Archibald, S., C. E. R. Lehmann, C. M. Belcher, W. J. Bond, R. A. Bradstock, A.-L. Daniau, K. G. Dexter, et al. 2018. Biological and geophysical feedbacks with fire in the Earth system. *Environmental Research Letters* 13: 033003.

Asner, G. P., D. E. Knapp, C. B. Anderson, R. E. Martin, and N. Vaughn. 2016. Large-scale climatic and geophysical controls on the leaf economics spectrum. *Proceedings of the National Academy of Sciences* 113.

Azevedo-Schmidt, L., and E. D., Currano. 2023. Leaf traits linked to structure and palatability drive plant-insect interactions within three forested ecosystems. *American Journal of Botany* e16263.

Balanda, K. P., and H. L. Macgillivray. 1988. Kurtosis: A Critical Review. *The American Statistician* 42: 111–119.

Baumgartner, A., and D. J. Peppe. 2021. Paleoenvironmental changes in the Hiwegi Formation (lower Miocene) of Rusinga Island, Lake Victoria, Kenya. *Palaeogeography, Palaeoclimatology, Palaeoecology* 574: 110458.

Beadle, N. C. W. 1966. Soil Phosphate and Its Role in Molding Segments of the Australian Flora and Vegetation, with Special Reference to Xeromorphy and Sclerophylly. *Ecology* 47: 992–1007.

Beck, H. E., N. E. Zimmermann, T. R. McVicar, N. Vergopolan, A. Berg, and E. F. Wood. 2018. Present and future Köppen-Geiger climate classification maps at 1-km resolution. *Scientific Data* 5: 180214.

Becker, P. 2000. Competition in the Regeneration Niche between Conifers and Angiosperms: Bond's Slow Seedling Hypothesis. *Functional Ecology* 14: 401–412.

Beverly, E. J., W. E. Lukens, and G. E. Stinchcomb. 2018. Paleopedology as a tool for reconstructing paleoenvironments and paleoecology. *In* D. A. Croft, S. W. Simpson, and D. F. Su [eds.], Methods in Paleoecology: Reconstructing Cenozoic Terrestrial Environments and Ecological Communities, update. Springer (Vertebrate Paleobiology and Paleoanthropology Series), Dordrecht.

Blonder, B., D. L. Royer, K. R. Johnson, I. Miller, and B. J. Enquist. 2014. Plant ecological strategies shift across the Cretaceous–Paleogene boundary. *PLoS biology* 12: e1001949.

Brett, M. T. 2004. When is a correlation between non-independent variables "spurious"? *Oikos* 105: 647–656.

Brodribb, T. J., J. Pittermann, and D. A. Coomes. 2012. Elegance versus Speed: Examining the Competition between Conifer and Angiosperm Trees. *International Journal of Plant Sciences* 173: 673–694.

Bruelheide, H., J. Dengler, O. Purschke, J. Lenoir, B. Jiménez-Alfaro, S. M. Hennekens, Z. Botta-Dukát, et al. 2018. Global trait–environment relationships of plant communities. *Nature Ecology & Evolution* 2: 1906–1917.

Burnham, R. J., S. L. Wing, and G. G. Parker. 1992. The reflection of deciduous forest communities in leaf litter: implications for autochthonous litter assemblages from the fossil record. *Paleobiology* 18: 30–49.

Butrim, M. J., and D. L. Royer. 2020. Leaf-economic strategies across the Eocene–Oligocene transition correlate with dry season precipitation and paleoelevation. *American Journal of Botany* 107: 1772–1785.

Butrim, M. J., A. J. Lowe, E. D. Currano. 2024. Leaf mass per area: an investigation into the uses of the ubiquitous functional trait from a paleobotanical perspective. *American Journal of Botany* XXX.

Carreño-Rocabado, G., M. Peña-Claros, F. Bongers, A. Alarcón, J.-C. Licona, and L. Poorter. 2012. Effects of disturbance intensity on species and functional diversity in a tropical forest. *Journal of Ecology* 100: 1453–1463.

Carvalho, M. R., C. Jaramillo, F. d. l. Parra, D. Caballero-Rodríguez, F. Herrera, S. Wing, B. L. Turner et al. 2021. Extinction at the end-Cretaceous and the origin of modern Neotropical rainforests. *Science* 372: 63-68.

Cayuela, L., I. Macarro, A. Stein, and J. Oksanen. 2021. Taxonstand: Taxonomic Standardization of Plant Species Names. R package version 2.4. https://CRAN.R-project.org/package=Taxonstand

Chabot, B. F., and D. J. Hicks. 1982. The Ecology of Leaf Life Spans. *Annual Review of Ecology and Systematics* 13: 229–259.

Chakrabarty, S., S. Sharma, S. Ganguly, A. Jezeera, N. Mohanbabu, and D. Barua. 2021. Quantitative estimates of deciduousness in woody species from a seasonally dry tropical forest are related to leaf functional traits and the timing of leaf flush. 2021.03.03.433407.

Chamberlain, S., and E. Szocs. 2013. taxize - taxonomic search and retrieval in R. F1000Research, 2:191. URL: https://f1000research.com/articles/2-191/v2

Chang, C. Y.-Y., K. Bräutigam, N. P. A. Hüner, and I. Ensminger. 2021. Champions of winter survival: cold acclimation and molecular regulation of cold hardiness in evergreen conifers. *New Phytologist* 229: 675–691.

Cheesman, A. W., H. Duff, K. Hill, L. A. Cernusak, and F. A. McInerney. 2020. Isotopic and morphologic proxies for reconstructing light environment and leaf function of fossil leaves: A modern calibration in the Daintree Rainforest, Australia. *American Journal of Botany* 107: 1165–1176.

Cornwell, W. K., J. H. C. Cornelissen, K. Amatangelo, E. Dorrepaal, V. T. Eviner, O. Godoy, S. E. Hobbie, et al. 2008. Plant species traits are the predominant control on litter decomposition rates within biomes worldwide. *Ecology Letters* 11: 1065–1071.

Enquist, B. J., L. P. Bentley, A. Shenkin, B. Maitner, V. Savage, S. Michaletz, B. Blonder, et al. 2017. Assessing trait-based scaling theory in tropical forests spanning a broad temperature gradient. *Global Ecology and Biogeography* 26: 1357–1373.

Enquist, B. J., J. Norberg, S. P. Bonser, C. Violle, C. T. Webb, A. Henderson, L. L. Sloat, and V. M. Savage. 2015. Scaling from Traits to Ecosystems. Advances in Ecological Research, 249–318. Elsevier.

Fick, S. E., and R. J. Hijmans. 2017. WorldClim 2: new 1-km spatial resolution climate surfaces for global land areas. *International Journal of Climatology* 37: 4302–4315.

Flynn, A. G., and D. J. Peppe. 2019. Early Paleocene tropical forest from the Ojo Alamo Sandstone, San Juan Basin, New Mexico, USA. *Paleobiology* 45: 612–635.

Fonseca, M. B., J. O. Silva, L. A. D. Falcão, M. G. V. Dupin, G. A. Melo, and M. M. Espírito-Santo. 2018. Leaf damage and functional traits along a successional gradient in Brazilian tropical dry forests. *Plant Ecology* 219: 403–415.

Fyllas, N. M., S. Patiño, T. R. Baker, G. Bielefeld Nardoto, L. A. Martinelli, C. A. Quesada, R. Paiva, et al. 2009. Basin-wide variations in foliar properties of Amazonian forest: phylogeny, soils and climate. *Biogeosciences* 6: 2677–2708.

Gillooly, J. F., J. H. Brown, G. B. West, V. M. Savage, and E. L. Charnov. 2001. Effects of Size and Temperature on Metabolic Rate. *Science* 293: 2248–2251.

HilleRisLambers, J., P. B. Adler, W. S. Harpole, J. M. Levine, and M. M. Mayfield. 2012. Rethinking Community Assembly through the Lens of Coexistence Theory. *Annual Review of Ecology, Evolution, and Systematics* 43: 227–248.

Jackson, D. A., and K. M. Somers. 1991. The spectre of 'spurious' correlations. *Oecologia* 86: 147–151.

Joswig, J. S., C. Wirth, M. C. Schuman, J. Kattge, B. Reu, I. J. Wright, S. D. Sippel, et al. 2021. Climatic and soil factors explain the two-dimensional spectrum of global plant trait variation. *Nature Ecology & Evolution* 6: 36–50.

Kattge, J., G. Bönisch, S. Díaz, S. Lavorel, I. C. Prentice, P. Leadley, S. Tautenhahn, et al. 2020. TRY plant trait database – enhanced coverage and open access. *Global Change Biology* 26: 119–188.

Kattge, J., S. Díaz, S. Lavorel, I. C. Prentice, P. Leadley, G. Bönisch, E. Garnier, et al. 2011. TRY – a global database of plant traits. *Global Change Biology* 17: 2905–2935.

Kattge, J., Bönisch, G., Günther, A., Wright, I., Zanne, A., Wirth, C., Reich, P.B. and the TRY Consortium. 2012. TRY - Categorical Traits Dataset. Data from: TRY - a global database of plant traits. TRY File Archive https://www.try-db.org/TryWeb/Data.php#3.

Keddy, P. A., and D. C. Laughlin. 2021. A Framework for Community Ecology: Species Pools, Filters and Traits. Cambridge University Press.

Kindt R. 2020. WorldFlora: An R package for exact and fuzzy matching of plant names against the World Flora Online taxonomic backbone data. *Applications in Plant Sciences* 8: e11388.

Kowalski, E. A., and D. L. Dilcher. 2003. Warmer Paleotemperatures for Terrestrial Ecosystems. *Proceedings of the National Academy of Sciences of the United States of America* 100: 167–170.

Kraft, N. J. B., R. Valencia, and D. D. Ackerly. 2008. Functional Traits and Niche-Based Tree Community Assembly in an Amazonian Forest. *Science* 322: 580–582.

Lammerant, R., A. Rita, M. Borghetti, and R. Muscarella. 2023. Water-limited environments affect the association between functional diversity and forest productivity. *Ecology and Evolution 13*: e10406.

Lourenço, J., E. A. Newman, C. R. D. Milanez, L. D. Thomaz, and B. J. Enquist. 2020. Assessing trait driver theory along abiotic gradients in tropical plant communities. *bioRxiv*. doi: 10.1101/2020.02.15.950139.

Lowe, A. J., D. R. Greenwood, C. K. West, J. M. Galloway, M. Sudermann, and T. Reichgelt. 2018. Plant community ecology and climate on an upland volcanic landscape during the Early Eocene Climatic Optimum: McAbee Fossil Beds, British Columbia, Canada. *Palaeogeography, Palaeoclimatology, Palaeoecology* 511: 433–448.

Lowe, A. J., A. G. Flynn, M. J. Butrim, A. Baumgartner, D. L. Royer, D. J. Peppe. 2024. Reconstructing terrestrial paleoclimate and paleoecology with fossil leaves using Digital Leaf Physiognomy and leaf mass per area. *Journal of Visualized Experiments*: In press.

Maire, V., I. J. Wright, I. C. Prentice, N. H. Batjes, R. Bhaskar, P. M. Van Bodegom, W. K. Cornwell, et al. 2015. Global effects of soil and climate on leaf photosynthetic traits and rates: Effects of soil and climate on photosynthetic traits. *Global Ecology and Biogeography* 24: 706–717.

Maréchaux, I., L. Saint-André, M. K. Bartlett, L. Sack, and J. Chave. 2020. Leaf drought tolerance cannot be inferred from classic leaf traits in a tropical rainforest. *Journal of Ecology* 108: 1030–1045.

Martin, R. E., G. P. Asner, L. P. Bentley, A. Shenkin, N. Salinas, K. Q. Huaypar, M. M. Pillco, et al. 2020. Covariance of Sun and Shade Leaf Traits Along a Tropical Forest Elevation Gradient. *Frontiers in Plant Science* 10: 1810.

Maynard, D. S., L. Bialic-Murphy, C. M. Zohner, C. Averill, J. Van Den Hoogen, H. Ma, L. Mo, et al. 2022. Global relationships in tree functional traits. *Nature Communications* 13: 3185.

McGlone, M. S., R. J. Dungan, G. M. J. Hall, and R. B. Allen. 2004. Winter leaf loss in the New Zealand woody flora. *New Zealand Journal of Botany* 42: 1–19.

Michaletz, S. T., D. Cheng, A. J. Kerkhoff, and B. J. Enquist. 2014. Convergence of terrestrial plant production across global climate gradients. *Nature* 512: 39-43.

Michaletz, S. T., M. D. Weiser, N. G. McDowell, J. Zhou, M. Kaspari, B. R. Helliker, and B. J. Enquist. 2016. The energetic and carbon economic origins of leaf thermoregulation. *Nature plants* 2: 1-9.

Michaletz, S. T., A. J. Kerkhoff, and B. J. Enquist. 2018. Drivers of terrestrial plant production across broad geographical gradients. Global Ecology and Biogeography, 27(2), 166-174.

Michaletz, S. T., and J. C. Garen. 2024. Hotter is not (always) better: Embracing unimodal scaling of biological rates with temperature. *Ecology Letters* 27: e14381.

Moles, A. T., S. E. Perkins, S. W. Laffan, H. Flores-Moreno, M. Awasthy, M. L. Tindall, L. Sack, et al. 2014. Which is a better predictor of plant traits: temperature or precipitation?,. *Journal of Vegetation Science* 25: 1167–1180.

Neyret, M., L. P. Bentley, I. Oliveras, B. S. Marimon, B. H. Marimon-Junior, E. Almeida de Oliveira, F. Barbosa Passos, et al. 2016. Examining variation in the leaf mass per area of dominant species across two contrasting tropical gradients in light of community assembly. *Ecology and Evolution* 6: 5674–5689.

Niinemets, Ü. 2001. Global-Scale Climatic Controls of Leaf Dry Mass per Area, Density, and Thickness in Trees and Shrubs. *Ecology* 82.

Niklas, K. J. 1994. Plant Allometry: The Scaling of Form and Process. University of Chicago Press.

Olson, M., J. A. Rosell, C. Martínez-Pérez, C. León-Gómez, A. Fajardo, S. Isnard, M. A. Cervantes-Alcayde, et al. 2020. Xylem vessel-diameter–shoot-length scaling: ecological significance of porosity types and other traits. *Ecological Monographs* 90.

Onoda, Y., I. J. Wright, J. R. Evans, K. Hikosaka, K. Kitajima, Ü. Niinemets, H. Poorter, et al. 2017. Physiological and structural tradeoffs underlying the leaf economics spectrum. *New Phytologist* 214: 1447–1463.

Ordoñez, J. C., P. M. Van Bodegom, J.-P. M. Witte, I. J. Wright, P. B. Reich, and R. Aerts. 2009. A global study of relationships between leaf traits, climate and soil measures of nutrient fertility. *Global Ecology and Biogeography* 18: 137–149.

Peppe, D. J., A. Baumgartner, A. Flynn, and B. Blonder. 2018. Reconstructing Paleoclimate and paleoecology using fossil leaves. *In* D. A. Croft, S. W. Simpson, and D. F. Su [eds.], Methods in Paleoecology: Reconstructing Cenozoic Terrestrial Environments and

Ecological Communities, update. Springer (Vertebrate Paleobiology and Paleoanthropology Series), Dordrecht.

Peppe, D. J., D. L. Royer, B. Cariglino, S. Y. Oliver, S. Newman, E. Leight, G. Enikolopov, et al. 2011. Sensitivity of leaf size and shape to climate: global patterns and paleoclimatic applications. *New Phytologist* 190: 724–739.

Peppe, D. J., Lemons, C. R., Royer, D. L., Wing, S. L., Wright, I. J., Lusk, C. H., and Rhoden, C. H. 2014. Biomechanical and leaf–climate relationships: a comparison of ferns and seed plants. *American Journal of Botany*, 101: 338-347.

Peterson, R. A. (2021). Finding Optimal Normalizing Transformations via bestNormalize. The R Journal, 13:1, 310-329, DOI:10.32614/RJ-2021-041.

Pinho, B. X., M. Tabarelli, C. J. F. Braak, S. J. Wright, V. Arroyo-Rodríguez, M. Benchimol, B. M. J. Engelbrecht, et al. 2021. Functional biogeography of Neotropical moist forests: Trait–climate relationships and assembly patterns of tree communities I. Simova [ed.],. *Global Ecology and Biogeography* 30: 1430–1446.

Poorter, H., Ü. Niinemets, L. Poorter, I. J. Wright, and R. Villar. 2009. Causes and consequences of variation in leaf mass per area (LMA): a meta-analysis. *New Phytologist* 182: 565–588.

R Core Team. 2013. R: A language and environment for statistical computing. R Foundation for Statistical Computing, Vienna, Austria. ISBN 3-900051-07-0, URL http://www.R-project.org/.

Reich, P. B. 1995. Phenology of tropical forests: patterns, causes, and consequences. *Canadian Journal of Botany* 73: 164–174.

Reich, P. B. 2014. The world-wide 'fast-slow' plant economics spectrum: a traits manifesto H. *Journal of Ecology* 102: 275–301.

Reich, P. B., I. J. Wright, and C. H. Lusk. 2007. Predicting leaf physiology from simple plant and climate attributes: a global GLOPNET analysis. *Ecological Applications* 17: 1982–1988.

Reichgelt, T., W. G. Lee, W. G., and D. E. Lee. 2022. The extinction of Miocene broad-leaved deciduous Nothofagaceae and loss of seasonal forest biomes in New Zealand. *Review of Palaeobotany and Palynology* 307: 104779.

Royer, D. L., I. M. Miller, D. J. Peppe, and L. J. Hickey. 2010. Leaf economic traits from fossils support a weedy habit for early angiosperms. *American Journal of Botany* 97: 438–445.

Royer, D. L., D. J. Peppe, E. A. Wheeler, and Ülo Niinemets. 2012. Roles of climate and functional traits in controlling toothed vs. untoothed leaf margins. *American Journal of Botany* 99: 915–922.

Royer, D. L., L. Sack, P. Wilf, C. H. Lusk, G. J. Jordan, Ülo Niinemets, I. J. Wright, et al. 2007. Fossil Leaf Economics Quantified: Calibration, Eocene Case Study, and Implications. *Paleobiology* 33: 574–589.

Russo, S. E., and K. Kitajima. 2016. The Ecophysiology of Leaf Lifespan in Tropical Forests: Adaptive and Plastic Responses to Environmental Heterogeneity. *In* G. Goldstein, and L.

S. Santiago [eds.], Tropical Tree Physiology: Adaptations and Responses in a Changing Environment, Tree Physiology, 357–383. Springer International Publishing, Cham.

Sack, L., M. T. Tyree, and N. M. Holbrook. 2005. Leaf hydraulic architecture correlates with regeneration irradiance in tropical rainforest trees. *New Phytologist* 167: 403–413.

Schneider, C. A., W. S. Rasband, and K. W. Eliceiri. 2012. NIH Image to ImageJ: 25 years of image analysis. *Nature Methods* 9: 671–675.

Šímová, I., C. Violle, J. Svenning, J. Kattge, K. Engemann, B. Sandel, R. K. Peet, et al. 2018. Spatial patterns and climate relationships of major plant traits in the New World differ between woody and herbaceous species. *Journal of Biogeography* 45: 895–916.

Simpson, A. H., S. J. Richardson, and D. C. Laughlin. 2016. Soil-climate interactions explain variation in foliar, stem, root and reproductive traits across temperate forests: Soil-climate interactions explain functional trait variation. *Global Ecology and Biogeography* 25: 964–978.

Soh, W. K., I. J. Wright, K. L. Bacon, T. I. Lenz, M. Steinthorsdottir, A. C. Parnell, and J. C. McElwain. 2017. Palaeo leaf economics reveal a shift in ecosystem function associated with the end-Triassic mass extinction event. *Nature plants* 3: 1-8.

Sokal, R. R., and F. J. Rohlf. 2012. Biometry : the principles and practice of statistics in biological research. 4th ed. W.H. Freeman, New York.

Su, T., R. A. Spicer, Y.-S. (C.) Liu, Y.-J. Huang, Y.-W. Xing, F. M. B. Jacques, W.-Y. Chen, and Z.-K. Zhou. 2013. Regional constraints on leaf physiognomy and precipitation regression models: a case study from China. *Bulletin of Geosciences*: 595–608.

Su, T., Y.-W. Xing, Y.-S. Liu, F. M. B. Jacques, W.-Y. Chen, Y.-J. Huang, and Z.-K. Zhou. 2010. Leaf margin analysis: a new equation from humid to mesic forests in China. *PALAIOS* 25: 234–238.

Swenson, N. G., B. J. Enquist, J. Pither, A. J. Kerkhoff, B. Boyle, M. D. Weiser, J. J. Elser, et al. 2012. The biogeography and filtering of woody plant functional diversity in North and South America: Functional trait biogeography. *Global Ecology and Biogeography* 21: 798–808.

Violle, C., B. J. Enquist, B. J. McGill, L. Jiang, C. H. Albert, C. Hulshof, V. Jung, and J. Messier. 2012. The return of the variance: intraspecific variability in community ecology. *Trends in Ecology & Evolution* 27: 244–252.

van de Weg, M. J., P. Meir, J. Grace, and O. K. Atkin. 2009. Altitudinal variation in leaf mass per unit area, leaf tissue density and foliar nitrogen and phosphorus content along an Amazon-Andes gradient in Peru. *Plant Ecology & Diversity* 2: 243–254.

Vogel, S. 2009. Leaves in the lowest and highest winds: temperature, force and shape. *New Phytologist* 183: 13-26.

Wagner, J. D., D. J. Peppe, J. M. K. O'Keefe, and C. Dennison. 2019. Plant Community Change Across the Paleocene-Eocene Boundary in the Gulf Coastal Plain, Central Texas. *Palaios* 38: 436-451.

Weiher, E., G. D. P. Clarke, and P. A. Keddy. 1998. Community Assembly Rules, Morphological Dispersion, and the Coexistence of Plant Species. *Oikos* 81: 309–322.

West, C. K., T. Reichgelt, and J. F. Basinger. 2021. The Ravenscrag Butte flora: Paleoclimate and paleoecology of an early Paleocene (Danian) warm-temperate deciduous forest near the vanishing inland Cannonball Seaway. *Palaeogeography, Palaeoclimatology, Palaeoecology* 576: 110488.

Westfall, P. H. 2014. Kurtosis as Peakedness, 1905–2014. R.I.P. *The American Statistician* 68: 191–195.

Wieczynski, D. J., B. Boyle, V. Buzzard, S. M. Duran, A. N. Henderson, C. M. Hulshof, A. J. Kerkhoff, et al. 2019. Climate shapes and shifts functional biodiversity in forests worldwide. *Proceedings of the National Academy of Sciences* 116: 587–592.

Wing, S. L., F. Herrera, C. A. Jaramillo, C. Gómez-Navarro, P. Wilf, and C. C. Labandeira. 2009. Late Paleocene fossils from the Cerrejón Formation, Colombia, are the earliest record of Neotropical rainforest. *Proceedings of the National Academy of Sciences* 106: 18627-18632.

Wright, I. J., P. B. Reich, J. H. C. Cornelissen, D. S. Falster, P. K. Groom, K. Hikosaka, W. Lee, et al. 2005. Modulation of leaf economic traits and trait relationships by climate: Modulation of leaf traits by climate. *Global Ecology and Biogeography* 14: 411–421.

Wright, I. J., P. B. Reich, M. Westoby, D. D. Ackerly, Z. Baruch, F. Bongers, J. Cavender-Bares, et al. 2004. The worldwide leaf economics spectrum. *Nature* 428: 821–827.

Zomer, R. J., J. Xu, and A. Trabucco. 2022. Version 3 of the Global Aridity Index and Potential Evapotranspiration Database. *Scientific Data* 9: 409.

Tables and Figures

TABLE 1. A glossary of abbreviations.

Abbreviation	Meaning
General terms	
LMA	Leaf dry mass per area (g/m^2)
PM	Petiole metric
LES	Leaf economic spectrum
WNMA	Woody non-monocot angiosperm
Percent evergreen	Percentage of evergreen species in a community
Climate variables	
MAT	Mean annual temperature (°C)
TS	Temperature seasonality
MART	Mean annual range of temperature (°C)
T warm Q	Temperature of the warm quarter (°C)
T cold Q	Temperature of the cold quarter (°C)
MAP	Mean annual precipitation (cm/year)
P wet Q	Precipitation of the wet quarter (cm)
P dry Q	Precipitation of the dry quarter (cm)
P wet M	Precipitation of the wettest month (cm)
P dry M	Precipitation of the driest month (cm)
PS	Precipitation seasonality
AI	Aridity index
PET	Potential evapotranspiration (mm)

TABLE 2. The terminology used in this study in reference to Köppen climate type abbreviations (Beck et al. 2018).

Major climate class	Climate type	Abbreviation	Köppen abbreviations
Tropical	Tropical everwet	TE	Af
Tropical	Tropical seasonally dry	TSD	Am
Tropical	Tropical seasonally very dry	TSVD	Aw
Arid	Arid	A	BWh, BWk, BSh, BSk
Temperate	Warm temperate dry summer	WTDS	Csa, Csb, Csc
Temperate	Warm temperate dry winter	WTDW	Cwa, Cwb, Cwc
Temperate	Warm temperate everwet	WTE	Cfa, Cfb, Cfc
Temperate	Cool temperate dry summer	CTDS	Dsa, Dsb, Dsc, Dsd
Temperate	Cool temperate dry winter	CTDW	Dwa, Dwb, Dwc, Dwd
Temperate	Cool temperate everwet	CTE	Dfa, Dfb, Dfc, Dfd

TABLE 3. A summary of hypotheses tested in this study, and their predictions, key results, and interpretation.

Hypotheses	Prediction	Key results	Interpretation
Prevalence of LES strategies			
Favorability	Fast LES strategies more prevalent in favorable (warm, wet) climates	Measured LMA mean is higher in warmer and less seasonal climates, following a trend of increasing percentage of evergreen species	Seasonality hypothesis better supported, particularly in temperate climates
Seasonality	Slow LES strategies more prevalent in warmer, less seasonal environments		
Diversity of LES strategies			
Abiotic filtering	How LES diversity in harsh (cold, dry) climates	Measured LMA variance highest in arid and warm temperate dry summer and lowest in cool temperate dry winter sites	Partially supported, habitat disparity in dry climates also important
Reconstructed LMA relates to measured LMA at community-scale			
PM-LMA correlation	LMA and PM correlate for community mean, variance, and kurtosis	Correlations are significant for mean and variance, weaker for the latter, and non-significant for kurtosis	Partially supported
Similar variables influence variation in reconstructed and measured LMA	Reconstructed and measured LMA have similar relationships to climatic and leaf habit variables	The trends across climate, and correlations with leaf habit, were similar between reconstructed and measured LMA	Supported
LMA distribution matching can be used to infer paleoclimates	Sites correctly match their LMA distribution to that of their true climate type at a high rate	In general, sites matched poorly with their true climate type	Not supported

TABLE 4. Variables required to calculate 95% prediction intervals for estimates of community mean and variance of LMA, using the formula for "predicting mean of $\bar{Y}i$ of k items for a given value Xi" presented in Sokal and Rohlf (2012 p. 489): $\log_{10}(\text{PI}) = \log_{10}(\text{rLMA}) \pm \sqrt{s^2{}_{Y \cdot X}\left[\frac{1}{k} + \frac{1}{n} + \frac{(X_i - \bar{X})^2}{\sum x^2}\right]} \times t_{0.05[n-2]}$, where PI = prediction interval, rLMA = reconstructed leaf mass per area central moment, $s^2{}_{Y \cdot X}$ = unexplained mean square or mean square error, $\bar{X}$ = mean $\log_{10}$(PM) of calibration data, $\sum x^2$ =sum of squares regression, $t_{0.05[n-2]}$ = critical value of Student's distribution for two-tailed significance level of 0.05 and (n-2) degrees of freedom.

Central moment	$S^2{}_{Y \cdot X}$	n	$\bar{X}$	$\sum x^2$	$t_{0.05[n-2]}$
Mean	0.01212861	70	-2.902972	1.154691	1.995469
Variance	0.1713672	70	-5.97104	5.085184	1.995469

Figure 1. Site map. Some sites are represented by leaf dry mass per area data (LMA; green triangles), some by petiole metric data (PM; orange diamonds), and some by both (purple circles). Sites include both novel and previously published data (see Appendix S1).

two columns

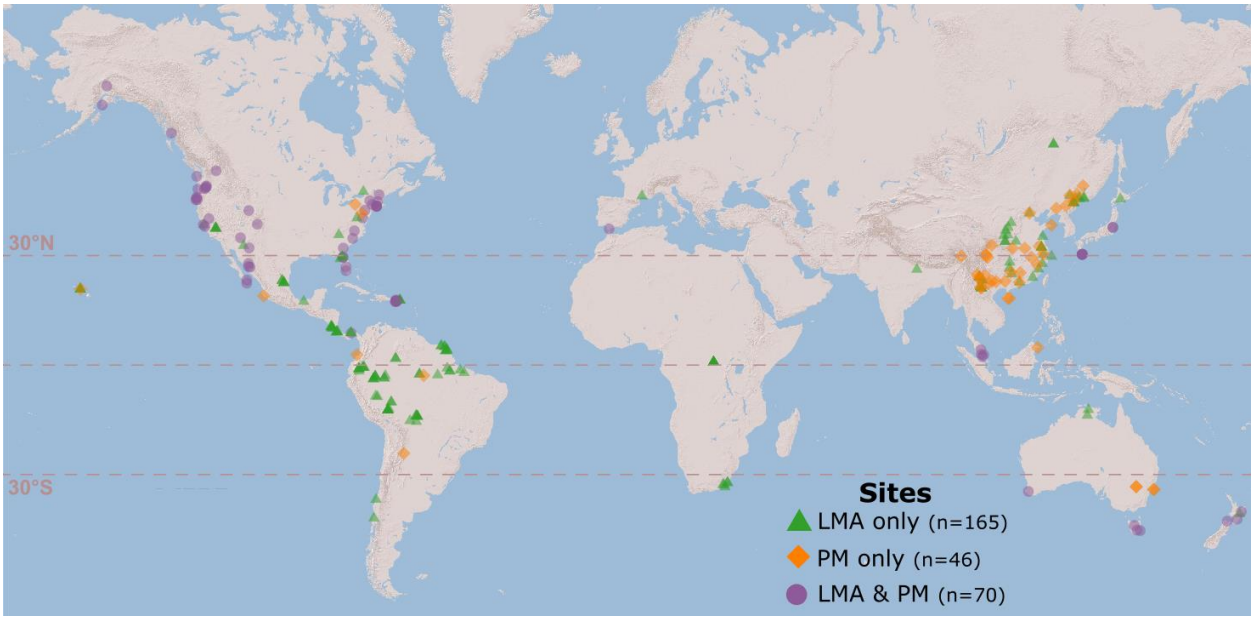

Figure 2. Leaf dry mass per area (LMA) central moments among differing climate types. No shared letters between climate types indicates statistical significance in LMA; **A-B)** Horizontal dotted lines represent cutoffs suggested by Royer et al. (2007), whereby leaves with leaf life spans of >1 or <1 year generally have species averaged LMA of > 129 g/m^2 (blue) and < ~87 g/m^2 (red), respectively. **A)** Measured LMA mean (g/m^2), **B)** Reconstructed LMA mean; **C)** Measured LMA variance ((g/m^2)^2); **D)** Reconstructed LMA variance.

two columns

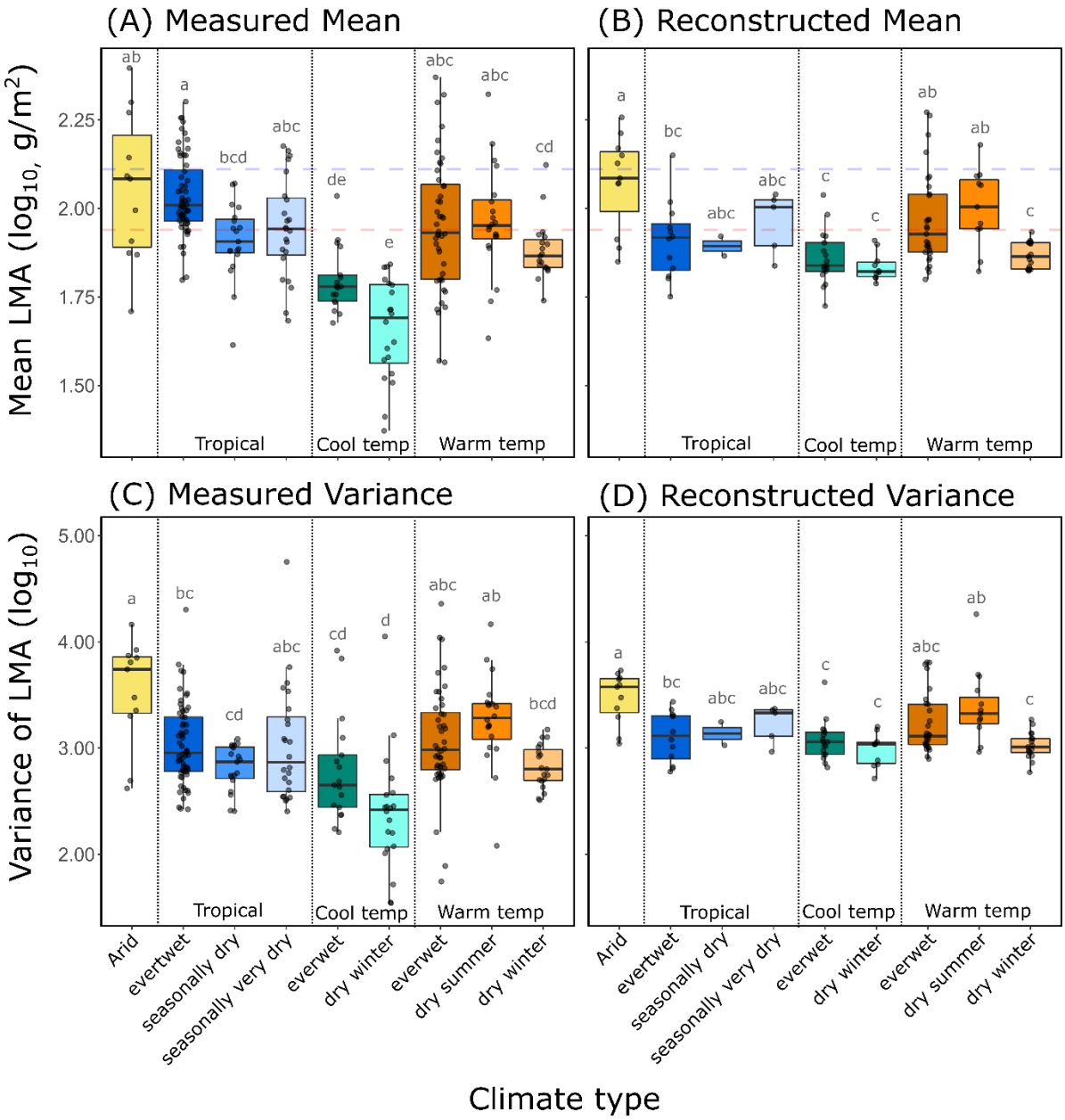

Figure 3. The strength of relationships between leaf dry mass per area (LMA) central moments and continuous climatic variables, expressed as R^2 values, for all, temperate, and tropical climate types. Negative R^2 values and warm colors designate negative relationships while positive values and cool colors designate positive relationships. Grey X's mark non-significant variables. Climate variables include temperature seasonality (TS), mean annual range of temperature (MART = maximum temperature of the warmest month – minimum temperature of the coldest month), temperature of the cold quarter (T cold Q), temperature of the warm quarter (T warm Q), mean annual temperature (MAT), mean annual precipitation (MAP), precipitation of the wet quarter (P wet Q), precipitation of the wet month (P wet M), precipitation of the dry quarter (P dry Q), precipitation of the dry month (P dry M), precipitation seasonality (PS), aridity index (AI), and potential evapo-transpiration (PET); **A)** Measured LMA mean and variance; **B)** Reconstructed LMA mean and variance.

two columns

(A)

	Measured Mean			Reconstructed Mean		
Climate	**All**	**Temp.**	**Tropics**	**All**	**Temp.**	**Tropics**
TS	**-0.24**	**-0.42**	X	-0.03	**-0.29**	X
MART	-0.18	-0.40	0.03	X	-0.28	X
T cold Q	0.17	0.29	-0.03	X	0.10	**-0.22**
T warm Q	X	X	X	X	-0.11	X
MAT	0.13	0.12	X	X	X	X
MAP	0.04	0.07	X	X	X	X
P wet Q	X	X	-0.03	-0.03	X	X
P wet M	X	X	**-0.05**	X	X	X
P dry Q	0.05	0.04	0.03	X	X	X
P dry M	0.05	0.03	0.04	X	X	X
PS	-0.03	X	**-0.05**	X	X	X
PET	0.10	0.09	X	**0.09**	X	X
AI	X	X	X	-0.03	X	X

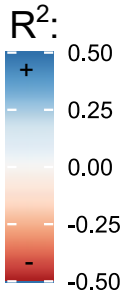

(B)

	Measured Variance			Reconstructed Variance		
Climate	**All**	**Temp.**	**Tropics**	**All**	**Temp.**	**Tropics**
TS	-0.03	-0.23	0.04	X	**-0.20**	X
MART	-0.02	**-0.25**	0.07	X	-0.19	X
T cold Q	0.01	0.13	**-0.08**	X	0.05	**-0.19**
T warm Q	X	-0.03	X	X	-0.12	X
MAT	X	0.03	X	X	X	X
MAP	X	0.12	-0.04	X	X	X
P wet Q	X	0.06	-0.05	-0.03	X	X
P wet M	X	0.06	-0.04	X	X	X
P dry Q	X	0.06	X	X	X	X
P dry M	X	0.04	X	X	X	X
PS	X	X	X	X	X	X
PET	**0.05**	X	0.04	**0.06**	X	X
AI	X	0.07	-0.05	X	X	X

Figure 4. The relationship between the percentage of evergreen species in a community and the mean leaf dry mass per area (LMA) of that community, separated by major climate class. A linear model was fitted to only temperate sites as relationships within arid and tropical climates were non-significant; **A)** Measured LMA mean; **B)** Difference of measured LMA mean between communities that are deciduous (D) and evergreen (E) dominated (i.e., >50% of species); **C)** Reconstructed LMA mean; **D)** Difference of reconstructed LMA mean between communities that are deciduous (D) and evergreen (E) dominated (i.e., >50% of species).

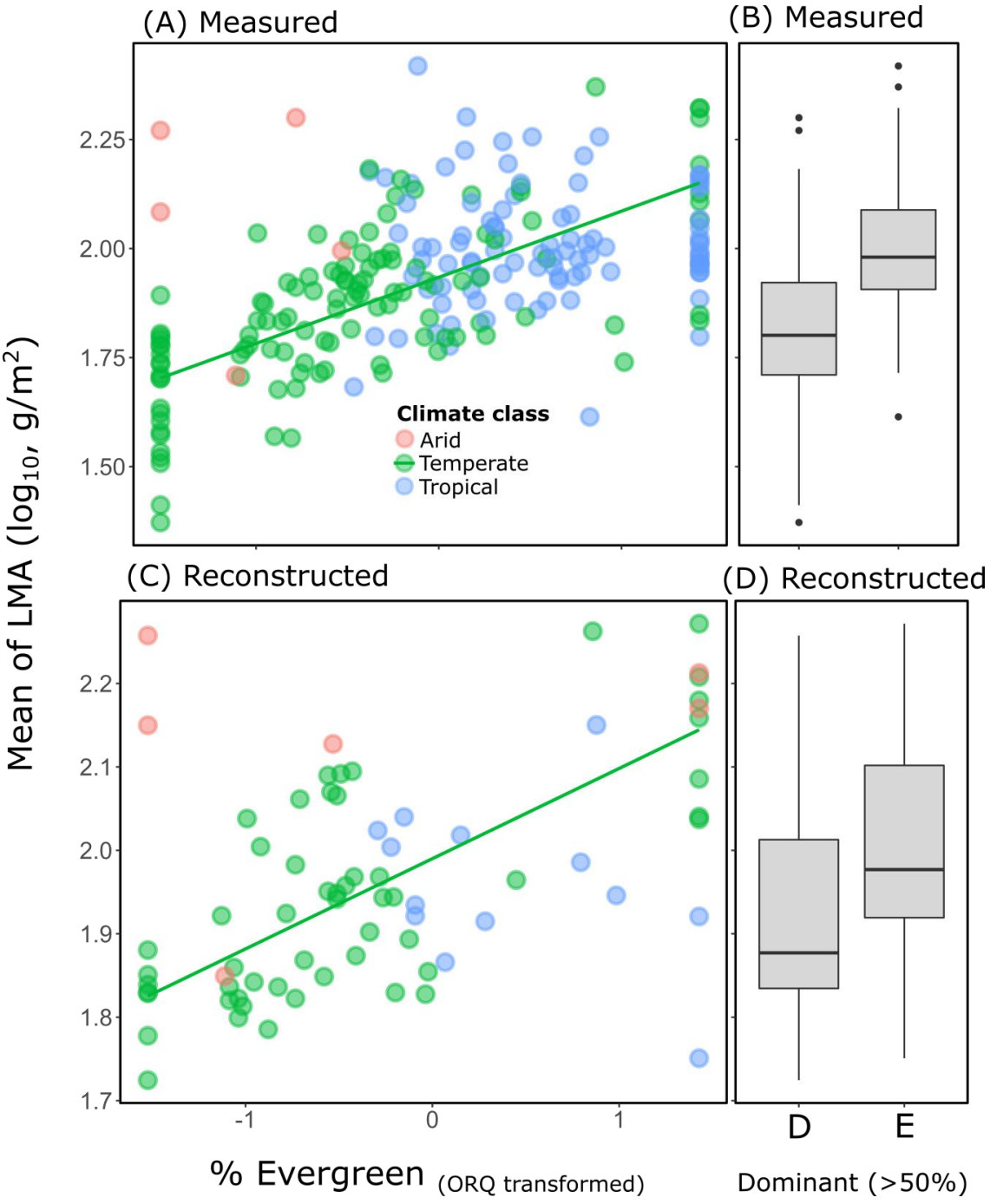

Figure 5. The relationship of site-specific species averaged leaf dry mass per area (LMA; y-axis) and the temperature seasonality (x-axis) for deciduous (orange; $p = 0.992$), and evergreen (green; Adj-$R^2 = 0.14$, $p = 0.017$) species. In addition, kernel density plots of site-specific species averaged LMA compared between deciduous and evergreen species. Only species from temperate climate types are included. *** indicates t-test results of $p<0.001$.

one column

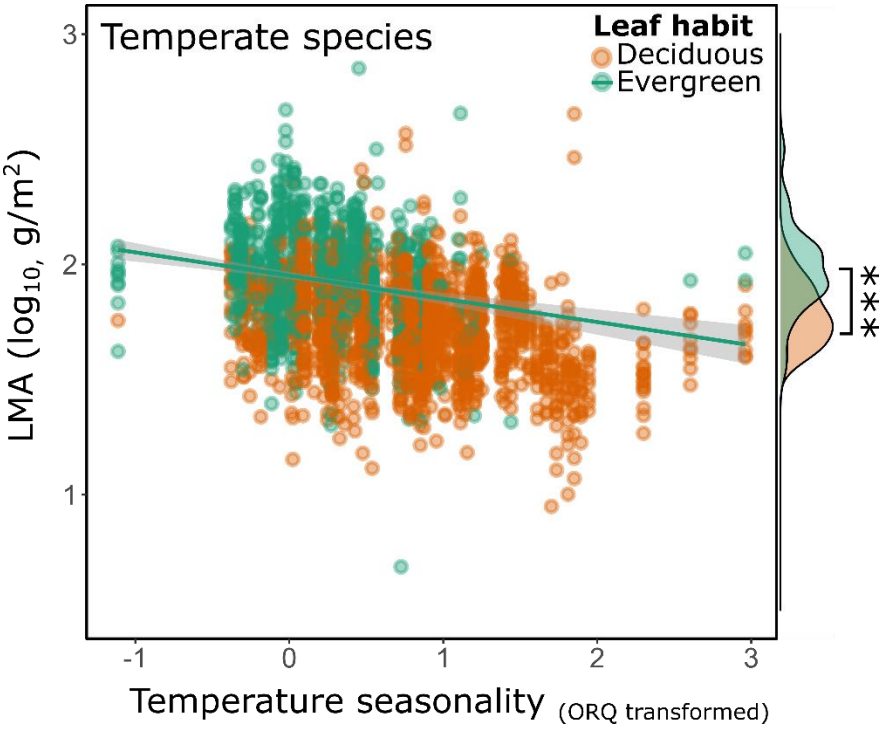

Figure 6. The scaling relationship between community-scale central moments of petiole metric (PM) and leaf dry mass per area (LMA) on a $\log_{10}$-$\log_{10}$ scale measured from leaves of woody non-monocot angiosperms; **A)** Community mean, the linear regression is $\log_{10}(\text{LMA}) = 2.954 + 0.345 \times \log_{10}(\text{PM})$; **B)** Community variance, the linear regression is $\log_{10}(\text{LMA}) = 5.028 + 0.302 \times \log_{10}(\text{PM})$; **C)** Community kurtosis, a linear regression is not provided as the relationship was not significant.

two columns

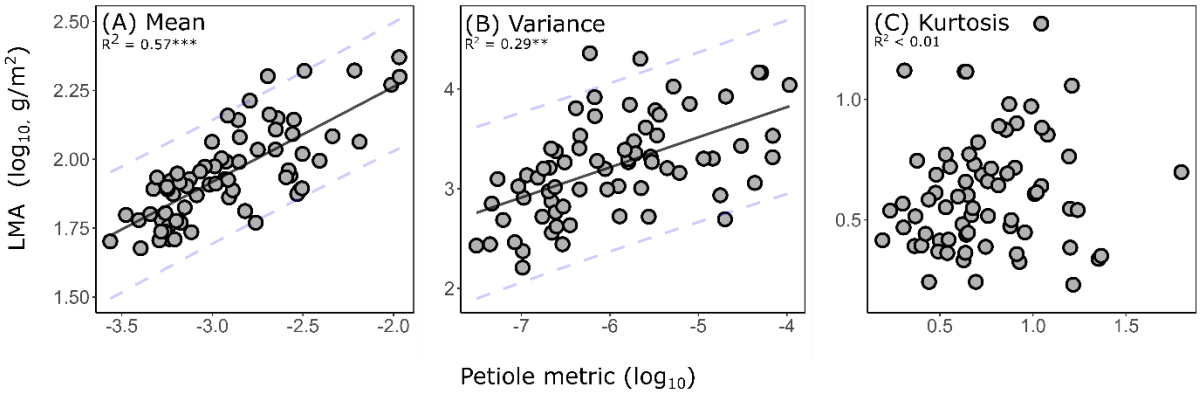

Figure 7. Determining the distinctiveness of leaf dry mass per area (LMA) distributions across climate types to test if LMA distributions from fossil sites can be reliably matched to a modern climate type to infer an analogous paleoclimate. Acronyms are listed in Table 2. **A)** An example to showcase the amount of variability observed within climate types. LMA distributions are plotted for all sites in WTE climates (green), an example used in previous work to typify this climate type (Pee Dee, SC; black), and the 'climate type distribution' meant provide a single characteristic distribution for this climate type; **B)** To simulate how fossil leaf assemblages would be quantitatively matched to a climate type distribution, LMA was reconstructed at the species level using PM, and the similarity of its reconstructed LMA cumulative density distribution (Pee Dee, SC [PD, SC] as an example) to each climate type distribution is shown, and was quantified using the Kolmogorov–Smirnov test statistic. **C-F)** Confusion matrices, where each row represents all sites belonging to a given climate type and the columns along that row representing what climate type each site best matched to. A darker blue corresponds to a higher percentage of matches. The diagonal cells represent the correct match rate expressed as a percentage. **C)** All climate types with reconstructed LMA ($rLMA_{[site]}$) compared to measured $LMA_{[climate\ type]}$; **D)** Coarser groupings of temperate climate types with $rLMA_{[site]}$ compared to measured $LMA_{[climate\ type]}$ **E)** All climate types with petiole metric ($PM_{[site]}$) compared to $PM_{[climate\ type]}$; **F)** Coarser groupings of temperate climate types, with $PM_{[site]}$ compared to $PM_{[climate\ type]}$.

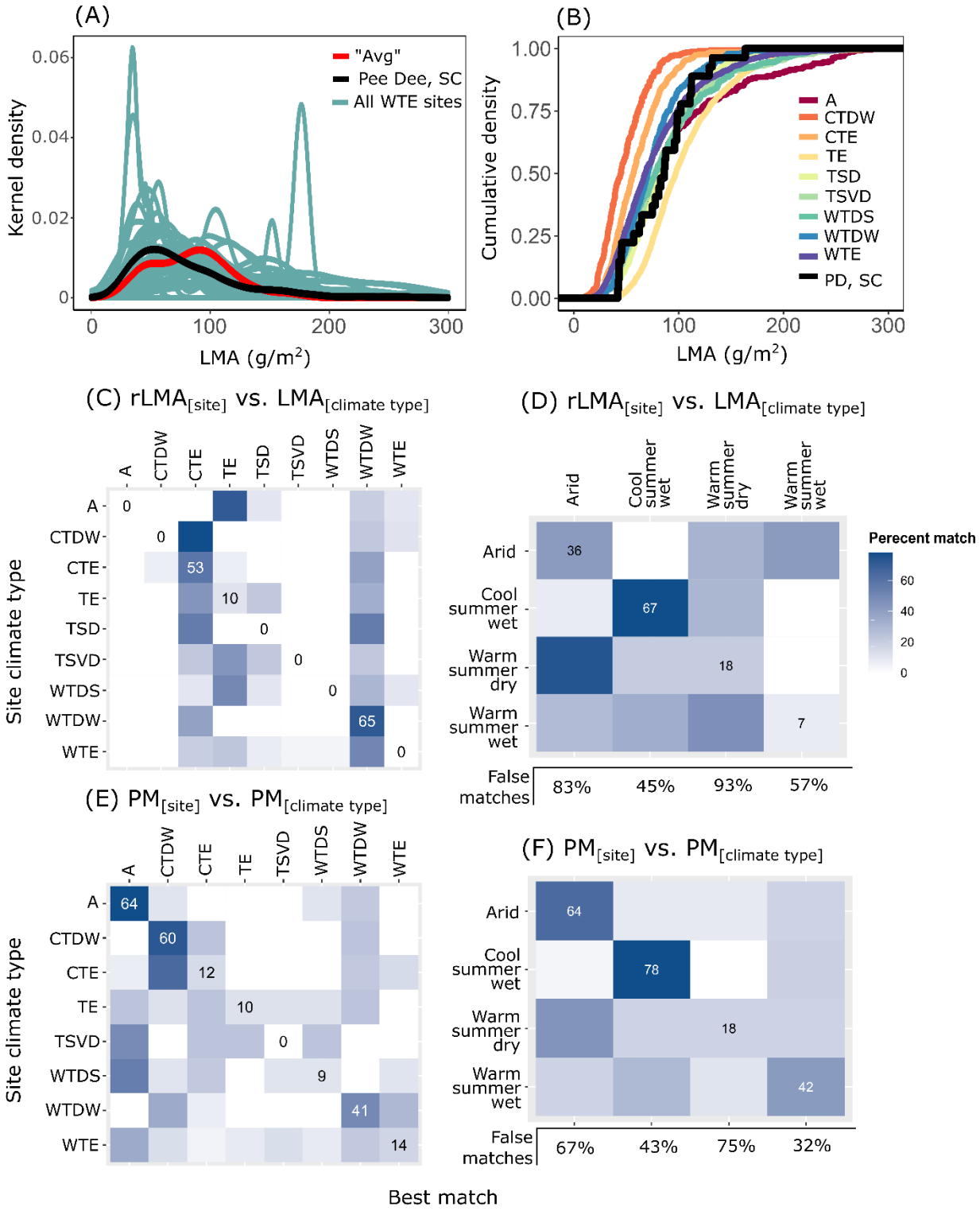
(A)
Kernel density
0.06
0.04
0.02
0
0
100
200
300
LMA (g/m²)
"Avg"
Pee Dee, SC
All WTE sites
(B)
Cumulative density
1.00
0.75
0.50
0.25
0.00
0
100
200
300
LMA (g/m²)
A
CTDW
CTE
TE
TSD
TSVD
WTDS
WTDW
WTE
PD, SC
(C) rLMA[site] vs. LMA[climate type]
Site climate type
A
CTDW
CTE
TE
TSD
TSVD
WTDS
WTDW
WTE
0
0
53
10
0
0
0
65
0
(D) rLMA[site] vs. LMA[climate type]
Arid
Cool summer wet
Warm summer dry
Warm summer wet
36
67
18
7
Perecent match
60
40
20
0
False matches
83%
45%
93%
57%
(E) PM[site] vs. PM[climate type]
Site climate type
A
CTDW
CTE
TE
TSVD
WTDS
WTDW
WTE
64
60
12
10
0
9
41
14
(F) PM[site] vs. PM[climate type]
Arid
Cool summer wet
Warm summer dry
Warm summer wet
64
78
18
42
False matches
67%
43%
75%
32%
Best match

Chapter 2. Links between leaf morphology and ecological strategy across secondary succession in a temperate deciduous forest (North Carolina, USA): implications for the fossil record

Alexander J. Lowe[1], Evonne Aguirre[1,2], Josephine Meier[1,3], Christopher Oishi[4], Caroline A.E. Strömberg[1]

[1]Department of Biology, Burke Museum of Natural History and Culture, University of Washington, Seattle, Washington, U.S.A.

[2]The Graduate Center, City University of New York, New York, New York, U.S.A.

[3]College of Forestry, Oregon State University, Corvallis, Oregon, USA

[4]United States Department of Agriculture Forest Service, Southern Research Station, Coweeta Hydrologic Laboratory, Otto, North Carolina, U.S.A.

Abstract

The fossil record offers important opportunities to reconstruct plant community response to past disturbance events. Yet, reconstructions are hindered by limited empirical evidence of successional variation in functional traits measurable on fossil leaves, including leaf morphology and δ13C. In addition, the role the leaf economic spectrum (LES) plays across succession within this forest type is unresolved. Lastly, it is unclear to what degree disturbance confounds the leaf morphology-climate relationships utilized in paleoclimate proxies.

We utilize a chronosequence spanning variously aged stands following logging (4, 21, 44, 94 years old), and one old growth stand, in North Carolina. Leaf traits of woody non-monocot angiosperms (WNMA) leaves, including all trees and prominent understory plants, were measured to document patterns relating to the LES (e.g., leaf mass per area [LMA]), patterns of leaf morphology and $\delta^{13}C$, and the confounding influence on climatic estimates using the digital leaf physiognomy proxy.

LMA increased across succession among trees, driven by variation in both leaf thickness and leaf density, supporting the role of the LES. The petiole metric (PM), which is biomechanically linked to LMA, increased across succession among trees as hypothesized, as did the proportion of entire-margined leaves and abundance-weighted leaf margin complexity. Measures of diversity (morphological and species richness, $\delta^{13}C$ and LMA variance) for all WNMAs were often highest in the old growth stand, reflecting structural and niche complexity, yet peaked in mid-succession among trees, reflecting a mixing of ecological strategies. Other leaf traits had complicated or subtle trends across succession that were difficult to reconcile and tie to function. Changes in leaf morphology across succession did not strongly confound the accuracy of paleoclimate reconstructions. Successional patterns of this study importantly highlight the utility

of PM, leaf margin, and leaf morphological richness in interpreting successional dynamics from fossil leaf assemblages sourced from temperate deciduous forests.

Introduction

The fossil record offers important examples of how plant communities respond to environmental perturbations ranging from relatively local (e.g., flooding; fire volcanic eruption; Currano et al. 2011; Lowe et al. 2018) to global disturbances (e.g., mass extinction; Lyson et al. 2019; Stiles et al. 2020). Such examples help disentangle the complexity of plant community assembly dynamics and aid in providing more informed predictions of anthropogenic impacts. In addition, understanding successional dynamics of paleovegetation may be important for paleoclimate inference, as certain successional stages ("climax vegetation") are thought to be in greater equilibrium with macroclimate than others (e.g., Taggart and Cross 1990; Schiller et al. In Press). Recognizing disturbance as a driving force in paleovegetation requires an understanding of how disturbance impacts the functional composition and diversity of plant communities in various vegetation- and climate types today.

A general model of vegetation succession in non-arid climates posits that high light availability following a disturbance favors the establishment of ecological strategies intolerant of shade that prioritize fast resource acquisition and growth. These strategies are eventually replaced by slower growing, shade-tolerant competitors (Bazzaz 1979; Poorter et al. 2024). Plant functional traits offer important insights to these ecological strategies by directly influencing plant fitness (Grime 2006; Enquist et al. 2015; Funk et al. 2017), providing important opportunity for paleoecological studies (McElwain et al. 2024). However, many traits linked by plant neo-ecologists to ecological strategy are impossible or difficult to directly measure from fossil plants (e.g., assimilation rates, nitrogen concentrations).

Nevertheless, previous work suggest traits measurable in the fossil plant record can be reflective of ecological strategy and successional dynamics, including leaf morphology, leaf carbon isotopes, leaf mass per area (through proxy reconstruction), plant diversity, and leaf herbivore damage (e.g., Currano et al. 2011; Resco et al. 2011). For example, early successional communities in wet tropical forests have been shown to have a greater proportion of species with toothed and lobed leaves compared to late succession (Kappelle and Leal 1996), suggesting links between leaf teeth/lobes and rapid growth strategies. However, there is a dearth of empirical evidence across succession in other vegetation types, including temperate deciduous forests, particularly at the community-scale (Currano et al. 2011). Successional patterns of quantitative leaf morphology traits have not been well explored, including the size and frequency of teeth, leaf circularity, and leaf area. Understanding whether leaf morphology does in fact vary across succession is important not just for tracking ecological strategies, but also to assess to what extent disturbance confounds relationships of leaf morphology and climate that form the basis for paleoclimate proxies such as digital leaf physiognomy (Peppe et al. 2011). This potential impact of disturbance on paleoclimate estimates has been minimally tested.

In addition to morphological traits, leaf carbon stable isotopic ratios ($\delta^{13}C$) can be measured on fossil leaf compressions and cuticle and may provide insight to ecological strategy during succession (Resco et al. 2011). Leaf $\delta^{13}C$ reflects the ratio of intercellular to ambient CO_2 concentration (c_i/c_a), sensitive to both assimilation and stomatal conductance rates, and the $\delta^{13}C$ of ambient CO_2 surrounding the leaf (Farquhar et al. 1982). Stronger vertical gradients of leaf $\delta^{13}C$ characterize more structurally complex forests, resulting from changes in plant water use efficiency with changing light and humidity levels (Farquhar et al. 1982; Garten and Taylor 1992), and potentially, gradients in the $\delta^{13}C$ of ambient CO_2 influenced by lower values of soil

respired CO_2 (Da Silveira et al. 1989; Graham et al. 2014). Thus, variation in assimilation rates, stomatal conductance, and forest structure throughout succession may drive variation in the mean and variance of leaf $\delta^{13}C$ in a plant community (e.g., Garten and Taylor 1992).

Leaf mass per area (LMA) has also been suggested as a useful trait in characterizing ecological strategy across succession (Currano et al. 2011; Lichstein et al. 2021). Although LMA cannot be measured directly on fossil leaves, it can be reconstructed for woody non-monocot angiosperms (WNMA) at the species- and community-scale using its relationship with the petiole metric (PM = petiole width^2 / leaf area) (Royer et al. 2007, 2010; Lowe et al. In Review). LMA is a component of the leaf economic spectrum (LES), which describes co-variation of leaf traits relating to resource acquisition and investment (Wright et al. 2004; Reich 2014; Onoda et al. 2017). The LES is hypothesized to play a role in successional dynamics, with, for example, early successional shade-intolerant plants having traits that confer fast resource acquisition through greater investment in low-density photosynthetic enzymes and lower resistance to within-leaf CO_2 flux (e.g., low LMA, high nitrogen concentration). In contrast, late successional plants are characterized by traits that confer shade tolerance and resource retention (e.g., high LMA, low nitrogen concentration) (Wright et al. 2004; Poorter and Bongers 2006; Onoda et al. 2017; Falster et al. 2018; Lichstein et al. 2021; Poorter et al. 2024).

However, the role of the LES in successional dynamics of deciduous-dominated humid forests is unclear, as shade-tolerant deciduous trees have repeatedly been shown to have lower LMA than shade-intolerant trees (Niinemets and Kull 1994; Niinemets et al. 1998; Aranda et al. 2004; Hallik et al. 2009). This may be explained by the complicating influence of leaf thickness—shade tolerance can be conferred by constructing large but thin leaves that maximize light interception and prevent within-leaf intra-cellular shading (Niinemets and Kull 1994; Green

and Kruger 2001). In addition, the co-variation of traits defining the LES are less pronounced among deciduous species (Wright et al. 2004), due in part to low variation in their leaf life span. Thus, resolving whether the LES, and reconstructions of LMA, are useful in reconstructing successional dynamics in deciduous-dominated forests requires direct testing using data on leaf traits related to the LES (e.g., LMA, leaf thickness and density, C:N) measured in situ for plant communities across successional gradients.

Lastly, much work has addressed patterns of plant diversity across succession. Often, species and functional diversity increase across succession as stronger filtering that selects for a narrow set of pioneer species that gives way to greater structural and abiotic complexity and niche differentiation (Currano et al. 2011; Poorter et al. 2024). However, alternative patterns are possible, including that diversity is highest in mid-succession where varying ecological strategies co-exist (e.g., Connell 1978), or that late successional forests are dominated by just a few number of strongly competitive tree species (Doyle 1981; Keddy and Drummond 1996). As discussed above, traits incorporated into measures of functional diversity by neo-ecologists are often not available in the fossil record. Leaf morphological diversity has been assessed in fossil leaf assemblages (e.g., Stiles et al. 2020), and while its relationship to climate has been explored (Butrim et al. 2024*a*; Roth-Nebelsick and Traiser 2024), its relationship to functional diversity (assessed using neo-ecological traits) and species diversity has been little explored.

To aid in more reliable interpretations of ecological strategy and successional dynamics from fossil leaf assemblages sourced from temperate deciduous forests, we analyze in situ, community-scale, WNMA leaf traits across a successional gradient in western North Carolina, USA. We utilize a chronosequence (i.e., space-for-time substitution) spanning various stages of secondary succession following disturbance by logging. This study is the first, to our knowledge,

to provide quantitative morphological measures of leaves sampled in situ and at the community-scale across a local chronosequence. Specifically, we test:

(1) The role of the LES across succession in temperate deciduous forests. We hypothesize that LMA will increase through succession and that there will be a stronger correlation of LMA with leaf density (approximated by leaf dry matter content [LDMC]) and carbon and nitrogen investment (C:N) than with leaf thickness. We also test for changes in species composition and their reported shade tolerance.

(2) Whether and how leaf morphology, $\delta^{13}C$, and diversity change across succession. We hypothesize that the petiole metric will follow patterns in LMA and that early succession will be characterized by more species with toothed and lobed leaves, consistent with patterns shown in tropical wet forests. We also hypothesize that species-, functional-, and morphological diversity will be lower in early succession and that high stomatal conductance in early succession leads to higher c_i/c_a and thus lower $\delta^{13}C$. Furthermore, we test for patterns in several additional quantitative leaf morphological traits, including the size and frequency of teeth, leaf circularity, and leaf area.

(3) For the confounding effects of disturbance in paleoclimate reconstructions by comparing mean annual temperature and precipitation estimates to true site climate across the chronosequence using the digital leaf physiognomy proxy.

Materials and Methods

As a clarification of terminology in this study, “sites” occur at the regional-landscape scale, “stands” occur within sites at the patch-scale and represent various successional stages, and “plots” are measurable units of the stand (e.g., Poorter et al. 2024).

Study site—The study site is in western North Carolina (NC), USA, in the Nantahala National Forest, and is in a region of mixed cove hardwood (i.e., mixed mesophytic), northern hardwood, oak, and oak-pine communities (Miniat et al. 2021). We incorporated four of the five chronosequence stands studied by Brantley et al. (2019), which were selected based on similar climate, soil, and local setting, with the furthest distance between any stand being ~30 km. At the time of sampling in 2021, these stands were 21, 44, and 94 years old (yo) following known logging activity, in addition to a previously unharvested old growth stand with many trees >200 yo. Due to access issues, we replaced the youngest stand of Brantley et al. (2019) with a separate 4 yo stand. The 4 yo stand was clearcut, the 21 yo stand represents shelterwood harvest, the 44 yo stand was clear cut, and the 94 yo stand was stump-cut removing all merchantable timber (Elliott and Swank 2008), all of which impart secondary succession. The site is characterized by a humid temperate climate, with mean annual temperature ranging from 12.8 °C at lower elevations (~700 m asl) to 10.8 °C at the slightly higher elevation old growth stand (~1,150 m asl), and mean annual precipitation from ~180 to ~260 cm/year depending on elevation (Miniat et al. 2021).

Plot Census and Leaf Sampling—Plots were established by prior work (see Miniat et al. 2021), including two 20 x 40 m plots (0.16 ha total) at each of the 21, 44, and old growth (>200) year old stands, and four 25 x 25 m plots at the 94 year old stand (0.25 ha total) (plot images in Appendix 1). Previous work in 2012 had identified every tree (≥ 10 cm diameter at breast height [DBH]) in each plot to species (Brantley et al. 2019), with one exception being trees identified to *Carya* spp. During the time of sampling in 2021, tree DBH was remeasured, incorporating new individuals which had since grown into the ≥10 cm DBH size class, and species identifications were confirmed and in rare cases revised. Given the very thick undergrowth at the 4 yo stand,

sampling was not done within a defined plot dimension, although the area covered was ~0.1 ha. At the 4 yo stand, no individuals had ≥10 cm DBH and instead every woody plant species encountered was sampled (dominant plants were *Liriodendron tulipifera* and *Robinia pseudoacacia*, which were ~2.5 m in height and <3 cm in DBH).

Leaves were sampled from all WNMA tree species ≥10 cm DBH in each stand, typically from the individual with the greatest DBH, but successively smaller individuals were considered if sampling the largest was not possible. In addition, prominent woody species restricted to the understory (as judged by careful observation) were sampled at each stand. In several cases, we did not identify understory plants to species, but instead to leaf morphotypes (Ellis et al. 2009), which were compared carefully across stands. Sunlit leaves were sampled from canopy trees and shaded leaves from understory plants using either an arborist throw-line launcher (Youngentob et al. 2016) or telescopic branch cutters (see Appendix 2 for additional detail).

Trait Measurements—Trait measurements for species are stand-specific. Leaf mass per area (LMA), leaf dry matter connect (LDMC), and leaf thickness were measured according to standardized protocols (Perez-Harguindeguy et al. 2013) on 8-14 leaves per individual of all species. $\delta^{13}C$ and C:N were measured on three leaves per species for 91% of species-stand pairs (2 leaves for 8% and 1 leaf for 1% of species) including all tree species (≥10 cm DBH), at stable isotope facilities at the University of Washington (see Appendix 2 for additional detail).

Leaf morphology was digitally measured from scanned images of fresh leaves on 5-17 leaves per species (76% of species have $n \geq 10$). To make morphological measurements comparable to paleobotanical approaches, we followed the digital leaf physiognomy approach originally devised as a paleoclimate proxy (Peppe et al. 2011; Lowe et al. In Press). The method measures morphological variables such as leaf area, blade circularity (via Feret diameter ratio),

margin complexity (via shape factor), blade toothiness, and the petiole metric (Table 1). For several leaves (n = 17) of *Quercus alba* and *Quercus velutina*, the lobe geometry was such that they qualified as very large teeth (i.e., were incised less than 25% the distance to the major vein; Royer et al. 2005; Lowe et al. In Press). We found that these outliers skewed stand-scale results, and instead prepared these leaves using a "isolated tooth" protocol, which effectively decreases the amount of leaf area held within each tooth (see Appendix 3 for further detail). To replicate the approach taken in paleoecology studies, the petiole metric was used to reconstruct community-scale LMA mean and variance using the equations of Lowe et al. (In Review). For all leaf trait measurements, leaflets of compound leaves were treated as leaves.

Analyses—All analyses were performed using R (version 4.3.2; R Core Team 2023). Species averages were first calculated for all traits. Species with toothed leaves were assigned a margin state of 0, untoothed leaves a 1, and species with both types of leaves a 0.5. Stand-scale mean and variance were calculated from species averages. Untoothed species were not included in calculating stand-level toothed variables, but untoothed leaves for mixed-margined species were included in the calculation of species averages by setting their tooth frequency and area to 0 and perimeter ratio to 1. Stand mean and variance were calculated both in a species-weighted (each species contributes equally) and abundance-weighted (each species contributes proportionally to their total stand basal area [SBA; calculated from DBH] in the stand). Abundance-weighting better reflects ecosystem-scale processes and the most successful trait value (i.e., those associated with the greatest plant biomass) (Grime 1998; Enquist et al. 2015), but excludes species with individuals < 10 cm DBH including the entire 4 yo stand. Paleoecological studies most often use a species-weighted approach because quantitative inference of original abundance is difficult to obtain from fossil records (but, see Soh et al.

2017). For the species-weighted approach, we consider both the entire WNMA community and only tree species (defined in this study as species with individuals ≥10 cm DBH in the stand), to better understand understory controls on WNMA traits and because trees are overrepresented in fossil leaf assemblages sourced from forests (Greenwood 2005).

Multivariate morphological diversity was assessed using the R package FD (Laliberté et al. 2014), where individual traits standardized to mean 0 and unit variance were included in a principal coordinate analysis (Laliberté and Legendre 2010). Of the diversity indices produced by FD, we included morphological richness, evenness, and dispersion because they are intuitive measures of diversity. Richness represents the amount of morphological space filled by the community, evenness represents how evenly species are distributed within that morphological space, and dispersion represents how dispersed species are from the centroid of morphological space (Laliberté and Legendre 2010). Both species- and abundance-weighted (by total SBA) analyses were performed for evenness and dispersion, but abundance-weighting is not possible for calculations of richness (Laliberté and Legendre 2010).

To consider how leaf trait variation reflects taxonomic composition, the similarity of taxonomic composition, in terms of presence/absence and abundance (by total SBA), was assessed across stands using non-metric multidimensional scaling. To do so, SBA of each species was first relativized by its proportion of total stand SBA for the abundance-weighted analysis, and 2D solutions were produced using Bray-Curtis dissimilarity matrices with *metaMDS()* in the vegan package (Oksanen et al. 2022).

We explored structural influences on LMA (leaf thickness, LDMC, and C:N), using the *lm()* function (R Core Team 2023). Because their values exhibited a right-skewed distribution across species, petiole metric, LMA, and leaf area were $\log_{10}$ transformed prior to regression analyses.

To assess the correlation of PM and LMA, we defined linear relationships of $\log_{10}$ transformed values using the *lm()* function (R Core Team 2023).

To test if succession confounds paleoclimate reconstructions, we produced stand-scale reconstructions of mean annual temperature (MAT) and mean annual precipitation (MAP) using the digital leaf physiognomy (DiLP) proxy method (Peppe et al. 2011). This method employs multiple linear regression models, including margin state, leaf circularity (Feret diameter ratio), and tooth count : internal perimeter for MAT, and leaf area, ln(tooth count : internal perimeter), and ln(perimeter ratio) for MAP (Royer et al. 2007; Peppe et al. 2011) (Table 1). We used the R package dilp to process data and produce climate reconstructions (Butrim et al. 2024*b*; Lowe et al. In Press).

Results

Species Composition, LMA, C:N, LDMC, and Leaf Thickness—Species composition varied across succession, with *Carya* spp., *Betula lenta*, *Robinia pseduoacacia* more abundant in early succession and *Liriodendron tulipifera*, *Quercus alba*, *Quercus rubra*, and *Acer rubrum* more abundant in late succession (Fig. 1; Appendix 4). There was a general increase in mean LMA and C:N mean across succession for trees using both species- and abundance-weighted approaches (Fig. 2). The increase in species-weighted tree LMA mean was strongly influenced by the occurrence of two high LMA species of evergreen woody understory shrubs, *Rhododendron maximum* and *Kalmia latifolia*—when these two taxa are excluded, LMA still increases, but to a lesser extent (i.e., by 8.2 g/m^2; Appendix 5). For the entire WNMA community, LMA peaked at mid-succession, and then decreased to late-succession (Fig. 2), alongside increased richness of species restricted to the understory (Appendix 6). LMA mean was positively correlated with both LDMC and leaf thickness at similar levels for the entire WNMA community (Adj-R^2 = 0.40 and

0.32, respectively) and for trees (Adj-R^2 = 0.26 and 0.31, respectively; Table 2). A slightly stronger correlation was found between LMA and C:N (Adj-R^2 = 0.42 for both all WNMA and trees; Table 2).

Species-weighted LMA variance increased through succession among trees but peaked in mid-succession for the entire WNMA community. Patterns among trees were again strongly influenced by the high LMA evergreen species, *R. maximum and K. latifolia* (Appendix 5). Abundance-weighted LMA variance peaked at mid-succession (Fig. 2) and was not influenced by *R. maximum and K. latifolia* because those species contribute minimally to stand total SBA.

Leaf Morphology and δ^{13}C—Several aspects of leaf morphology varied across succession (Fig. 2; see Appendix 7 for visual with leaf images). Petiole metric, and thus reconstructed LMA, increased across succession following the trend of measured LMA (Fig. 2). In fact, reconstructed LMA correlated strongly with LMA at the stand-scale for trees (Adj-R^2=0.90), although the correlation was non-significant when understory plants are included, and weak at the species-scale for both trees and the entire WNMA community (Adj-R^2 = 0.17 and 0.11, respectively; Fig. 3). In most cases, values fall below the 1:1 line, indicating that LMA reconstructions from PM often overestimated measured LMA.

The proportion of untoothed species increased through succession among trees but was relatively invariable for the entire WNMA community. Among toothed species, tooth frequency (TC:IP) varied little among trees but was highest at the old growth (>200 yo) site for the entire WNMA community. Tooth size (TA:BA) showed no notable trend across succession for trees or the entire WNMA community. Leaf margin complexity increased (shape factor decreased) across succession only when weighted by abundance (Fig. 2) and did not vary appreciably for species-weighted measurements. Leaf circularity (Feret diameter ratio) generally decreased across

succession for both species-weighted approaches, although only subtly, encompassing ~16% of total variation across the species of this study. When abundance-weighted, leaf circularity spiked at the 44 yo stand, but did not vary otherwise (Fig. 2).

$\delta^{13}C$ mean showed mixed patterns, being relatively invariable across succession among trees when species-weighted, spiking at mid-succession (44 yo stand) when trees were abundance-weighted, and peaked at mid-succession for the entire WNMA community (Fig. 2). $\delta^{13}C$ variance also showed mixed patterns, with trees having low variance at mid-late succession when species-weighted, generally decreasing variance when abundance-weighted, and with maximum variance in the old growth (>200 yo) stand for the entire WNMA community (Fig. 2).

Leaf morphological richness peaked at mid-succession among trees and increased through succession for the entire WNMA community (Fig. 4A). This pattern mirrored trends in species richness (Fig. 4B). Patterns of morphological evenness were variable, peaking at mid-succession for the entire WNMA community, fluctuating for trees when species-weighted, and decreasing across succession when trees were abundance-weighted (Fig. 4D). Morphological dispersion peaked in mid-succession for the entire WNMA community but was variable for trees when species- and abundance-weighted (Fig. 4G). Species evenness had a fluctuating trend across succession (Fig. 4E).

Climate Reconstructions—The multivariate morphological space of each stand, and the combined stands, falls within the DiLP calibration space, allowing reliable climate reconstructions (Peppe et al., 2011; Appendix 8; Lowe et al., In Press). Reconstructions of mean annual temperature (MAT) varied from 10.1 to 15.3 °C and matched well with true MAT (10.8 - 12.8 °C) (Fig. 5A). The average error was 1.1 °C across all stands, but lower for the two oldest stands (0.4 °C) than the three youngest (1.8 °C). When data were combined across all stands (i.e.,

site scale), the reconstructed MAT was 12.8 °C. Reconstructions of mean annual precipitation (MAP) ranged from 149.6 to 173.4 cm/yr, and 165.7 cm/yr for the combined data, all similar to, but less than, the true range of MAP (180-206 cm/yr) (Fig. 5B).

Discussion

LMA and the Role of the LES—Across a successional gradient (i.e., chronosequence) in an eastern U.S. temperate deciduous forest, LMA mean increased across succession among trees when species- and abundance-weighted, providing some support for the role of the LES across succession (Fig. 2). Increasing LMA is accompanied by shifts in taxonomic composition among deciduous canopy dominants, with greatest dissimilarity between the 21 yo stand and those older (Fig. 1A). Compositional changes reflect, in part, differing shade tolerance strategies, with 21 yo stand dominants *Robinia pseudoacacia*, *Carya* spp., *Quercus velutina*, and *Betula lenta* having low-intermediate tolerance of shade, while older stand dominants *Quercus rubra*, *Quercus alba*, and *Acer rubrum* have an intermediate-high tolerance of shade (Burns and Honkala 1990).

The increase of species-weighted LMA among trees is primarily driven by the growth of high LMA evergreen species *Rhododendron maximum* and *Kalmia latifolia*, which are absent from the two youngest stands, and present but < 10 cm DBH at the 44 yo stand (Appendix 5). Both species mature as small shade tolerant woody shrubs in forest understories (Monk et al. 1985) and have increased in abundance regionally in response to suppressed disturbance (e.g., fire and grazing; McGee and Smith 1967; Elliott et al. 1997). Increases in the prevalence of evergreen, over deciduous, WNMAs across succession has also been reported from subtropical forests of China (Wang et al. 2007; Kröber et al. 2012). These points suggest that increasing LMA resulting from a greater prevalence of evergreen tree species across succession may apply to both subtropical and temperate humid forests.

When species restricted to the understory (i.e., < 10 cm DBH) are included for all stands, the LMA increase is reversed from mid to late succession (Fig. 2), as low LMA deciduous understory elements become more diverse (Appendix 6), reflecting the greater structural complexity of the old growth stand. This highlights the sensitivity of community-scale interpretations to the extent to which understory elements are considered, which can have lower LMA than canopy trees in temperate humid forests (e.g., Nomura et al. 2023).

In contrast to the LES model of succession, previous work has found that shade tolerant tree species, which prevail in late successional environments, have lower LMA, driven in part by large and thin leaves that maximize light interception for a given investment (Niinemets and Kull 1994; Niinemets et al. 1998; Aranda et al. 2004; Hallik et al. 2009). We find that leaf thickness across succession in this study did not drive variation in LMA considerably more than leaf density, as approximated by LDMC (Garnier and Laurent 1994; Perez-Harguindeguy et al. 2013), although correlations were never very strong (Adj-$R^2 \leq 0.40$; Table 2). Instead, resource allocation patterns, as assessed by C:N, correlated most strongly with LMA (Adj-$R^2 = 0.42$; Table 2). This suggests that complicated influences of both leaf thickness and leaf density drive LMA variation across succession in this temperate deciduous forest.

Previous reports of negative LMA-shade tolerance relationships in deciduous taxa were mainly assessed at the species-scale (Niinemets and Kull 1994; Niinemets et al. 1998; Aranda et al. 2004; Hallik et al. 2009). However, one study assessing abundance-weighted LMA mean at the community-scale found it to be lower for tree species growing in previously clearcut, relative to unmanaged old growth temperate forests of Japan (Nomura et al. 2023), supporting our results. Nevertheless, our findings may not be applicable in all contexts. For example, species of *Fagus*, which have low LMA and thin leaves relative to other deciduous species (Aranda et al.

2004; Legner et al. 2014) are often canopy dominants of old growth temperate deciduous forests (Braun 1964; Burns and Honkala 1990), but were not in the late successional stands of this study. Therefore, this study provides some support for the LES model of succession in temperate deciduous forests but further documentation of LMA at the community-scale—a scale that best captures how ecological strategies are filtered and assemble within forest stands—will aid in understanding the universality of these results.

Leaf morphology and $\delta^{13}C$ as indicators of ecology and succession

Petiole Metric—The petiole metric (PM), which was used to reconstruct LMA following established paleoecological methods (Royer et al. 2007; Lowe et al. In Review), increased across succession for mean and variance, mirroring trends in measured LMA, particularly for trees (Figs. 2, 3, 4), in support of our hypothesis. This further corroborates the utility of PM in reconstructing LES strategies at the community-scale (Royer et al. 2007; Peppe et al. 2018, Butrim et al. 2024*a*; Lowe et al. In Review). In contrast, reconstructed (from PM) and measured LMA corresponded less at the species-scale (Fig. 3A, D), and correlations were weaker than previous work integrating across larger spatial scales (Royer et al. 2007, 2010). The greater correspondence for community mean, relative to species mean, of this study results from a predominant influence of just a few high LMA evergreen species. When evergreen species *R. maximum* and *K. latifolia* are removed from the analysis, the community-scale relationship is weaker (Adj-R^2 = 0.30 vs. 0.90) and insignificant (Student's t-test; $p > 0.05$). This suggests that comparisons of reconstructed LMA among deciduous species in temperate humid forests should be made with caution and highlights open questions about the scales and contexts at which PM-LMA relationships are strongest.

Toothiness.—In support of our hypothesis, a greater proportion of tree species with toothed leaves comprised early successional stands (Fig. 2), following the pattern documented in a tropical wet forest (Kappelle and Leal 1996). This pattern also corroborates previous work suggesting that leaf teeth may help confer rapid growth strategies in high-light and disturbed environments (Kowalski and Dilcher 2003; Greenwood 2005; Royer and Wilf 2006; Royer et al. 2009, 2012). The link between leaf teeth, growth strategy, and early succession may result from enhanced early season transpiration and photosynthesis (Baker-Brosh and Peet 1997; Royer and Wilf 2006) and efficient packing of leaves in over-wintering buds (Edwards et al. 2016). There is no correspondence between the proportion of untoothed species and the (small) differences in elevation and temperature of our stands, contrary to predictions of established MAT-leaf margin relationships (e.g., Peppe et al. 2011), suggesting little confounding effect on leaf morphological patterns (Appendix 9).

Species growing only in the understory of early successional environments were disproportionately untoothed, and their inclusion in analyses tempers the increasing trend of untoothed species (Fig. 2). However, trees better capture those strategies that are most successful in growing to occupy the early successional canopy and thus better reflect successful ecological strategies in terms of biomass. Among trees, there was no clear pattern in the number or size of teeth across succession (Fig. 2), suggesting these characters may be less functional at a regional scale, compared to a continental or global scale across gradients of climate (Royer et al. 2005; Peppe et al. 2011).

Leaf Margin Complexity.—In contrast to our hypothesis and the pattern documented in a tropical wet forest (Kappelle and Leal 1996), abundance-weighted leaf margin complexity increases, rather than decreases, across succession (Fig. 2). This reflects the increasing

dominance of lobed-leaved *Acer rubrum,* a shade tolerant species, and species of *Quercus* classified as mid-tolerant (Barnes and Spurr 1998). Lobed leaves, through efficient bud packing and heightened early season photosynthetic and transpiration rates (Baker-Brosh and Peet 1997; Edwards et al. 2016), may help confer shade tolerance to juvenile understory trees that leaf out early to intercept high irradiance before the canopy closes—a behavior known in shade tolerant species of *Acer* (Seiwa 1999; Augspurger and Bartlett 2003; Richardson and O'Keefe 2009). Alternatively, or in addition, lobed leaves may help an understory plant ramp up growth during canopy gap formation (Abrams 1998), by increasing hydraulic efficiency (Sisó et al. 2001) and countering the influence of low wind speed in forest understories on increased boundary layer resistance (Givnish 1979; Leigh et al. 2017). Many understory plants in tropical environments have leaves with dissected margins (Givnish 1979), suggesting a potential link between margin complexity and shade tolerance. In addition, complex margins are associated with colder and more seasonal temperatures in North America (Royer et al. 2005), where rapid growth during a short growing season is advantageous (Lowe et al. In Review). However, increasing margin complexity among tree dominants alongside a greater prevalence of untoothed tree species is difficult to reconcile, and several other shade tolerant species prevalent in old growth temperate deciduous forests do not have lobed leaves (e.g., species of *Fagus* and *Tilia*; Burns and Honkala 1990), complicating links drawn between margin complexity and shade tolerance.

Diversity.—Morphological richness varied across succession alongside other measures of diversity, providing some insight into its functional significance (Fig. 4). Trends of morphological and species richness, and of $\delta^{13}C$ and LMA variance, often differed depending on whether the entire WNMA community or just trees were considered. For the entire WNMA community, the old growth stand showed the highest morphological and species richness (Fig.

4), the highest $\delta^{13}C$ variance (Fig. 2), and among the highest LMA variance. The old-growth stand also had the greatest richness of species restricted to the understory aside from the 4 yo stand. Thus, we interpret an increase in structural complexity and available niche space in our old growth stand to have influenced a higher diversity of species displaying a greater range of leaf morphologies, water use efficiency, and resource acquisition strategies (Currano et al. 2011; Graham et al. 2014; Poorter et al. 2024), corroborating suggested potential links between morphological and functional diversity (Roth-Nebelsick and Traiser 2024).

Among trees, morphological and species richness was lowest in the youngest (21 yo) stand, but peaked at mid-succession (Fig. 4A, B). Abundance-weighted LMA variance also peaked at mid-succession (Fig. 4C), showcasing patterns among tree dominants. When understories are not included, structural complexity is a less important factor, and instead, a mixing of shade tolerance strategies among canopy trees in mid succession likely drives patterns in tree richness (e.g., Connell 1978). In contrast, abundance-weighted $\delta^{13}C$ variance decreased through succession (Fig. 2), suggesting potentially greater convergence in water use efficiency strategies among canopy dominants (Cernusak 2020).

Additional Traits.—Several additional traits had subtle or complicated patterns across succession that are difficult to tie to function and apply to the fossil record. For example, leaf area was largest among saplings in the 4 yo stand (Fig. 2), including a very large-leafed and invasive *Paulownia tomentosa* (avg. leaf area = 727 cm^2), and generally decreased through mid- to late succession. However, the trend was not apparent for abundance-weighted area (Fig. 2), and it contradicts previous work finding that shade tolerant deciduous species are typically characterized by larger leaves that maximize light interception (Niinemets and Kull 1994; Niinemets et al. 1998). Leaf circularity decreased slightly across succession for species-weighted

values, but sharply increased at the 44 yo stand when abundance-weighted (Fig. 2), reflecting the dominance of *Liriodendron tulipifera* (70% of total stand SBA; Fig. 1), whose leaves are relatively circular (Appendix 7)—it is unclear whether this pattern relates to function. Discordant patterns among morphological and species evenness, and morphological dispersion are difficult to reconcile. Although there was little change in $\delta^{13}C$ mean through succession among trees (Fig. 2), a spike in abundance-weighted $\delta^{13}C$ occurs at the 44 yo stand, reflecting the strong dominance of *L. tulipifera* which had relatively high $\delta^{13}C$. A large drawdown of c_i, relative to c_a, indicative of a high water use efficiency, may have helped confer rapid growth known to characterize this shade intolerant and isohydric species (Burns and Honkala 1990; Benson et al. 2022) and help explain its strong dominance in the canopy of this mid-successional stand.

Application to Reconstructing Successional Dynamics in the Fossil Record—Results of this study offer utility for some leaf morphological traits in reconstructing successional dynamics in ancient temperate deciduous forests, corroborating work in other vegetation types (Table 3; Kappelle and Leal 1996; Currano et al. 2011). We place emphasis on leaf trait patterns among tree species as they are likely overrepresented in fossil leaf assemblages sourced from forests. For example, leaf abundance in humid temperate forest leaf litter best correlates with a species total SBA (Burnham et al. 1992; Steart et al. 2005), demonstrating a lower probability of understory plants with lower SBA becoming fossilized. However, this probability increases with fossil sample size and several prior studies do report fossil taxa inferred as shrubs or small trees from ancient forested environments (e.g., Chaney and Axelrod 1959; Wolfe and Wehr 1987; Kvacek 2004). Thus, in some cases, patterns of the entire WNMA community may be more applicable (e.g., very well sampled assemblages).

Leaf traits patterns across succession suggest that disturbed stands in temperate deciduous forests may contain tree species with more toothed leaves and lower reconstructed LMA, as compared to late successional and old growth stands (Table 3). LMA variance increases across succession following increases in evergreen WNMA abundance (Appendix 4). The fact that the presence of high LMA evergreen outliers are an important driving factor in patterns of community-scale LMA and PM should be considered when interpreting fossil records (e.g., Lowe et al. In Review). Morphological richness may be expected to reflect species richness and both can peak when pooling ecological strategies typical of early and late succession, including in mid-succession (Fig. 4; Table 3), when low severity disturbances occur frequently (Connell 1978; Miller et al. 2011), or when integrating across an area where disturbance occurs in a patchy manner (White and Pickett 1985). The increase in margin complexity among dominant trees is likely not applicable to the fossil record, as the same trend was not apparent for species-weighted measures of trees most utilized in paleoecological studies, and it is unclear how abundance-weighting by fossil leaf counts (e.g., Soh et al. 2017) correlates to mean weighted by total SBA.

Succession has both predictable and unpredictable components (Poorter et al. 2024), and the universality of successional patterns of this study relies on mechanistic links between traits and fitness. Patterns of PM and leaf margin across succession in this study agree with independent lines of evidence linking leaf traits to function and fitness (Table 3). However, additional traits are known to be important in conferring ecological strategies across succession, including those related to seed production and dispersal, physiological traits influencing photosynthetic and respiration rates and saturation, and expressions of phenotypic plasticity (Woods and Turner 1971; Abrams 1998; Oguchi et al. 2005; Wilfahrt et al. 2014; Poorter et al. 2024). Patterns are

also likely to differ depending on the forest type. For example, in tropical dry forests, high irradiance in early succession increases soil water limitation and may favor drought resistance traits and strategies (e.g., Fonseca et al. 2018).

Natural disturbances act on various spatial and temporal scales, from tree fall gaps to volcanic eruptions, or even asteroid impacts (Poorter et al. 2024), and varying depositional environments and fossil sampling methodologies differ in their spatial and temporal resolution (Wing and DiMichele 1995). For example, if disturbances are infrequent and with low severity they may be difficult to detect, because even narrow ranges of stratigraphy can average across hundreds or thousands of years—exceptions being instantaneous events such as thick volcanic ash burying vegetation in situ (e.g., Wing et al. 2012). Larger scale disturbances (e.g., high severity volcanic processes, large-scale crown fires, large-scale herbivory or pathogen outbreak) and/or disturbances that occur at high frequency (e.g., frequent fire regime; volcanically active or flood-prone landscapes) are instead those most detectable in most fossil records (e.g., Currano et al. 2011; Lowe et al. 2018).

The Influence of Disturbance on Paleoclimate Reconstructions—Variation in leaf morphology across succession has the potential to confound leaf physiognomy-based paleoclimate proxies, which rely on macroclimate as a predominant correlate. In our study, we found that the effect of successional stage was minimal using the DiLP proxy, as the average error of reconstructed MAT and MAP was consistently low, averaging 1.1 °C and 15.3 cm/yr, respectively, all within the uncertainty bands of the estimates (Fig. 5). In addition, we reconstructed climate at the site-scale by combining stands to simulate the spatial and temporal averaging that may occur in some fossil assemblages. These combined reconstructions also helped increase species richness to the minimum number (~15 WNMAs) suggested by previous

work (Wolfe 1993; Lowe et al. In Press), as only the 44 yo stand had ≥15 tree species. MAT and MAP reconstructions for combined stands were similarly accurate compared to individual stands (Fig. 5). These results suggest that MAT and MAP reconstructions made using the DiLP proxy on fossil macrofloras from analogous paleovegetation types may be relatively robust to successional status or degrees of spatial averaging, more so than what has been proposed by previous work using pollen assemblages (e.g., Taggart and Cross 1990; Schiller et al. 2024).

Patterns of MAT estimates do not directly correspond to patterns in the proportion of untoothed species, known to be an important influence on the leaf morphology-MAT relationship. For example, among trees, reconstructed MAT is most similar between the 21 yo and >200 yo stands (11.1 vs. 10.8 °C, respectively) where the proportion of untoothed species is most dissimilar (19 and 30%, respectively). This outcome reflects the influence of other variables in the regression, including leaf circularity (FDR) and tooth frequency (TC:IP), and suggests that the DiLP proxy may be less sensitive to confounding effects of disturbance than univariate proxies that rely on leaf margin alone (i.e., leaf margin analysis; Wing and Greenwood 1993).

Conclusions

Using a community-scale dataset of in situ leaf traits sampled across a chronosequence in temperate deciduous forests of North Carolina, USA, we aimed to 1) test the role of the LES in this forest type, with the prediction that lower LMA leaves with higher nutrient concentrations have greater prevalence in early succession, 2) test for links between leaf morphology and plant ecological strategies across succession and provide tools for reconstructing successional dynamics in the fossil record, and 3) consider how disturbance may impact paleoclimate estimates using the digital leaf physiognomy proxy.

The role of the LES across succession was partly supported in our study, as trees had higher LMA in older stands, comprised of a greater number of shade-tolerant species, and leaf thickness did not drive LMA variation more than leaf density (approximated by LDMC) or relative nitrogen concentration (C:N). However, LMA did not increase appreciably when considering the entire WNMA community due to increased richness of low LMA understory plants.

Leaf morphology and $\delta^{13}C$ patterns across succession highlight the utility of leaf teeth, PM, and leaf morphological diversity in inferring community-scale ecological strategy and successional status. Patterns among trees in closed canopy forests may be most applicable to the fossil record given relationships of leaf abundance in litter and SBA (Burnham et al. 1992). PM and measured LMA both increased across succession among trees for community mean and variance. A greater prevalence of toothed tree species in early succession is consistent with the previously proposed links of leaf teeth and faster growth strategies. Species of *Acer* and *Quercus* with high leaf margin complexity came to dominate late successional stands, suggesting a relationship between margin complexity and shade intolerance strategies. However, the pattern has limited application to the fossil record because species-weighted measures most utilized in paleoecological studies were much less variable. Structural diversity and a species-rich understory in the old growth stand influenced high morphological and species richness for the entire WNMA community, as well as high LMA and $\delta^{13}C$ variance, highlighting the importance of the increased niche space promoted in late succession. In contrast, when trees are considered alone and structural complexity is less of a factor, species and morphological richness, as well as LMA variance among tree dominants, is highest in mid-succession, likely a result of mixing shade tolerance- and ecological strategies. Other traits, such as leaf area, circularity, $\delta^{13}C$, and the

number and size of teeth, as well as morphological evenness and dispersion, had complicated or subtle trends across succession that were difficult to reconcile.

Changes in leaf morphology across succession did not strongly confound the accuracy of paleoclimate reconstructions using digital leaf physiognomy. In summary, this study provides important insight into ties between leaf morphology and ecological strategy that can be applied to the fossil record to infer successional dynamics in ancient temperate deciduous forests.

Acknowledgments

We thank the University of Washington Team Leaf (year 2021) for preforming leaf morphological measurements, Chelcy Miniat for help in project inception and technical assistance, and Christine Sobek and Joel Scott at Coweeta Hydrological Laboratory for technical assistance in the field. Funding for initial research plot establishment was supported by U.S. Department of Agriculture (USDA) National Institute of Food and Agriculture (NIFA), Agriculture and Food Research Initiative Competitive Grant 2012-67019-19484. Further funding supported field work and research expenses from NSF PNW EAR-1924390 to C.A.E.S. and the American Philosophical Society Lewis and Clark Grant, the Paleontological Society Student Research Grant, and the University of Washington Department of Biology Margo and Tom Wyckoff award to A.J.L. We thank Andy Schauer and Gordon Holtgrieve (University of Washington) for their assistance with stable isotope analyses. The findings and conclusions in this publication are those of the author(s) and should not be construed to represent an official USDA, Forest Service, or U.S. Government determination or policy.

Literature Cited

Abrams, M. D. 1998. The red maple paradox. BioScience 48:355–364.

Aranda, I., F. Pardo, L. Gil, and J. A. Pardos. 2004: Anatomical basis of the change in leaf mass per area and nitrogen investment with relative irradiance within the canopy of eight temperate tree species. Acta Oecologica 25:187–195.

Augspurger, C. K., and E. A. Bartlett. 2003. Differences in leaf phenology between juvenile and adult trees in a temperate deciduous forest. Tree physiology 23:517–525.

Baker-Brosh, K., and R. K. Peet. 1997. The ecological significance of lobed and toothed leaves in temperate forest trees. Ecology 78:1250–1255.

Barnes, B. V., and S. Hopkins. Spurr. 1998. Forest ecology. Wiley, New York.

Bazzaz, F. A. 1979. The physiological ecology of plant succession. Annual review of Ecology and Systematics 10:351–371.

Benson, M. C., C. F. Miniat, A. C. Oishi, S. O. Denham, J. Domec, D. M. Johnson, J. E. Missik, R. P. Phillips, J. D. Wood, and K. A. Novick. 2022. The xylem of anisohydric *Quercus alba* L. is more vulnerable to embolism than isohydric codominants. Plant, Cell & Environment 45:329–346.

Brantley, S. T., C. F. Miniat, and P. V. Bolstad. 2019. Rainfall partitioning varies across a forest age chronosequence in the southern Appalachian Mountains. Ecohydrology 12:e2081.

Braun, E. L. 1964. Deciduous forests of eastern North America. Hafner Pub. Co., New York.

Burnham, R. J., S. L. Wing, and G. G. Parker. 1992. The reflection of deciduous forest communities in leaf litter: implications for autochthonous litter assemblages from the fossil record. Paleobiology 18:30–49.

Burns, R. M., and B. H. Honkala. 1990. Silvics of North America: Volume 2. Hardwoods. United States Department of Agriculture (USDA), Forest Service, Agriculture Handbook 654.

Butrim, M. J., A. J. Lowe, and E. D. Currano. 2024a. Leaf mass per area: An investigation into the application of the ubiquitous functional trait from a paleobotanical perspective. American Journal of Botany 111:e16419.

Butrim, M. J., A. J. Lowe, A. G. Flynn, A. Baumgartner, D. J. Peppe, and D. L. Royer. 2024b. Dilp: Reconstruct Paleoclimate and Paleoecology with Leaf Physiognomy. R package version 1.1.0.

Cernusak, L. A. 2020. Gas exchange and water-use efficiency in plant canopies. Plant Biology 22:52–67.

Chaney, R. W., and D. L. Axelrod. 1959. Miocene floras of the Columbia Plateau. Carnegie Institution of Washington Publication 617.

Connell, J. H. 1978. Diversity in Tropical Rain Forests and Coral Reefs. Science 199:1302–1310.

Currano, E. D., B. F. Jacobs, A. D. Pan, and N. J. Tabor. 2011. Inferring ecological disturbance in the fossil record: A case study from the late Oligocene of Ethiopia. Palaeogeography, Palaeoclimatology, Palaeoecology 309:242–252.

Da Silveira, L., L. Sternberg, S. S. Mulkey, and S. J. Wright. 1989. Ecological interpretation of leaf carbon isotope ratios: influence of respired carbon dioxide. Ecology 70:1317–1324.

Doyle, T. W. 1981. The Role of Disturbance in the Gap Dynamics of a Montane Rain Forest: An Application of a Tropical Forest Succession Model. *In* D. C. West, H. H. Shugart, and D. B. Botkin, eds. Forest Succession. Springer, New York:56–73.

Edwards, E. J., E. L. Spriggs, D. S. Chatelet, and M. J. Donoghue. 2016. Unpacking a century-old mystery: Winter buds and the latitudinal gradient in leaf form. American Journal of Botany 103:975–978.

Elliott, K. J., and W. T. Swank. 2008. Long-term changes in forest composition and diversity following early logging (1919–1923) and the decline of American chestnut (Castanea dentata). Plant Ecology 197:155–172.

Elliott, K. J., L. R. Boring, W. T. Swank, and B. R. Haines. 1997. Successional changes in plant species diversity and composition after clearcutting a southern Appalachian watershed. Forest Ecology and Management 92:67–85.

Ellis, B., D. C. Daly, L. J. Hickey, K. R. Johnson, J. D. Mitchell, P. Wilf, and S. L. Wing. 2009. Manual of leaf architecture. Cornell University Press, Ithaca, NY.

Enquist, B. J., J. Norberg, S. P. Bonser, C. Violle, C. T. Webb, A. Henderson, L. L. Sloat, and V. M. Savage. 2015. Scaling from Traits to Ecosystems: Developing a General Trait Driver Theory via Integrating Trait-Based and Metabolic Scaling Theories. *In* S. Pawar, G. Woodward, and A. I. Dell, eds. Advances in Ecological Research. Academic Press 52:249–318.

Falster, D. S., R. A. Duursma, and R. G. FitzJohn. 2018. How functional traits influence plant growth and shade tolerance across the life cycle. Proceedings of the National Academy of Sciences 115:E6789–E6798.

Farquhar, G. D., M. H. O'Leary, and J. A. Berry. 1982. On the relationship between carbon isotope discrimination and the intercellular carbon dioxide concentration in leaves. Functional Plant Biology 9:121–137.

Fonseca, M. B., J. O. Silva, L. A. D. Falcão, M. G. V. Dupin, G. A. Melo, and M. M. Espírito-Santo. 2018. Leaf damage and functional traits along a successional gradient in Brazilian tropical dry forests. Plant Ecology 219:403–415.

Funk, J. L., J. E. Larson, G. M. Ames, B. J. Butterfield, J. Cavender-Bares, J. Firn, D. C. Laughlin, A. E. Sutton-Grier, L. Williams, and J. Wright. 2017. Revisiting the Holy Grail: using plant functional traits to understand ecological processes. Biological Reviews 92:1156–1173.

Garnier, E., and G. Laurent. 1994. Leaf anatomy, specific mass and water content in congeneric annual and perennial grass species. New Phytologist 128:725–736.

Garten, C. T., and G. E. Taylor. 1992. Foliar $\delta^{13}C$ within a temperate deciduous forest: spatial, temporal, and species sources of variation. Oecologia 90:1–7.

Givnish, T. 1979. On the adaptive significance of leaf form. *In* O. T. Solbrig, S. Jain, G. B. Johnson, and P. H. Raven, eds. Topics in Plant Population Biology. Macmillan Education UK, London:375–407.

Graham, H. V., M. E. Patzkowsky, S. L. Wing, G. G. Parker, M. L. Fogel, and K. H. Freeman. 2014. Isotopic characteristics of canopies in simulated leaf assemblages. Geochimica et Cosmochimica Acta 144:82–95.

Green, D. S., and E. L. Kruger. 2001. Light-mediated constraints on leaf function correlate with leaf structure among deciduous and evergreen tree species. Tree Physiology 21:1341–1346.

Greenwood, D. R. 2005. Leaf margin analysis: Taphonomic constraints. PALAIOS 20:498–505.

Grime, J. P. 1998. Benefits of plant diversity to ecosystems: immediate, filter and founder effects. Journal of Ecology 86:902–910.

Grime, J. P. 2006. Plant strategies, vegetation processes, and ecosystem properties. John Wiley & Sons, p.

Hallik, L., Ü. Niinemets, and I. J. Wright. 2009. Are species shade and drought tolerance reflected in leaf-level structural and functional differentiation in Northern Hemisphere temperate woody flora? New Phytologist 184:257–274.

Kappelle, M., and M. E. Leal. 1996. Changes in leaf morphology and foliar nutrient status along a successional gradient in a Costa Rican upper montane Quercus forest. Biotropica:331–344.

Keddy, P. A., and C. G. Drummond. 1996. Ecological Properties for the Evaluation, Management, and Restoration of Temperate Deciduous Forest Ecosystems. Ecological Applications 6:748–762.

Kowalski, E. A., and D. L. Dilcher. 2003. Warmer paleotemperatures for terrestrial ecosystems. Proceedings of the National Academy of Sciences of the United States of America 100:167–170.

Kröber, W., M. Böhnke, E. Welk, C. Wirth, and H. Bruelheide. 2012. Leaf Trait-Environment Relationships in a Subtropical Broadleaved Forest in South-East China. PLOS One 7:e35742.

Kvacek, Z. 2004. Early Miocene freshwater and swamp ecosystems of the Most Basin (northern Bohemia) with particular reference to the Bílina Mine section. Journal of Geosciences 49:1–40.

Laliberté, E., and P. Legendre. 2010. A distance-based framework for measuring functional diversity from multiple traits. Ecology 91:299–305.

Laliberté, E., P. Legendre, and B. Shipley. 2014. FD: measuring functional diversity from multiple traits, and other tools for functional ecology. R package version 1.0-12.

Legner, N., S. Fleck, and C. Leuschner. 2014. Within-canopy variation in photosynthetic capacity, SLA and foliar N in temperate broad-leaved trees with contrasting shade tolerance. Trees 28:263–280.

Leigh, A., S. Sevanto, J. D. Close, and A. B. Nicotra. 2017. The influence of leaf size and shape on leaf thermal dynamics: does theory hold up under natural conditions? Plant, Cell & Environment 40:237–248.

Lichstein, J. W., B. T. Peterson, J. Langebrake, and S. A. McKinley. 2021. Leaf Economics of Early- and Late-Successional Plants. The American Naturalist 198:347–359.

Lowe, A. J., D. R. Greenwood, C. K. West, J. M. Galloway, M. Sudermann, and T. Reichgelt. 2018. Plant community ecology and climate on an upland volcanic landscape during the Early Eocene Climatic Optimum: McAbee Fossil Beds, British Columbia, Canada. Palaeogeography, Palaeoclimatology, Palaeoecology 511:433–448.

Lowe, A. J., A. G. Flynn, M. J. Butrim, A. Baumgartner, D. Royer L., and D. J. Peppe. In Press. Reconstructing Terrestrial Paleoclimate and Paleoecology with Fossil Leaves Using Digital Leaf Physiognomy and Leaf Mass Per Area. Journal of Visualized Experiments.

Lowe, A. J., D. L. Royer, D. J. Wieczynski, M. J. Butrim, T. Reichgelt, L. Azevedo-Schmidt, D. J. Peppe, B. J. Enquist, and C. A. E. Strömberg. In Review. Global patterns in community-scale leaf mass per area distributions of woody non-monocot angiosperms and their utility in the fossil record. American Journal of Botany.

Lyson, T. R., I. M. Miller, A. D. Bercovici, K. Weissenburger, A. J. Fuentes, W. C. Clyde, J. W. Hagadorn, M. J. Butrim, K. R. Johnson, R. F. Fleming, R. S. Barclay, S. A. Maccracken, B. Lloyd, G. P. Wilson, D. W. Krause, and S. G. B. Chester. 2019. Exceptional continental record of biotic recovery after the Cretaceous–Paleogene mass extinction. Science 366:977–983.

McElwain, J. C., W. J. Matthaeus, C. Barbosa, C. Chondrogiannis, K. O' Dea, B. Jackson, A. B. Knetge, K. Kwasniewska, R. Nair, J. D. White, J. P. Wilson, I. P. Montañez, Y. M. Buckley, C. M. Belcher, and S. Nogué. 2024. Functional traits of fossil plants. New Phytologist 242:392–423.

McGee, C. E., and R. C. Smith. 1967. Undisturbed rhododendron thickets are not spreading. Journal of Forestry 65:334–335.

Miller, A. D., S. H. Roxburgh, and K. Shea. 2011. How frequency and intensity shape diversity–disturbance relationships. Proceedings of the National Academy of Sciences 108:5643–5648.

Miniat, C. F., A. C. Oishi, P. V. Bolstad, C. R. Jackson, N. Liu, J. P. Love, C. M. Pringle, K. J. Solomon, and N. Wurzburger. 2021. The Coweeta Hydrologic Laboratory and the Coweeta Long-Term Ecological Research Project. Hydrological Processes 35:e14302.

Monk, C. D., D. T. McGinty, and F. P. Day. 1985. The Ecological Importance of *Kalmia latifolia* and *Rhododendron maximum* in the Deciduous Forest of the Southern Appalachians. Bulletin of the Torrey Botanical Club 112:187–193.

Niinemets, Ü., and K. Kull. 1994. Leaf weight per area and leaf size of 85 Estonian woody species in relation to shade tolerance and light availability. Forest Ecology and Management 70:1–10.

Niinemets, Ü., O. Kull, and J. D. Tenhunen. 1998. An analysis of light effects on foliar morphology, physiology, and light interception in temperate deciduous woody species of contrasting shade tolerance. Tree Physiology 18:681–696.

Nomura, Y., T. Matsuo, T. Ichie, K. Kitayama, and Y. Onoda. 2023. Quantifying functional trait assembly along a temperate successional gradient with consideration of intraspecific variations and functional groups. Plant Ecology 224:669–682.

Oguchi, R., K. Hikosaka, and T. Hirose. 2005. Leaf anatomy as a constraint for photosynthetic acclimation: differential responses in leaf anatomy to increasing growth irradiance among three deciduous trees. Plant, Cell & Environment 28:916–927.

Oksanen, J., G. L. Simpson, F. G. Blanchet, R. Kindt, P. Legendre, P. R. Minchin, R. B. O'Hara, P. Solymos, M. H. H. Stevens, E. Szoecs, H. Wagner, M. Barbour, M. Bedward, B. Bolker, D. Borcard, G. Carvalho, M. Chirico, M. D. Caceres, S. Durand, H. B. A. Evangelista, R. FitzJohn, M. Friendly, B. Furneaux, G. Hannigan, M. O. Hill, L. Lahti, D. McGlinn, M.-H. Ouellette, E. R. Cunha, T. Smith, A. Stier, C. J. F. T. Braak, and J. Weedon. 2022. Vegan: Community Ecology Package. R package version 2.6-4.

Onoda, Y., I. J. Wright, J. R. Evans, K. Hikosaka, K. Kitajima, Ü. Niinemets, H. Poorter, T. Tosens, and M. Westoby. 2017. Physiological and structural tradeoffs underlying the leaf economics spectrum. New Phytologist 214:1447–1463.

Peppe, D. J., A. Baumgartner, A. Flynn, and B. Blonder. 2018. Reconstructing Paleoclimate and paleoecology using fossil leaves. *In* D. A. Croft, S. W. Simpson, and D. F. Su, eds. Methods in Paleoecology: Reconstructing Cenozoic Terrestrial Environments and Ecological Communities. Springer, Dordrecht:289–318.

Peppe, D. J., D. L. Royer, B. Cariglino, S. Y. Oliver, S. Newman, E. Leight, G. Enikolopov, M. Fernandez-Burgos, F. Herrera, J. M. Adams, E. Correa, E. D. Currano, J. M. Erickson, L. F. Hinojosa, J. W. Hoganson, A. Iglesias, C. A. Jaramillo, K. R. Johnson, G. J. Jordan, N. J. B. Kraft, E. C. Lovelock, C. H. Lusk, Ü. Niinemets, J. Peñuelas, G. Rapson, S. L. Wing, and I. J. Wright. 2011. Sensitivity of leaf size and shape to climate: global patterns and paleoclimatic applications. New Phytologist 190:724–739.

Perez-Harguindeguy, N., S. Diaz, E. Garnier, S. Lavorel, H. Poorter, P. Jaureguiberry, M. S. Bret-Harte, W. K. Cornwell, J. M. Craine, and D. E. Gurvich. 2013. New handbook for standardised measurement of plant functional traits worldwide. Australian Journal of Botany 61:167–234.

Poorter, L., and F. Bongers. 2006. Leaf traits are good predictors of plant performance across 53 rain forest species. Ecology 87:1733–1743.

Poorter, L., M. T. van der Sande, L. Amissah, F. Bongers, I. Hordijk, J. Kok, S. G. Laurance, M. Martínez-Ramos, T. Matsuo, and J. A. Meave. 2024. A comprehensive framework for vegetation succession. Ecosphere 15:e4794.

R Core Team. 2023. R: A Language and Environment for Statistical Computing. R Foundation for Statistical Computing, Vienna, Austria.

Reich, P. B. 2014. The world-wide 'fast-slow' plant economics spectrum: a traits manifesto. Journal of Ecology 102:275–301.

Resco, V., J. P. Ferrio, J. A. Carreira, L. Calvo, P. Casals, Á. Ferrero-Serrano, E. Marcos, J. M. Moreno, D. A. Ramírez, M. T. Sebastià, F. Valladares, and D. G. Williams. 2011. The stable isotope ecology of terrestrial plant succession. Plant Ecology & Diversity 4:117–130.

Richardson, A. D., and J. O'Keefe. 2009. Phenological Differences Between Understory and Overstory. *In* A. Noormets, ed. Phenology of Ecosystem Processes. Springer, New York:87–117.

Roth-Nebelsick, A., and C. Traiser. 2024. Diversity of leaf architecture and its relationships with climate in extant and fossil plants. Palaeogeography, Palaeoclimatology, Palaeoecology 634:111932.

Royer, D. L., and P. Wilf. 2006. Why do toothed leaves correlate with cold climates? Gas exchange at leaf margins provides new insights into a classic paleotemperature proxy. International journal of plant sciences 167:11–18.

Royer, D. L., R. M. Kooyman, S. A. Little, and P. Wilf. 2009. Ecology of leaf teeth: A multi-site analysis from an Australian subtropical rainforest. American Journal of Botany 96:738–750.

Royer, D. L., I. M. Miller, D. J. Peppe, and L. J. Hickey. 2010. Leaf economic traits from fossils support a weedy habit for early angiosperms. American Journal of Botany 97:438–445.

Royer, D. L., D. J. Peppe, E. A. Wheeler, and Ü. Niinemets. 2012. Roles of climate and functional traits in controlling toothed vs. untoothed leaf margins. American Journal of Botany 99:915–922.

Royer, D. L., P. Wilf, D. A. Janesko, E. A. Kowalski, and D. L. Dilcher. 2005. Correlations of climate and plant ecology to leaf size and shape: potential proxies for the fossil record. American Journal of Botany 92:1141–1151.

Royer, D. L., L. Sack, P. Wilf, C. H. Lusk, G. J. Jordan, Ü. Niinemets, I. J. Wright, M. Westoby, P. D. Coley, A. D. Cutter, K. R. Johnson, C. C. Labandeira, A. T. Moles, and F. Valladares. 2007. Fossil Leaf Economics Quantified: Calibration, Eocene Case Study, and Implications. Paleobiology 33:574–589.

Schiller, C., M., A. J. Lowe, T. A. Dillhoff, P. F. Fields, R. E. Taggart, M. Schmitz D., and C. A. E. Strömberg. In Press. Mechanisms of short-term ($<10^6$ years) plant community change from the Miocene Succor Creek flora, Oregon and Idaho (USA). PLOS One.

Seiwa, K. 1999. Changes in leaf phenology are dependent on tree height in *Acer mono*, a deciduous broad-leaved tree. Annals of Botany 83:355–361.

Sisó, S., J. J. Camarero, and E. Gil-Pelegrín. 2001. Relationship between hydraulic resistance and leaf morphology in broadleaf *Quercus* species: a new interpretation of leaf lobation. Trees 15:341–345.

Soh, W. K., I. J. Wright, K. L. Bacon, T. I. Lenz, M. Steinthorsdottir, A. C. Parnell, and J. C. McElwain. 2017. Palaeo leaf economics reveal a shift in ecosystem function associated with the end-Triassic mass extinction event. Nature plants 3:1–8.

Steart, D. C., D. R. Greenwood, and P. I. Boon. 2005. Paleoecological implications of differential biomass and litter production in canopy trees in Australian *Nothofagus* and *Eucalyptus* forests. PALAIOS 20:452–462.

Stiles, E., P. Wilf, A. Iglesias, M. A. Gandolfo, and N. R. Cúneo. 2020. Cretaceous–Paleogene plant extinction and recovery in Patagonia. Paleobiology 46:445–469.

Taggart, R. E., and A. T. Cross. 1990. Plant successions and interruptions in Miocene volcanic deposits, Pacific Northwest. *In* M. G. Lockley and A. Rice, eds. Volcanism and Fossil Biotas. Geological Society of America: 57–68

Wang, X.-H., M. Kent, and X.-F. Fang. 2007. Evergreen broad-leaved forest in Eastern China: Its ecology and conservation and the importance of resprouting in forest restoration. Forest Ecology and Management 245:76–87.

White, P. S., and S. T. A. Pickett. 1985. Natural disturbance and patch dynamics: an introduction. *In* S. T. A. Pickett and P. S. White, eds. The Ecology of Natural Disturbance and Patch Dynamics. Academic Press, Orlando, Fl:3–13

Wilfahrt, P. A., B. Collins, and P. S. White. 2014. Shifts in functional traits among tree communities across succession in eastern deciduous forests. Forest Ecology and Management 324:179–185.

Wing, S. L., and D. R. Greenwood. 1993. Fossils and fossil climate: The case for equable continental interiors in the Eocene. Philosophical Transactions: Biological Sciences 341:243–252.

Wing, S. L., and W. A. DiMichele. 1995. Conflict between local and global changes in plant diversity through geological time. PALAIOS:551–564.

Wing, S. L., C. A. Strömberg, L. J. Hickey, F. Tiver, B. Willis, R. J. Burnham, and A. K. Behrensmeyer. 2012. Floral and environmental gradients on a Late Cretaceous landscape. Ecological Monographs 82:23–47.

Wolfe, J. A. 1993. A method of obtaining climatic parameters from leaf assemblages. United States Geological Survey Bulletin 2040.

Wolfe, J. A., and W. Wehr. 1987. Middle Eocene dicotyledonous plants from Republic, northeastern Washington. United States Geological Survey Bulletin 1597.

Woods, D. B., and N. C. Turner. 1971. Stomatal response to changing light by four species of varying shade tolerances. New Phytologist 70:77–84.

Wright, I. J., P. B. Reich, M. Westoby, D. D. Ackerly, Z. Baruch, F. Bongers, J. Cavender-Bares, T. Chapin, J. H. C. Cornelissen, M. Diemer, J. Flexas, E. Garnier, P. K. Groom, J. Gulias, K. Hikosaka, B. B. Lamont, T. Lee, W. Lee, C. Lusk, J. J. Midgley, M.-L. Navas, Ü. Niinemets, J. Oleksyn, N. Osada, H. Poorter, P. Poot, L. Prior, V. I. Pyankov, C. Roumet, S. C. Thomas, M. G. Tjoelker, E. J. Veneklaas, and R. Villar. 2004. The worldwide leaf economics spectrum. Nature 428:821–827.

Youngentob, K. N., C. Zdenek, and E. van Gorsel. 2016. A simple and effective method to collect leaves and seeds from tall trees. Methods in Ecology and Evolution 7:1119–1123.

Tables and Figures

Table 1. Leaf traits measured in this study. Measurements were made on fresh leaves (before drying), unless stated otherwise.

Leaf trait	Abbreviation	Description
Leaf dry mass per area (g/m^2)	LMA	Leaf dry mass / fresh leaf area
Leaf thickness (mm)		Thickness of the leaf in the middle region between the primary vein and margin, and apex and base.
Carbon : Nitrogen	C : N	Ratio of %C and %N on a dry mass basis.
Leaf dry matter content (%)	LDMC	Leaf dry mass / fresh mass * 100, reflects leaf density.
Petiole metric	PM	Petiole $width^2$ / leaf area, used to reconstruct LMA.
Leaf area (cm^2)		Summed blade and petiole area
Feret diameter ratio	FDR	Feret diameter, or the diameter of a circle with same area of the leaf / major axis length. Measures leaf circularity.
Shape factor		$4\pi \cdot$ blade area/$perimeter^2$. Measures margin complexity.
Tooth count : internal perimeter (#/cm)	TC : IP	Internal perimeter is the leaf perimeter measured once teeth are digitally removed.
Tooth area : blade area	TA : BA	Tooth area is measured between primary sinuses, which includes the area of subsidiary teeth if present.
Perimeter ratio		Length of the blade perimeter / length of internal blade perimeter, after teeth are digitally removed

Table 2. The strength of linear relationships between leaf mass per area (LMA) and traits considered to influence LMA directly including leaf dry matter content (LDMC), which approximates leaf density, leaf thickness, and carbon : nitrogen ratio (C:N). A plus sign (+) signifies a positive slope.

	Trees + Understory			Trees		
Trait	***p***	**Adj-R^2**	**slope**	***p***	**Adj-R^2**	**slope**
LDMC	<0.005	0.40	+	<0.005	0.26	+
Leaf thickness	<0.005	0.32	+	<0.005	0.31	+
C:N	<0.005	0.42	+	<0.005	0.42	+

Table 3. Results of this study that are most relevant to application in the fossil record. Successional patterns are described for trees only. LMA = leaf mass per area, LES = leaf economic spectrum, PM = petiole metric, WNMA = woody non-monocot angiosperm.

Trait	Successional pattern	Functional inferences
LMA and PM/reconstructed LMA	Increase of mean and variance across succession	LMA mean and variance increase across succession, as evergreen WNMA trees become more prevalent, providing evidence for the role of the LES in temperate deciduous forests. Petiole metric also increases in mean and variance, reflecting biomechanical links between petiole width and leaf mass, however these links are strongest when contrasting deciduous and evergreen species, and weaker among deciduous species.
Margin type	More toothed species in early succession	Teeth may confer rapid growth strategies through enhanced early season transpiration and photosynthetic rates and/or more efficient bud packing. However, the inclusion of understory elements may confound this trend.
Morphological richness	Peaked in mid succession.	A close reflection of species richness. A peak in mid succession suggest a high richness of leaf morphologies may represent a mixing of ecological strategies and be tied to functional diversity.

Figure 1. Changes in taxonomic composition of different aged stands assessed by nonmetric multidimensional scaling (NMDS). A, species weighted by relative abundance (i.e., proportion of total SBA), with the top five most abundant species listed. B, the analysis only includes the presence/absence of taxa.

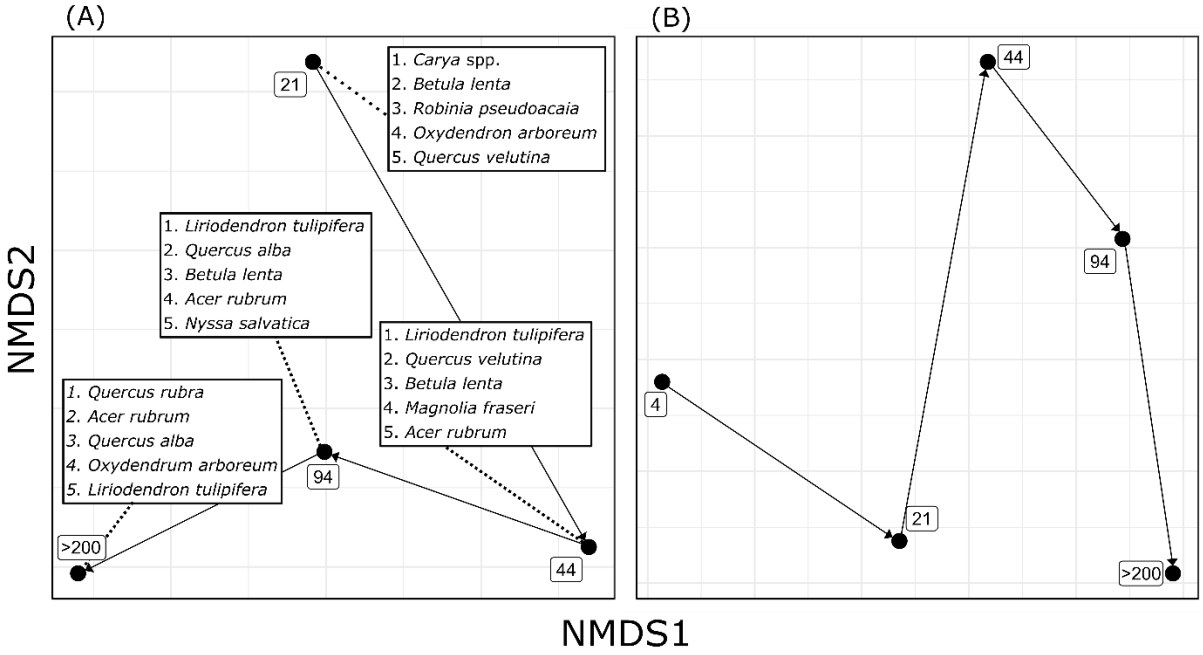

Figure 2. Changes in community leaf traits across ecological succession, including those related to ecological strategy, leaf $\delta^{13}C$, leaf size and shape, and leaf toothiness. Leaf traits are analyzed using three different approaches. Rec. LMA = reconstructed LMA, other abbreviations follow Table 1.

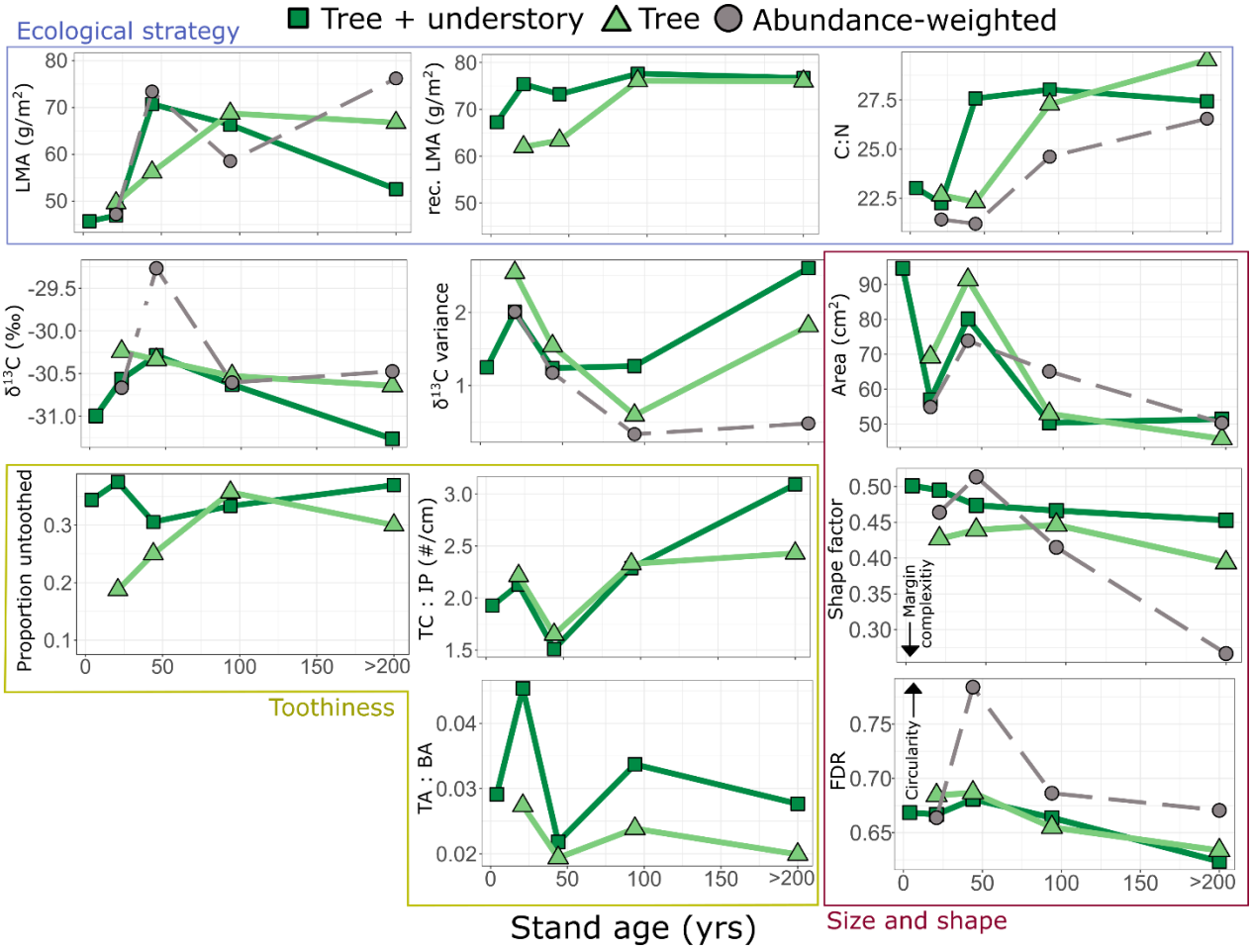

Figure 3. The relationships between reconstructed and measured leaf mass per area (LMA) across different aged stands (shown by point color), compared to a 1:1 relationship (dotted line). A-C, analyses including trees and understory plants, for (A) species mean, (B) stand mean, and (C) stand variance. D-F, analyses limited to trees, for (D) species mean, (E) stand mean, and (F) stand variance.

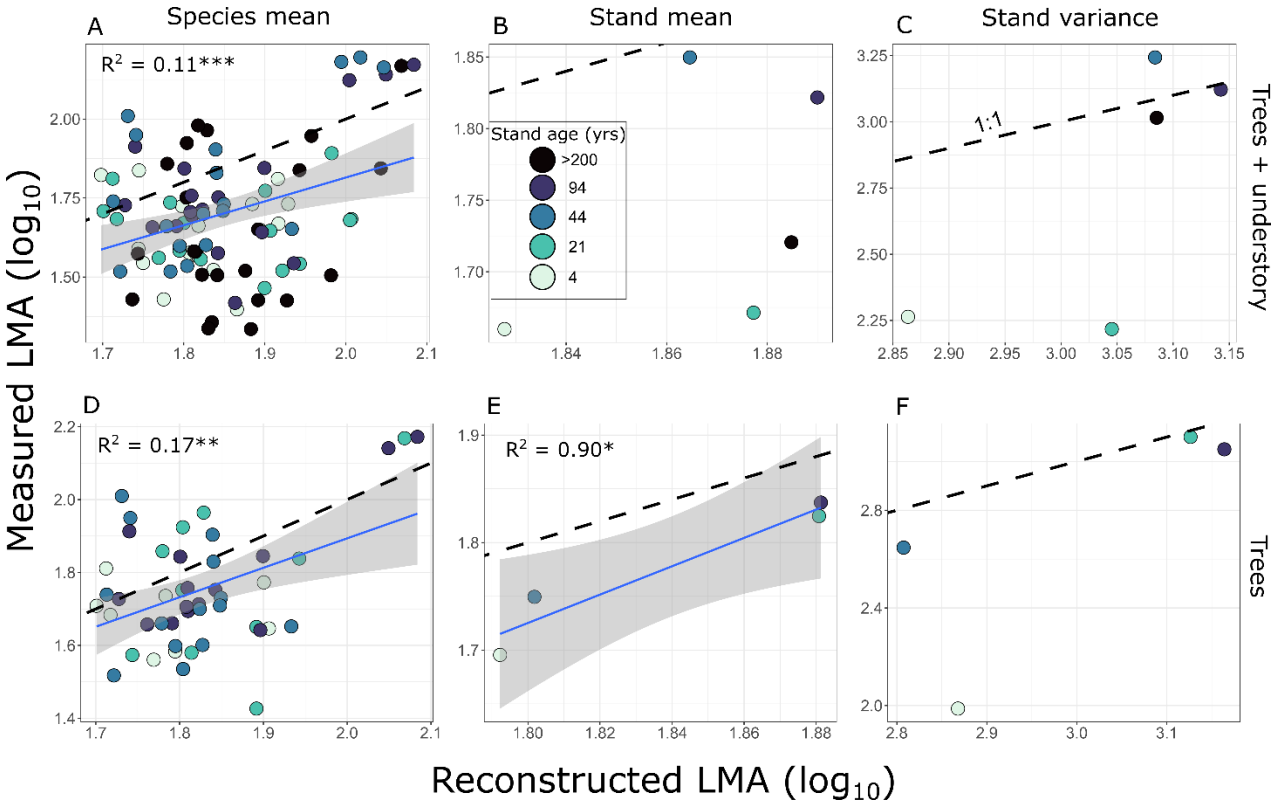

Figure 4. Diversity indices for various aged stands, including those related to leaf morphological diversity (A, D, G), species diversity (B, E), and the diversity of leaf economic spectrum (LES) strategies assessed by both (C) measured and (F) reconstructed (rec.) leaf mass per area (LMA). Leaf traits are analyzed using three different approaches. Note, species richness represents all taxa censused in the plot, including those not sampled (see Appendix 4).

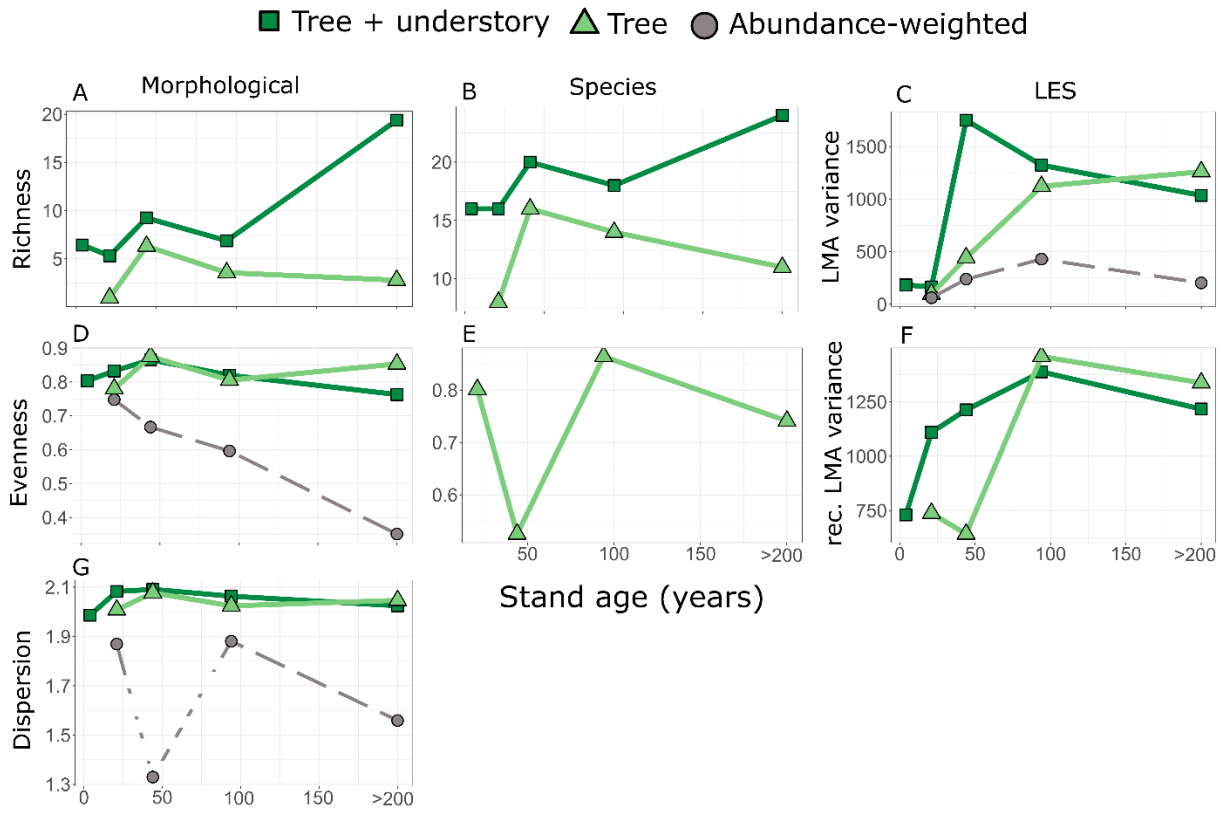

Figure 5. Estimated climatic variables using the digital leaf physiognomy proxy across various aged stands and by combining data across all stands (i.e., site level; "combined"). Estimations are done for both trees only and trees and understory plants combined. The gold bar marks the true climate variable. A, Estimated mean annual temperature (MAT), with true site temperature at the old growth stand adjusted to reflect its slightly higher elevation, and (B) mean annual precipitation (MAP), with the bar width capturing values across all stands.

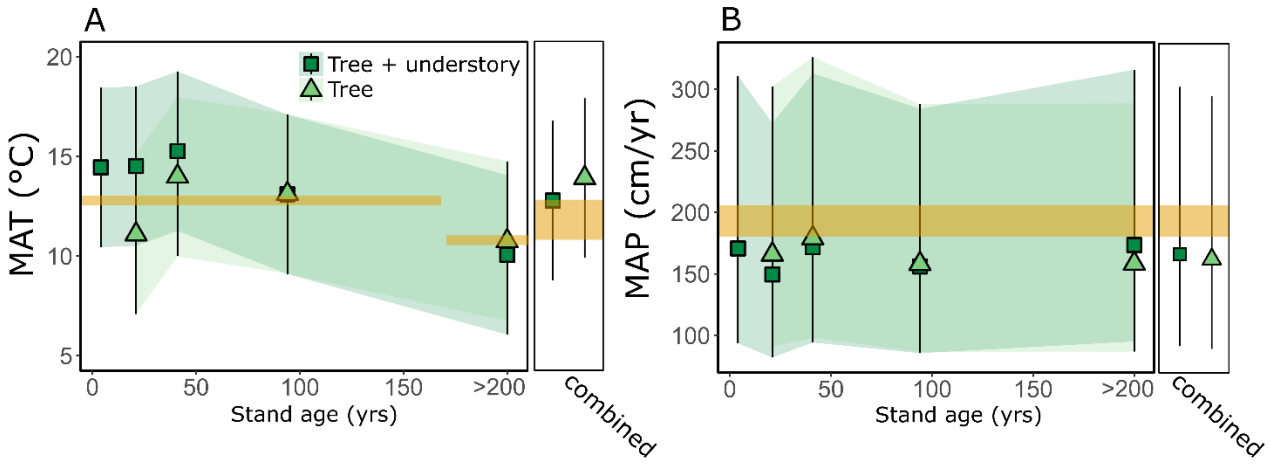

Chapter 3. Pacific Northwest plant community and climate response across global climatic events of the Miocene within a refined temporal framework.

Alexander J. Lowe[1,2], Richard Dillhoff[2], Thomas Dillhoff[2], Mark Schmitz[3], Christopher Schiller[2,4], William Rember[5], Patrick Fields[6], Tammo Reichgelt[7], Fransisco Nares[1,8], Caroline A.E. Strömberg[1,2]

[1]Department of Biology, University of Washington, Seattle, Washington, U.S.A.

[2]Burke Museum of Natural History and Culture, Seattle, Washington, U.S.A.

[3]Boise State University, Boise, ID, U.S.A.

[4]Pacific Lutheran University, Tacoma, WA, U.S.A.

[5]Department of Earth and Spatial Sciences, University of Idaho, Moscow, ID, U.S.A.

[6]Orma J. Smith Museum, College of Idaho, Caldwell, ID, U.S.A.

[7]Department of Earth Sciences, University of Connecticut, Storrs, CT, USA

[8]Department of Biology, University of Florida, Gainesville, FL, U.S.A.

Abstract

The Miocene is marked by two global events—warming of the Miocene Climatic Optimum (MCO) and cooling of the Middle Miocene Climatic Transition (MMCT)—that occurred in a relatively modern world. As such, the Miocene offers critical insights for our warming future. Regional records are key in arriving at such insights because global events manifest differently in varying locations. Twelve fossil plant sites in the Pacific Northwest (PNW; USA), were used to reconstruct a regional record of climate and vegetation across the MCO and MMCT. To do so, we provide new temporal constraints with U-Pb geochronology, unify and document parataxonomic frameworks, and combine three complimentary lines of evidence (macrofossils, palynomorphs, and phytoliths).

Our study shows that the PNW during the MCO had an average mean annual temperature (MAT) 3.7 °C warmer than modern, hosting mixed mesophytic closed canopy forests and lacking summer drought. Across the MMCT, winter temperatures decreased by 3.0 °C, as did the percentage of evergreen angiosperms. Annual temperatures and precipitation decreased in the interior Snake River Plain (SRP) but changes were tempered in the more coastal Puget lowland, reflecting continentality. Considerable morphotype turnover occurred in the SRP across the MMCT, but genera were a nested subset of earlier MCO floras, suggesting diversification or immigration within persistent genera. The number of exotic taxa (i.e., no longer native to the west coast) decreased in the SRP, reflecting a step in the modernization of PNW ecosystems, although several persist in the wetter and warmer Puget lowlands. Phytolith evidence and *Ephedra* pollen indicate some open-habitat vegetation in the SRP post-MMCT, consistent with regional drying. Global cooling during the MMCT, rather than regional uplift, seems the most likely driver of regional climate change based on published thermochronology and

paleobotanical evidence. These results shed light on the PNW in a world of elevated CO_2 and temperature consistent with high-end future predictions, and constrain important steps in its modernization.

Introduction

The Miocene epoch (23-5 Ma) presents a key period in modernization of ecosystems and climates, and offers important insights into plant community sensitivity and response to global climate change (e.g., Steinthorsdottir et al. 2021*b*). Global climatic events include Miocene Climatic Optimum (MCO) warming and Middle Miocene Climatic Transition (MMCT) cooling. The MCO was a 2.2 million year period (16.9-14.7 Ma) of sustained global warmth that interrupted a cooling trend over much of the Cenozoic (Flower and Kennett 1994; Zachos et al. 2008; Westerhold et al. 2020, Steinthorsdottir et al. 2021*b*; Holbourn et al. 2022). The MCO is marked by elevated ocean and terrestrial temperatures (Flower and Kennett 1994; Bruch et al. 2007; Goldner et al. 2014; Burls et al. 2021), likely elevated CO_2 levels (Ji et al. 2018; Super et al. 2018; Hönisch et al. 2023), a lower latitudinal temperature gradient (Wolfe 1981; Goldner et al. 2014), and pronounced Milankovitch-scale cyclicity in both $\delta^{18}O$ and $\delta^{13}C$ marine records (Woodruff and Savin 1991; Flower and Kennett 1994; Holbourn et al. 2007, 2014). The driver of the MCO is currently debated, but may involve release of CO_2 from the near concurrent eruption of the Columbia River Basalts and/or enhanced ocean crustal production and volcanic degassing rates (Kasbohm and Schoene 2018; Herbert et al. 2022; Tian and Buck 2022). Difficulty in identifying MCO drivers stems in part from its positive, rather than negative, carbon isotope excursion (the Monterey Excursion; Woodruff and Savin 1991; Holbourn et al. 2015) and the prolonged duration of both $\delta^{13}C$ and $\delta^{18}O$ excursions, suggesting complicated feedbacks within the global carbon cycle (Sosdian et al. 2020; Holbourn et al. 2022).

The MMCT (14.7 – 13.8 Ma) marks the termination of the MCO and complete glaciation of Antarctica following expansion of the east Antarctic ice sheet (Flower and Kennett 1994; Shevenell et al. 2008, Steinthorsdottir et al. 2021*b*). Ocean and terrestrial temperatures generally

cool across the MMCT (Mosbrugger et al. 2005; Shevenell et al. 2008; Herbert et al. 2022), along with a likely decrease in CO_2 (Badger et al. 2013; Ji et al. 2018; Super et al. 2018; Hönisch et al. 2023), increase in the latitudinal temperature gradient (Flower and Kennett 1994; Pound et al. 2012), and greater temperature seasonality, continentality, and terrestrial ecosystem heterogeneity (Wolfe 1981; Mosbrugger et al. 2005; Bruch et al. 2007, 2011; Pound et al. 2012; Bouchal et al. 2018). The drivers of the MMCT are also debated, but may relate to enhanced organic carbon burial and/or reduction in ocean production and volcanic degassing rates (Badger et al. 2013; Herbert et al. 2022). Climates continued to cool throughout the late Miocene and Pliocene, ushering in final stages in the establishment of many modern climate and ecosystem types (Herbert et al. 2016; Westerhold et al. 2020).

The MCO and MMCT occurred during a time when Earth's continental configuration and were relatively modern, compared to older well-studied global climatic events (e.g., the Paleocene-Eocene Thermal Maximum; McInerney and Wing 2011). If current reconstructions are correct, the MCO also marks the last time CO_2 was consistently higher than at present (Steinthorsdottir et al. 2021*a*; Hönisch et al. 2023). As such, the Miocene has been called the "future of the past" and offers critical insight for impacts of current and future climatic changes (Steinthorsdottir et al. 2021*b*). However, regional responses to global events in the past, and predicted for the future, are variable, particularly for precipitation (Pfahl et al. 2017; Harris et al. 2020; Botsyun et al. 2022; Pratap and Markonis 2022). Thus, regional-scale records are critical pieces for synthesizing an understanding of the response of the Earth system to past global climatic events that can inform our future.

The U.S. Pacific Northwest (PNW) encompasses the states of Washington (WA), Oregon (OR), and Idaho (ID), and hosts a suite of well-preserved fossil floras (Chaney and Axelrod

1959; Wolfe 1969; Graham 1999) that span the MCO and MMCT. Many were deposited in ancient lakes whose formation and preservation was influenced by prevalent regional volcanism (Reidel and Tolan 2013; Ebinghaus et al. 2020). Silicic volcanic centers in the ancestral Cascade Volcanic Chain of WA and OR, and along a time-progressive tract in the Snake River Plain initiating at the McDermitt Volcanic Field near the borders of Nevada, ID, and OR (Fig. 1), spread ash fall and flows across the PNW (Peck et al. 1964; Wood and Clemens 2002; Benson et al. 2017). In addition, the Columbia River Basalts (CRBs) erupted large volumes (~210,000 km^3) in the PNW over only 800,000 years (16.7-15.9 Ma; Fig. 1) (Reidel et al. 2013*a*; Kasbohm and Schoene 2018; Kasbohm et al. 2023). In addition to promoting the preservation of fossil floras, regional volcanism may have imparted significant disturbance and influenced plant community dynamics across Miocene (e.g., Taggart and Cross 1990; Ebinghaus et al. 2015; Schiller et al. 2024).

There is a long and rich history of study of PNW Neogene floras (Table 1), providing an important baseline understanding of regional plant community and climatic change (reviewed below). However, ecological and climatic inferences from these prior studies are limited by several factors relating to parataxonomic approaches, methods of ecology/climate inference, temporal constraints, and the isolated analysis of various fossil types. These are reviewed individually below.

Parataxonomy.—The taxonomic frameworks established by many earlier studies (e.g., Berry 1929; Brown 1937; Axelrod 1944, 1964; Chaney and Axelrod 1959), which relied heavily on fossil foliage, used an approach previous authors have termed “picture matching” (see discussion in Wolfe and Schorn 1990). In this approach, the primary objective was to match a fossil, or group of fossils, to an extant species, from which generic affinity was applied. In doing

so, considerations of trait variation within the genus and its diagnostic value are generally ignored. More recent work has emphasized the importance of the leaf morphotype as a fundamental unit for fossil foliage parataxonomy (i.e., classification based on "morphospecies"; Wilf 2008; Ellis et al. 2009). In this approach, emphasis is first placed on delimiting fossil morphotypes based on patterns of leaf morphology and venation architecture. Subsequent considerations of fossil taxonomy are then made with greater focus on taxonomic synapomorphies.

In addition, different researchers have published taxonomic frameworks at different PNW Neogene floras (e.g., Table 1), often with clashing ideologies on taxonomic approaches (e.g., Daniel Axelrod and Jack Wolfe; see Wolfe and Schorn 1990). Thus, comparison across these floras are subject to investigator bias. Lastly, assignments of taxonomic affinity and delineations of species were often accompanied by very little, if any, justification or discussion of confidence. In addition, fossil photographs figured in previous publications offer only limited detail of leaf architecture and were in many cases altered through subsequent re-drawing. Thus, reproducing or reassessing the (para)taxonomic frameworks from previous work, and results and conclusions drawn from them, is difficult, time-intensive, and expensive. This problem is made worse by the inclusion of several unpublished floras in regional scale analyses (e.g., Wolfe 1969, 1995). These points likely explain, at least in part, the limited number of site-level ecology and climates studies published over the last 50 years following up on earlier Neogene PNW floral studies.

Ecological and climatic inference.—Climatic and ecological analyses in previous work often relied on the ranges and ecology of extant species thought to best match morphologically with a fossil taxon (e.g., Chaney and Axelrod 1959). The reliability of such inferences are limited by large uncertainty to whether morphological similarities of leaves compared across 10^7 of

years, which were sometimes drawn superficially, reflects taxonomic similarity at the species level (e.g., Wilf 2008). In addition, such analyses assume limited evolution in ecological niches and climatic tolerances at the species-level and ignore the diversity of these preferences spanned across extant species within the applied generic of familial affinity. Lastly, many floras lack reliable census counts, and even when reported, they may be strongly influenced by collector's bias as a clear indication of the use of census collection methods (all identifiable specimens counted) is never stated. Inference of diversity is then typically based on raw richness, without quantitative standardization to sample size of sample completeness.

Temporal constraints.—Many sites were dated by previous studies using fossil plant biostratigraphic correlation, which has been shown in many cases to give erroneous results (Schorn et al. 2007). Several other sites were dated using K-Ar, a technique now known to be susceptible to undetected Ar loss leading to erroneous ages (Kelley 2002). To provide two examples, in the well-cited Cenozoic climate curve produced by Wolfe (1994, 1995), whose Neogene sites are all from the PNW, the only flora placed within the MCO (Cape Blanco flora; via plant biostratigraphy) was subsequently re-dated as early Miocene using more reliable 40Ar-39Ar methods (Emerson 2009), thus precluding interpretations of the MCO entirely. Second, the Alvord Creek fossil site of southeastern Oregon was assigned to middle Miocene (Fuller 1931), early Pliocene (Axelrod 1944), and then late Eocene (Wolfe and Tanai 1987) using plant biostratigraphy, a site now known to be latest Oligocene from new U-Pb dating (see results).

Disparate fossil plant types.—Many sites offer three complementary lines of palaeobotanical evidence—macrofossils (e.g., leaves, fruits, flower, cones, seeds), palynomorphs (pollen, spores), and phytoliths (microscopic silica bodies)—with potential to provide an integrated perspective of regional vegetation and habitat structure. However, previous work often

studied these fossil types in isolation, sometimes arriving at different conclusions which are difficult to reconcile given several potential explanatory factors, including differences in time, location, and biases introduced through each fossil type (Strömberg et al. 2018). In addition, the use of phytoliths in habitat reconstruction in the PNW Neogene is underexplored, limited to only two prior published studies (Dillhoff et al. 2014; Harris et al. 2017).

These limitations call for a reinvigoration of the PNW Neogene paleofloral record using updated approaches and methods. To do so, we study 12 well-preserved PNW fossil sites (Fig. 1) to provide well resolved and reproducible reconstructions of climate and ecology during this critical period in Earth history. The objectives of this study were to (1) revise the temporal framework utilizing silicic tuffs and high precision U-Pb dating, (2) build a digital macrofossil image library, (3) reconsider the macrofossil morphotype frameworks of each site while providing detailed discussion and justification of decisions made (e.g., in better alignment with FAIR principals; Wilkinson et al. 2016), (4) analyze fossil palynomorph and phytolith assemblages alongside macrofossils for an integrated perspective of local-regional vegetation and climate, (5) resample macrofossils using a census collection technique for more reliable inference of diversity and relative abundance, (6) precisely tie all samples into measured and described stratigraphic sections, and (7) incorporate recent and novel methods for climatic and ecological reconstructions.

Hypotheses

Climate.—We hypothesize that regional PNW climates changed in response to global changes at the MCO onset. These changes included an increase in winter and annual temperatures and annual precipitation, to values higher than those of modern PNW climates

(H1). During the MMCT, we hypothesize that annual and winter temperatures and annual precipitation decreased with stronger patterns of continentality (H2).

Vegetation.—Regional PNW vegetation changed in response to global changes at the MCO onset. These changes included an increase in plant diversity, the percentage of evergreen angiosperm species, the prevalence of "slow" leaf economic spectrum strategies, and the establishment of mixed mesophytic and closed canopy forests (H3). During the MMCT, we hypothesize that global cooling drove a reversal of this pattern, with compositional changes reflecting a decrease in the percentage of evergreen angiosperm species, a greater prevalence of "fast" leaf economic strategies, and increased prevalence of conifers, and that regional drying lead to more open habitat vegetation types (H4). We also hypothesize that the MMCT was an important step in the modernization of PNW plant communities and climates (H5).

Geologic and Chronologic Background

Oligocene to Miocene fossil plant localities of this study occur within depositional basins of the Western Cascades, Puget lowland, Columbia River Basalt Province, including the more northern Columbia Basin and more southern Oregon Plateau, and Snake River plain (Fig. 1). These regions mark distinct structural regimes, and themselves are comprised of smaller divisions of structural, depositional, and volcanic domains (Wood and Clemens 2002, Reidel et al. 2013*b*).

Western Cascades.—The middle Miocene Moose Mountain flora, also called the Cascadia flora, represents a single locality in the Western Cascades of Oregon (Fig. 1), a belt of Eocene-Miocene volcanic formations that filled a broad northward trending downwarp basin (Peck et al. 1964). Miocene volcanic rocks and minor sedimentary interbeds include the

following sequence (oldest to youngest): the Little Butte Volcanic Series, the CRBs (Grande Ronde and Wanapum members), and the Sardine Formation. The Moose Mountain site (USGS paleobot. loc. 9350) was mapped as part of the Little Butte Volcanic Series (Peck et al. 1964; with subsequent local revisions by Beaulieu et al. 1974; Walker and Duncan 1989). The Little Butte Volcanic Series interfingers with marine sandstones at the border of the Willamette Valley (Peck et al. 1964; Beaulieu et al. 1974), but the fossil site occurs further east and closer to mapped silicic vent structures (tuff, flows, and domes of dacite and rhyodacite; Fig. 1) and the inferred location of a north-trending volcanic chain (Peck et al. 1964). In fact, Miocene silicic vents are mapped immediately adjacent to the fossil site (Walker and Duncan 1989). Thus, considerable relief may have existed between these volcanic centers and the Miocene coastline, which occurred in modern Willamette valley.

The age of the site was originally reported as early Miocene (Wolfe 1962; Peck et al. 1964) then late Oligocene (Wolfe and Tanai 1987) based on its floral character. More recently, $^{40}Ar/^{39}Ar$ dates were reported from an interbedded tuff at the Moose Mountain site at 14.91 ± 0.23 Ma by Manchester et al. (2018). In this study, the same tuff dated by $^{40}Ar/^{39}Ar$ was resampled and dated by $^{206}Pb/^{238}U$ to provide more precise age constraints.

Puget Lowland.—The Puget lowlands occur west of the Cascade Range but east of the Olympic Range (Fig. 1) and represents a forearc basin of the (ancestral and modern) Cascade arc. The late Miocene Vasa Park flora, represented by a single locality, is exposed near the axis Seattle Fault Zone near Seattle, WA (Liberty and Pratt 2008), and is part of an unnamed sequence of Miocene tuffaceous and sedimentary rocks (Booth et al. 2012). As summarized by Dillhoff et al. (2014), the site is a 17 m thick section of matrix-supported pebble/cobble conglomerate, tuffaceous siltstone, sandy siltstone, and silty sandstones. The lithology and associated

sedimentary structures suggest deposition in high-energy braided streams, and associated flood plains, draining the ancestral Cascades. Fossil plants occur in both fine-grained laminated sandstone and mudstone, likely representing flood plain environments.

The fossil site was originally considered Quaternary in age due to the low degree of lithification, subsequent K-Ar dates were reported at 9.3-14.7 Ma, while most recently, an $^{40}Ar/^{39}Ar$ laser fusion date was reported at 11.40 ± 0.61 Ma (Booth et al. 2012).

Columbia Basin.—The Columbia Basin marks regions covered by Columbia River Basalt north of the Blue Mountains, including the eastern St. Maries and Clearwater embayments (sensu Reidel et al. 2013*b*; Fig. 1). While much of the central Columbia Basin, including the Palouse slope, would have likely been a broad and generally featureless plain, areas at the margins of the CRB show evidence of considerable paleo-relief (Reidel et al. 2013*b*). In these locations, CRBs and associated sedimentary deposits, overly structurally competent Precambrian granite and shist along a surface of varying elevation, and basement rocks often occur above CRBs without evidence for a post-depositional deformation cause (Pardee and Bryan 1926, Reidel et al. 2013*b*). It is in these more marginal locations that fossil sites of this study occur (Fig. 1).

Middle Miocene floras in the Columbia Basin include Spokane, Clarkia, and Juliaetta. All occur in the Latah Formation, which includes tuffaceous sedimentary deposits interbedded within flows of the Columbia River Basalts. Although the Latah Fm. was originally restricted to the Spokane River Watershed, in area of Spokane, WA (Pardee and Bryan 1926; Gray and Kittleman 1967), it is now recognized to include sedimentary interbeds further west (around Grand Coulee, WA) and in the St. Maries and Clearwater embayments of northern Idaho (Kirkham and Johnson 1929; Reidel and Tolan 2013).

The Spokane flora represents several sub-localities near Spokane, WA (Fig. 1), many which are no longer accessible due to urban development. We restricted our study to those closest to Spokane, excluding Cour D'Alene, Mica, and Vera. The Spokane flora was thought to be deposited in lowlands containing lakes and swamps, fed by streams sourced from nearby mountains to the west (Pardee and Bryan 1926; Griggs 1976).

Early work on basalt stratigraphy in the Spokane area was done by Pardee and Bryan (1926), but has been subsequently revised (Griggs 1976; Joseph 1990). As revised, most of the Latah Fm. near Spokane occurs between Grande Ronde and Wanapum members, although at the Deep Creek sub-locality, the exposed Latah Fm. is interbedded within Grande Ronde N_2 (Joseph 1990). The oldest Grande Ronde date comes from the Wapshilla Ridge Member (Kasbohm and Schoene 2018), which was the first Grande Ronde flow to enter the Spokane region (Reidel et al. 2013*c*), and stratigraphically underlies the Grande Ronde N_2, which is most widespread unit in the Spokane region (Joseph 1990, Reidel et al. 2013*c*). Thus, we consider the Latah flora to be well bracketed between the age of the upper Wapshilla Ridge Member at 16.254 ± 0.034 Ma and the upper boundary of the Wanapum basalts, at 15.895 ± 0.019 Ma (Kasbohm and Schoene 2018).

The Clarkia flora represents several sub-localities near Clarkia, ID (Fig. 1). We restricted our study to the most well-sampled and correlated P33 and P37 sub-localities. Fossil plants occur in well-laminated lacustrine shales throughout much of the exposed stratigraphy at both sub-localities (Smiley and Rember 1985*a*). It is thought that the ancient lake was dammed by the Priest Rapids flow (Wanapum Member of the CRBs), whose localized outcrops showcase pillow structures indicating deposition in water (Smiley and Rember 1985*b*). The modern topography is defined by resistant hills of Precambrian schist rising above, but stratigraphically underlying the

Latah Fm., suggesting considerable relief at the time of its deposition (Smiley and Rember 1985*b*).

The P37 and P33 sub-localities are tied into a common depth scale through coring at the Emerald Creek site, and glass major and trace element tephrostratigraphic correlation (Ladderud et al., 2015; Geraghty, 2017). A single tuff (Unit 5B of Yang et al., 1995) from the P33 has been recently dated by CA-IDTIMS U-Pb geochronology at 15.780 ± 0.035 Ma (single youngest zircon) by Höfig et al. (2020). We provide U-Pb dates from both P33 to P37 to constrain deposition of the entire lacustrine sequence.

Lastly, the Jualietta flora, also known as Potlatch Creek flora (i.e., Station 24 of Kirkham and Johnson 1929; Kvaček et al. 2000) is represented by a single locality near Juliaetta, Idaho (Fig. 1). It is interbedded within Grande Ronde basalts (Pine Creek interbeds of Bond 1963) at the north end of Clearwater Embayment. Basalt interbeds in this embayment record a lowland of swamps, lakes, and rivers whose outlet was likely dammed along the northeastern front of the basalt field (Bond 1963; Ebinghaus et al. 2020). Prior work has suggested considerable relief of the pre-depositional surface in the Clearwater embayment (Bond 1963 and references therein).

The Juliaetta site is characterized by poorly-moderately laminated siltstone overlain by ~18 m of massive sandstone. Royer et al. (2003) interpret the site as a deltaic deposit, but no inclined foresets were observed in our investigation. The upward transition to sandstone may then represent the progradation of a delta front or the shallowing of the lake. A large basalt lobe occurs near the middle of the outcrop and is surrounded by sedimentary rocks (Appendix 1). We suggest this represents an invasive subaerial basalt lobe which burrowed into the unconsolidated lake sediments upon entering the lake (e.g., Schmincke 1967; Camp 1981; Ebinghaus et al.

2020). Many signs of soft sediment deformation are associated with the basalt lobe, likely resulting from its emplacement (Appendix 1).

The site is interbedded locally within Grande Ronde R_1 member (Lewis et al. 2005), constraining the age between $^{206}Pb/^{238}U$ of the underlying Imnaha at 16.572 ± 0.018 and the overlying Wapshilla Ridge Member (Grande Ronde) at 16.288 ± 0.039, although we provide a more precise U-Pb date directly from the site.

Blue Mountains.—The Blue Mountains separate the Columbia Basin to the North and the Oregon Plateau to the south (Fig. 1), and represent a highly deformed anticlinorium involving a diverse suite of volcanic and sedimentary rocks (Walker 1990, Reidel et al. 2013*b*). Deformation initiated during the middle Oligocene, creating a barrier to sediment and tuff distribution at its northwestern front, shown by distinct eastern and western facies of the Oligocene John Day Formation (Robinson et al. 1984), and by distribution patterns of the CRBs (Reidel et al. 2013*b*, *a*). The northwestern front may have also acted as a barrier to atmospheric moisture, leading to decreased rainfall on the eastern leeward side (Kukla et al. 2021). In contrast, uplift along the eastern portion of the Blue Mountains, including the Wallowa Mountains mostly postdated the CRB eruptions (Reidel and Tolan 2013; Schoettle-Greene et al. 2022). The Blue Mountains host the eruptive site (Monument dike swarm) of the Picture Gorge Basalt member of the CRBs (Cahoon et al. 2023).

The Mascall flora is comprised of several sub-localities near Dayville, OR (Fig. 1), none of which were excluded from this study. The Mascall Formation overlies the Picture Gorge Basalts and is subdivided into Lower, Middle, and Upper members (Bestland et al., 2008). In the Mascall Fm. type area, the Mascall tuff divides the lower and middle members and dated by $^{206}Pb/^{238}U$ at 15.122 ± 0.017 Ma (Maguire et al. 2018). Silicic tuffaceous interbeds in the Mascall

Fm., including the Mascall tuff, are thought to be distally sourced, potentially from the ancestral Cascades or McDermitt volcanic field (Smith et al. 1989; Bestland et al. 2008). There is a rarity of basalt fragments in the Mascall Formation, which may suggest rivers traversed a low relief landscape leeward of the Blue Mountain uplift front, dominated by internal reworking of floodplain soils and ash, rather than prominent erosion of the pre-Mascall basaltic surface (Bestland et al. 2008).

The White Hills and Riverbank/Van Horn's Ranch sub-localities were historically most heavily collected and occur ~25 km east of the Mascall Formation type area. Discontinuous exposures and a lack a key marker beds makes direct correlation of these two areas difficult (Chaney and Axelrod 1959; Bestland et al. 2008). The fossil plant sub-localities, comprised largely of diatomite and lignite, are placed in the lower member as similar lithologies occur only in the lower member in the type area (Bestland et al. 2008). New U-Pb dates are provided at White Hills to more reliably correlate it with the geochronological framework of the Mascall Fm. type area.

Oregon Plateau.—The Oregon Plateau hosts the late Oligocene Alvord Creek flora and the middle Miocene Watersnake flora (part of the Succor Creek flora) of this study (Fig. 1). The Alvord Creek flora is comprised of two sub-localities, South Fork and Scarp (equivalent to 601 and 601N of Axelrod 1944, respectively), part of the Alvord Creek Formation and within a greater sequence of sedimentary and volcanic sequence exposed in Steens Mountain. This sequence is as follows (oldest to youngest): the Alvord Creek Fm., the Pike Creek Fm., the Steens Mountain Volcanics, and the Steens Basalt (Fuller 1931; Walker and Repenning 1965, Minor et al. 1987*c*). Fossil plants occur within moderately- to well-laminated lacustrine shales. Axelrod (1944) reports evidence for regional signs of volcanic centers at the time of deposition,

but suggests the prevalence of fine-grained deposits indicates they occurred at considerable distance to depositional lake basin.

There have been several conflicting reports of age based on plant biostratigraphy, including “Mascall age” (i.e., middle Miocene; Fuller 1931; MacGinitie 1933), lower Pliocene (late Miocene by current standards; Axelrod 1944) and late Eocene (Wolfe and Tanai 1987). K-Ar dates were reported by Evernden and James (1964) from an overlying basalt at 21.3 Ma (early Miocene). New U-Pb dates are provided in this study to reconcile these widely varying reports.

The middle Miocene Trout Creek flora consists of four sub-localities spanning only ~200 m lateral distance, although the “West Quarry” was the most heavily collected by previous work (Graham 1965). The flora is part of the Trout Creek Formation, a ~140 m thick fluvio-lacustrine sequence in the northern McDermitt volcanic field (Fig. 1) as was dated by K-Ar at 13.1 Ma (Evernden and James 1964). The plant macrofossils occur within well-laminated diatomite.

After floral monographs were published for Trout Creek flora (MacGinitie 1933; Chaney and Axelrod 1959; Graham 1965), the Trout Creek Fm. was shown to represent lacustrine in-fill of the ~13 x 12 km Whitehorse Caldera (Rytuba et al. 1981; Barrow 1983; Benson et al. 2017), which formed following eruption of the Tuff of Whitehorse Creek at 15.556 ± 0.019 Ma (Benson et al. 2017) whose maximum thickness was ~100 m (Rytuba et al. 1981; Rytuba and McKee 1984; Benson et al. 2017). Subsequent rhyolitic lavas and dome eruptions occured along the caldera margins from 15.464 to 15.369 Ma (Rytuba et al. 1981; Benson et al. 2017). The eruption of the Tuff of Whitehorse Creek occurred on a landscape impacted by both earlier silicic eruptions of the McDermitt volcanic field (Benson et al. 2017), and the Steens Basalt (CRB), which erupted from a source only ~50 km to the northwest ~1 million years prior (Kasbohm and

Schoene 2018). In this study, we provide U-Pb radiometric dates for the Trout Creek flora (Table 1) to refine the age of intra-caldera deposition.

The middle Miocene Succor Creek flora is comprised of ~100 sub localities along the central Oregon-Idaho border (Fields 1996). To focus the scope and spatio-temporal resolution, we incorporate only the Watersnake sub-locality in the South Bend Area (Fig. 1; Fields 1996). The sub-locality comprises 68 m of fluvio-lacustrine deposits interbedded with two thick rhyolite ash flow tuffs (Schiller et al. 2024). Fossils occur in the lower 10 m of the section (WS Zone 1 of Schiller et al. 2024), in lacustrine sequence of well laminated shales and massive sandstones. The Succor Creek flora at large occurs within the Sucker Creek Formation (Kittleman et al. 1965) which was deposited along the eastern and northeastern margin of the Lake Owyhee Volcanic Field (Rytuba et al. 1991; Benson and Mahood 2016). This area occurs near the transition of the Oregon Plateau and the western Snake River Plain (Fig. 1; Reidel et al. 2013*b*).

Deposition of the Succor Creek Formation occurred both before and after nearby caldera eruptions. Reports are made of either two tuffs from two separate caldera sources, i.e., the tuff of Leslie Gulch and tuff of Spring Creek from the Mahogany Mountain and Three Fingers calderas, respectively (e.g., Rytuba et al. 1991; Ferns et al. 2017), or a single tuff and caldera, i.e., the tuff of Leslie Gulch from the Rooster Comb Caldera, whose eruption is dated by $^{40}Ar/^{39}Ar$ at 15.8 Ma (Benson and Mahood 2016). In either case, the closest caldera margin is inferred only ~20 km northwest of the Watersnake site (Fig. 1). The Succor Creek Formation also occurs along the eastern margin of the Oregon-Idaho graben, that began subsiding at 15.5 Ma (Cummings et al. 2000). New U-Pb dates reported in Schiller et al. (2024) show deposition of the fossil plants of the Watersnake sub locality occurred at 15.546 ± 0.018 Ma (Table 2), and deposition of the Sucker Creek Formation at large occurred, at a minimum, from 15.782 – 14.799 Ma,

demonstrating complex interplays with local volcanism and graben-based subsidence. Lacustrine sedimentation at 15.546 Ma challenges the prior claim that the eruption of the Tuff of Leslie Gulch at 15.81 Ma drove a change from lacustrine to fluvial environments (Benson et al. 2017).

Snake River Plain.—The Snake River Plain (SRP) is currently divided into eastern and western segments (Fig. 1), each with a unique structural regime. The western SRP is interpreted as a fault-bounded rift basin, while the eastern SRP a structural downwarp (Wood and Clemens 2002). During the late Miocene (~11 Ma), volcanism prevalent in the Owhyee and McDermitt volcanic fields of Oregon and Nevada waned, with silicic volcanism was mainly restricted to the Bruneau-Jarbidge region at the margin of the western Snake River Plain (Fig. 1; Wood and Clemens 2002). While rhyolite flows and domes occur near the western Snake River Plain margin, they do not form thick accumulations within its center, suggesting the plain may have been higher than the surrounding margins (Wood and Clemens 2002).

The late Miocene Pickett Creek flora consists of two sub localities only a few hundred meters apart, and is placed within the Chalk Hills Formation (Buechler et al. 2007), an early stage of sedimentation of relatively thin packages along margins of the western Snake River plain (Wood and Clemens 2002). The Pickett Creek site is comprised of moderately- to well-laminated lacustrine diatomite with fairly thin tuffaceous interbeds (Buechler et al. 2007). Mapping of shoreline features and lake sediments suggests the ancient lake was 2-4 km^2 and the shoreline at the current elevation of 1250-1280 m (Buechler et al. 2007). An age of 8.5-10.5 Ma was reported for the Pickett Creek site using tephrachornologic correlations of volcanic glass to tuffs of the Twin Falls region (Buechler et al. 2007). We provide a new U-Pb date to refine this age constraint.

The Late Miocene Trapper Creek flora was collected from a single main locality and occurs at the southern margin of the eastern Snake River Plain and northern margin of the Basin and Range province (Fig. 1). In this region, a fairly thick section (400-900 m) of Neogene tuffaceous sedimentary deposits occur within the Goose Creek Basin (Axelrod 1964; Perkins et al. 1995). The flora occurs in moderately-laminated siltstones and associated tuffs of the lowest unit, the Beaverdam Formation (Axelrod 1964). This formation is overlain by the Tuff of Ibex Peak, whose lower contact is exposed at the Trapper Creek site, which is overlain by the Cassia Formation (Axelrod 1964; Perkins et al. 1995; Knott et al. 2016). Tuff interbedded within the Beaverdam Formation, and making up the Tuff of Ibex Peak, were likely sourced from silicic eruptions of the Bruneau-Jarbridge volcanic field, whose center was ~130 km northwest of Trapper Creek (Fig. 1; Perkins et al. 1995; Sarna-Wojcicki et al. 2023). This includes the widespread Ibex Hollow tuff, within the Tuff of Ibex Peak, which is thought to have dispersed across an area of ~2.7 million km^2, from North Dakota to Baja, Mexico (Sarna-Wojcicki et al. 2023).

The presence of well sorted pebble to small-sized cobble conglomerate in the Beaverhead Fm. suggested to Axelrod (1964) that relatively broad streams drained a well-dissected topography. However, the Cassia Hills, which currently border the Goose Creek Basin to the west, were likely of low relief during the Miocene (Axelrod 1964), and the drainage direction was likely instead to the south (Perkins et al. 1995 and references therein). $^{40}Ar/^{39}Ar$ ages reported by Perkins et al. (1995) bracketed the fossil site, which occurs in the upper 10 meters of the Beaverdam Formation, and constrained the age between 12.82 ± 0.04 (TC89-20A) and 11.81 ± 0.03 (TC89-21B). When updated to a Fish Canyon Tuff sanidine (FCs) fluence monitor age of 28.021 Ma, these ages are recalculated to 13.09 ± 0.08 and 12.06 ± 0.08 Ma. We note this

recalculations differ slightly from those reported in Sarna-Wojcicki et al. (2023), likely a result of different assigned Fish Canyon Tuff sanidine monitor ages. In this study, we provide a new U-Pb date for Tuff of Ibex Peak, 40 cm above its contact with the Beaverdam, to better constrain deposition of the fossil assemblage.

Review of prior work on Miocene terrestrial ecosystem and climatic response

Two events during the Oligocene to early Miocene set the scene for middle and late Miocene North American environments. The first was the Eocene-Oligocene transition, marking a shift from "warmhouse" to "coolhouse" conditions, with drops in global temperatures, increased temperature seasonality, and the establishment of temperate deciduous biomes in lowlands of western North America (Meyer and Manchester 1997). The second was increased continentality during the late Oligocene to early Miocene, with expansion of open habitat grasslands in the Great Plains region (Strömberg 2005), potentially driven by decreasing winter precipitation (Kukla et al. 2022), while closed forests dominated much of the western US (Peck et al. 1964; Wolfe 1981).

The MCO.—Global floral records generally record considerable changes in plant communities and climate across the MCO onset. For example, taxa typical of warmer and less seasonal climates today (e.g., laurophyllous taxa), increase in abundance across southern and central Europe (Mosbrugger et al. 2005, Utescher et al. 2007*a*), and phytolith evidence from Patagonia suggest expansion of more closed canopy forests (Dunn et al. 2015). During the MCO, low latitudinal temperature gradients promoted the establishment of relatively warmer vegetation types at high latitudes, including woody tundra (e.g., *Nothofagus,* Podocarpaceae) and relatively thermophilic fungi on Antarctica (Lewis et al. 2008; Warny et al. 2009; Pilie et al. 2023), and

mixed deciduous forests at high latitudes of the Northern Hemisphere where boreal forest exists today (White et al. 1997; Williams et al. 2008; Pound et al. 2012).

In the PNW, reports of vegetation and climatic change are mixed. Wolfe (1969) reports little change in taxonomic composition across the MCO onset, with persistent mixed mesophytic forests—a forest type reported by several additional authors in PNW lowlands during the MCO (Chaney and Axelrod 1959; Graham 1965, Smiley and Rember 1985*a*). Despite stable floral composition, Wolfe (1969) reports an increasing proportion of entire-margined species (Wolfe 1969). In fact, leaf physiognomic changes from the PNW were some of the earliest evidence for recognizing the MCO as global climatic event (Wolfe and Hopkins 1967). Phytolith evidence from the Idaho/Montana border instead suggests minimal change across the MCO onset, with persistent mixed grassland and open woodlands in semi-arid, seasonal, and warm climates (Harris et al. 2017, 2020). Arid climates are known elsewhere during the MCO including southern California (Smiley et al. 2018). Volcanic disturbance during the MCO has also been suggested as an important driver of plant community change, potentially masking global climatic influences (Taggart and Cross 1990; Schiller et al. 2024).

Quantitative precipitation reconstructions across the MCO in the PNW are limited. Using the $\delta^{13}C$ of fossil equid enamel, Drewicz and Kohn (2018) reconstructed variable precipitation during the MCO, peaking at the Mascall site, but anomalously low at other MCO sites (e.g., Succor Creek at ~20-30 cm/yr), inconsistent with most paleobotanical evidence (Graham 1965; Fields 1996; Schiller et al. 2024). Evidence from paleosols also suggested peaked, but variable precipitation within the MCO (Retallack 2007). Paleoclimate models suggest a positive relationship between pCO_2 and PNW precipitation, with precipitation higher than modern during MCO (Krapp and Jungclaus 2011).

The MMCT.—Considerable changes in plant communities and climate across the MMCT are recorded in several flora around the globe. For example, boreal forests replaced mixed deciduous forest above 60° N (Pound et al. 2012), and high latitude migration pathways between North America, Asia, and Europe were likely restricted, potentially initiating genetic divergence among modern disjunct taxa (Manchester 1999; Wen 1999; Chen et al. 2018). Subtropical and warm temperate biomes were restricted globally (Utescher et al. 2007*b*; Pound et al. 2012). Taxa typical of cooler and more seasonal climates today became more prevalent, with broadleaf deciduous forests replacing mixed mesophytic forest throughout much of western and southwestern Eurasia (Mosbrugger et al. 2005; Syabryaj et al. 2007, Utescher et al. 2007*a*, *b*; Bruch et al. 2011; Kayseri-Özer 2017; Kovar-Eder et al. 2021). In Patagonia, MCO regreening was reversed, as open forests and shrublands replaced closed canopy forests (Dunn et al. 2015).

In the PNW, many taxa of the MCO mixed mesophytic forests became regionally extinct, and the taxonomic composition became more modern-like, consistent with both a cooling and drying climate (Wolfe 1981; Axelrod 1992; Axelrod and Schorn 1994)—although exotic taxa (i.e., those that no longer grow in the PNW) sensitive to drought persist in several PNW floras (Smiley 1963; Mustoe and Leopold 2014). A decrease in the proportion of entire-margined species, consistent with decreased annual temperatures, (Wolfe 1969, 1995), along with greater spatial heterogeneity in floras (i.e., floristic provincialism) characterize the western US (Wolfe 1981). Volcanic disturbance may have continued to play an important role. Ebinghaus et al. (2015) found plant community changes across the MMCT were best explained by volcanic disturbance from ash fall, than changes in global climate.

Materials and Methods

Field Work and Sampling

All floras were referenced or published in prior work (Table 1). Field work was carried out at all sites of this study except Fossil High School (HS) and Vasa Park where new sampling was not required. Field work involved relocating sections described and sampled by previous work, sampling rocks for subsequent pollen and phytolith extraction, tuff or tuffaceous rocks for radiometric dating, and plant macrofossils (e.g., leaves, fruits, flowers, cones, seeds), and placing them within a newly described and measured (correcting for dip) stratigraphic section. To permit reliable inference of diversity and relative abundance, macrofossil census collections were made when possible, accounting for all specimens preserved sufficiently enough to be assigned to fossil morphotypes (e.g., Lowe et al. 2018). Specimens encompassed in such census counts include those collected, those photographed in the field and not collected, and those simply tallied in the field. At several sites census collections were not possible because, for example, productive horizons were no longer present, or were not a priority given reliable counts published in previous work. Additional detail regarding field work is included in Appendix 1.

U-Pb Dating

Sample preparation.—Zircon crystals were separated from approximately 1 kg of tuff sample by a combination of crushing, milling, ultrasonic vortical washing removal of clays (Hoke et al. 2014), and water shaking table concentration, followed by conventional heavy liquid and magnetic methods. A selection of hand-picked zircon crystals were placed in a muffle furnace at 900°C for 60 hours in quartz beakers to anneal minor radiation damage; annealing enhances cathodoluminescence (CL) emission (Nasdala et al. 2002), promotes more reproducible interelement fractionation during laser ablation inductively coupled plasma mass spectrometry

(LA-ICPMS) (Allen and Campbell 2012), and prepares the crystals for subsequent chemical abrasion isotope dilution thermal ionization mass spectrometry (CA-IDTIMS) (Mattinson 2005). Following annealing, individual grains were hand-picked and mounted, polished and imaged on a Hitachi TM4000PlusII table-top scanning electron microscope outfitted with a low vacuum secondary electron (SE) - cathodoluminescence (CL) UVD detector. From these compiled images, the location of spot analyses for LA-ICPMS or single grain CA-IDTIMS were selected.

LA-ICPMS analysis.—LA-ICPMS analysis utilized a ThermoFisher Scientific iCAP RQ quadrupole inductively coupled plasma mass spectrometer coupled to a Teledyne Photon Machines Analyte Excite+ 193 nm excimer laser ablation system. In-house analytical protocols, standard materials, and data reduction software were used for acquisition and calibration of U-Pb dates and a suite of high field strength elements (HFSE) and rare earth elements (REE). Zircon was ablated with a laser spot of 20 μm wide using fluence and pulse rates of ~2 J/cm^2 and 10 Hz, during a 35 second analysis (15 sec gas blank, 20 sec ablation) that excavated a pit ~10 μm deep. Ablated material was carried by a combined 1.2 L/min He gas stream from the two-volume ablation cell to the nebulizer flow of the plasma. Quadrupole dwell times were: 2 ms for ^{89}Y, ^{91}Zr, ^{177}Hf; 10 ms for ^{29}Si ^{139}La, ^{141}Pr, ^{202}Hg, ^{204}Pb, ^{232}Th, and ^{238}U; 100 ms for ^{49}Ti; 60 ms for ^{207}Pb, 40 ms for ^{206}Pb, 20 ms for ^{208}Pb, and 5 ms for all other REE, ^{93}Nb, ^{181}Ta, and ^{31}P; total sweep duration is 371 ms. Background count rates for each analyte were obtained prior to each spot analysis and subtracted from the raw count rate for each analyte.

For concentration calculations, background-subtracted count rates for each analyte were internally normalized to ^{29}Si and calibrated with respect to NIST SRM-610 and -612 glasses as the primary standards. Ablations pits that appear to have intersected glass or mineral inclusions were identified based on Ti and P signal excursions, and associated sweeps were generally

discarded. U-Pb dates from these analyses are considered valid if the U-Pb ratios appear to have been unaffected by the inclusions. Signals at mass 204 were normally indistinguishable from zero following subtraction of mercury backgrounds measured during the gas blank (<100 cps ^{202}Hg), and thus dates are reported without common Pb correction. Rare analyses that appear contaminated by common Pb were rejected.

For U-Pb and $^{207}Pb/^{206}Pb$ dates, instrumental fractionation of the background-subtracted ratios was corrected and dates were calibrated with respect to interspersed measurements of zircon standards and reference materials. The primary standard Plešovice zircon (Sláma et al. 2008) was used to monitor time-dependent instrumental fractionation based on two analyses for every 10 analyses of unknown zircon. A polynomial fit to the primary standard analyses versus time yields each sample-specific fractionation factor. A secondary bias correction of generally less than 2% may be subsequently applied to unknowns on the basis of the residual age bias as a linear function of radiogenic Pb count rate in standard materials including Seiland, Zirconia, and Plesovice zircon, or similar materials of known age and variable Pb content. Radiogenic isotope ratio and age error propagation for all analyses includes uncertainty contributions from counting statistics and background subtraction. Ages are reported with and without uncertainties from the standard calibrations propagated into the errors on each date. These calibration uncertainties are the local standard deviations of the polynomial fits to the interspersed primary standard measurements versus time for the time-dependent, relatively larger U/Pb fractionation factor, and the standard errors of the means of the consistently time-invariant and smaller $^{207}Pb/^{206}Pb$ fractionation factor. Method metadata and sample data are reported using the community standards of Horstwood et al. (2016), and additional details of methodology and reproducibility are reported in Macdonald et al. (2018).

ID-TIMS analysis.—Zircon crystals selected on the basis of CL zoning and LA-ICPMS spot analysis were removed from the expoxy mounts, and subjected to a modified version of the chemical abrasion method of Mattinson (2005), whereby single crystals were partially dissolved in a single step with concentrated hydrofluoric acid at 190°C for 12 hours. After rinsing and ultrasonication, residual crystals were spiked with the BSU-1B mixed ^{205}Pb-^{233}U-^{235}U tracer solution calibrated against EARTHTIME gravimetric standards (Condon et al. 2015), fully dissolved in concentrated hydrofluoric acid at 220° for 48 hours, dried and redissolved in 6M hydrochloric acid at 180° for 12 hours. U and Pb were purified by anion exchange chromatography (Krogh 1973), eluted together and loaded on a single zone-refined rhenium filament with a mixed silica gel and dilute phosphoric acid solution for mass spectrometry (Gerstenberger and Haase 1997). U-Pb geochronology methods for isotope dilution thermal ionization mass spectrometry (ID-TIMS) follow those reported in Macdonald et al. (2018). Pb and U isotope ratios were measured on an IsotopX Isoprobe-T thermal ionization mass spectrometer by single collector peak jumping on a Daly conversion dynode ion-counting detector (Pb^+) or static multicollection on Faraday cups fitted with 10^{12} W resistor amplifiers (UO_2^+).

U-Pb dates and uncertainties for each analysis were calculated using the algorithms of Schmitz and Schoene (2007), the U decay constants of Jaffey et al. (1971), and the ^{238}U/^{235}U ratio of Hiess et al. (2012). Propagated uncertainties are based upon non-systematic analytical errors, including counting statistics, instrumental fractionation, tracer subtraction, and blank subtraction. Uncertainties for sample weighted mean dates are reported in the text and tables at the 95% confidence interval (c.i.), which is the internal error expanded by the square root of the MSWD (mean square of weighted deviations), Wendt and Carl (1991) and the Student's t

multiplier for n-1 degrees of freedom (Ludwig 2003). These error estimates should be considered when comparing our $^{206}Pb/^{238}U$ dates with those from other laboratories that used tracer solutions calibrated against the EARTHTIME gravimetric standards. When comparing our dates with those derived from other decay schemes (e.g., $^{40}Ar/^{39}Ar$, ^{187}Re-^{187}Os), the uncertainties in tracer calibration (0.03%; Condon et al., 2015; McLean et al., 2015) and U decay constants and natural isotopic ratio (Jaffey et al. 1971; Hiess et al. 2012) should be added to the internal error in quadrature. Quoted errors for calculated weighted means are thus of the form ±X(Y)[Z], where X is solely analytical uncertainty, Y is the combined analytical and tracer uncertainty, and Z is the total analytical, tracer and decay constant uncertainty.

Macrofossils

Macrofossils were included from both prior and new collections. New collections included census and taxonomic (non-census) collections. Prior collections included those housed at the Burke Museum of Natural History and Culture (UWBM), University of California Museum of Paleontology (UCMP), Smithsonian National Museum of Natural History (NMNH), University of Michigan Museum of Paleontology (UMMP), Orma J. Smith Museum at the College of Idaho (OJSM), Florida Museum of Natural History (UF), and in private collections of Robert Rosé. Fossil specimens were photographed in high resolution, and in many cases, fine detail of leaf architecture (e.g., minor veins) were imaged under a stereoscope. In addition to digitizing type material, we digitized non-type specimens including many that were un-cataloged in museum collections, to better represent variation beyond the type material and incorporate potential hidden diversity. Uncataloged specimens were assigned unique image IDs.

We established a unified macrofossil morphotype framework using our digital library. This framework was carefully built from prior monographs (Table 1) and subsequent revisions,

but morphotype delineations within sites, assignments of taxonomic affinity, and synonymy of fossil morphotypes across sites for all prior established taxa were re-considered and, in many cases, revised. Our emphasis was unifying morphotype delineation frameworks and approaches to ascribing taxonomic affinity, not formal taxonomy and nomenclature—thus, revisions do not constitute formal taxonomic nomenclatural changes. In our approach, morphotype delineations within sites were considered first by analyzing aspects of vegetative and reproductive morphology and foliar venation architecture (e.g., Ellis et al. 2009). Each morphotype was assigned a unique site-specific number. Then we considered taxonomic affinity, which, if assigned, feed back into inferences of morphotype delineation by considering intraspecific variation within extant members of the taxon. Morphotypes were left without affinity in several cases. Lastly, morphotypes were compared across sites of this study and synonymy was drawn where characters strongly overlap. Synonymy was applied using either an established epithet, if we think our concept agrees well with that previously published, or an arbitrary study morphotype name when it departs or no taxonomic affinity was applied (e.g., Fabaceae foliage M1, entire foliage M8). We take a conservative "hypothesis-testing" approach, with specimens considered to represent the same morphotype (e.g., null hypothesis) unless sufficient evidence supports their separation (e.g., alternative hypothesis).

The morphotype framework is represented in a custom FileMaker Pro database. Justifications were explicitly discussed for all morphotype delineations, assignments of taxonomic affinity, and morphotype synonymies in the database, or in supplemental files, to ameliorate the limited documentation in many previous studies. To better represent uncertainty inherent in many assignments of taxonomic affinity, particularly for fossil foliage (e.g., Wilf 2008), and explore its impacts on downstream analyses, we established a confidence scoring

system (see Appendix 2 for additional detail). A score of high confidence (1), medium confidence (2), or low confidence (3) was first assigned to each macrofossil morphotype in isolation (i.e., considering the single organ at the single site) considering traits that are consistent and/or diagnostic of the taxa, and if they had been studied in detail by previous work. Confidence was considered for the finest taxonomic rank applied among family, subfamily, or genus. The confidence score was then increased (score decreased by 1) if additional organs with higher confidence (i.e., pollen or reproductive organs) occurred at the same site for the same taxon. Lastly, confidence scores were adjusted according to morphotype synonymy. All morphotypes held in synonymy were assigned the highest confidence (lowest score) found across that synonymy. Confidence score adjustments were applied using R (version 4.3.2; R Core Team 2023) to ensure consistency and reproducibility (final confidence scores listed in Appendix 4).

We utilized many resources for establishing the morphotype framework and the workflow described above, including previous monographs on sites of this study (Table 1), detailed taxonomic studies involving sites and material of this study (e.g., Smiley and Huggins 1981; Edwards 1983; Manchester 1987, 1999; Wolfe and Tanai 1987; Baghai 1988; Manchester and Donoghue 1995; Fields 1996; Erwin and Schorn 2000; Kvaček and Rember 2007; Buechler 2008; Burge and Manchester 2008; Smith and Manchester 2019; Huegele et al. 2020; Latchaw and Manchester 2024), taxonomic studies of other Cenozoic sites in North America and beyond (e.g., Buzek 1971; Hummel 1983; Hill 1986; Wolfe and Schorn 1990; Kvaček 1999; Sakala 2000; Denk and Meller 2001; Kunzmann et al. 2009; Xing et al. 2013; Jud et al. 2021), modern cleared leaf collections (Wilf et al. 2021, particularly the National Museum of Nature and Science, Tokyo, online collection), modern herbaria (e.g., The Smithsonian US National

Herbarium), and taxonomic studies of modern taxa (e.g., Meyerhoff 1952; Merrill 1978; Farjon 1990, 2005; Andrés-Hernández and Terrazas 2009), among others.

Palynology

In addition to new samples collected from our field work, a rock sample was provided from Fossil High School (HS) of the Bridge Creek flora, from the dark shale horizon exposed high in the exposed section, as discussed in Meyer and Manchester (1997), by Dr. Steve Manchester (U. of Florida). Prepared palynological slides were provided from Moose Mountain by Robert Rosé, collected from ~2.3 m below the productive leaf layer (Appendix 3).

New rock samples were prepared for palynomorph analysis following the Faegri-Iverson method (Faegrie and Iverson 1964). The samples were washed, dried, and then ~3 g of material was crushed to less than 2 mm in size with a mortar and pestle. The crushed samples were treated with 1 M hydrochloric acid (HCl) to remove carbonates and then rinsed with deionized water. A 10% solution of potassium hydroxide was added, and the samples were treated in a hot water bath to remove humic acid, followed by an additional rinse step. The remaining sample was then treated with cold 50% hydrofluoric acid and allowed to react overnight to remove silicate minerals. After additional rinsing, the samples were filtered through 185 µm and 7 µm mesh Nitex filters to remove coarse and fine particles. The sample remaining on the 7 µm mesh was then treated by acetolysis to remove excess organics. Slides were prepared using glycerin jelly treated with 2% safranin dye as a mounting medium.

Prepared slides were examined under 400x magnification using an optical light microscope. At least one slide from each processed sample was examined across transects spaced 1 mm apart to characterize the palynoflora, identify palynomorphs for inclusion in the

presence/absence matrix, and mark representative examples of each palynomorph for imaging. Samples were then counted to obtain at least three hundred identified palynomorphs. Identifications were made using both modern and fossil pollen references (Wodehouse 1935; Erdtman 1952, 1957; Gray 1958, 1985; Graham 1965; McAndrews et al. 1973; Taggart 1973; Kapp 2000; Zetter and Ferguson 2001; Reinink-Smith and Leopold 2005; Mustoe and Leopold 2014; Reinink-Smith et al. 2017; Tang et al. 2020). New palynological data were supplemented with published data from Vasa Park (Dillhoff et al. 2014).

Phytoliths

Rock samples were prepared for phytolith analyses using a series of chemical and mechanical steps to isolate biosilica particles (see Strömberg et al. 2018). To do so, ~1 g of sample was broken down using a mortar and pestle, after which the sample was treated with HCl to remove carbonates. The sample was passed through a 250 μm sieve to remove coarse particles and subsequently boiled with Schultze's solution to remove organic matter. A second round of sieving (53 μm) was done to disaggregate finer particles, such that clay particles could be removed by repeated washing, centrifuging, and decanting. Lastly, biogenic silica was isolated using heavy liquid floatation ($ZnBr + HCl + H_2O$; specific gravity 2.38). Extracted biosilica was washed with ethanol, then dried, and finally mounted on microscopy slides using Cargille Meltmount™, which were scanned and counted at 1,000x magnification under a compound optical light microscope.

Phytoliths were classified using the morphotype scheme developed by Strömberg and coauthors (e.g., Strömberg 2004, 2005, Strömberg et al. 2007*b*, *a*, 2013). The morphotypes were grouped into major phytolith-based plant functional groups (e.g., Strömberg et al. 2018), including the following diagnostic types: (1) forest indicator phytoliths, known to form primarily

in (a) palms (PALM), (b) Zingiberales and other monocotyledonous (sub)tropical herbaceous plants (ZINGI); and (c) woody and herbaceous non-monocot angiosperms, conifers, and ferns (FI), as well as (2) grass silica short cell phytoliths (GSSCP), formed exclusively by grasses, including (a) forms indicative of closed-habitat grasses, such as bambusoid and early-diverging grasses (APPBO), and forms diagnostic of various primarily open-habitat grasses, such as members of (b) Pooideae, which are all C_3, currently dominant in cooler climates and high elevation (POOID TOT), and members of the PACMAD clade, including (c) Panicoideae, which are mostly C4, typical of warmer and relatively humid climates (PANI), and (d) Chloridoideae, which are all C_4, typical of warmer and arid climates (CHLOR), (e) remaining PACMAD grasses, which contain both C_3 and C_4 taxa typical in warmer climates (PACMAD general) (e.g., Soreng et al. 2017, 2022), and (f) GSSCP that are not possible to assign to a taxonomic group because their production is not tied to a specific group or because they are not well enough preserved to classify (OTHG). Phytoliths that are less useful for inferring vegetation type, so-called non-diagnostic phytoliths, were also counted, including (3) phytoliths typical of sedges, *Equisetum*, and aquatic monocotyledons (AQ), (4) non-diagnostic phytoliths typical of grasses and other monocotyledons, as well as, in some cases, conifers (NDG), and (5) non-diagnostic phytoliths that are widely produced among land plants, whose production is unknown, or that are not possible to classify because they are broken or otherwise not sufficiently well preserved (NDO). At least 200 diagnostic forms (groups 1 and 2) were counted to ensure statistically robust relative abundance estimates (Strömberg 2009).

Vegetation type was reconstructed by comparing the relative abundances of diagnostic phytolith-based plant functional types, with sampling error on phytolith frequencies calculated as 95% confidence intervals using bootstrapping (Strömberg 2009). For example, habitat openness

was estimated through comparing open-habitat vs. closed-habitat grasses and other forest indicators using visual inspection (e.g., Harris et al. 2017; Strömberg et al. 2018). Furthermore, presence/abundance of phytoliths from plants such as palms, Zingiberales, and C_4 chloridoids helped constrain climate (Chen and Smith 2013; Crifò and Strömberg 2020). New phytolith data were supplemented with published data from Vasa Park (Dillhoff et al. 2014), and data from Mascall were counted by Dr. Regan Dunn (Los Angelos Natural History Museum) and included in Strömberg and Dunn (2014).

Analyses

All analyses were performed in R (version 4.3.2; R Core Team 2023).

Paleovegetation.—Paleovegetational analyses, excluding those phytolith-based, included only terrestrial woody gymnosperms and angiosperms as they are best represented in fossil assemblages and sensitive recorders of environments (Greenwood 1991). Community composition was assessed in terms of both presence-absence and relative abundance. For relative abundance analyses, we include both new census collections and count data published in prior work from Trout Creek (Graham 1965), Trapper Creek (Axelrod 1964), and Pickett Creek (Buechler et al. 2007). At Pickett Creek, we only included a stratigraphic span of the most productive horizons to minimize temporal averaging (the N, O, P, Q, and R horizons of Buechler et al. 2007). Published count data were aligned with the morphotype framework of this study. At Alvord Creek, new census collections were made from both the South Fork (601) and Scarp (601N) sub-localities, but given their relatively low morphotyped specimen counts (297 and 476 specimens total, respectively), they were combined for all analyses. For macrofossil count data, each isolated specimen contributed a single count. For example, to account for production and transport biases, isolated branchlets of conifers were considered one count regardless of size or

number of branches, rather than individual needle or scale leaves, but attached leaves/leaflets were counted individually (i.e., leaflets count as leaves) (e.g., Wing et al. 1993, 2012; Wing and DiMichele 1995).

Changes in community composition (H3, H4) was assessed with nonmetric multidimensional scaling (NMDS) using the *metaMDS()* function in the vegan package (Oksanen et al. 2022) with the following parameter set: engine = monoMDS, k = 2 or 3, weakties = TRUE, model = global, maxit = 400, try = 40, trymax = 100. The distance measures used were Jaccard for presence-absence and Bray-Curtis for abundance data, the latter first relativized as a proportion of the site total. Morphotype composition (corresponding roughly to species composition) was assessed considering foliage only to account for differing taphonomic biases acting on various plant organs. To explore which species were most influential to calculations of dissimilarity across sites, or groups of sites, we used Indicator Species Analysis (ISA) with the *multipatt()* function of the indicspecies package (Cáceres and Legendre 2009), and Similarity Percentage (SIMPER), with the *simper()* function of the vegan package (Oksanen et al. 2022).

To quantify diversity across sites with count data, we used a coverage-based approach that relativizes species diversity to sample completeness, rather than sample size. This approach accounts for the fact that environments of different diversity will reach a complete sample (i.e., all taxa represented) with a varying minimum number of individuals (Chao and Jost 2012). In addition, assemblages are either extrapolated or rarified to meet a common completeness value, instead of all assemblages (expect the smallest) being rarified with greater exclusion of abundance information. The package iNEXT (Chao et al. 2014; Hsieh et al. 2024) was used to calculate species diversity, and associated uncertainty, in terms of richness (q=0) and evenness via the Simpson's Index (q=2).

To estimate the percentage of evergreen woody non-monocot angiosperms (WNMA) species at each site, a novel probability-based approach was employed. In this approach, each taxon is represented by a probability of being evergreen, proportional to the number of extant evergreen species in that taxon, instead of simply applying a binary assignment of evergreen or deciduous. The analysis was restricted to macrofossil morphotypes to ensure equal treatment to sites that had no palynology data. All confidence scores are included (1-3), as many untoothed morphotypes are assigned to Lauraceae with low confidence (3) given the generally limited presence of diagnostic characters found in that leaf type (i.e., untoothed, pinnately veined, with looped secondary veins). As untoothed leaves are more often evergreen than toothed leaves (Royer et al. 2012), filtering by confidence score would bias against evergreen leaves.

As a first step in our novel approach, for each extant taxon assigned in this study (i.e., genus, or family if genus not assigned), an estimate of the percentage of evergreen species within that taxon was determined. This was done using the TRY - Categorical Traits Dataset (Kattge et al. 2012). We consider this calculation an estimate because leaf habit data of all species of each taxon were not available in this dataset. An iterative workflow followed: For each taxon at a site, 100 records (empty dataframe rows) were generated, and each record was assigned to evergreen or deciduous depending on the percentage defined for that taxon. A record was then randomly selected and constituted the leaf habit assignment for that taxon. This was repeated for each taxon at a site and a % evergreen value was calculated for the site. This iteration was then repeated 1000 times, resulting in 1000 estimates of % evergreen per site. Mean and standard deviation were calculated from these values. Values for each taxa are included in Appendix 4.

Leaf mass per area (M_A) reflects plant economic strategies along a “fast” and “slow” resource acquisition spectrum (Wright et al. 2004*b*; Reich 2014). M_A can be reconstructed for

WNMA fossil leaves using its relationship to the petiole metric (PM = petiole width^2 / leaf area; Royer et al. 2007). Both reconstructed and measured site mean M_A has been shown to vary with winter temperatures in temperate climates, being higher in less seasonal climates comprised of a greater number of evergreen WNMA species (Lowe et al. In Review*b*). In addition, site M_A is sensitive to impacts of disturbance, with low M_A taxa more prevalent at disturbed earlier successional sites (Currano et al. 2011, Lowe et al. In Review*a*). Thus, site mean M_A is reconstructed here to consider variation in leaf economic strategies, the prevalence of evergreen species, and to consider patterns in temperature seasonality and disturbance.

Site mean M_A was reconstructed following protocols of Royer et al. (2007) and Lowe et al. (2024, In Review*b*). To briefly summarize, petiole width was measured perpendicular to the petiole at its basal most insertion to the leaf blade, and leaf area included both blade and petiole (when preserved) area. In several cases, damaged portions of the leaf margin were digitally reconstructed. Site mean M_A mean was reconstructed from site mean PM with the *lma()* function of the dilp package (Butrim et al. 2024), using regression equations reported in Lowe et al. (In Review*b*).

To assess modernization of floras across the MMCT (H5), each fossil taxon (typically genus, although sometimes family or subfamily when genus not applied) was assigned as "exotic" or "remnant" by referencing online sources and regional published floras (Hitchcock et al. 2018) (assignments in Appendix 4). We define exotic as those whose native ranges do not include the west coast (WA, OR, and CA). Confidence scores were filtered to include only medium (2) and high (1) confidence.

Paleoclimate.—Paleoclimate (H1, H2) was reconstructed from fossil plants using two main approaches: leaf physiognomy proxies and the nearest living relative proxy Bioclimatic

Analysis. Leaf physiognomy methods included the univariate proxies leaf margin analysis, which reconstructs mean annual temperature (MAT) through its relationship to the proportion of untoothed WNMA morphotypes or species in a flora (i.e., leaf margin state), and leaf area analysis which reconstructions mean annual precipitation (MAP) through its relationship to mean leaf area in a flora (see summary of methods in Peppe et al. 2018). In addition, the multivariate proxy Digital Leaf Physiognomy (DiLP) was used, which relates multiple continuous physiognomic measurements of leaf shape, size, and toothiness to MAT and MAP (Peppe et al. 2011).

To do so, fossil WNMA leaves were prepared and measured following Lowe et al. (2024), a protocol built from prior work (Huff et al. 2003; Royer et al. 2005; Peppe et al. 2011). Morphotypes with toothed leaves were assigned a margin state of 0, untoothed leaves a 1, and those with both 0.5, regardless of if they were preserved well enough for quantitative measurements. We used the R package dilp to process data and produce climate reconstructions for all leaf physiognomy proxies (Butrim et al. 2024; Lowe et al. 2024). We used the leaf margin analysis equations reported in Wing and Greenwood (1993) and Peppe et al. (2011), with associated binomial sampling error calculated following Wilf (1997). In addition, we used leaf area analysis equations reported in Wilf et al. (1998) and Peppe et al. (2011).

A modified Bioclimatic Analysis (Greenwood et al. 2005) employing probability density functions was used here (see West et al. 2020, 2024; Reichgelt et al. 2023), and restricted to high (1) and medium (2) confidence scores (the impacts of filtering levels are assessed in Appendix 5). Occurrences of extant species belonging to fossil taxa of this study (typically genera, but families or subfamilies were used when genus was not assigned; Appendix 4) were obtained from Global Biodiversity Information Facility (GBIF.org. 2023. Global Biodiversity Information

Facility. Website: https://www.gbif.org [accessed 2023]) and subsequently filtered and resampled to exclude non-native taxa, erroneous entries, and regional overrepresentation. Climatic envelopes were generated from each point using WorldCLIM maps with the dismo R package (Hijmans et al. 2023). A random set of over 800,000 unique combinations of MAT, cold quarter temperature (CQT), MAP, and precipitation of the driest month (DMP) were then generated. The likelihood of a taxon (*t*) occurring at any of the climatic combinations was determined by calculating the product of probabilities (*f*) using the means (μ) and standard deviations (σ) of their modern range, for each climatic variable (*c*), with equation (1),

$$f(t_n) = \prod_{i=1}^{5} \pi/2\sigma_c^2 \times e^{(x_c-\mu_c)/2\sigma_c^2} \quad (1)$$

where x_c represents a value of MAT, CQT, MAP, or DMP that generates a unique combination from which the likelihood of the taxon occurring in the climate can be calculated. Reconstructing the probability of a taxon occurring at a combination of climatic variables, rather than considering each climate variable in isolation, reduces the likelihood for high probability to be calculated for a multivariate climate space not actually occupied by the modern taxon (Grimm and Potts 2016). To scale to the site-level, the likelihood for all taxa at a site (*n*) combined was calculated with equation (2),

$$f(z) = \prod_{i=1}^{n} t_n \quad (2)$$

where the highest probability density $f(z)$ represents the most likely climate in which the fossil assemblage was growing. A 95% confidence interval was established by calculating the maximum range of climatic variables, with $f(z) \geq 5\%$ of maximum $f(z)$.

Paleoclimate reconstructions are compared to a range of modern PNW climates east and west of the Cascades. To do so, climatic variables were extracted using WorldCLIM (Hijmans et al. 2023) from randomly selected coordinates in the PNW (n = 788 amd 2809 west and east of the Cascades, restively), filtered to only include lowland elevations (< 900 m above sea level; see Appendix 6 for more detail).

Results

Stratigraphy and sedimentology

All fossil sites where field work was intended were re-located, and macrofossil collection horizons of prior work were re-located at most sites (see further detail in Appendix 1). Rather, productive macrofossil horizons were found stratigraphically near prior collecting horizons at Alvord Creek and either near or overlapping at Juliaetta. At the Deep Creek sub-locality (Spokane), only poorly preserved plant fossils were found, and at Trapper Creek, only poorly-moderately preserved fossils in fairly low abundance and diversity were found, either near or overlapping with collections from prior work.

Illustrated local stratigraphic sections with the precise location of sampled macrofossils, rocks for palynomorphs/phytoliths, and tuff for radiometric dating, are included in Appendix 3. Sections ranged from 5.5 to 37 m in thickness, while the full Watersnake section was 68 m in thickness and published in Schiller et al. (2024). Plant macrofossils occur in silt- to clay-sized, moderately- to well-laminated, shales. Fossiliferous shales are often tuffaceous and diatomaceous, and fossiliferous diatomite occured at Mascall (White Hills and Riverside/Van Horn's Ranch; at the latter weathered rocks will float in water), Trout Creek, and Pickett Creek. Coarser grained massive sandstones, conglomerates, and/or volcanic breccia occur within local

sections at nearly all sites. Volcanic tuff or largely tuffaceous horizons were also found in local stratigraphy at all sites, ranging in thickness from sub-cm to a 17 m tuff at Watersnake (Appendix 3; Watersnake tuff illustrated in Schiller et al. 2024).

U-Pb dating

Pickett Creek—A 3 cm thick, medium ash, gray vitroclastic tuff (Appendix 3) defining the datum of Site I of Buechler et al. (2007) produced abundant euhedral, elongate, prismatic zircon crystals, of which eight were successfully analyzed for CA-IDTIMS. Four crystals produced concordant and equivalent U-Pb isotope ratios, with a weighted mean 206Pb/238U date of 11.372 ± 0.029 (0.029) [0.032] Ma (95% confidence interval; MSWD = 0.81; n=4; Table 2). Another four crystals produced an older cluster of ca 11.51 Ma dates, and are interpreted as older antecrysts recycled into the volcanic eruption. As most of the macroflora collected at this site comes from laminated siltstone and diatomite 1 to 2 meters below this datum, the dated horizon represents a minimum age for the flora. However if the millimetric laminations in the sedimentary rocks are seasonal then the macroflora collections likely are within the error of the eruption age of the tuff. This data is older than that previously reported at Pickett Creek (10.5-8.5 Ma; Buechler et al. 2007), and older than ages typically cited for both the Chalk Hills Formation, and the underlying (or overlapping?) Poison Creek Formation (Love et al. 2023 and references therein), and may aid future work in constraining the earliest phase of sedimentation in the western Snake River Plain (Wood and Clemens 2002).

Trapper Creek.—A 5 cm thick, medium ash, normally graded, gray vitric tuff was sampled from the tuff of Ibex Peak unit, 40 cm above its basal contact with the Beaverdam Formation (Appendix 3). This sample yielded abundant elongate prismatic zircon, from which five crystals selected for CA-IDTIMS produced 206Pb/238U dates ranging from 12.962 to

12.828 Ma. The youngest two crystals define a weighted mean 206Pb/238U date of 12.830 ± 0.082 (0.082) [0.083] Ma (95% confidence interval; MSWD = 0.20; n=2; Table 2). Our dated tuff is stratigraphically between (80 meters above TC89-20A and 170 meters below TC89-21B) and intermediate in age to the two bracketing $^{40}Ar/^{39}Ar$ ages reported by Perkins et al. (1995), revised by us to 12.82 ± 0.04 and 11.81 ± 0.03. Our new date of the Tuff of Ibex Peak, immediately overlying the macrofossil horizon, provides an upper bracket, while the revised 40Ar/39Ar date of the upper Beaverdam Fm. from Perkins et al. (1995) provides a lower bracket, constraining the fossil flora within a ~260 kyr interval between to 13.09 ± 0.08 and 12.830 ± 0.082. The age of our dated tuff is also consistent with a recalculated $^{40}Ar/^{39}Ar$ age of Cougar Point Tuff III of 12.83 ± 0.08 Ma (Bonnichsen et al. 2008), which was correlated on the basis of glass chemistry by Perkins et al. (1995) to a horizon near the base of the tuff of Ibex Peak unit.

Mascall.—The base of the White Hills section is defined by a very thick (6.5 m) gray, massive vitric tuff near apparent fault contact with Dayville Basalt (Appendix 3). The massive basal tuff produced abundant elongate prismatic zircon, with 12 crystals selected for CA-IDTIMS producing a weighted mean $^{206}Pb/^{238}U$ date of 16.131 ± 0.011 (0.012) [0.021] Ma (95% confidence interval; MSWD = 1.73; n=12; Table 2). This date constrains a minimum age for the Lower Mascall Formation (likely unit 1 of Downs 1956) and indicates a minimum depositional duration of the lower member at ~1 million years (16.131 ± 0.011 - 15.122 ± 0.017 Ma; Maguire et al. 2018). This result is also within error of the single crystal laser fusion $^{40}Ar/^{39}Ar$ plagioclase age of 16.06 ± 0.02 Ma (calibrated to FCs = 28.021 Ma) for Unit 1 of the Dinner Creek Tuff suite (Brogan Tuff) reported by Streck et al. (2015).

Watersnake (Succor Creek)—U-Pb dates from the Watersnake sub-locality of the Succor Creek flora, including a Bayesian age model extending through the entire section, were

published recently by Schiller et al. (2024). Supplementary detail to that publication follows. A thin bentonitic volcanic tuff (21-WS-T-01) sampled at 4 meters above the section base (Appendix 3) produced sparse but homogeneous in form prismatic volcanic zircons, of which 5 of 8 crystals selected for CA-IDTIMS U-Pb geochronology produced concordant and equivalent isotope ratios with a weighted mean $^{206}Pb/^{238}U$ date of 15.546 ± 0.018 (0.019) [0.025] Ma (95% confidence interval; MSWD = 0.71; n=5; Table 2). Three significantly older crystals (15.65 Ma) are interpreted as recycled antecryts within the volcanic horizon. The lower thick ash-flow tuff (+18 to 26.5 meters above base) consists of white, bedded to laminated, fine to medium grained originally vitric ash, largely altered to zeolitized clay. The sample (21WS-02) from this tuff produced abundant elongate volcanic zircon with abundant glass inclusions, of which 9 crystals successfully analyzed by CA-IDTIMS produced a younger cluster with a weighted mean $^{206}Pb/^{238}U$ date of 15.512 ± 0.025 (0.026) [0.031] Ma (95% confidence interval; MSWD = 0.13; n=5), and four crystals with resolvably older ages attributed to inheritance. The upper Watersnake ash-flow tuff (+45 to 61 m above base) consists of gray to white, bedded, normally graded, fine to medium grained vitric ash and lapilli, altered to clay in many intervals. This tuff also produced abundant, highly elongate, prismatic zircon with abundant glass inclusions, from which 6 of 8 crystals successfully analyzed by CA-IDTIMS produced a weighted mean $^{206}Pb/^{238}U$ date of 15.512 ± 0.022 (0.022) [0.028] Ma (95% confidence interval; MSWD = 0.37; n=6). While the ages of the two ash flow tuffs are identical within error, they are clearly discrete, stacked event beds in the measured section within a single fault block. Schiller et al. (2024) applied a Bayesian age modeling algorithm (Bacon; Blaauw and Christen 2011) to this measured section with three geochronological likelihoods to estimate a short duration of deposition of 34 kyr and a rapid rock accumulation rate of 2 m/kyr (no correction for compaction). The plant

macrofossil census collection is firmly dated by the lower bentonite age of 15.546 ± 0.018 Ma (Table 2).

Trout Creek.—Thin (2-16 cm) beds of fine to medium vitric tuffs were collected at 8.61 (A), 9.06 (B), 9.71 (C), 10.95 (D), and 34.5 (E) meters above base in the "West Quarry" section (Appendix 3). Sample 20TROUT-A at 8.61 meters produced abundant elongate prismatic zircon, and six crystals selected for CA-IDTIMS analysis yielded two clusters of concordant and equivalent $^{206}Pb/^{238}U$ dates. The younger cluster of three crystals is assigned a weighted mean $^{206}Pb/^{238}U$ date of 15.452 ± 0.022 (0.023) [0.028] Ma (95% confidence interval; MSWD = 0.07; n=3; Table 2), which is interpreted as the eruption and depositional age of the event bed. A slightly older cluster of dates at 15.48 Ma is interpreted as epiclastic reworking of older volcanic products into the eruption column.

Sample 20TROUT-D at 10.95 meters produced abundant highly elongate prismatic zircon, and six crystals selected for CA-IDTIMS analysis yielded concordant and equivalent isotope ratios with a weighted mean $^{206}Pb/^{238}U$ date of 15.450 ± 0.009 (0.010) [0.020] Ma (95% confidence interval; MSWD = 1.41; n=6; Table 2), which is interpreted as the eruption and depositional age of the event bed. The statistically indistinguishable dates for these two tuffs over 2.34 meters of section suggest that this age may be safely extrapolation downward to the productive plant layers ≤0.8 meters below. This date agrees well previous work, indicating the fossil flora was deposited in the intra-caldera lake ~100 kyr after the eruption of the Tuff of Whitehorse Creek at 15.556 ± 0.019 Ma that formed the caldera, and concurrent with eruption of ring fracture rhyolites along the caldera margin from 15.464 to 15.369 Ma (Benson et al. 2017).

Moose Mountain.—A thin 3 cm gray vitric tuff at 2.9 meters above the base of the section, and 20 cm above a productive macrofossil horizon was sampled (Appendix 3). This tuff

produced abundant colorless, transparent, prismatic zircon crystals, and four crystals analyzed by CA-IDTIMS yielded concordant and equivalent isotope ratios with a weighted mean $^{206}Pb/^{238}U$ date of 15.678 ± 0.033 (0.034) [0.038] Ma (95% confidence interval; MSWD = 0.54; n=4; Table 2), which is interpreted as the eruption and depositional age of the event bed. A single crystal with a slightly older date of 16.076 Ma is interpreted as inherited epiclastic zircon. Our new U-Pb zircon age is slightly older but significantly more precise than a previous $^{40}Ar/^{39}Ar$ plagioclase date reported by Manchester et al. (2018) of 15.00 ± 0.46 Ma (after recalculation to the Fish Canyon Tuff sanidine fluence monitor age of 28.201 Ma). The site dates younger than the duration of the Grande Ronde and Wanapum CRB members (Kasbohm and Schoene 2018), suggesting its place in the Sardine Formation, rather than the previously cited Little Butte Volcanic Series which underlies the CRBs (Peck et al. 1964; Beaulieu et al. 1974; Walker and Duncan 1989).

Clarkia.—We collected a suite of volcanic tuffs equivalent to a subset of the sampling of Ladderud et al. (2015) and Geraghty (2017), which can be correlated in turn to the sampling of Yang et al. (1995). Two tuff samples from each outcrop were successfully dated and used as the input likelihoods to a Bayesian age model of deposition. Our sample 19P33-2064 from the Racetrack section is the stratigraphically lowest sample from a 2 cm thick gray fine ash tuff 21 cm below the P33-2bv1 horizon of Ladderud et al. (2015) and Geraghty (2017). Six small, elongate, prismatic zircon crystals successfully analyzed by CA-IDTIMS from this sample produced a weighted mean $^{206}Pb/^{238}U$ date of 15.909 ± 0.016 (0.016) [0.024] Ma (95% confidence interval; MSWD = 0.82; n=6; Table 2), interpreted as the eruption and depositional age of the tuff. Our sample 19P33-1771 also from the Racetrack section is equivalent to the P33-5b horizon of Ladderud et al. (2015) and Geraghty (2017) and the Unit 5B of Yang et al. (1995)

and Höfig et al. (2021). Seven small equant prismatic zircon crystals were successfully analyzed from this tuff, and six of those crystals produced a weighted mean $^{206}Pb/^{238}U$ date of 15.903 ± 0.041 (0.041) [0.044] Ma (95% confidence interval; MSWD = 0.77; n=6; Table 2). A single crystal produced a substantially older date of 15.97 Ma interpreted as a reworked epiclastic crystal.

Our stratigraphically lowest sample 19P37B-13.85 from the Emerald Creek locale was sampled at the bottom of the excavated pit and is a distinctive 26 cm thick gray, coarse crystal-vitric tuff equivalent to the P37-10 horizon of Geraghty (2017). Fifteen relatively small and low U, elongate, prismatic zircon crystals were successfully analyzed via CA-IDTIMS. The youngest cluster of eight crystals exhibit concordant and equivalent isotope ratios, with a weighted mean $^{206}Pb/^{238}U$ date of 15.888 ± 0.013 (0.014) [0.022] Ma (95% confidence interval; MSWD = 0.89; n=8; Table 2). There are a number of older crystals in this sample, ranging in age from 15.97 to 16.66 Ma, which are interpreted as antecrysts from recycled older volcanics. Our stratigraphically highest dated sample 19P37B-5.46 from Emerald Creek is equivalent to the P37-4 horizon of Ladderud et al. (2015) and Geraghty (2017). This 4 cm thick tuff produced abundant relatively large zircon crystals, and 9 of 11 crystals successfully analyzed by CA-IDTIMS produced a weighted mean $^{206}Pb/^{238}U$ date of 15.831 ± 0.009 (0.010) [0.020] Ma (95% confidence interval; MSWD = 0.79; n=9; Table 2). Our new Miocene U-Pb zircon ages obtained from the Clarkia paleolake are consistent in timing with an origin through damming of the paleo-St. Maries River by basalt flows of the Priest Rapids Member from the Wanapum Basalt of the Columbia River Basalt Group (15.895 ± 0.019 Ma; Kasbohm and Schoene 2018). Moreover, our age model demands a fairly short lifetime for the lake, on the order of <100 thousand years.

Juliaetta.—A 13 cm thick gray vitroclastic tuff within a prominent 2 m thick diatomite layer was sampled from 24 meters above the base of the section, and ~18 m above the macrofossil census layer (Appendix 3). This sample (19P6-A) produced abundant zircon with a distinctive flattened prismatic morphology, and six crystals successfully analyzed by CA-IDTIMS yielded a weighted mean $^{206}Pb/^{238}U$ date of 16.577 ± 0.012 (0.013) [0.022] Ma (95% confidence interval; MSWD = 0.63; n=6; Table 2). This date is interpreted as the eruption and depositional age of the tuff and provides a minimum age for the macroflora. In addition, this date provides precise constraints on eruption of the Grande Ronde R1 member (Lewis et al. 2005), which, to our knowledge, has not been dated using U-Pb on zircon-bearing silicic tuff interbeds.

Alvord Creek.—The lowest tuff bed sampled at the South Fork sub-locality (601 of Axelrod 1944), sample 20ALV-A, is a 30 cm thick pumiceous vitroclastic tuff along strike of and approximately 22.5 meters below the leaf fossil quarry site (Appendix 3). This tuff produced abundant colorless, transparent, equant and slightly flattened tabular zircon crystals, of which five were successfully analyzed by CA-IDTIMS and produced a weighted mean $^{206}Pb/^{238}U$ date of 25.574 ± 0.042 (0.043) [0.051] Ma (95% confidence interval; MSWD = 0.68; n=5; Table 2).

The Alvord Creek Formation is locally overlain by the Pike Creek Volcanics, and in Pike Creek we collected a 2 m thick crystal vitric pyroclastic ash flow tuff layer within tuffaceous siltsone and sandstone, about 2 meters below the contact with the overlying 'lower platy rhyolite' (Tprl) of Minor et al. (1987*a*). This sample 20PCV-A produced abundant equant to elongate prismatic zircon, of which six were analyzed by CA-IDTIMS. The three youngest zircon crystals produced a weighted mean $^{206}Pb/^{238}U$ date of 25.585 ± 0.040 (0.041) [0.049] Ma (95% confidence interval; MSWD = 0.73; n=3; Table 2), which is interpreted as the eruption age of the

tuff bed. The remainder of the crystals are interpreted as older antecrysts recycled into the volcanic eruption.

These results supplement addition information to suggest the Alvord Creek Fm. may have been deposited in a caldera lake. This suggestion follows the observation that (1) the Pike Creek Formation displays dome and flow facies (Minor et al. 1987*c*), (2) is ~600 m thick south of the fossil plant localities (near Pike Creek), but completely pinches out laterally further north (near Big Alvord Creek) prior to reaching the fossil beds (Minor et al. 1987*c*, *b*, *a*), and (3) the Pike Creek and Alvord fms. are roughly contemporaneous (Table 2). Thus, the two formations may showcase rhyolitic ring fracture eruptions that surrounded a topographically high caldera lake.

Fossil HS (Bridge Creek).—Zircon was separated from a sample of fossil-bearing tuffaceous shale (collected by Dr. Regan Dunn) from the macroflora bearing strata at Wheeler High School in Fossil, Oregon. These rocks contain a diverse leaf flora described by Manchester and Meyer (1997) and previously dated by the $^{40}Ar/^{39}Ar$ single crystal sanidine technique by McIntosh et al. (1997).

Twelve zircon crystals selected for CA-IDTIMS produced concordant and equivalent U-Pb isotope ratios, with $^{206}Pb/^{238}U$ dates ranging from 33.379 to 33.058 Ma. The youngest six crystal define a cluster with a weighted mean $^{206}Pb/^{238}U$ date of 33.079 ± 0.024 (0.026) [0.044] Ma (95% confidence interval; MSWD = 1.41; n=6; Table 2). The remainder of the crystals are interpreted as older antecrysts recycled into the volcanic eruption. This new age is consistent with, but an order of magnitude more precise than the previous $^{40}Ar/^{39}Ar$ sanidine date of McIntosh et al. (1997) after updating of the decay constant values and the Fish Canyon Tuff sanidine fluence monitor age (the previous $^{40}Ar/^{39}Ar$ sanidine date of 32.58 ± 0.26 Ma is recalculated to 33.00 ± 0.26 Ma).

Composition of macrofossil and palynomorph records

Macrofossil and palynomorph frameworks.—Across sites of study, our compiled digital library includes ~14,000 images, 429 of which are details of finer venation imaged under a stereoscope. This includes images from Fossil HS (Bridge Creek), Ellensburg, and Willamette although they were not subsequently included in our morphotype framework study. Our established macrofossil morphotype framework involved the study of ~11,000 specimens, and is comprised of 673 total morphotypes, resulting in 307 study-scale morphotypes once across-site synonymy was applied (Table 3; see further details in Appendix 7). Alterations to taxon-concepts presented by previous work were most often in the form of "lumping". Of the total morphotypes, 592 were assigned either familial, sub-familial, or generic affinity, and after confidence scores were adjusted according to organ co-occurrence and across-site synonymy, 72% were assigned with high confidence (1), 19% with medium (2), and 9% with low (3) (Appendix 4). A greater percentage of high confidence scores were given to reproductive, compared to foliar, morphotypes (83% vs. 65%).

New palynomorph assemblages were analyzed from nine sites (Table 3). We identified 56 unique palynomorph types, including 1 lycophyte (*Salaginella*), 5 pteridophytes, 10 gymnosperms, 30 woody angiosperms, 7 herbaceous angiosperms, and 3 aquatic angiosperms, and several more undifferentiated types.

Patterns in community composition.—Macrofossil census collections were made at Alvord Creek, Juliaetta, Mascall, Clarkia, and Watersnake. Specimens identified to morphotype from census collections vary from 672 to 857 total, 489 to 822 total foliage, and 282 to 609 woody non-monocot angiosperm (WNMA) foliage specimens (Table 3).

NMDS analyses (all with stress values < 0.1) indicate that pre- and post-MCO floras never fall within the ordination space defined by MCO floras (i.e., their convex hull) for both macrofossils and palynomorphs, and abundance and presence-absence analyses (Fig. 2). Alvord Creek is distinct from all other floras as it contains several unique morphotypes, including some of its most dominant ones (e.g., *Sorbus harneyensis*, *Prunus harneyensis*, Alv002, and *Acer alvordense*), and lacks prevalent MCO morphotypes (e.g., *Quercus simulata*, *Taxodium distichium*). All palynomorphs with pre-MCO occurrences persist across the MCO onset (and MMCT, except *Tilia*) and several new palynomorphs appear alongside them (Fig. 3C). For example, 48% of MCO angiosperm palynomorphs do not have pre-MCO occurrences, including several genera whose macrofossils also first appear in the MCO, even when considering Fossil HS macrofossils (e.g., *Aesculus, Celtis, Ilex, Liquidambar, Nyssa*; Fig. 3; Meyer and Manchester 1997).

Within the MCO, composition varies considerably (Fig. 2). Among foliar morphotypes (presence-absence), Columbia Basin floras (Clarkia, Spokane, Juliaetta) cluster with the Mascall flora (Fig. 2A), driven by some shared occurrences of several morphotypes (e.g., *Alnus relatus*, *Alnus fairii*, *Quercus pseudolyrata*, *Liquidambar pachyphyllum, Populus lindgreni, Taxodium dubium, Ginkgo adiantoides*, *Nyssa* M1, *Zizyphoides aurciulata*). Moose Mountain is distinct in having several unique or uncommon morphotypes and lacking several others typical of MCO floras. Trout Creek (southeastern Oregon Plateau) shows greater similarity to post-MCO floras Trapper Creek and Pickett Creek (Snake River Plain) than to other MCO floras (Fig. 2A). Similarity in these three floras is driven by the shared presence of several morphotypes (e.g., *Acer schorni*, *Betula lacustris*, *Salix payettensis*, *Populus* foliage M1, *Populus* washoensis, and *Berberis reticulata*) and by lacking several other prevalent MCO morphotypes (e.g., *Platanus*

dissecta, Fagus washoensis, Liquidambar pachyphyllum, and *Taxodium distichium*), including several exotic taxa (Fig. 4A). Watersnake plots intermediate between the Trout Creek and the Columbia Basin/Mascall cluster (Fig. 2A), differing from the latter by lacking several morphotypes (e.g., *Alnus relatus*, Fabaceae foliage M1, *Liquidambar pachyphyllum, Populus lindgreni,* and *Quercus pseduolyrata)*, and having several not found in the other floras (e.g., *Acer oregonianum, Berberis reticulata, Chamaecyparis* foliage M1, Fabaceae foliage M5, *Abies* foliage M1, and *Viburnum* foliage M2).

Foliar morphotype composition in terms of relative abundance is also variable among MCO floras, including those that shared similarity in presence-absence (Fig. 2B, C). For example, Clarkia, Juliaetta, and Mascall share few morphotypes among the top 5 most abundant in each flora (Appendix 8). In contrast, similarities between MCO floras Watersnake and Trout Creek and the post-MCO site Trapper Creek hold when considering relative abundance, as all three share a hyper-dominance of *Quercus simulata* (> 55% dicot foliage). The relative similarity of Trout Creek and Trapper Creek extends beyond *Q. simulata*, as the pattern remains when *Q. simulata* is removed from NMDS analyses (Appendix 9). In contrast, the similarity of Watersnake to Trout Creek/Trapper Creek in terms of relative abundance is driven only by the shared hyper-dominance of *Q. simulata* (Appendix 9).

Foliar morphotype composition again shifts across the MMCT (excluding Trout Creek), but differs between inland Snake River Plain floras (Trapper Creek and Pickett Creek) and the more coastal Puget lowland Vasa Park flora (Fig. 2). Compared to MCO floras, Snake River Plain floras are distinct in their shared presence of *Populus* M1, *Acer schorni, Betula lacustris, Salix payettensis,* and *Acer oregonianum*, and lack of *Taxodium dubium*, *Arbutus idahoensis, Magnolia* M1*, Alnus relatus, Liquidambar pachyphyllum, Q. pseduolyrata, Betula* M2, *Fagus*

washoensis, and *Glyptostrobus oregonensis*. Range-through plots illustrate several foliar morphotypes and genera which do not appear to persist across the PNW in the Snake River Plain (Fig. 3). This loss of taxa reflects a reduction in the number of exotics, from an average of 49% (excluding Trout Creek and Moose Mountain, see below) to 21% (Fig. 4A). Lost exotic taxa tend to occupy warmer and wetter modern climates without summer drought, relative to climates occupied by remnant taxa in the modern, including climates of the modern PNW (Fig. 5).

Of the genera that do occur in post-MCO floras, all except one (*Sequoiadendron* at Trapper Creek) persist from the MCO (Fig. 3B). Of the genera that persist, 30% occur only within the more coastal Vasa Park flora (47% among angiosperms; Fig. 3B). For example, the following taxa, most of which are exotics (marked with an "E"), are present in either the Vasa Park macrofossil or palynomorph record, but absent from both the Snake River Plain floras: *Aesculus, Celtis, Cercidiphyllum* (E), *Fagus* (E), *Hydrangea* (E), *Ilex* (E), *Liquidambar* (E), *Nyssa* (E), *Paulownia* (E), *Platanus.* Accordingly, Vasa Park does not decrease in the proportion of exotic taxa across the MMCT in contrast with Snake River Plain floras (Fig. 4A). Among foliar morphotypes (roughly corresponding to species), there is a greater number of first appearances across the MMCT, compared to genera. For example, only 59% that occur in post-MCO floras persist from the MCO (Fig. 3A).

Community ecology and structure (macrofossil, palynomorph, and phytolith assemblages)

Diversity.—Despite Alvord, Mascall, and Watersnake census collections having considerable specimen counts (>790 specimens; Table 3), the collections are of low completeness, leading to large error surrounding estimates of richness (Appendix 10). This uncertainty limits inference of diversity from richness, so inferences are instead focused on

evenness, which is less sensitive and is an important descriptor of modern mixed mesophytic forests (Wang 1961; Braun 1964).

Evenness changes little across the MCO onset and is strongly varied within the MCO (Fig. 4B, C). Clarkia has the highest evenness when considering both all and WNMA foliage. A strong dominance of *Taxodium dubium* at Juliaetta results in low evenness; however, evenness among WNMAs is considerably higher (Fig. 4B, C). Trout Creek and Watersnake show low evenness in both measures, with the former having a hyper-dominance of *Q. simulata* and *Quercus* M1 (79% relative abundance), and the latter a hyper-dominance of *Q. simulata* and *Glyptostrobus oregonensis* (79% relative abundance). Both floras are those most intimately associated with silicic volcanic centers during the MCO (Fig. 1). Across the MMCT, there is a decrease in evenness in the Snake River Plain floras (Trapper Creek and Pickett Creek) relative to those MCO floras less intimately associated with silicic volcanic centers, particularly among WNMAs (Fig. 4B, C).

MA and prevalence of evergreen dicots.—All floras were reconstructed to be dominated by deciduous, relative to evergreen, WNMAs (Fig. 6A). During the MCO, % evergreen reconstructions overlap (via visual inspection) more with modern plant communities in warm temperate climates (Köppen Cf and Cs) compared to cool temperate climates (Köppen Df). Across the MMCT, there is a decrease in % evergreen reconstruction, from an average of 22% to 7%, to values instead more consistent with cool temperate climates (Fig. 6A).

Leaf mass per area (M_A) was reconstructed for 44-73% of WNMA foliar morphotypes per site (Appendix 11). Site mean M_A decreases slightly across the MCO onset, and reconstructions are similar within the MCO (77.6-84.3 g/m^2), with greatest overlap (via visual inspection) with modern plant communities in warm temperate climates (Fig. 6B). Across the MMCT, the Trapper

Creek site is reconstructed with the highest M_A of all sites, although only 13.1 g/m^2 higher than the MCO average, while Pickett Creek falls within the range of MCO sites. In contrast, Vasa Park shows a decrease in M_A, 18.8 g/m^2 lower than the MCO average, and similar to modern plant communities in both cool temperate and warm temperate climates (Fig. 6B). There appears to be general correspondence between % evergreen and mean M_A reconstructions, with Trapper Creek, which is reconstructed as the driest Miocene site, falling the greatest distance from the trendline (Fig. 6C).

Functional groups.—Macrofossil and palynomorph relative diversity and macrofossil relative abundance in nearly all floras are dominated by WNMAs. Juliaetta is an exception given numerical dominance of riparian conifers (*Taxodium dubium*; Fig 6B). In contrast, conifer pollen dominates in nearly all floras in terms of relative abundance (Fig. 7D). The pre-MCO Alvord Creek flora has a relatively high proportion of non-riparian conifer abundance and diversity in the macrofossil record, and the highest relative abundance of Pinaceae pollen, all of which generally decreases across the MCO onset, particularly in terms of relative abundance (Fig. 7).

During the MCO, riparian conifers are prevalent (*Taxodium, Glyptostrobus, Metasequoia*) in most macrofloras, but lacking completely from Trout Creek and Moose Mountain (Fig. 7A, B). Accordingly, Cupressaceae/Taxaceae (C/T) pollen is prevalent during the MCO but is in relatively low abundance at Moose Mountain (no pollen recovered from Trout Creek; Fig. 7D). Across the MMCT, non-riparian conifers do not persist and C/T pollen generally decreases. Snake River Plain floras differ in their abundance of non-riparian conifers, as Trapper Creek has high abundance and diversity in both the macrofossil and pollen records, while Pickett Creek is lower in both. Pollen of *Ephedra*, a taxon typical of arid climates today (Leopold and Denton 1987; Barbolini et al. 2020), occurs at both Snake River Plain floras, not at Vasa Park, and at

only one MCO flora (Spokane; Fig. 7C). Vasa Park has a lower relative diversity of non-riparian conifer macrofossils relative to Trapper Creek but shares fairly similar relative abundance and diversity of conifer pollen.

Phytoliths and canopy structure.—Preliminary phytolith analyses are presented, including completed counts from an initial set of four fossil floras (Mascall, Clarkia, Trapper Creek, Pickett Creek). During the MCO, forest indicator phytoliths dominate nearly all assemblages (65-85%; Fig. 7E). One exception is a single sample from Mascall, with a relatively higher relative abundance (40%) of open-habitat grasses (i.e., Pooideae, Panicoideae, and other PACMAD grasses), as well as ginger, palm, and closed habitat grass phytoliths, coincident with a bamboo leaf fossil (a modern closed-habitat grass) in the Mascall flora. Across the MMCT, the relative abundance of open-habitat grasses, particularly Pooideae, increase in the Snake River Plain floras (to 59-63%), but not in the more coastal Vasa Park flora where forest indicators remain the dominant type (Fig. 7E). One exception is a single sample at Vasa Park with a relatively high relative abundance of PACMAD grass phytoliths (34%).

Paleoclimate

Relatively cool MAT was reconstructed at Moose Mountain (via leaf physiognomy) and Trout Creek (via bioclimatic analysis). For example, reconstructed MAT at Moose Mountain was 5-7 °C lower than for other MCO sites, driven by a lower margin state percentage (17% vs. avg. of 37%). Trout Creek had MAT and CQT reconstructions 1.9 °C and 2.6°C colder than other MCO sites, respectively (Fig. 8). These results, combined with independent lines of evidence, suggest the floras represent higher paleoelevations (see Discussion section); for this reason we excluded them from the following calculations of average lowland paleoclimate variables.

Leaf physiognomy.—The number of WNMA morphotypes included in leaf physiognomy analyses varied from 17 to 56, all above the suggested minimal sample size for analyses (Burnham et al. 1992, 2005; Wolfe 1993). Of those, 63-95% (avg. 83%), were preserved well enough to contribute quantitative leaf area data, totaling 1251 specimens. Of the non-entire morphotypes (toothed and mixed margin), 72-100% (avg. 93%), contributed tooth count: internal perimeter data to DiLP analyses, totaling 899 specimens (Appendix 11). All fossil floras fall within the multivariate leaf physiognomic space of the calibration dataset, permitting reliable inference (Appendix 12; Lowe et al., 2024).

MAT reconstructions during the MCO range from 11.5 to 16.9 °C (avg. 13.4 °C), depending on the site and method (Fig. 8). Temperature trends across the MCO onset are unclear, as average MAT during the MCO is ~5.8 °C higher than the pre-MCO Alvord Creek flora but overlaps with the pre-MCO Fossil HS flora, which is 7.5 million years older than Alvord Creek (Fig 7). MCO reconstructed temperature is generally higher than the range of modern PNW temperatures, and ~4.1 and ~3.4°C higher than average MAT east and west of the Cascades, respectively. Across the MMCT, MAT decreases by 3.9 °C in the PNW interior, 2.5 °C for the more coastal Vasa Park site, with greater overlap with modern PNW climates (Fig. 8). One exception is the DiLP reconstruction for Vasa Park, which is 3.5 °C higher than that produced by leaf margin analysis, driven by a relatively high mean Feret Diameter ratio (i.e., more circular leaf shapes). MAT reconstructions from various methods are in general agreement, although DiLP typically reconstructs slightly cooler MAT relative to leaf margin analyses (Appendix 13).

Changes in precipitation are reconstructed across the MCO onset and MMCT, although the large uncertainty inherent in leaf physiognomy methods results in overlap of error bars across all site estimates (Fig. 9). Nevertheless, all MCO sites (120-157 cm/yr) are reconstructed with

higher average MAP relative to pre-MCO Alvord Creek site (100 cm/yr), suggesting increased precipitation across the MCO onset. Precipitation during the MCO is in line with modern precipitation on the wetter west side of the Cascade Range. Across the MMCT, the two interior sites (93-113 cm/yr) are reconstructed as drier than all MCO sites, and occupy values intermediate to those on east and west of the Cascades today (Fig. 9). The more coastal post-MCO Vasa Park site instead has the highest reconstructed MAP of all sites of this study (175 cm/year). MAP reconstructions from various methods are in general agreement, although DiLP in all but one case reconstructs higher values compared to the leaf area analysis equation of Peppe et al. (2011), and in all cases reconstructs lower values compared to the leaf area analysis equation of Wilf et al. (1998) (Appendix 13).

Bioclimatic analysis.—The number of unique taxa included in Bioclimatic Analyses ranged from 14 at Vasa Park to 52 at Clarkia (Appendix 11). Estimates of MAT, MAP, and CQT, were mostly insensitive to the level of filtering in confidence scores (Appendix 5). MAT increases across the MCO onset by an average of 4.7 °C (Fig. 8). Reconstructions of MAT within the MCO vary between 12.4 to 13.9 °C and are on average 3.9 and 3.2 °C warmer than mean MAT east and west of the Cascades today, respectively. Across the MMCT, MAT decreases in the PNW interior by 3.4°C, in line with modern PNW temperatures; however, there is no discernable change in MAT for the more coastal Vasa Park site (Fig. 8). Reconstructions of CQT closely parallel MAT, increasing by 6.6 °C at the MCO onset, to values consistent with modern climates west of, but higher than climates east of, the Cascades (Fig. 8). Across the MMCT, CQT decreases for both the SRP (Trapper Creek and Pickett Creek) and more coastal Vasa Park sites by an average of 3.3 °C, to values intermediate of modern climates east and west of the Cascades (Fig. 8).

MAP reconstructions using Bioclimatic Analysis are similar to those from leaf physiognomy methods (Fig. 9). MAP increases across the MCO onset by 30.2 cm/yr, and varies from 98 to 115 cm/yr within the MCO, consistent with modern climates on the wetter west side of the Cascades. Across the MMCT, precipitation decreases in the Snake River Plain by 20.2 cm/yr, although the more coastal Vasa Park site had the highest MAP reconstructed across all sites of this study, at 117 cm/yr (Fig. 9).

Discussion

The Miocene Climatic Optimum

The MCO is well represented in this study, with seven sites representing a ~1 million year interval between ~15.5 and ~16.6 Ma (Table 2). Changes of paleoclimate and paleovegetation across the MCO onset are evident when comparing the pre-MCO flora of Alvord Creek to those in the MCO, in most cases consistent with our hypotheses (H1, H3). These include an increase in the prevalence of taxa typical of warm and wet climates today (Figs. 7, 8), the appearance of new genera and morphotypes including riparian conifers (Figs. 3, 6), and a decrease in non-riparian conifers and site M_A (Figs. 5, 6). However, reliable tests of generalized patterns across the MCO onset for the PNW, as proposed in our hypotheses, are strongly limited by only a single pre-MCO flora included in nearly all analyses, as well-sampled early Miocene floras, particularly east of the modern Cascade Mountains, are exceedingly rare (e.g., Graham 1999). Even when Fossil HS is included in certain analyses (i.e., leaf margin analysis, palynomorph analyses), the early Oligocene age of this flora (33.1 Ma or 16 myr prior to the MCO onset) limits interpretations of conditions leading up to the MCO warming. A collection of potentially early Miocene localities occur in the western Cascades (Peck et al. 1964; Wolfe 1969)

and offer future potential for addressing the MCO onset through providing reliable radiometric dates and renewed investigation of paleoclimate and paleovegetation.

Paleoeleveation Patterns.—Differences of paleoelevation among floras potentially confound interpretations of regional climatic response to Miocene global change events. Anomalously cool MAT was reconstructed at Moose Mountain (via leaf physiognomy) and Trout Creek (via bioclimatic analysis) (Fig. 8). In addition, the morphotype composition of both floras deviates from other MCO floras, with Trout Creek most similar to post-MCO floras also reconstructed as relatively cooler, and Moose Mountain relatively distinct from all others (Fig. 2). Both floras are the only two MCO floras of this study where riparian conifers, typical of more lowland swamps (e.g., *Taxodium*, *Glyptostrobus*), are absent and pollen of the Cupressaceae/Taxaceae, the group to which these conifer taxa belong, is in relatively low abundance (although pollen were not recovered from Trout Creek; Fig. 7). Taphonomic factors are unlikely to be the cause of these differences as fossils of both sites were deposited in lacustrine shales, consistent with other MCO floras.

Our inferences from floral analysis are consistent with previous paleobotanical interpretations and independent evidence indicating that Moose Mountain and Trout Creek represent relatively higher paleoelevations. Prior work on the Trout Creek flora suggested it was deposited in an upland lake based on floral composition and comparison to modern relatives (MacGinitie 1933; Axelrod 1964; Graham 1965). Axelrod (1964) also noted taxonomic similarity between Trout Creek and the post-MCO Trapper Creek, likening both to a mixed conifer-hardwood forest (although he considered them to be concurrent in age). Subsequent reinterpretation of the Trout Creek Formation indicates lacustrine deposition within the

Whitehorse Caldera (Rytuba et al. 1981; Benson et al. 2017), which agrees well with our date of Trout Creek Fm. deposits (Table 2), and is consistent with local-regional high elevations.

The compositional distinctness of Moose Mountain relative to other MCO floras (e.g., Fig. 2), including a lack of pinnately lobed *Quercus*, led to an incorrect age assignment of late Oligocene to early Miocene (Wolfe 1962; Peck et al. 1964; Wolfe and Tanai 1987). However, the flora was grouped with several others whose floral character was said to represent a subtropical to "very warm temperate" climate (Peck et al. 1964). Our revised morphotype framework also does not indicate a taxonomic composition consistent with cooler climates (Fig. 8C, D), and includes a prevalence of genera more common in Eocene and Oligocene floras (e.g., *Trochodendron, Concavistylon, Exbucklandia,* and a foliar morphotype reminiscent of *Fagopsis* [MM014]). Instead, cooler temperature reconstructions are driven by a low percentage of entire-margined leaves (17%).

High paleoelevations at Moose Mountain are also suggested by geologic mapping. Silicic vent structures (e.g., those of stratovolcanoes) of the Little Butte Volcanic Series are mapped along a north-south trend in the Western Cascades, proposed to represent a volcanic chain. The Moose Mountain flora occurs near this axis, further east from other western Cascade Oligocene-Miocene sites (Fig. 1; Peck et al. 1964). However, this interpretation is complicated by our U-Pb dates (Table 2) which more likely places Moose Mountain in the Sardine Fm. On the other hand, many exposures previously mapped as Little Butte Volcanic Series have been subsequently mapped in the Sardine Fm. (Beaulieu et al. 1974; Walker and Duncan 1989) and both formations are predominantly volcanic. Alternatively, volcanic disturbance may have influenced a lower margin percentage within an otherwise warm temperate forest (e.g., Kappelle and Leal 1996, Lowe et al. In Review*a*), explaining the discrepancy between temperature reconstructions from

leaf physiognomy and bioclimatic analysis. That said, many other MCO sites are also intimately associated with volcanism but do not have such low margin states. Thus, we find the preponderance of evidence most consistence with Moose Mountain occupying high paleoelevations. As noted above, we exclude both Trout Creek and Moose Mountain from the following of lowland MCO climate.

Paleoclimate in MCO (lowlands).—Reconstructions during the MCO suggest an average MAT of 12-15°C, MAP of 117-146 cm/yr, and CQT of 5-6°C. MCO temperature was generally higher than what occurs in modern PNW lowlands (Fig. 8), consistent with our hypothesis (H1). The presence of several exotic taxa in MCO floras that are today sensitive to summer drought (Fig. 5), suggests an ever-wet or summer-wet, rather than the summer-dry (Mediterranean) climate that characterizes the PNW today. Annual precipitation amount appears similar to that occurring in PNW lowlands on the wetter west of the Cascades today (Fig. 9). Such climatic parameters are consistent with the establishment of mixed broadleaf evergreen and deciduous forests and mixed mesophytic forests (Wolfe 1979).

PNW temperature and precipitation reconstructions during the MCO generally agree with that proposed by previous paleobotanical studies based on climatic preferences of modern relatives (e.g., Chaney and Axelrod 1959; Graham 1965, Smiley and Rember 1985*a*), including an inferred ever-wet or summer-wet precipitation regime (e.g., Mustoe and Leopold 2014; O'Keefe et al. 2024). In contrast, an integrated record of clay and carbonate $\delta^{18}O$ across much of the Cenozoic reconstrued the PNW as summer-dry (Mediterranean) during the MCO and persisting across the MMCT, with prevalent open habits (marking the "open habitat transition") and woody taxa restricted to areas where "conditions remained favorable" (e.g., riparian zones) (Kukla et al. 2022). We suspect that the richness of woody plants in both macrofossil and pollen

records, including several exotic taxa that do not occur today in summer-dry climates, and dominance of closed forest indicator phytoliths observed in our MCO fossil floras, is inconsistent with the restriction of closed canopy forests to riparian zones. We encourage further work to reconcile these diverging interpretations from PNW paleobotanical and geochemical evidence. Our precipitation estimates are much less variable, and generally wetter than those using $\delta^{13}C$ of fossil teeth, particularly for the Succor Creek where an arid climate was previously reconstructed (Drewicz and Kohn 2018). Our MCO temperature estimates roughly agree with global terrestrial proxy compilations (predominately palaeobotanical-based), albeit on the cooler end, and paleoclimate modeling results of mid-latitudes (Krapp and Jungclaus 2011; Goldner et al. 2014).

General character of paleovegetation.—During the MCO, lowland forests of the Pacific Northwest are reconstructed as dominated by deciduous angiosperms with intermixed evergreen angiosperms, riparian conifers, and non-riparian conifers, with a minor contribution of predominately Pooideae grasses (Fig. 7). Preliminary results of phytolith analyses suggest that MCO vegetation represents closed canopy forests (Fig. 7E). These vegetational characters are consistent with a mixed mesophytic forest type (Wang 1961; Braun 1964; Wolfe 1979; Dyer 2006), in support of our hypothesis (H3). MCO floras were rich in exotic taxa (40.7-52.4%), including gymnosperms (e.g., *Cunninghamia, Metasequoia, Taxodium, Glyptostrobus, Ginkgo, Amentotaxus,* and *Tetraclinis*), and angiosperms (e.g., *Magnolia, Liquidambar, Pterocarya, Fagus, Nyssa, Liriodendron, Mezoneuron, Cedrela, Exbucklandia, Comptonia, Cercidiphyllum, Ailanthus*, and rare occurrences of bamboos [Bambusoideae], palms [Arecaceae], and gingers and relatives [Zingiberales]). Prevalent taxa in MCO forests that still occur along the west coast today include conifers such as *Abies*, *Picea, Tsuga, Pinus, Calocedrus,* and *Sequoia*, and angiosperms such as *Acer, Quercus, Betula, Alnus, Fraxinus, Platanus, Fabaceae, Berberis,* and

Amelanchier. This floristic composition is generally similar to mixed mesophytic forests of the eastern US and east Asia (Wang 1961; Braun 1964). In addition, the PNW MCO forests contained several extinct genera, including *Pseudofagus, Nordenskioldia/Zizyphoides, Ozakia,* and *Diplodipelta*.

Our reconstruction of paleovegeation type agrees well with that of prior work (e.g., Table 1), and other regional floras including the Red Lake flora of southern British Columbia (Greenwood et al. 2020). Similar warm temperate evergreen broadleaf and mixed forests types have been reconstructed across mid latitudes of the Northern Hemisphere during the MCO (Pound et al. 2012). Phytolith evidence suggesting open habitat vegetation near the Idaho-Montana border (Harris et al. 2017), which may reflect a Rocky Mountain environment distinct from the PNW.

Spatial heterogeneity in lowland paleovegetation.—Spatial heterogeneity characterized PNW lowland floras during the MCO. For example, the composition of Watersnake plots intermediate in similarity between Trout Creek and the Columbia Basin (Clarkia, Spokane, Juliaetta)/Mascall cluster. Several taxa prevalent in the latter cluster are absent in Watersnake (e.g., *Alnus relatus,* Fabaceae foliage M1 [*Sophora*-like]) including several that are either rare or absent in the greater Succor Creek flora (e.g., *Liquidambar pachyphyllum, Populus lindgreni, Quercus pseudolyrata*; Fields 1996). Fields (1996) also noted the similarity of Succor Creek and Trout Creek, relative to Columbia Basin floras and Mascall, suggesting their shared proximity to calderas and volcanic activity as a likely explanation (Fig. 1). In agreement with a volcanic influence, the Watersnake and Trout Creek floras have the two lowest evenness values among woody non-monocot angiosperms (WNMAs), consistent with strong filtering acting in early succession environments (Currano et al. 2011; Poorter et al. 2024). These points indicate that

deviation of Watersnake from Columbia Basin/Mascall floras may be a result from enhanced volcanic disturbance from silicic eruptions (e.g., Taggart and Cross 1990; Schiller et al. 2024), in contrast to the several other MCO sites that are closely associated with basalt volcanism (Fig. 1). We note that Watersnake is also intermediate between Columbia Basin/Mascall sites and Trout Creek in both age (Table 2) and location (Fig. 1), and thus consider this question of relative similarity unresolved.

Columbia Basin floras and the Mascall flora are less similar to one another when considering relative abundance. Modern mixed mesophytic forests are characterized by the shared dominance of several species (high evenness), which results in considerable differences in the composition and relative abundance in local habitats within the general forest type (Wang 1961; Braun 1964; Wolfe 1979; Dyer 2006). For example, oak and hickory (most abundant at Mascall) often dominate in the western mixed mesophytic forests, swamp cypress, oak, poplar, and alder (most abundant at Juliaetta) can dominate in lowland alluvial plains, and mixed forests of swamp cypress, oaks, chestnuts, birches, beech, and legumes (most abundant at Clarkia) are consistent with both mixed mesophytic forests and alluvial plains (Braun 1964; Dyer 2006). While we do not suggest that these offer exact analogs for the fossil sites, we find the differences in relative abundance within the Columbia Basin/Mascall cluster to be consistent with that found in modern mixed mesophytic forests.

The Middle Miocene Climatic Transition

Paleoclimate (lowlands).—Paleoclimate reconstructions across the MMCT are variable regionally within the PNW. Pronounced climatic change is recorded for the Snake River Plain (SRP; Pickett Creek and Trapper Creek), including decreased annual and winter temperatures by 3.4 and 3.3 °C, respectively (Fig. 8), and a likely decrease in mean annual precipitation by ~27

cm/yr (Fig. 9). Cooling of annual temperatures resulted in modern-like values, with winter temperatures intermediate of those occurring east and west of the Cascades today (Fig. 8), while annual precipitation was still consistent with the wetter west side of the range (Fig. 9). Post-MCO reconstructions agree with prior work at Trapper Creek which utilized floral composition and comparison to modern relatives (Axelrod 1964), but MAT is higher than previously published at Pickett Creek using the leaf physiognomy technique CLAMP (10.0 °C vs. 13.4 °C; Buechler et al. 2007). This is influenced (at least in part) by the greater number of entire-margined Fabaceae foliar morphotypes (Appendix 7) and thus higher leaf margin percentage in the framework of Buechler et al. (2007) (54% vs. 27%). The post-MCO climate reconstructed for the SRP is consistent with the establishment of mixed broad leaf deciduous forests, mixed coniferous forests (where summer temperature and/or precipitation is relatively low), and mixed northern hardwood forests (Wolfe 1979).

Paleoclimatic changes in the SRP are accompanied by a loss of exotic taxa (Fig. 4A) that today grow in relatively warmer and wetter climates that lack summer drought (Fig. 5). This pattern was noted by several earlier studies who attribute the change to decreased summer rain (Wolfe 1981; Axelrod 1992; Axelrod and Schorn 1994; Fields 1996; Graham 1999). Suggested drivers of seasonal precipitation onset include increasing latitudinal temperature gradients intensifying subtropical high pressure systems (Wolfe 1981), the cooling of the Pacific sea surface and strengthening of ocean-land temperature gradients (Axelrod 1992), and the establishment of the California current ~10-7.6 Ma (Barron et al. 2002; Kohn and Fremd 2008). In contrast, Mustoe and Leopold (2014) found that late Miocene floras from the western Columbia Basin share high taxonomic similarity to modern summer-wet eastern US deciduous forests throughout the late Miocene. Trapper Creek was found to be more dissimilar to these

modern eastern US forests, but the authors posit that the presence of several deciduous hardwood taxa still indicated summer-wet climates. We consider the question of exactly when and why summer-dry (Mediterranean) climates established in the Pacific Northwest an open and intriguing question, which would benefit from collaboration with earth system modelers and paleooceanographers.

In the Puget lowlands, climatic reconstructions at the Vasa Park site are mixed, with DiLP and BA reconstructing no change in MAT across the MMCT, while leaf margin analysis reconstructed change comparable to the SRP (Fig. 8). We favor the interpretation that MAT change across the MMCT was tempered along the coast, with the Puget lowland ~1.7 °C higher in MAT than the SRP, given the agreement between two different proxies (DiLP and BA) and a greater number of physiognomic characters included in DiLP, relative to leaf margin analysis. Further, Dillhoff et al. (2014) reconstructed MAT at Vasa Park consistent with our DiLP and BA reconstructions (11.6-16.6 °C) using a separate data source (pollen) and proxy (coexistence analysis). However, reconstructed winter temperatures decreased across the MMCT, comparable to the SRP (Fig. 8D), which along with similar decreases in the percentage of evergreen species (see below), suggest that tempered MAT near the coast may have been driven by warmer summers.

Depositional environments vary between Vasa Park and the SRP sites (fluvial and lacustrine, respectively), which may confound comparisons of climate and vegetation. Fossil plants deposited in fluvial environments are typically sourced from a smaller area (Wing and DiMichele 1995) with greater bias toward riparian species, relative to lacustrine environments. A local riparian bias is consistent with relatively few conifers represented as macrofossils at Vasa Park, yet moderate counts of more widely dispersed conifer pollen, and the abundance of *Alnus*

leaves, a common riparian plant today. However, bias towards riparian environments is also associated with a greater proportion of toothed leaves, driving colder, not warmer, paleoclimate estimates (Greenwood 1991; Kowalski and Dilcher 2003; Royer et al. 2009). In addition, the Vasa Park pollen assemblage, which is less sensitive to local riparian biases, is most similar in composition to the warm and wet Clarkia assemblage, and relatively dissimilar to SRP assemblages (Fig. 2D).

In summary, we find that annual and winter temperatures and annual (and potentially summer) precipitation decreased in the PNW interior but that this decrease was tempered near the coast where temperature and precipitation remained at MCO-like condition, in support of our hypothesis (H2). These results are consistent with many previous studies reconstructing cooling and drying of continental climates using paleobotanical-based proxies across the MMCT in Eurasia and beyond (Mosbrugger et al. 2005; Syabryaj et al. 2007, Utescher et al. 2007*a*, *b*; Bruch et al. 2011; Pound et al. 2012; Dunn et al. 2015; Kayseri-Özer 2017; Kovar-Eder et al. 2021).

Paleovegetation.—Post-MCO floras of the PNW record considerable changes in plant community composition, ecology, and structure across the MMCT. As with paleoclimate, patterns of change vary regionally within the PNW. However, both the SRP (Trapper Creek, Pickett Creek) and Puget lowlands (Vasa Park) record a reduction in the number of evergreen WNMA taxa to percentages intermediate of modern communities in cool and warm temperate climates (Fig. 6A), in support of our hypothesis (H4). This pattern is consistent with decreases in winter temperature reconstructed in both regions (Fig 7D), and indicates a change from the warm temperate mixed mesophytic forests of the MCO to more cool temperate vegetation. These changes are accompanied by considerable turnover in foliar morphotypes (Fig. 3A). At the

genus-level, however, there is a lack of significant turnover and instead nearly all genera (except *Sequoiadendron* in the SRP) persist from the MCO (Fig 3B). This pattern of compositional change is known as nestedness and is an important component of beta diversity (Baselga 2010). For example, in modern forests of China, spatial transitions from mixed mesophytic to more deciduous-dominated northern hardwood forests also involve nestedness, as most tree genera of the latter are represented in the former but by distinct species (Wang 1961). Thus temporal transitions documented here match with spatial transitions in similar modern forest types, and suggest that dynamics of change may be similar—reminiscent of Braun (1964)'s suggestion that mixed mesophytic forests are the ancestors to other deciduous-dominated humid forest types.

For the SRP, nestedness across the MMCT is accompanied with a loss of several genera in both the macrofossil and palynomorph records (Fig. 3), and a general reduction in the evenness of WNMAs (Fig. 4B, C), in support of our hypothesis (H5). There is a disproportionate loss among exotic, relative to remnant, taxa (Fig. 4A), including all riparian conifers, several non-riparian conifers (e.g., *Amentotaxus, Tetraclinis, Cunninghamia*, and *Cathaya*), and many angiosperms (e.g., *Cedrela, Exbucklandia, Ilex, Liquidambar, Liriodendron, Magnolia, Paliurius, Tilia, Cercidiphyllum, Fagus, Hydrangea*, and *Nyssa*). However, several exotic taxa persist, including *Comptonia, Ostrya, Pterocarya, Ulmus,* and *Sassafras.* These changes reveal a step in the modernization of interior PNW floras during the MMCT, but show that modernization was not completed, with late Miocene forests still fairly distinct from those in the PNW today.

Phytolith evidence indicates an increase in open-habitat grasses across the MMCT in the SRP (Fig. 7E), suggesting a local-regional mixed grassland-forest mosaic or a relatively open woodland. Morphotypes typical of Pooideae grasses were the most abundant among grass phytoliths, a clade that includes C_3 taxa prevalent in relatively cooler climates today, including

the PNW (Leopold and Denton 1987). Thus, phytolith and macrofossil evidence both indicate that the MMCT represents an important step in the modernization of PNW vegetation. The establishment of more open-habitat vegetation was likely influenced by reconstructed drying in the SRP and potentially a shift to a more frequent fire regime (Sankaran et al. 2005; Lehmann et al. 2014), as observed in other regions during the late Miocene (e.g., Karp et al. 2018; Loughney et al. 2023). Lower precipitation can also lead to a greater prevalence of "slow" leaf economic strategies (i.e., high M_A) (Wright et al. 2004*a*), and confound the positive relationship between % evergreen and temperature seasonality (Lowe et al. In Review*b*), likely explaining why Trapper Creek has a high M_A despite having low % evergreen (Fig. 6).

Vegetation differences were observed not just between the coast and interior, but also among the interior SRP floras. Conifer macrofossils are more abundant and diverse, and conifer pollen more abundant, at Trapper Creek compared to Pickett Creek (Fig. 7). In addition, lobed oaks were the most abundant leaf at Pickett Creek (56.4 %), where similarity was drawn to California oak woodlands (Buechler et al. 2007), but are absent from Trapper Creek. Axelrod (1964) considered Trapper Creek to represent a relatively high elevation montane conifer-hardwood forest, and considered lobed oaks to indicate warmer lower elevations, through comparison to MCO floras of the PNW which he considered at the time contemporaneous. Trapper Creek and Pickett Creek offer more reliable points of comparison as both occur after the MMCT and span two structural regions (western vs. eastern Snake River Plain), although ~1.6 million years of time separates them. It is true that, in deciduous dominated forests, lobed oaks are less prevalent in the cooler mixed northern hardwood forests (Wang 1961; Braun 1964). However, considering the modern distribution of all taxa identified in these two floras, and

patterns of leaf physiognomy, we find no evidence for differences temperature or precipitation (Figs 7D, 8C), suggesting no major elevational difference.

Thus, differences in conifer diversity and relative abundance (Fig. 7), and in the numerical dominants of foliar morphotypes and palynomorphs (Fig. 2) likely reflects spatial heterogeneity across a region with relatively similar macroclimate. Heterogeneity may be related to disturbance, considering differences in WNMA evenness between the two floras (Fig. 4B, C) and evidence for relatively open habitats where fire may have been important (Sankaran et al. 2005), or minor differences in landscape position (e.g., slope aspect). Similar transitions can occur between ecotones of oak hardwood and mixed evergreen forests in lowlands of Oregon and California, which may offer a rough analog (Franklin and Dyrness 1973; Wolfe 1979). Alternatively, differences may result from varying taphonomic biases (e.g., preservation, transport), as the Pickett Creek flora occurs in a diatomite with many exceptionally preserved fossils, while the Trapper Creek flora occurs in moderately-laminated siltstones with a poorer quality of preservation.

In the more coastal Puget lowlands, changes in plant community composition post-MCO is shown through dissimilarity of foliar morphotypes (presence-absence) between Vasa Park and MCO floras (Fig. 2). While several MCO genera do not occur in the Vasa Park flora, the loss of genera is less severe compared to the SRP (Fig. 3). For example, several exotic genera that do not persist in the SRP occur in the warmer and wetter Vasa Park flora (Figs. 3, 4A), including *Cercidiphyllum*, *Fagus*, *Hydrangea*, *Ilex*, *Liquidambar*, *Nyssa*, and *Paulownia*. Although non-riparian conifers are also absent at Vasa Park, *Taxodium* occurs along with several other exotic taxa at late Miocene floras along the western Columbia Basin (Smiley 1963; Leopold and Denton 1987; Mustoe and Leopold 2014). Phytolith evidence from Vasa Park suggests a closed

canopy forest and of the grasses present, the relatively thermophilic PACMAD group dominated (Fig. 7E), consistent with generally warm climate reconstructions. Given relatively cooler winter temperatures (Fig. 8) and a reduction in the percentage of evergreen species (Fig. 6A), Vasa Park paleovegetation is consistent with a mixed broad leaf deciduous forest (Wolfe 1979).

These results suggest a tempering of climate change near the coast influenced a less severe loss of exotic taxa, and further points to a west-east continentality gradient. A decrease in the percentage of evergreen species across the MMCT agrees with prior work in the PNW (Wolfe 1981) and recorded transitions of mixed mesophytic forests to broadleaf deciduous forests throughout much of western and southwestern Eurasia (Mosbrugger et al. 2005; Syabryaj et al. 2007, Utescher et al. 2007*a*, *b*; Bruch et al. 2011; Kayseri-Özer 2017; Kovar-Eder et al. 2021). An increase in open habitats across the MMCT was also found in Patagonia (Dunn et al. 2015). Lastly, our results contrast with a prior palynological study that found that volcanic disturbance rather than climate was the primary influence of plant community change in the Columbia Basin across the MMCT (Ebinghaus et al. 2015), and highlight the utility of combining fossil plant types for an integrated view of local-regional paleoclimate and paleovegetation.

Global climate or regional uplift?—Changes in paleoclimates and paleovegetation recorded across the MMCT by SRP floras may result from either global climate change or regional uplift. Similarly, differences between the Puget lowlands and the SRP in the late Miocene may result from coast-interior climatic gradients or regional uplift. We argue that while the influence of regional uplift is difficult to fully dismiss, global climatic changes is a likely driver.

Regional uplift of the Cascade Mountains has potential to affect climate of the PNW interior, particularly through the development of a leeward rain shadow. However, timing of the

uplift of the Cascades to significant, near-modern heights is currently debated. The presence of an arc-related volcanic chain (i.e., the "ancestral Cascades") since at least the Oligocene time is clear (Robinson et al. 1984; Tabor et al. 1984; du Bray and John 2011). Studies reconstructing gradients of stable isotopic composition of precipitation across the southern Cascade axis (WA and OR) consistently report a rainout effect in keeping with considerable topography from late Oligocene or middle Miocene (Kohn et al. 2002; Takeuchi and Larson 2005; Bershaw et al. 2019; Pesek et al. 2020; McLean and Bershaw 2021), but not in the late Eocene to early Oligocene (Methner et al. 2016). Integrated clays and carbonate $\delta^{18}O$ point towards decreased winter precipitation during the late Oligocene to early Miocene in the PNW, Rocky Mountains, and Great Plains, which the authors suggest was driven by the rise of the Cascades (Kukla et al. 2022). A shift from temperate wet to arid ecosystems at 10-5 Ma in the Columbia Basin was interpreted through gradients of pedogenic carbonate $\delta^{13}C$ across the Cascade axis, which the authors attribute to the rise of Cascades (Takeuchi et al. 2010). In addition, the distribution of middle Miocene CRBs suggest that the ancestral Cascades were a prominent barrier to flow, with CRBs crossing the Cascade axis only through the Columbia trans-arc lowland, along the present-day Columbia River (Reidel et al. 2013*a*).

In contrast, post-deposition deformation of the CRBs point to significant uplift occurring more recent than the middle Miocene (Cheney 1997), agreeing with increased exhumation rates calculated for the late Miocene (12-8 Ma) using thermochronology methods (Reiners et al. 2002). Fossil plants offer an important opportunity to assess the strength of the rain shadow by considering emergent effects of sensitive ecosystems. Late Miocene floras of the western Columbia Basin share high taxonomic similarity with humid eastern US deciduous forests, comprised of several taxa that today are known only from humid environments (e.g., *Taxodium,*

Liquidambar, Nyssa), and to late Miocene floras on the west side of the Cascade range (Leopold and Denton 1987; Mustoe and Leopold 2014), including Vasa Park. Thus, paleobotanical evidence suggest no evidence for a significant rain shadow until the latest Miocene or Pliocene. Clearly there is a pressing need to reconcile different patterns in isotopic and palaeobotanical studies, but we currently favor interpretations involving more direct evidence of ecosystem impact afforded by fossil plant records, suggesting a lack of significant rain shadow from the Cascade Mountains during the middle and late Miocene.

Alvord Creek, Pickett Creek, and Trapper Creek occur adjacent to, or within, Basin and Range mountains (i.e., Steens Mountain, Owyhee Mountains, and Cassia Mountains, respectively) whose uplift could have impacted local-regional climate. However, Basin and Range extension initiated in the middle Miocene (Colgan and Henry 2009), precluding its influence on the late Oligocene Alvord Creek flora. In addition, the ~11 Ma Jump Creek rhyolite is exposed in higher elevations of the Owyhee Range suggesting significant post-depositional uplift (Bonnichsen et al. 2016). Lastly, the Cassia Mountains appeared to have not been a high elevation center during deposition of the Trapper Creek flora (Axelrod 1964), or during deposition of the overlying Cassia Formation (Knott et al. 2016). Thus, we consider Basin and Range mountain building as an unlikely driver of regional macroclimate patterns recorded in this study.

Today, the Yellowstone hotspot creates a topographic swell up to 1 km in height and ~350-400 km across, driven mainly from dynamic and thermal buoyancy above the plume (Pierce and Morgan 1990; Vogl et al. 2014), and may have driven high local-regional elevation during late Miocene. Flexural uplift resulting from surface and mid-crustal emplacement of dense mantle-derived magma in the eastern Snake River plain may also contribute to uplift of

basin margins (Vogl et al. 2014; Knott et al. 2016). During deposition of the Trapper Creek and Pickett Creek floras, the Yellowstone hotspot fed the Bruneau-Jarbridge volcanic field that occurred between them (Fig. 1; Bonnichsen et al. 2008), and may have influenced paleoelevation in a similar manner to the hotspot today. In fact, we infer relatively high elevations for the MCO Trout Creek flora which was situated over the hotspot in the McDermitt Volcanic Field during the MCO (Benson et al. 2017).

Studies of exhumation based on thermochronologic methods provide important insight to this issue. In the eastern Snake River Plain, cooling ages indicate rapid exhumation of Pioneer-Boulder Mountains on the north margin of the Snake River Plain and a similar longitude to Trapper Creek from 11-8 Ma (Vogl et al. 2014), but after deposition of the Trapper Creek flora (Table 2). In the western Snake River plain where Pickett Creek occurs, mountain fronts on the SW and NW margins show evidence for limited Miocene exhumation, suggesting that extensional-related subsidence of the western SRP was accommodated instead by intra-basin faulting and basalt diking (Wetzel and Stanley 2022). Detrital zircon analyses indicated the presence of a topographic swell over the Twin Falls volcanic field by 9 Ma, but do not provide evidence for uplift during the time of fossil deposition (Beranek et al. 2006). Lastly, Yellowstone hotspot volcanics in the Cassia Hills (11.3 – 8.1 Ma), immediately west of the Trapper Creek site and overlying the Beaverdam Fm., point to eruption in a topographically depressed basinal setting, suggesting that elevated topography of the modern Yellowstone hotspot did not characterize all Snake River plain eruptive centers (Knott et al. 2016). Thus, we conclude relatively cooler temperatures of the SRP floras to be unlikely driven by the presence of a hotspot-driven topographic swell.

Similar paleoclimate estimates between the two sites, which occur in two separate structural domains (eastern vs. western SNP), may be more easily explained by a far-reaching global climatic influence, as compared to local-regional tectonics. In addition, plant community changes, including a reduction in exotic taxa, have been reported across the MMCT among interior floras beyond the SRP (e.g., Axelrod 1992; Axelrod and Schorn 1994).

Rather than invoking rain shadows and other tectonic influences, differences in climate and vegetation between the more coastal Vasa Park and interior SRP sites could potentially be explained by coast-interior climatic gradients. Oceans are well known to buffer seasonal variation in climate and drive coast-interior variation in temperate, particularly in winter temperatures, but sometimes in annual temperatures as well (e.g., France to Germany). It is, however, difficult to reconcile a lack of coast-interior gradient reconstructed for CQT (Fig. 8). Coast-interior gradients in precipitation can be strong with progressive rain out, particularly along the primary moisture transport vector, even without the influence of mountains and rain shadows (e.g., southern Spain, northern France, the UK).

In summary, given thermochronologic evidence which points to limited exhumation in the Snake River Plain during Trapper Creek and Pickett Creek deposition, similar paleovegetation and paleoclimate estimates despite occurring in distinct structural domains, and reports of similar plant community changes in the western US beyond the SRP, we favor the interpretation that global climatic changes of the MMCT drove regional changes in paleoclimate and palevegetation, that were more pronounced in the interior relative and tempered near coast, reflecting the influence continentality of coast-interior climate gradients. These changes thus mark important steps in the modernization of PNW climates and ecosystems. We however recognize that patterns of paleoclimate and paleovegetation across the western US more broadly

are heterogenous and likely influenced in part by patterns of regional uplift (Strömberg 2005; Harris et al. 2017, 2020; Kukla et al. 2022).

Conclusions

Reconstructions of plant community ecology and climate using an integrated suite of fossil plant types within a refined temporal framework demonstrate important influences of global Miocene climate on PNW environments. Generalizable interpretations of changes at the MCO onset are limited by a small sample of pre-MCO sites. Nevertheless, fossil plant-based paleoclimate estimates suggest the MCO was warmer and wetter relative to the pre-MCO Alvord Creek site, with relatively distinct plant community composition including a greater abundance of non-riparian conifers and lacking riparian conifers.

During the MCO, lowland PNW annual and winter temperatures were elevated relative to modern, by ~3.7 °C, broadly agreeing with proxy compilations and modeling results of Northern Hemisphere mid-latitudes. Precipitation was similar to the modern (wetter) west side of the Cascade Range but was likely ever- or summer-wet. Integrated fossil evidence indicates that MCO plant communities represented mixed mesophytic closed canopy forests and associated swampy lacustrine margins, with some variation in dominant taxa between floras.

Global cooling of the MMCT impacted PNW climate and plant communities, with a considerable drop in winter temperatures (by 3.0 °C) and, accordingly, the percentage of evergreen WNMA taxa. A drop in annual temperature (by 3.7 °C) and precipitation (by 26.8 cm/yr) occurred in the PNW interior but was tempered closer to the coast, demonstrating the influence of continentality. In the interior SRP, morphotypes (roughly equivalent to species) record consider turnover and a general decrease of WNMA diversity, while genera present in all

but one case were also present during the MCO. A pattern of nestedness for genera, but turnover among species, can be explained by in situ diversification or immigration of novel species within persistent genera, a pattern found across humid deciduous forests today. Not all MCO genera persisted across the MMCT however, and the SRP records a considerable decrease in the number of exotic taxa, that today live in relatively warmer and wetter climates that lack summer drought, representing an important stage in the modernization of PNW vegetation. Phytolith and pollen evidence indicates the presence of open habitat vegetation in the SRP, consistent with regional drying and unchanging M_A despite a relatively fewer number of evergreen species. Tempered climatic changes in the more coastal Puget lowland also tempered the loss of exotic taxa while there, where closed canopy forests persisted with an increasing prevalence of 'fast' leaf economic strategies, favored in shorter (colder winters) yet more productive (wetter) growing seasons.

Although there is a possibility that regional uplift in the SRP driven by the underlying Yellowstone hotspot influenced reconstructed climatic change, we find thermochronology and paleobotanical evidence to suggest a global climatic driver, and associated coast-interior climatic gradients, as the most likely driver of regional change. This contrasts with previous palynological work in the Columbia Basin, suggesting limited influence of regional climate on plant communities across MMCT, and highlights the utility of integrating complimentary lines of paleobotanical evidence.

Acknowledgments

Funding was supported by NSF PNW EAR-1924390 to C.A.E.S., by a Geological Society of America Graduate Student Research grant to A.J.L. We thank Regan Dunn for assistance in the field and providing phytolith counts from Mascall. We thank Robert Rosé for

assistant and the field, access to private collections, and for donations to the Burke Museum. We thank several collections managers and staff for logistical support including Paige Wilson-Deibel, Katherine Anderson, Ron Eng, Diane Erwin, Adam Rountrey, and Scott Wing. We thank the many students and volunteers who assisted with fossil collection, cataloging, photography, and preparation, and members of the UW undergraduate "Team Fossil Leaf" for assistance with Digital Leaf Physiognomy measurements. Thank you to Alex Arrendale and Abigail Riley for preparing phytolith slides. We thank Steve Manchester, Herbert Meyer, Abby Swann, and Janneke Hille Ris Lambers for helpful insight, discussion, and/or edits to this manuscript.

Literature cited

Allen, C. M., and I. H. Campbell. 2012: Identification and elimination of a matrix-induced systematic error in LA–ICP–MS $^{206}Pb/^{238}U$ dating of zircon. Chemical Geology 333:157–165.

Andrés-Hernández, A. R., and T. Terrazas. 2009: Leaf architecture of *Rhus* s.str. (Anacardiaceae). Feddes Repertorium 120:293–306.

Ashlee, T. R. 1932: A contribution to the Latah flora of Idaho. Northwest Science 6:69–82.

Axelrod, D. I. 1964: The Miocene Trapper Creek flora of southern Idaho. University of California Publications in the Geological Sciences 51:148.

Axelrod, D. I. 1992: Miocene floristic change at 15 Ma, Nevada to Washington, USA. Journal of Palaeosciences 41:234–239.

Axelrod, D. I., and H. E. Schorn. 1994: The 15 Ma Floristic Crisis At Gillam Spring, Washoe County, Northwestern Nevada. PaleoBios 16:1–7.

Axelrod, D. L. 1944: The Alvord Creek flora. Carnegie Institution of Washington 553:225–262.

Badger, M. P. S., C. H. Lear, R. D. Pancost, G. L. Foster, T. R. Bailey, M. J. Leng, and H. A. Abels. 2013: CO_2 drawdown following the middle Miocene expansion of the Antarctic Ice Sheet. Paleoceanography 28:42–53.

Baghai, N. L. 1988: *Liriodendron* (Magnoliaceae) from the Miocene Clarkia flora of Idaho. American Journal of Botany 75:451–464.

Barbolini, N., A. Woutersen, G. Dupont-Nivet, D. Silvestro, D. Tardif, P. M. C. Coster, N. Meijer, C. Chang, H.-X. Zhang, A. Licht, C. Rydin, A. Koutsodendris, F. Han, A. Rohrmann, X.-J. Liu, Y. Zhang, Y. Donnadieu, F. Fluteau, J.-B. Ladant, G. Le Hir, and C. Hoorn. 2020: Cenozoic evolution of the steppe-desert biome in Central Asia. Science Advances 6:eabb8227.

Barron, J. A., M. Lyle, and I. Koizumi. 2002: Late Miocene and early Pliocene biosiliceous sedimentation along the California margin. Revista Mexicana de Ciencias Geologicas 19:161–169.

Barrow, K. T. 1983: Trout Creek Formation Southeastern Oregon: Stratigraphy and Diatom Paleoecology.vM.S. thesis, Stanford University, Stanford, California, 121 pp.

Baselga, A. 2010: Partitioning the turnover and nestedness components of beta diversity. Global Ecology and Biogeography 19:134–143.

Beaulieu, J. D., P. W. Hughes, and R. K. Mathiot. 1974: Environmental geology of western Linn County, Oregon. Oregon Department of Geology and Minderal Industries, Portland, Oregon.

Benson, T. R., and G. A. Mahood. 2016: Geology of the Mid-Miocene Rooster Comb Caldera and Lake Owyhee Volcanic Field, eastern Oregon: Silicic volcanism associated with Grande Ronde flood basalt. Journal of Volcanology and Geothermal Research 309:96–117.

Benson, T. R., G. A. Mahood, and M. Grove. 2017: Geology and 40Ar/39Ar geochronology of the middle Miocene McDermitt volcanic field, Oregon and Nevada: Silicic volcanism associated with propagating flood basalt dikes at initiation of the Yellowstone hotspot. Bulletin 129:1027–1051.

Beranek, L. P., P. K. Link, and C. M. Fanning. 2006: Miocene to Holocene landscape evolution of the western Snake River Plain region, Idaho: Using the SHRIMP detrital zircon provenance record to track eastward migration of the Yellowstone hotspot. Geological Society of America Bulletin 118:1027–1050.

Berry, E. W. 1929: A revision of the flora of the Latah Formation. USGS Professional Paper 154-H:255–265.

Bershaw, J., E. J. Cassel, T. B. Carlson, A. R. Streig, and M. J. Streck. 2019: Volcanic glass as a proxy for Cenozoic elevation and climate in the Cascade Mountains, Oregon, USA. Journal of Volcanology and Geothermal Research 381:157–167.

Bestland, E. A., M. S. Forbes, E. S. Krull, G. J. Retallack, and T. Fremd. 2008: Stratigraphy, paleopedology, and geochemistry of the middle Miocene Mascall Formation (type area, central Oregon, USA). PaleoBios 28:41–61.

Blaauw, M., and J. A. Christen. 2011: Flexible paleoclimate age-depth models using an autoregressive gamma process. Bayesian analysis 6:457–474.

Bond, J. G. 1963: Geology of the Clearwater Embayment. Idaho Bureau of Mines and Geology, Moscow, Idaho.

Bonnichsen, B., S. Boroughs, M. M. Godchaux, and J. Wolff. 2016: From land to lake: Basalt and rhyolite volcanism in the western Snake River Plain, Idaho *in* Exploring the Geology of the Inland Northwest, R. Lewis, K. Schmidt [eds.]. Geological Society of America 41.

Bonnichsen, B., W. P. Leeman, N. Honjo, W. C. McIntosh, and M. M. Godchaux. 2008: Miocene silicic volcanism in southwestern Idaho: geochronology, geochemistry, and evolution of the central Snake River Plain. Bulletin of Volcanology 70:315–342.

Booth, D. B., T. J. Walsh, K. Goetz Troost, and S. A. Shimel. 2012: Geologic map of the east half of the Bellevue South 7.5' x 15' quadrangle, Issaquah area, King County, Washington. U.S. Geological Survey.

Botsyun, S., T. A. Ehlers, A. Koptev, M. Böhme, K. Methner, C. Risi, C. Stepanek, S. G. Mutz, M. Werner, D. Boateng, and A. Mulch. 2022: Middle Miocene Climate and Stable Oxygen Isotopes in Europe Based on Numerical Modeling. Paleoceanography and Paleoclimatology 37:e2022PA004442.

Bouchal, J. M., T. H. Güner, and T. Denk. 2018: Middle Miocene climate of southwestern Anatolia from multiple botanical proxies. Climate of the Past 14:1427–1440.

Braun, E. L. 1964: Deciduous forests of eastern North America. Hafner Pub. Co., New York.

du Bray, E. A., and D. A. John. 2011: Petrologic, tectonic, and metallogenic evolution of the Ancestral Cascades magmatic arc, Washington, Oregon, and northern California. Geosphere 7:1102–1133.

Brown, R. W. 1937: Additions to some fossil floras of the western United States. USGS Professional Paper 186J.

Bruch, A. A., D. Uhl, and V. Mosbrugger. 2007: Miocene climate in Europe — Patterns and evolution. Palaeogeography, Palaeoclimatology, Palaeoecology 253:1–7.

Bruch, A. A., T. Utescher, and V. Mosbrugger. 2011: Precipitation patterns in the Miocene of Central Europe and the development of continentality. Palaeogeography, Palaeoclimatology, Palaeoecology 304:202–211.

Buechler, W. K. 2008: Revision of fossil willows: *Salix hesperia-S. inquirenda* and *Salix* subgenus Longifoliae groups. Paleobios 28: 62-75.

Buechler, W. K., M. T. Dunn, and W. C. Rember. 2007: Late Miocene Pickett Creek flora of Owyhee County, Idaho. Contributions from the Museum of Paleontology, the University of Michigan 31:305–362.

Burge, D. O., and S. R. Manchester. 2008: Fruit Morphology, Fossil History, and Biogeography of *Paliurus* (Rhamnaceae). International Journal of Plant Sciences 169:1066–1085.

Burls, N. J., C. D. Bradshaw, A. M. De Boer, N. Herold, M. Huber, M. Pound, Y. Donnadieu, A. Farnsworth, A. Frigola, E. Gasson, A. S. Von Der Heydt, D. K. Hutchinson, G. Knorr, K. T. Lawrence, C. H. Lear, X. Li, G. Lohmann, D. J. Lunt, A. Marzocchi, M. Prange, C. A. Riihimaki, A. -C. Sarr, N. Siler, and Z. Zhang. 2021: Simulating Miocene Warmth: Insights From an Opportunistic Multi-Model Ensemble (MioMIP1). Paleoceanography and Paleoclimatology 36:e2020PA004054.

Burnham, R. J., S. L. Wing, and G. G. Parker. 1992: The reflection of deciduous forest communities in leaf litter: implications for autochthonous litter assemblages from the fossil record. Paleobiology 18:30–49.

Burnham, R. J., B. Ellis, and K. R. Johnson. 2005: Modern tropical forest taphonomy: does high biodiversity affect paleoclimatic interpretations? PALAIOS 20:439–451.

Butrim, M. J., A. J. Lowe, A. G. Flynn, A. Baumgartner, D. J. Peppe, and D. L. Royer. 2024: Dilp: Reconstruct Paleoclimate and Paleoecology with Leaf Physiognomy. R package version 1.1.0.

Buzek, C. 1971: Tertiary flora from the northern part of the Petipsy area (North-Bohemian Basin). Rozpravy Úst redního Ústavu geologického, Stuttgart, Germany.

Cáceres, M. D., and P. Legendre. 2009: Associations between species and groups of sites: indices and statistical inference. Ecology 90:3566–3574.

Cahoon, E. B., M. J. Streck, and A. A. Koppers. 2023: Picture Gorge Basalt: Internal stratigraphy, eruptive patterns, and its importance for understanding Columbia River Basalt Group magmatism. Geosphere 19:406–430.

Camp, V. E. 1981: Geologic studies of the Columbia Plateau: Part II. Upper Miocene basalt distribution, reflecting source locations, tectonism, and drainage history in the Clearwater embayment, Idaho. Geological Society of America Bulletin 92:669–678.

Chaney, R. W. 1925: The Mascall flora--Its distribution and climatic relation. Pp.23–48 *in* Studies on the Fossil Flora and Fauna of the Western United States. Vol. 349. Carnegie Institution of Washington.

Chaney, R. W. 1927: Geology and palaeontology of the Crooked River Basin, with special reference to the Bridge Creek flora. Carnegie Institution of Washington, p.

Chaney, R. W., and D. L. Axelrod. 1959: Miocene floras of the Columbia Plateau. Carnegie Institution of Washington Publication 617.

Chao, A., and L. Jost. 2012: Coverage-based rarefaction and extrapolation: standardizing samples by completeness rather than size. Ecology 93:2533–2547.

Chao, A., N. J. Gotelli, T. C. Hsieh, E. L. Sander, K. H. Ma, R. K. Colwell, and A. M. Ellison. 2014: Rarefaction and extrapolation with Hill numbers: a framework for sampling and estimation in species diversity studies. Ecological Monographs 84:45–67.

Chen, S. T., and S. Y. Smith. 2013: Phytolith variability in Zingiberales: a tool for the reconstruction of past tropical vegetation. Palaeogeography, Palaeoclimatology, Palaeoecology 370:1–12.

Chen, Y.-S., T. Deng, Z. Zhou, and H. Sun. 2018: Is the East Asian flora ancient or not? National Science Review 5:920–932.

Cheney, E. S. 1997: What is the age and extent of the Cascade Magmatic Arc? Washington Geology 25:28–32.

Colgan, J. P., and C. D. Henry. 2009: Rapid middle Miocene collapse of the Mesozoic orogenic plateau in north-central Nevada. International Geology Review 51:920–961.

Condon, D. J., B. Schoene, N. M. McLean, S. A. Bowring, and R. R. Parrish. 2015: Metrology and traceability of U-Pb isotope dilution geochronology (EARTHTIME Tracer Calibration Part I). Geochimica et Cosmochimica Acta 164:464–480.

Crifò, C., and C. A. Strömberg. 2020: Small-scale spatial resolution of the soil phytolith record in a rainforest and a dry forest in Costa Rica: applications to the deep-time fossil phytolith record. Palaeogeography, palaeoclimatology, palaeoecology 537:109107.

Cummings, M. L., J. G. Evans, M. L. Ferns, and K. R. Lees. 2000: Stratigraphic and structural evolution of the middle Miocene synvolcanic Oregon-Idaho graben. GSA Bulletin 112:668–682.

Currano, E. D., B. F. Jacobs, A. D. Pan, and N. J. Tabor. 2011: Inferring ecological disturbance in the fossil record: A case study from the late Oligocene of Ethiopia. Palaeogeography, Palaeoclimatology, Palaeoecology 309:242–252.

Denk, T., and B. Meller. 2001: Systematic Significance of the Cupule/Nut Complex in Living and Fossil *Fagus*. International Journal of Plant Sciences 162:869–897.

Dillhoff, R. M., T. A. Dillhoff, A. P. Jijina, and C. A. Strömberg. 2014: The Vasa Park flora, King County, Washington, USA: A Window into the Late Miocene of the Pacific Northwest. Pp.64–97 *in* Paleobotany and Biogeography: A Festschrift for Alan Graham in His 80th Year. Missouri Botanical Garden, St. Louis.

Downs, T. 1956: The Mascall fauna from the Miocene of Oregon. University of California Publications in Geological Sciences 31.

Drewicz, A. E., and M. J. Kohn. 2018: Stable isotopes in large herbivore tooth enamel capture a mid-Miocene precipitation spike in the interior Pacific Northwest. Palaeogeography, Palaeoclimatology, Palaeoecology 495:1–12.

Dunn, R. E., C. A. E. Strömberg, R. H. Madden, M. J. Kohn, and A. A. Carlini. 2015: Linked canopy, climate, and faunal change in the Cenozoic of Patagonia. Science 347:258–261.

Dyer, J. M. 2006: Revisiting the Deciduous Forests of Eastern North America. BioScience 56:341.

Ebinghaus, A., D. W. Jolley, and A. J. Hartley. 2015: Extrinsic forcing of plant ecosystems in a large igneous province: The Columbia River flood basalt province, Washington State, USA. Geology:G37276.1.

Ebinghaus, A., R. Taylor, A. Barker, A. J. Hartley, D. W. Jolley, and M. J. Hole. 2020: Development of inter-lava drainage systems in LIPs: The Columbia River Flood Basalt Province (USA) as a case study. Journal of Sedimentary Research 90:1346–1369.

Edwards, S., W. 1983: Cenozoic history of Alaskan and Port Orford Chamaecyparis cedars. Dissertation, University of California Berkeley.

Ellis, B., D. C. Daly, L. J. Hickey, K. R. Johnson, J. D. Mitchell, P. Wilf, and S. L. Wing. 2009: Manual of leaf architecture. Cornell University Press, Ithaca, NY.

Emerson, L. F. 2009: The early Miocene Cape Blanco flora of coastal Oregon. Dissertation, University of Oregon.

Erdtman, G. 1952: Pollen Morphology and Plant Taxonomy: Angiosperms. Almqvist & Wiksell, Stockholm.

———. 1957: Pollen and Spore Morphology and Plant Taxonomy: Gymnospermae, Pteridophyta, Bryophyta. Almqvist & Wiksell, Stockholm.

Erwin, D. M., and H. E. Schorn. 2000: Revision of *Lyonothamnus* A. Gray (Rosaceae) from the Neogene of Western North America. International Journal of Plant Sciences 161:179–193.

Evernden, J. F., and G. T. James. 1964: Potassium-argon dates and the Tertiary floras of North America. American Journal of Science 262:945–974.

Faegrie, K., and J. Iverson. 1964: Textbook of Pollen Analysis. Hafner Publishing Company, New York, NY.

Farjon, Aljos. 1990: Pinaceae, drawings and descriptions of the Genera : Abies, Cedrus, Pseudolarix, Keteleeria, Nothotsuga, Tsuga, Cathaya, Pseudotsuga, Larix and Picea. Regnum Vegetabile 121. Koeltz Scientific Books, Köenigstein, Germany.

———. 2005: A monograph of Cupressaceae and Sciadopitys. *in Cupressaceae and Sciadopitys*. Royal Botanic Gardens, Kew, Richmond, Surrey, UK.

Ferns, M. L., M. J. Streck, and J. D. McClaughry. 2017: Field-trip guide to Columbia River flood basalts, associated rhyolites, and diverse post-plume volcanism in eastern Oregon. Scientific Investigations Report 2017-5022O. Reston, VA.

Fields, P. F. 1996: The Succor Creek flora of the middle Miocene Sucker Creek Formation, southwestern Idaho and eastern Oregon: systematics and paleoecology. Dissertation, Michigan State University.

Flower, B. P., and J. P. Kennett. 1994: The middle Miocene climatic transition: East Antarctic ice sheet development, deep ocean circulation and global carbon cycling. Palaeogeography, Palaeoclimatology, Palaeoecology 108:537–555.

Franklin, J. F., and C. T. Dyrness. 1973: Natural Vegetation of Oregon and Washington. U.S. Government Printing Office.

Fuller, R. E. 1931: The geomorphology and volcanic sequence of Steens Mountain in southeastern Oregon. University of Washington Publications in Geology 3:1–130.

Geraghty, C. S. 2017: Tephrochronology of mid-Miocene Clarkia Lake sedimentary deposits. Washington State University.

Gerstenberger, H., and G. Haase. 1997: A highly effective emitter substance for mass spectrometric Pb isotope ratio determinations. Chemical Geology 136:309–312.

Gillette, N. J. 1940: Some Miocene plants from north central Idaho. Northwest Science:51–55.

Goldner, A., N. Herold, and M. Huber. 2014: The challenge of simulating the warmth of the mid-Miocene climatic optimum in CESM1. Climate of the Past 10:523–536.

Graham, A. 1965: The Sucker Creek and Trout Creek Miocene Floras of Southeastern Oregon. Kent State University Bulletin, Research Series IX, Kent, Ohio.

———. 1999: Late Cretaceous and Cenozoic History of North American Vegetation (North of Mexico). Oxford University Press.

Gray, J. 1958: Plant Microfossils from the Miocene of the Columbia Plateau, Oregon. Dissertation, University of California Berkeley.

———. 1985: Interpretation of co-occurring megafossils and pollen: A comparative study with Clarkia as an example. Pp.185–244 *in* C. J. Smiley, ed. Late Cenozoic History of the Pacific Northwest. Pacific Division of the AASP, San Francisco, California.

Gray, J., and L. R. Kittleman. 1967: Geochronometry of the Columbia River Basalt and associated floras of eastern Washington and western Idaho. American Journal of Science 265:257–291.

Greenwood, D. R. 1991: The taphonomy of plant macrofossils. The processes of fossilization:141–169.

Greenwood, D. R., C. K. West, and J. F. Basinger. 2020: The Miocene Red Lake macroflora of the Deadman River Formation (Chilcotin Group), Interior Plateau, British Columbia, Canada. Acta Palaeobotanica 60:213–250.

Greenwood, D. R., B. S. Archibald, R. W. Mathewes, and P. T. Moss. 2005: Fossil biotas from the Okanagan Highlands, southern British Columbia and northeastern Washington State: climates and ecosystems across an Eocene landscape. Canadian Journal of Earth Sciences 42:167–185.

Griggs, A. B. 1976: The Columbia River Basalt Group in the Spokane Quadrangle, Washington, Idaho, and Montana. Vol. 1413. US Government Printing Office.

Grimm, G. W., and A. J. Potts. 2016: Fallacies and fantasies: the theoretical underpinnings of the Coexistence Approach for palaeoclimate reconstruction. Climate of the Past 12:611–622.

Harris, E. B., M. J. Kohn, and C. A. E. Strömberg. 2020: Stable isotope compositions of herbivore teeth indicate climatic stability leading into the mid-Miocene Climatic Optimum, in Idaho, U.S.A. Palaeogeography, Palaeoclimatology, Palaeoecology 546:109610.

Harris, E. B., C. A. E. Strömberg, N. D. Sheldon, S. Y. Smith, and D. A. Vilhena. 2017: Vegetation response during the lead-up to the middle Miocene warming event in the Northern Rocky Mountains, USA. Palaeogeography, Palaeoclimatology, Palaeoecology 485:401–415.

Herbert, T. D., K. T. Lawrence, A. Tzanova, L. C. Peterson, R. Caballero-Gill, and C. S. Kelly. 2016: Late Miocene global cooling and the rise of modern ecosystems. Nature Geoscience 9:843–847.

Herbert, T. D., C. A. Dalton, Z. Liu, A. Salazar, W. Si, and D. S. Wilson. 2022: Tectonic degassing drove global temperature trends since 20 Ma. Science 377:116–119.

Hiess, J., D. J. Condon, N. McLean, and S. R. Noble. 2012: 238U/235U systematics in terrestrial uranium-bearing minerals. Science 335:1610–1614.

Hijmans, R. J., S. Phillips, J. Leathwick, and J. Elith. 2023: Dismo: Species Distribution Modeling. R package version 1.3-14.

Hill, R. S. 1986: Lauraceous leaves from the Eocene of Nerriga, New South Wales. Alcheringa: An Australasian Journal of Palaeontology 10:327–351.

Hitchcock, C. L. (Charles L., A. Cronquist, D. Giblin, B. Legler, P. F. Zika, R. G. Olmstead, J. R. Janish, J. H. Rumely, C. Shin, and N. Porcino. 2018: Flora of the Pacific Northwest: an illustrated manual. University of Washington Press, Seattle.

Höfig, D., Y. G. Zhang, L. Giosan, Q. Leng, J. Liang, M. Wu, B. Miller, and H. Yang. 2021: Annually resolved sediments in the classic Clarkia lacustrine deposits (Idaho, USA) during the middle Miocene Climate Optimum. Geology 49:916–920.

Hoke, G. D., M. D. Schmitz, and S. A. Bowring. 2014: An ultrasonic method for isolating nonclay components from clay-rich material. Geochemistry Geophysics Geosystems 15:492–498.

Holbourn, A., W. Kuhnt, M. Schulz, J.-A. Flores, and N. Andersen. 2007: Orbitally-paced climate evolution during the middle Miocene “Monterey” carbon-isotope excursion. Earth and Planetary Science Letters 261:534–550.

Holbourn, A., W. Kuhnt, K. G. D. Kochhann, N. Andersen, and K. J. Sebastian Meier. 2015: Global perturbation of the carbon cycle at the onset of the Miocene Climatic Optimum. Geology 43:123–126.

Holbourn, A., W. Kuhnt, K. G. D. Kochhann, K. M. Matsuzaki, and N. Andersen. 2022: Middle Miocene climate–carbon cycle dynamics: Keys for understanding future trends on a warmer Earth? Pp.93–111 *in* I. W. Aiello, J. A. Barron, and A. C. Ravelo, eds. Understanding the Monterey Formation and Similar Biosiliceous Units across Space and Time. Geological Society of America.

Holbourn, A., W. Kuhnt, M. Lyle, L. Schneider, O. Romero, and N. Andersen. 2014: Middle Miocene climate cooling linked to intensification of eastern equatorial Pacific upwelling. Geology 42:19–22.

Hönisch, B., D. L. Royer, D. O. Breecker, P. J. Polissar, G. J. Bowen, M. J. Henehan, Y. Cui, M. Steinthorsdottir, J. C. McElwain, M. J. Kohn, A. Pearson, S. R. Phelps, K. T. Uno, A. Ridgwell, E. Anagnostou, J. Austermann, M. P. S. Badger, R. S. Barclay, P. K. Bijl, T. B. Chalk, C. R. Scotese, E. De La Vega, R. M. DeConto, K. A. Dyez, V. Ferrini, P. J. Franks, C. F. Giulivi, M. Gutjahr, D. T. Harper, L. L. Haynes, M. Huber, K. E. Snell, B. A. Keisling, W. Konrad, T. K. Lowenstein, A. Malinverno, M. Guillermic, L. M. Mejía, J. N. Milligan, J. J. Morton, L. Nordt, R. Whiteford, A. Roth-Nebelsick, J. K. C. Rugenstein, M. F. Schaller, N. D. Sheldon, S. Sosdian, E. B. Wilkes, C. R. Witkowski, Y. G. Zhang, L. Anderson, D. J. Beerling, C. Bolton, T. E. Cerling, J. M. Cotton, J. Da, D. D. Ekart, G. L. Foster, D. R. Greenwood, E. G. Hyland, E. A. Jagniecki, J. P. Jasper, J. B. Kowalczyk, L. Kunzmann, C. E. Lawrence, C. H. Lear, M. A. Martínez-Botí, D. P. Maxbauer, P. Montagna, B. D. A. Naafs, J. W. B. Rae, M. Raitzsch, G. J. Retallack, S. J. Ring, O. Seki, J. Sepúlveda, A. Sinha, T. F. Tesfamichael, A. Tripati, J. Van Der Burgh, J. Yu, J. C. Zachos, L. Zhang, and The Cenozoic CO_2 Proxy Integration Project (CenCOPIP) Consortium. 2023: Toward a Cenozoic history of atmospheric CO_2. Science 382:eadi5177.

Horstwood, M. S. A., J. Košler, G. Gehrels, S. E. Jackson, N. M. McLean, C. Paton, N. J. Pearson, K. Sircombe, P. Sylvester, P. Vermeesch, J. F. Bowring, D. J. Condon, and B. Schoene. 2016: Community-Derived Standards for LA-ICP-MS U-(Th-)Pb Geochronology - Uncertainty Propagation. Age Interpretation and Data Reporting. Geostandards and Geoanalytical Research 40:311–332.

Hsieh, T. C., K. H. Ma, and A. Chao. 2024: iNEXT: Interpolation and Extrapolation for Species Diversity.

Huegele, I. B., R. J. Spielbauer, and S. R. Manchester. 2020: Morphology and systematic affinities of Platanus dissecta Lesquereux (Platanaceae) from the Miocene of western North America. International Journal of Plant Sciences 181:324–341.

Huff, P. M., P. Wilf, and E. J. Azumah. 2003: Digital future for paleoclimate estimation from fossil leaves? Preliminary results. Palaios 18:266–274.

Hummel, A. 1983: The Pliocene leaf flora from Ruszow near Zary in Lower Silesia, SW Poland. Prace Muzeum Ziemi 36.

Jaffey, A. H., K. F. Flynn, L. E. Glendenin, W. C. Bentley, and A. M. Essling. 1971: Precision measurements of half-lives and specific activities of 235U and 238U. Physical Review C 4:1889–1906.

Ji, S., J. Nie, A. Lechler, K. W. Huntington, E. O. Heitmann, and D. O. Breecker. 2018: A symmetrical CO2 peak and asymmetrical climate change during the middle Miocene. Earth and Planetary Science Letters 499:134–144.

Joseph, N. L. 1990: Geologic map of the Spokane 1: 100,000 quadrangle. Washington–Idaho: Washington Division of Geology and Earth Resources, Open File Report:90–17.

Jud, N. A., S. E. Allen, C. W. Nelson, C. L. Bastos, and J. G. Chery. 2021: Climbing since the early Miocene: The fossil record of Paullinieae (Sapindaceae). PLoS One 16:e0248369.

Kapp, R. O. 2000: Pollen and Spores. American Association of Stratigraphic Palynologists Foundation Publication.

Kappelle, M., and M. E. Leal. 1996: Changes in leaf morphology and foliar nutrient status along a successional gradient in a Costa Rican upper montane Quercus forest. Biotropica:331–344.

Karp, A. T., A. K. Behrensmeyer, and K. H. Freeman. 2018: Grassland fire ecology has roots in the late Miocene. Proceedings of the National Academy of Sciences 115:12130–12135.

Kasbohm, J., and B. Schoene. 2018: Rapid eruption of the Columbia River flood basalt and correlation with the mid-Miocene climate optimum. Science Advances 4:eaat8223.

Kasbohm, J., B. Schoene, D. F. Mark, J. Murray, S. Reidel, D. Szymanowski, D. Barfod, and T. Barry. 2023: Eruption history of the Columbia River Basalt Group constrained by high-precision U-Pb and 40Ar/39Ar geochronology. Earth and Planetary Science Letters 617:118269.

Kattge, J. S., G. Bönisch, A. Günther, I. Wright, A. Zanne, C. Wirth, P. B. Reich, and the TRY Consortium. 2012: TRY - Categorical Traits Dataset. Data from: TRY - a global database of plant traits. TRY File Archive https://www.try-db.org/TryWeb/Data.php#3.

Kayseri-Özer, M. S. 2017: Cenozoic vegetation and climate change in Anatolia — A study based on the IPR-vegetation analysis. Palaeogeography, Palaeoclimatology, Palaeoecology 467:37–68.

Kelley, S. 2002: K-Ar and Ar-Ar Dating. Reviews in Mineralogy and Geochemistry 47:785–818.

Kirkham, V. R. D., and M. M. Johnson. 1929: The Latah Formation in Idaho. The Journal of geology 37:483–504.

Kittleman, L. R., A. R. Green, A. R. Hagood, A. M. Johnson, J. M. McMurray, R. G. Russel, and D. A. Weeden. 1965: Cenozoic stratigraphy of the Owyhee Region, Southeastern Oregon. Bulletin of the Museum of Natural History 1, University of Oregon, Eugene, Oregon.

Knott, T. R., M. J. Branney, M. K. Reichow, D. R. Finn, R. S. Coe, M. Storey, D. Barfod, and M. McCurry. 2016: Mid-Miocene record of large-scale Snake River–type explosive volcanism and associated subsidence on the Yellowstone hotspot track: The Cassia Formation of Idaho, USA. Bulletin 128:1121–1146.

Kohn, M. J., and T. J. Fremd. 2008: Miocene tectonics and climate forcing of biodiversity, western United States. Geology 36:783.

Kohn, M. J., J. L. Miselis, and T. J. Fremd. 2002: Oxygen isotope evidence for progressive uplift of the Cascade Range, Oregon. Earth and Planetary Science Letters 204:151–165.

Kovar-Eder, J., P. Mazouch, V. Teodoridis, A. Roth-Nebelsick, C. Traiser, and J. Wypich. 2021: Modern vegetation proxies reflect Palaeogene and Neogene vegetation evolution and climate change in Europe, Turkey, and Armenia. Palaeontologia Electronica.

Kowalski, E. A., and D. L. Dilcher. 2003: Warmer paleotemperatures for terrestrial ecosystems. Proceedings of the National Academy of Sciences of the United States of America 100:167–170.

Krapp, M., and J. H. Jungclaus. 2011: The Middle Miocene climate as modelled in an atmosphere-ocean-biosphere model. Climate of the Past 7:1169–1188.

Krogh, T. E. 1973: A low-contamination method for hydrothermal decomposition of zircon and extraction of U and Pb for isotopic age determinations. Geochimica et Cosmochimica Acta 37:494.

Kukla, T., J. K. C. Rugenstein, D. E. Ibarra, M. J. Winnick, C. A. E. Strömberg, and C. P. Chamberlain. 2022: Drier Winters Drove Cenozoic Open Habitat Expansion in North America. AGU Advances 3:e2021AV000566.

Kukla, T., D. E. Ibarra, J. K. C. Rugenstein, J. T. Gooley, C. E. Mullins, S. Kramer, D. Y. Moragne, and C. P. Chamberlain. 2021: High-Resolution Stable Isotope Paleotopography of the John Day Region, Oregon, United States. Frontiers in Earth Science 9:635181.

Kunzmann, L., Z. Kvaček, D. H. Mai, and H. Walther. 2009: The genus Taxodium (Cupressaceae) in the Palaeogene and Neogene of Central Europe. Review of Palaeobotany and Palynology 153:153–183.

Kvaček, Z. 1999: An ancient Calocedrus (Cupressaceae) from the European Teriary. Flora 194:237–248.

Kvaček, Z., and W. Rember. 2007: Calocedrus robustior (Cupressaceae) and Taxus schornii (Taxaceae): two new conifers from the middle Miocene Latah Formation of northern Idaho. Paleobios 27:68–79.

Kvaček, Z., S. R. Manchester, and H. E. Schorn. 2000: Cones, Seeds, and Foliage of *Tetraclinis Salicornioides* (Cupressaceae) from the Oligocene and Miocene of Western North America: A Geographic Extension of the European Tertiary Species. International Journal of Plant Sciences 161:331–344.

Ladderud, J. A., J. A. Wolff, W. C. Rember, and M. E. Brueseke. 2015: Volcanic Ash Layers in the Miocene Lake Clarkia Beds: Geochemistry, Regional Correlation, and Age of the Clarkia Flora. Northwest Science 89:309–323.

Latchaw, G., and S. R. Manchester. 2024: Fruits of Sabia (Sabiaceae) from the Miocene of western North America and their biogeographic significance. Acta Palaeobotanica 64:51–59.

Lehmann, C. E. R., T. M. Anderson, M. Sankaran, S. I. Higgins, S. Archibald, W. A. Hoffmann, N. P. Hanan, R. J. Williams, R. J. Fensham, J. Felfili, L. B. Hutley, J. Ratnam, J. San Jose, R. Montes, D. Franklin, J. Russell-Smith, C. M. Ryan, G. Durigan, P. Hiernaux, R. Haidar, D. M. J. S. Bowman, and W. J. Bond. 2014: Savanna Vegetation-Fire-Climate Relationships Differ Among Continents. Science 343:548–552.

Leopold, E. B., and M. F. Denton. 1987: Comparative age of grassland and steppe east and west of the northern rocky mountain. Annals of the Missouri Botanical Garden:841–867.

Lewis, A. R., D. R. Marchant, A. C. Ashworth, L. Hedenäs, S. R. Hemming, J. V. Johnson, M. J. Leng, M. L. Machlus, A. E. Newton, J. I. Raine, J. K. Willenbring, M. Williams, and A. P. Wolfe. 2008: Mid-Miocene cooling and the extinction of tundra in continental Antarctica. Proceedings of the National Academy of Sciences 105:10676–10680.

Lewis, R. S., J. H. Bush, R. F. Burmester, J. D. Kauffman, D. L. Garwood, D. L. Myers, and K. L. Othberg. 2005: Geologic Map of the Potlatch 30 x 60 Minute Quadrangle, Idaho. Idaho Geological Survey.

Liberty, L. M., and T. L. Pratt. 2008: Structure of the eastern Seattle fault zone, Washington State: New insights from seismic reflection data. Bulletin of the Seismological Society of America 98:1681–1695.

Loughney, K. M., A. Harkness, and C. Badgley. 2023: Middle Miocene fire activity and C4 vegetation expansion in the Barstow Formation, California, USA. Geology 51:763–767.

Love, R. L., R. S. Lewis, S. H. Wood, D. M. Feeney, and M. D. Schmitz. 2023: U–Pb zircon ages, mapping, and biostratigraphy of the Payette Formation and Idaho Group north of the western Snake River Plain, Idaho: Implications for hydrocarbon system correlation. Rocky Mountain Geology 58:83–113.

Lowe, A. J., E. Aguirre, J. Meier, C. Oishi, and C. A. E. Strömberg. In Review*a*: Links between leaf morphology and ecological strategy across secondary succession in a temperate deciduous forest (North Carolina, USA): implications for the fossil record. Paleobiology.

Lowe, A. J., D. R. Greenwood, C. K. West, J. M. Galloway, M. Sudermann, and T. Reichgelt. 2018: Plant community ecology and climate on an upland volcanic landscape during the Early Eocene Climatic Optimum: McAbee Fossil Beds, British Columbia, Canada. Palaeogeography, Palaeoclimatology, Palaeoecology 511:433–448.

Lowe, A. J., A. G. Flynn, M. J. Butrim, A. Baumgartner, D. L. Royer, D. J. Peppe, and D. J. Peppe. 2024: Reconstructing Terrestrial Paleoclimate and Paleoecology with Fossil Leaves Using Digital Leaf Physiognomy and Leaf Mass Per Area. JoVE:e66838.

Lowe, A. J., D. L. Royer, D. J. Wieczynski, M. J. Butrim, T. Reichgelt, L. Azevedo-Schmidt, D. J. Peppe, B. J. Enquist, and C. A. E. Strömberg. In Review*b*: Global patterns in community-scale leaf mass per area distributions of woody non-monocot angiosperms and their utility in the fossil record. American Journal of Botany.

Ludwig, K. R. 2003: Isoplot 3.00: a geochronological toolkit for Microsoft Excel. Berkeley Geochronology Center Special Publication 4:1–71.

Macdonald, F. A., M. D. Schmitz, J. V. Strauss, G. P. Halverson, T. M. Gibson, A. Eyster, G. Cox, P. Mamrol, and J. L. Crowley. 2018: Cryogenian of Yukon. Precambrian Research 319:114–143.

MacGinitie, H. D. 1933: The Trout Creek flora of southeastern Oregon. Carnegie Institution of Washington, Contributions to Paleontology, Washington, D.C.

Maguire, K. C., J. X. Samuels, and M. D. Schmitz. 2018: The fauna and chronostratigraphy of the middle Miocene Mascall type area, John Day Basin, Oregon, USA. PaleoBios 35.

Manchester, S. R. 1987: The fossil history of the Juglandaceae. Monographs in Systematic *Botany* 21. Missouri Botanical Garden, St. Louis, Missouri.

———. 1999: Biogeographical Relationships of North American Tertiary Floras. Annals of the Missouri Botanical Garden 86:472.

Manchester, S. R., and M. J. Donoghue. 1995: Winged Fruits of Linnaeeae (Caprifoliaceae) in the Tertiary of Western North America: *Diplodipelta* gen. nov. International Journal of Plant Sciences 156:709–722.

Manchester, S. R., K. B. Pigg, Z. Kvaček, M. L. DeVore, and R. M. Dillhoff. 2018: Newly Recognized Diversity in Trochodendraceae from the Eocene of Western North America. International Journal of Plant Sciences 179:663–676.

Mattinson, J. M. 2005: Zircon U-Pb chemical abrasion ("CA-TIMS") method: combined annealing and multi-step partial dissolution analysis for improved precision and accuracy of zircon ages. Chemical Geology 220:47–66.

McAndrews, J. H., A. A. Berti, and G. Norris. 1973: Key to the Quaternary Pollen and Spores of the Great Lakes Region. Royal Ontario Museum Life Sciences Miscellaneous Publication.

McInerney, F. A., and S. L. Wing. 2011: The Paleocene-Eocene Thermal Maximum: A Perturbation of carbon cycle, climate, and biosphere with implications for the future. Annual Review of Earth & Planetary Sciences 39:489–516.

McIntosh, W. C., S. R. Manchester, and H. W. Meyer. 1997: Age of the plant-bearing tuffs of the John Day Formation at Fossil, Oregon, based upon $^{40}Ar/^{39}Ar$ single-crystal dating. Oregon Geology v. 59:3–7.

McLean, A., and J. Bershaw. 2021: Molecules to mountains: A multi-proxy investigation into ancient climate and topography of the Pacific Northwest, USA. Frontiers in Earth Science 9:624961.

Merrill, E. K. 1978: Comparison of Mature Leaf Architecture of Three Types in Sorbus L. (Rosaceae). Botanical Gazette 139:447–453.

Methner, K., J. Fiebig, U. Wacker, P. Umhoefer, C. P. Chamberlain, and A. Mulch. 2016: Eocene-Oligocene proto-Cascades topography revealed by clumped (Δ_{47}) and oxygen isotope ($\delta^{18}O$) geochemistry (Chumstick Basin, WA, USA). Tectonics 35:546–564.

Meyer, H. W., and S. R. Manchester. 1997: Oligocene Bridge Creek flora of the John Day Formation, Oregon. University of California Press.

Meyerhoff, A. A. 1952: A study of leaf venation in the Betulaceae with its application to paleobotany. Dissertation, Stanford University.

Minor, S. A., J. J. Rytuba, C. A. Goeldner, and K. J. Tegtmeyer. 1987a: Geologic Map of the Alvord Hot Spring quadrangle, Harney County, Oregon. USGS Miscellaneous Field Studies Map MF-1916.

———. 1987b: Geologic map of the Wildhorse Lake quadrangle, Harney County, Oregon. USGS Miscellaneous Field Studies Map MF-1915.

Minor, S. A., J. J. Rytuba, M. J. Grubensky, D. B. Vander Meulen, C. A. Goeldner, and K. J. Tegtmeyer. 1987c: Geologic map of the High Steens and Little Blitzen Gorge Wilderness Study area Harney County, Oregon. USGS Miscellaneous Field Studies Map MF-1876.

Mosbrugger, V., T. Utescher, and D. L. Dilcher. 2005: Cenozoic continental climatic evolution of Central Europe. Proceedings of the National Academy of Sciences 102:14964–14969.

Mustoe, G. E., and E. B. Leopold. 2014: Paleobotanical evidence for the post-Miocene uplift of the Cascade Range. Canadian Journal of Earth Sciences 51:809–824.

Nasdala, L., C. L. Lengauer, J. M. Hanchar, A. Kronz, R. Wirth, P. Blanc, A. K. Kennedy, and A. M. Seydoux-Guillaume. 2002: Annealing radiation damage and the recovery of cathodoluminescence. Chemical Geology 191:121–140.

O'Keefe, J. M. K., M. J. Pound, I. C. Romero, N. B. Nuñez Otaño, M. E. Gibson, J. McCoy, M. E. Alden, C. J. Fairchild, J. Fitzpatrick, E. Hodgson, T. Horsfall, S. Jones, J. E. Lennex-Stone, C. A. Marsh, A. A. Patel, T. M. Spears, L. Tarlton, L. F. Smallwood, O. L. VanderEspt, J. R. Cabrera, C. F. Eble, W. C. Rember, J. E. Starnes, M. H. Alford, A. Brink, and S. Warny. 2024: Summer-Wet Hydrologic Cycle during the Middle Miocene of the United States: New Evidence from Fossil Fungi. Research 7:0481.

Oksanen, J., G. L. Simpson, F. G. Blanchet, R. Kindt, P. Legendre, P. R. Minchin, R. B. O'Hara, P. Solymos, M. H. H. Stevens, E. Szoecs, H. Wagner, M. Barbour, M. Bedward, B. Bolker, D. Borcard, G. Carvalho, M. Chirico, M. D. Caceres, S. Durand, H. B. A. Evangelista, R. FitzJohn, M. Friendly, B. Furneaux, G. Hannigan, M. O. Hill, L. Lahti, D. McGlinn, M.-H. Ouellette, E. R. Cunha, T. Smith, A. Stier, C. J. F. T. Braak, and J. Weedon. 2022: Vegan: Community Ecology Package. R package version 2.6-4.

Pardee, J. T., and K. Bryan. 1926: Geology of the Latah Formation in relation to the lavas of the Columbia Plateau near Spokane, Washington. Shorter Contribution to General Geology. US Government Printing Office.

Peck, D. L., A. B. Griggs, H. G. Schlicker, F. G. Wells, and H. M. Dole. 1964: Geology of the central and northern parts of the western Cascade Range in Oregon. Geological Survey Professional Paper 449.

Peppe, D. J., A. Baumgartner, A. Flynn, and B. Blonder. 2018: Reconstructing Paleoclimate and paleoecology using fossil leaves *in* D. A. Croft, S. W. Simpson, and D. F. Su, eds. Methods in Paleoecology: Reconstructing Cenozoic Terrestrial Environments and Ecological Communities. Springer, Dordrecht.

Peppe, D. J., D. L. Royer, B. Cariglino, S. Y. Oliver, S. Newman, E. Leight, G. Enikolopov, M. Fernandez-Burgos, F. Herrera, J. M. Adams, E. Correa, E. D. Currano, J. M. Erickson, L. F. Hinojosa, J. W. Hoganson, A. Iglesias, C. A. Jaramillo, K. R. Johnson, G. J. Jordan, N. J. B. Kraft, E. C. Lovelock, C. H. Lusk, Ü. Niinemets, J. Peñuelas, G. Rapson, S. L. Wing, and I. J. Wright. 2011: Sensitivity of leaf size and shape to climate: global patterns and paleoclimatic applications. New Phytologist 190:724–739.

Perkins, M. E., W. P. Nash, F. H. Brown, and R. J. Fleck. 1995: Fallout tuffs of Trapper Creek, Idaho—A record of Miocene explosive volcanism in the Snake River Plain volcanic province. Geological Society of America Bulletin 107:1484–1506.

Pesek, M. E., N. D. Perez, A. Meigs, C. C. Rowden, and S. M. Giles. 2020: Exhumation Timing in the Oregon Cascade Range Decoupled From Deformation, Magmatic, and Climate Patterns. Tectonics 39:e2020TC006078.

Pfahl, S., P. A. O'Gorman, and E. M. Fischer. 2017: Understanding the regional pattern of projected future changes in extreme precipitation. Nature Climate Change 7:423–427.

Pierce, K. L., and L. A. Morgan. 1990: The track of the Yellowstone hotspot: Volcanism, faulting, and uplift. USGS Open-File Report 90-415.

Pilie, M., M. E. Gibson, I. C. Romero, N. B. Nuñez Otaño, M. J. Pound, J. M. K. O'Keefe, and S. Warny. 2023: Miocene Climatic Optimum fungal record and plant-based CREST climatic reconstruction from southern McMurdo Sound, Antarctica. Journal of Micropalaeontology 42:291–307.

Poorter, L., M. T. van der Sande, L. Amissah, F. Bongers, I. Hordijk, J. Kok, S. G. Laurance, M. Martínez-Ramos, T. Matsuo, and J. A. Meave. 2024: A comprehensive framework for vegetation succession. Ecosphere 15:e4794.

Pound, M. J., A. M. Haywood, U. Salzmann, and J. B. Riding. 2012: Global vegetation dynamics and latitudinal temperature gradients during the Mid to Late Miocene (15.97–5.33Ma). Earth-Science Reviews 112:1–22.

Pratap, S., and Y. Markonis. 2022: The response of the hydrological cycle to temperature changes in recent and distant climatic history. Progress in Earth and Planetary Science 9:30.

R Core Team. 2023: R: A Language and Environment for Statistical Computing. R Foundation for Statistical Computing, Vienna, Austria.

Reich, P. B. 2014: The world-wide 'fast-slow' plant economics spectrum: a traits manifesto. Journal of Ecology 102:275–301.

Reichgelt, T., A. Baumgartner, R. Feng, and D. A. Willard. 2023: Poleward amplification, seasonal rainfall and forest heterogeneity in the Miocene of the eastern USA. Global and Planetary Change 222:104073.

Reidel, S. P., and T. L. Tolan. 2013: The late Cenozoic evolution of the Columbia River system in the Columbi River flood basalt province. Pp.201–230 *in* S. P. Reidel, ed. The Columbia River Flood-Basalt Province. The Geological Society of America, Boulder, Colorado.

Reidel, S. P., V. E. Camp, T. L. Tolan, and B. S. Martin. 2013a: The Columbia River flood basalt province: Stratigraphy, areal extent, volume, and physical volcanology. Pp.0 *in* S. P. Reidel, V. E. Camp, M. E. Ross, J. A. Wolff, B. S. Martin, T. L. Tolan, and R. E. Wells, eds. The Columbia River Flood Basalt Province. Geological Society of America.

Reidel, S. P., V. E. Camp, T. L. Tolan, J. D. Kauffman, and D. L. Garwood. 2013b: Tectonic evolution of the Columbia River flood basalt province. Pp.*in* S. P. Reidel, ed. The Columbia River Flood-Basalt Province. The Geological Society of America, Boulder, Colorado.

Reidel, S. P., T. L. Tolan, V. E. Camp, M. E. Ross, J. A. Wolff, B. S. Martin, and R. E. Wells. 2013c: The Grande Ronde Basalt, Columbia River Basalt Group. The Columbia River Flood Basalt Province: Geological Society of America Special Paper 497:117–153.

Reiners, P. W., T. A. Ehlers, J. I. Garver, S. G. Mitchell, D. R. Montgomery, J. A. Vance, and S. Nicolescu. 2002: Late Miocene exhumation and uplift of the Washington Cascade Range. Geology 30:767.

Reinink-Smith, L. M., and E. B. Leopold. 2005: Warm climate in the late Miocene of the south coast of Alaska and the occurrence of Podocarpaceae pollen. Palynology 29:205–262.

Reinink-Smith, L. M., S. Zaborac-Reed, and E. B. Leopold. 2017: Clamgulchian (Miocene–Pliocene) pollen assemblages of the Kenai Lowland, Alaska, and the persistence of the family Podocarpaceae. Palynology 42:66–101.

Retallack, G. J. 2007: Cenozoic Paleoclimate on Land in North America. The Journal of Geology 115:271–294.

Robinson, P. T., G. F. Brem, and E. H. Mckee. 1984: John Day Formation of Oregon: A distal record of early Cascade volcanism. Geology 12:11915.

Royer, D. L., L. J. Hickey, and S. L. Wing. 2003: Ecological conservatism in the “living fossil” Ginkgo. Paleobiology 29:84–104.

Royer, D. L., R. M. Kooyman, S. A. Little, and P. Wilf. 2009: Ecology of leaf teeth: A multi-site analysis from an Australian subtropical rainforest. American Journal of Botany 96:738–750.

Royer, D. L., D. J. Peppe, E. A. Wheeler, and Ü. Niinemets. 2012: Roles of climate and functional traits in controlling toothed vs. untoothed leaf margins. American Journal of Botany 99:915–922.

Royer, D. L., P. Wilf, D. A. Janesko, E. A. Kowalski, and D. L. Dilcher. 2005: Correlations of climate and plant ecology to leaf size and shape: potential proxies for the fossil record. American Journal of Botany 92:1141–1151.

Royer, D. L., L. Sack, P. Wilf, C. H. Lusk, G. J. Jordan, Ü. Niinemets, I. J. Wright, M. Westoby, P. D. Coley, A. D. Cutter, K. R. Johnson, C. C. Labandeira, A. T. Moles, and F. Valladares. 2007: Fossil Leaf Economics Quantified: Calibration, Eocene Case Study, and Implications. Paleobiology 33:574–589.

Rytuba, J. J., and E. H. McKee. 1984: Peralkaline ash flow tuffs and calderas of the McDermitt Volcanic Field, southeast Oregon and north central Nevada. Journal of Geophysical Research: Solid Earth 89:8616–8628.

Rytuba, J. J., S. A. Minor, and E. H. McKee. 1981: Geology of the Whitehorse Caldera and caldera-fill deposits, Malheur County, Oregon. USGS Open-File Report 81-1092.

Rytuba, J. J., D. B. Vander Meulen, V. E. Barlock, and M. L. Ferns. 1991: Hot spring gold deposits in the Lake Owyhee Volcanic Field, Eastern Oregon. Pp.633–712 *in* Great Basin Symposium: The Geology and Ore Deposits of the Great Basin: Field Trip Guidebook Compendium. Geological Society of Nevada, Reno, NV.

Sakala, J. 2000: Flora and vegetation of the roof of the main lignite seam in the Bílina Mine (Most Basin, Lower Miocene). Acta Mus. Nat. Pragae, Ser. B, Hist. Nat 56:49–84.

Sankaran, M., N. P. Hanan, R. J. Scholes, J. Ratnam, D. J. Augustine, B. S. Cade, J. Gignoux, S. I. Higgins, X. Le Roux, and F. Ludwig. 2005: Determinants of woody cover in African savannas. Nature 438:846–849.

Sarna-Wojcicki, A. M., J. R. Knott, J. A. Westgate, J. R. Budahn, J. Barron, C. J. Bray, G. A. Ludvigson, C. E. Meyer, D. M. Miller, and R. E. Otto. 2023: Ibex Hollow Tuff from ca. 12 Ma supereruption, southern Idaho, identified across North America, eastern Pacific Ocean, and Gulf of Mexico. Geosphere 19:1476–1507.

Schiller, C., M., A. J. Lowe, T. A. Dillhoff, P. F. Fields, A. M. Riley, R. E. Taggart, M. Schmitz D., and C. A. E. Strömberg. 2024: Mechanisms of rapid plant community change from the Miocene Succor Creek flora, Oregon and Idaho (USA). PLOS One 19:e0312104.

Schmincke, H.-U. 1967: Fused tuff and peperites in south-central Washington. Geological Society of America Bulletin 78:319–330.

Schmitz, M. D., and B. Schoene. 2007: Derivation of isotope ratios, errors and error correlations for U-Pb geochronology using 205Pb-235U-(233U)-spiked isotope dilution thermal ionization mass spectrometric data. Geochemistry Geophysics Geosystems 8, Q08006.

Schoettle-Greene, P., A. R. Duvall, and P. D. Crowley. 2022: Multiphase Topographic and Thermal Histories of the Wallowa and Elkhorn Mountains, Blue Mountains Province, Oregon, USA. Tectonics 41:e2021TC006704.

Schorn, H. E., J. A. Myers, and D. M. Erwin. 2007: An updated chronology of Neogene paleofloras from the western United States. Courier Forschungsinstitut Senckenberg 258:139-146.

Shevenell, A. E., J. P. Kennett, and D. W. Lea. 2008: Middle Miocene ice sheet dynamics, deep-sea temperatures, and carbon cycling: A Southern Ocean perspective. Geochemistry, Geophysics, Geosystems 9:2007GC001736.

Sláma, J., J. Kosler, D. Condon, J. Crowley, A. Gerdes, J. Hanchar, M. Horstwood, G. Morris, L. Nasdala, and N. Norberg. 2008: Plesovice zircon–A new natural reference material for U-Pb and Hf isotopic microanalysis. Chemical Geology 249:1–35.

Smiley, C. J. 1963: The Ellensburg flora of Washington. Publications in Geological Sciences, University of California Press.

Smiley, C. J., and L. M. Huggins. 1981: *Pseudofagus idahoensis*, n. gen. et sp. (Fagaceae) from the Miocene Clarkia flora of Idaho. American Journal of Botany 68:741–761.

Smiley, C. J., and W. C. Rember. 1985a: Composition of the Miocene Clarkia flora. Late Cenozoic History of the Pacific Northwest 95:112.

Smiley, C. J., and W. C. Rember. 1985b: Physical setting of the Miocene Clarkia Fossil Beds, northern Idaho. Pp.11–32 *in* Late Cenozoic History of the Pacific Northwest. California Academy of Sciences, San Francisco, California.

Smiley, T. M., E. G. Hyland, J. M. Cotton, and R. E. Reynolds. 2018: Evidence of early C_4 grasses, habitat heterogeneity, and faunal response during the Miocene Climatic Optimum in the Mojave Region. Palaeogeography, Palaeoclimatology, Palaeoecology 490:415–430.

Smith, G. A., B. N. Bjornstad, and K. R. Fecht. 1989: Neogene terrestrial sedimentation on and adjacent to the Columbia Plateau; Washington, Oregon, and Idaho. Pp.0 *in* S. P. Reidel and P. R. Hooper, eds. Volcanism and Tectonism in the Columbia River Flood-Basalt Province. Geological Society of America.

Smith, M., and S. Manchester. 2019: A new species of "gigantic" capsular fruits of Vaccinioideae from the Miocene of Idaho. Palaeontologia Electronica 22.3.65:1-7.

Soreng, R. J., P. M. Peterson, K. Romaschenko, G. Davidse, J. K. Teisher, L. G. Clark, P. Barberá, L. J. Gillespie, and F. O. Zuloaga. 2017: A worldwide phylogenetic classification of the Poaceae (Gramineae) II: An update and a comparison of two 2015 classifications. Journal of Systematics and Evolution 55:259–290.

Soreng, R. J., P. M. Peterson, F. O. Zuloaga, K. Romaschenko, L. G. Clark, J. K. Teisher, L. J. Gillespie, P. Barberá, C. A. D. Welker, E. A. Kellogg, D. Li, and G. Davidse. 2022: A worldwide phylogenetic classification of the Poaceae (Gramineae) III: An update. Journal of Systematics and Evolution 60:476–521.

Sosdian, S. M., T. L. Babila, R. Greenop, G. L. Foster, and C. H. Lear. 2020: Ocean Carbon Storage across the middle Miocene: a new interpretation for the Monterey Event. Nature Communications 11:134.

Steinthorsdottir, M., P. E. Jardine, and W. C. Rember. 2021a: Near-Future pCO_2 During the Hot Miocene Climatic Optimum. Paleoceanography and Paleoclimatology 36:e2020PA003900.

Steinthorsdottir, M., H. K. Coxall, A. M. De Boer, M. Huber, N. Barbolini, C. D. Bradshaw, N. J. Burls, S. J. Feakins, E. Gasson, J. Henderiks, A. E. Holbourn, S. Kiel, M. J. Kohn, G. Knorr, W. M. Kürschner, C. H. Lear, D. Liebrand, D. J. Lunt, T. Mörs, P. N. Pearson, M. J. Pound, H. Stoll, and C. A. E. Strömberg. 2021b: The Miocene: The Future of the Past. Paleoceanography and Paleoclimatology 36:e2020PA004037.

Streck, M. J., M. L. Ferns, and W. McIntosh. 2015: Large, persistent rhyolitic magma reservoirs above Columbia River Basalt storage sites: The Dinner Creek Tuff eruptive center, eastern Oregon. Geosphere 11:226–235.

Strömberg, C. A. 2004: Using phytolith assemblages to reconstruct the origin and spread of grass-dominated habitats in the great plains of North America during the late Eocene to early Miocene. Palaeogeography, Palaeoclimatology, Palaeoecology 207:239–275.

———. 2009: Methodological concerns for analysis of phytolith assemblages: does count size matter? Quaternary International 193:124–140.

Strömberg, C. A., L. Werdelin, E. M. Friis, and G. Saraç. 2007a: The spread of grass-dominated habitats in Turkey and surrounding areas during the Cenozoic: phytolith evidence. Palaeogeography, Palaeoclimatology, Palaeoecology 250:18–49.

Strömberg, C. A., E. M. Friis, L. Ming-Mei, L. Werdelin, and Z. Yu-Liang. 2007b: Palaeoecology of an Early-Middle Miocene lake in China: preliminary interpretations based on phytoliths from the Shanwang Basin. Vertebrata Palasiatica 45:145.

Strömberg, C. A., R. E. Dunn, R. H. Madden, M. J. Kohn, and A. A. Carlini. 2013: Decoupling the spread of grasslands from the evolution of grazer-type herbivores in South America. Nature communications 4:1478.

Strömberg, C. A. E. 2005: Decoupled taxonomic radiation and ecological expansion of open-habitat grasses in the Cenozoic of North America. Proceedings of the National Academy of Sciences 102:11980–11984.

Strömberg, C. A. E., R. E. Dunn, C. Crifò, and E. B. Harris. 2018: Phytoliths in Paleoecology: Analytical Considerations, Current Use, and Future Directions. Pp.235–287 *in* D. A. Croft, D. F. Su, and S. W. Simpson, eds. Methods in Paleoecology. Springer International Publishing, Cham.

Super, J. R., E. Thomas, M. Pagani, M. Huber, C. O'Brien, and P. M. Hull. 2018: North Atlantic temperature and pCO2 coupling in the early-middle Miocene. Geology 46:519–522.

Syabryaj, S., T. Utescher, S. Molchanoff, and A. A. Bruch. 2007: Vegetation and palaeoclimate in the Miocene of Ukraine. Palaeogeography, Palaeoclimatology, Palaeoecology 253:153–168.

Tabor, R. W., V. A. Frizzell, J. A. Vance, and C. W. Naeser. 1984: Ages and stratigraphy of lower and middle Tertiary sedimentary and volcanic rocks of the central Cascades, Washington: Application to the tectonic history of the Straight Creek fault. Geological Society of America Bulletin 95:26.

Taggart, R. E. 1973: Additions to the Miocene Sucker Creek flora of Oregon and Idaho. American Journal of Botany 60:923–928.

Taggart, R. E., and A. T. Cross. 1990: Plant successions and interruptions in Miocene volcanic deposits, Pacific Northwest. Pp.57–68 *in* M. G. Lockley and A. Rice, eds. Volcanism and Fossil Biotas. Geological Society of America.

Takeuchi, A., and P. B. Larson. 2005: Oxygen isotope evidence for the late Cenozoic development of an orographic rain shadow in eastern Washington, USA. Geology 33:313.

Takeuchi, A., M. T. Hren, S. V. Smith, C. P. Chamberlain, and P. B. Larson. 2010: Pedogenic carbonate carbon isotopic constraints on paleoprecipitation: Evolution of desert in the Pacific Northwest, USA, in response to topographic development of the Cascade Range. Chemical Geology 277:323–335.

Tang, L., L. Mao, J. Shu, C. Li, C. Shen, and Z. Zhou. 2020: Atlas of Quaternary Pollen and Spores in China. Science Press and Springer Nature, Singapore.

Tian, X., and W. R. Buck. 2022: Intrusions induce global warming before continental flood basalt volcanism. Nature Geoscience 15:417–422.

Utescher, T., D. Djordjevic-Milutinovic, A. Bruch, and V. Mosbrugger. 2007a: Palaeoclimate and vegetation change in Serbia during the last 30 Ma. Palaeogeography, Palaeoclimatology, Palaeoecology 253:141–152.

Utescher, T., B. Erdei, L. François, and V. Mosbrugger. 2007b: Tree diversity in the Miocene forests of Western Eurasia. Palaeogeography, Palaeoclimatology, Palaeoecology 253:226–250.

Vogl, J. J., K. Min, A. Carmenate, D. A. Foster, and A. Marsellos. 2014: Miocene regional hotspot-related uplift, exhumation, and extension north of the Snake River Plain: Evidence from apatite (U-Th)/He thermochronology. Lithosphere 6:108–123.

Walker, G. W. 1990: Overview of the Cenozoic geology of the Blue Mountains region. *in* G. W. Walker, ed. Geology of the Blue Mountains Region of Oregon, Idaho, and Washington: Cenozoic Geology of the Blue Mountains Region. U.S Geological Survey.

Walker, G. W., and C. A. Repenning. 1965: Reconnaissance geologic map of the Adel quadrangle, Lake, Harney, and Malheur counties, Oregon. U.S. Geological Survey, Miscellaneous Geologic Investigations Map I-446.

Walker, G. W., and R. A. Duncan. 1989: Geologic map of the Salem 1 by 2 degree quadrangle, Western Oregon. US Geological Survey. Miscellaneous Investigations Map I-1893.

Wang, C.-W. 1961: The forests of China with a survey of grassland and desert vegetation. Maria Moors Cabot Foundation. Harvard University, Cambridge, MA.

Warny, S., R. A. Askin, M. J. Hannah, B. A. R. Mohr, J. I. Raine, D. M. Harwood, F. Florindo, and the SMS Science Team. 2009: Palynomorphs from a sediment core reveal a sudden remarkably warm Antarctica during the middle Miocene. Geology 37:955–958.

Wen, J. 1999: Evolution of Eastern Asian and Eastern North American Disjunct Distributions in Flowering Plants. Annual Review of Ecology and Systematics 30:421–455.

Wendt, I., and C. Carl. 1991: The statistical distribution of the mean squared weighted deviation. Chemical Geology 86:275–285.

West, C. K., D. R. Greenwood, T. Reichgelt, A. J. Lowe, J. M. Vachon, and J. F. Basinger. 2020: Paleobotanical proxies for early Eocene climates and ecosystems in northern North America from middle to high latitudes. Climate of the Past 16:1387–1410.

West, C. K., T. Reichgelt, A. V. Reyes, S. D. Buryak, K. J. Staniszewska, and J. F. Basinger. 2024: Paleobotanical Evidence for Mediterranean Climates in the Western Canadian Paleoarctic During the Late Middle Eocene. Paleoceanography and Paleoclimatology 39:e2024PA004874.

Westerhold, T., N. Marwan, A. J. Drury, D. Liebrand, C. Agnini, E. Anagnostou, J. S. K. Barnet, S. M. Bohaty, D. De Vleeschouwer, F. Florindo, T. Frederichs, D. A. Hodell, A. E. Holbourn, D. Kroon, V. Lauretano, K. Littler, L. J. Lourens, M. Lyle, H. Pälike, U. Röhl, J. Tian, R. H. Wilkens, P. A. Wilson, and J. C. Zachos. 2020: An astronomically dated record of Earth's climate and its predictability over the last 66 million years. Science 369:1383–1387.

Wetzel, K. F., and J. R. Stanley. 2022: Linking exhumation, paleo-relief, and rift formation to magmatic processes in the western Snake River Plain, Idaho, using apatite (U-Th)/He thermochronology. Geosphere 18:885–909.

White, J. M., T. A. Ager, D. P. Adam, E. B. Leopold, G. Liu, H. Jetté, and C. E. Schweger. 1997: An 18 million year record of vegetation and climate change in northwestern Canada and Alaska: tectonic and global climatic correlates. Palaeogeography, Palaeoclimatology, Palaeoecology 130:293–306.

Wilf, P. 1997: When are leaves good thermometers? A new case for leaf margin analysis. Paleobiology 23:373–390.

———. 2008: Fossil angiosperm leaves: Paleobotany's difficult children prove themselves. Paleontological Society Papers 14:319–333.

Wilf, P., S. L. Wing, D. R. Greenwood, and C. L. Greenwood. 1998: Using fossil leaves as paleoprecipitation indicators: An Eocene example. Geology 26:203–208.

Wilf, P., S. L. Wing, H. W. Meyer, J. A. Rose, R. Saha, T. Serre, N. R. Cúneo, M. P. Donovan, D. M. Erwin, and M. A. Gandolfo. 2021: An image dataset of cleared, x-rayed, and fossil leaves vetted to plant family for human and machine learning. PhytoKeys 187:93.

Wilkinson, M. D., M. Dumontier, Ij. J. Aalbersberg, G. Appleton, M. Axton, A. Baak, N. Blomberg, J.-W. Boiten, L. B. da Silva Santos, P. E. Bourne, J. Bouwman, A. J. Brookes, T. Clark, M. Crosas, I. Dillo, O. Dumon, S. Edmunds, C. T. Evelo, R. Finkers, A. Gonzalez-Beltran, A. J. G. Gray, P. Groth, C. Goble, J. S. Grethe, J. Heringa, P. A. C. 't Hoen, R. Hooft, T. Kuhn, R. Kok, J. Kok, S. J. Lusher, M. E. Martone, A. Mons, A. L. Packer, B. Persson, P. Rocca-Serra, M. Roos, R. van Schaik, S.-A. Sansone, E. Schultes, T. Sengstag, T. Slater, G. Strawn, M. A. Swertz,

M. Thompson, J. van der Lei, E. van Mulligen, J. Velterop, A. Waagmeester, P. Wittenburg, K. Wolstencroft, J. Zhao, and B. Mons. 2016: The FAIR Guiding Principles for scientific data management and stewardship. Scientific Data 3:160018.

Williams, C. J., E. K. Mendell, J. Murphy, W. M. Court, A. H. Johnson, and S. L. Richter. 2008: Paleoenvironmental reconstruction of a Middle Miocene forest from the western Canadian Arctic. Palaeogeography, Palaeoclimatology, Palaeoecology 261:160–176.

Wing, S. L., and D. R. Greenwood. 1993: Fossils and fossil climate: The case for equable continental interiors in the Eocene. Philosophical Transactions: Biological Sciences 341:243–252.

Wing, S. L., and W. A. DiMichele. 1995: Conflict between local and global changes in plant diversity through geological time. PALAIOS:551–564.

Wing, S. L., L. J. Hickey, and C. C. Swisher. 1993: Implications of an exceptional fossil flora for Late Cretaceous vegetation. Nature 363:342–344.

Wing, S. L., C. A. Strömberg, L. J. Hickey, F. Tiver, B. Willis, R. J. Burnham, and A. K. Behrensmeyer. 2012: Floral and environmental gradients on a Late Cretaceous landscape. Ecological Monographs 82:23–47.

Wodehouse, R. P. 1935: Pollen Grains, Their Structure Identification and Significance in Science and Medicine. McGraw-Hill Book Company.

Wolfe, J., and T. Tanai. 1987: Systematics, phylogeny, and distribution of Acer (maples) in the Cenozoic of western North America. Journal of the Faculty of Science. Hokkaido University, Series 4: Geology and Mineralogy 22.

Wolfe, J. A. 1962: A Miocene pollen sequence from the Cascade Range of northern Oregon. U.S. Geological Survey, C81–C84 p.

———. 1969: Neogene floristic and vegetational history of the Pacific Northwest. Madroño 20:83–110.

———. 1979: Temperature parameters of humid to mesic forests of eastern Asia and relation to forests of other regions of the northern hemisphere and Australasia. US Geological Survey Professional Paper 1106. United States Gov. Print. Off, Washington.

———. 1981: Paleoclimatic signficance of the Oligocene and Neogene floras of the northwestern United States. Pp.79–101 *in* Paleobotany, Paleoecology, and Evolution 2:79-101.

———. 1993: A method of obtaining climatic parameters from leaf assemblages. USGS Bulletin 2040.

———. 1994: Tertiary climatic changes at middle latitudes of western North America. Palaeogeography, Palaeoclimatology, Palaeoecology 108.3-4:195–205.

———. 1995: Paleoclimatic estimates from Tertiary leaf assemblages. Annual Review of Earth and Planetary Sciences 23:119–142.

Wolfe, J. A., and D. M. Hopkins. 1967: Climatic changes recorded by Tertiary land floras in northwestern North America. Pp.67–76 *in* Tertiary Correlations and Climatic Changes in the Pacific. Sasaki Printing and Publishing Co. Ltd., Sendai, Japan.

Wolfe, J. A., and H. E. Schorn. 1990: Taxonomic revision of the Spermatopsida of the Oligocene Creede flora, southern Colorado. US Geological Survey Bulletin 1923.

Wood, S. H., and D. M. Clemens. 2002: Geologic and tectonic history of the western Snake River Plain, Idaho and Oregon. Tectonic and Magmatic Evolution of the Snake River Plain Volcanic Province: Idaho Geological Survey Bulletin.

Woodruff, F., and S. Savin. 1991: Mid-Miocene isotope stratigraphy in the deep sea: High-resolution correlations, paleoclimatic cycles, and sediment preservation. Paleoceanography 6:755–806.

Wright, I. J., P. K. Groom, B. B. Lamont, P. Poot, L. D. Prior, P. B. Reich, E.-D. Schulze, E. J. Veneklaas, and M. Westoby. 2004a: Leaf trait relationships in Australian plant species. Functional plant biology 31:551–558.

Wright, I. J., P. B. Reich, M. Westoby, D. D. Ackerly, Z. Baruch, F. Bongers, J. Cavender-Bares, T. Chapin, J. H. C. Cornelissen, M. Diemer, J. Flexas, E. Garnier, P. K. Groom, J. Gulias, K. Hikosaka, B. B. Lamont, T. Lee, W. Lee, C. Lusk, J. J. Midgley, M.-L. Navas, Ü. Niinemets, J. Oleksyn, N. Osada, H. Poorter, P. Poot, L. Prior, V. I. Pyankov, C. Roumet, S. C. Thomas, M. G. Tjoelker, E. J. Veneklaas, and R. Villar. 2004b: The worldwide leaf economics spectrum. Nature 428:821–827.

Xing, Y.-W., Y. C. Liu, T. Su, F. M. Jacques, and Z.-K. Zhou. 2013: A new Tsuga species from the upper Miocene of Yunnan, southwestern China and its palaeogeographic significance. Palaeoworld 22:159–167.

Yang, H., C. J. Smiley, K. F. Sprenke, W. C. Rember, and C. R. Knowles. 1995: Subsurface evidence for a rapid formation of the Clarkia Miocene lake in northern IDaho. Northwest Science 69:52–59.

Zachos, J. C., R. E. Zeebe, and G. R. Dickens. 2008: An early Cenozoic perspective on greenhouse warming and carbon-cycle dynamics. Nature 451:279–283.

Zetter, R., and D. K. Ferguson. 2001: Trapaceae pollen in the Cenozoic. Acta Palaeobot 41:321–339.

Tables and Figures

Table 1. Previous floral monographs and the starting point for constructing macrofossil morphotype frameworks of this study.

Sites	Previous floral monographs
Pickett Creek	Buechler et al. (2007)
Vasa Park	Dillhoff et al. (2014)
Trapper Creek	Axelrod (1964)
Trout Creek	MacGinitie (1933), Graham (1965)
Succor Creek (Watersnake)	Fields (1996)
Moose Mountain	Jack Wolfe in Peck et al. (1964)
Clarkia	Smiley and Rember (1985), Rember (1991)
Mascall	Chaney (1925), Chaney and Axelrod (1959)
Spokane	Knowlton (1926), with subsequent revisions E. Berry and R. Brown, among others.
Juliaetta	Studied in part by Kirkham and Johnson (1929), Ashlee (1932), and Gillette (1940)
Alvord Creek	Axelrod (1944)
Bridge Creek (Fossil HS)	Chaney (1927), Meyer and Manchester (1997)

Table 2. Summary of new CA-IDTIMS U-Pb ages.

Site	Formation	Sample	Weighted mean $^{206}Pb/^{238}U$ ages
Pickett Creek	Chalk Hills	19P2-0.00	11.372 ± 0.029
Trapper Creek	Tuff of Ibex Peak	21TC-T-02	12.830 ± 0.082
Mascall (White Hills)	Mascall	21MF-07-T-1 bottom	16.131 ± 0.011
Succor Creek (Watersnake)[1]	Sucker Creek	21-WS-T-01	15.546 ± 0.018
Trout Creek	Trout Creek	20TROUT-A	15.452 ± 0.022
		20TROUT-D	15.450 ± 0.009
Moose Mountain	Little Butte Volcanic Series	21MM-2	15.678 ± 0.033
Clarkia (P33)	Latah	19P33-2064	15.909 ± 0.016
		19P33-1771	15.903 ± 0.041
Clarkia (P37)		19P37B-13.85	15.888 ± 0.013
		19P37B-5.46	15.831 ± 0.009
Juliaetta	Latah	19P6-A	16.577 ± 0.012
Alvord Creek	Alvord Creek	20ALV-A	25.574 ± 0.042
Alvord Creek	Pike Creek Volcanics	20PCV-A	25.585 ± 0.040
Bridge Creek (Fossil HS)	John Day	-	33.079 ± 0.024

[1]Published in Schiller et al. (2024)

Table 3. Summary of sample sizes per site, including the number of macrofossil morphotypes and macrofossil specimens assessed in this study, the number of macrofossil specimens represented by count data (census) and the extent of stratigraphy they were pooled across (in parenthesis). Note, some census collections were made as part of this study and others were incorporated from previous work. Lastly, the number of pollen and phytolith samples studied and the extent of stratigraphy pollen samples were pooled across (in parentheses); phytolith samples are analyzed individually. F = Foliage, R = Reproductive, O = Other.

Abb.	Site	Morphotypes			Macro. specimens studied	Census	Pollen samples	Phyto. samples
		F	R	O				
PC	Pickett Creek	29	14	3	342	721[1] (0.74 m)	-	-
VP	Vasa Park	26	4	1	520	-	3 (8 m)	3
TraC	Trapper Creek	31	18	1	396	3797[2] (?)	1	2
TroC	Trout Creek	45	27	2	676	5261[3] (~17 m)	-	-
WS	Watersnake (Succor Creek)	31	22	1	1178	866 (2.8 m)	5 (1.8 m)	-
MM	Moose Mountain	27	13		541	-	1[4]	-
Clk	Clarkia	72	49		1635	746 (0.3 m)	6 (0.21 m)	2
Mas	Mascall	49	31	1	1885	794 (0.6 m)	-	4
Spok	Spokane	66	32	3	984	-	3 (0.5 m)	-
Jul	Juliaetta	27	12	1	1273	864 (2.8 m)	6 (2.85 m)	-
AC	Alvord Creek	22	12	1	1506	815 (?)	3 (?)	-
FHS	Fossil HS (Bridge Creek)	-	-	-	-	-	1[5]	-
	Totals	425	234	14				
	Study-scale morphotypes	213	90	4				

[1]Counts reported in Buechler et al. (2007)
[2]Counts reported in Axelrod (1964)
[3]Counts reported in Graham (1965)
[4]Prepared slides provided by Robert Rosé
[5]Sample provided by Steven Manchester. Pollen were not well preserved and thus counts were not made

Figure 1. Map of the Pacific Northwest and location of sites of this study with color and symbol type denoting their occurrence in time relative to the Miocene Climatic Optimum (MCO). Major depositional basins, physiographic provinces, and volcanic fields mentioned throughout the text are labelled and redrawn from Reidel et al. (2013*a*), Benson and Mahood (2016), and Wetzl and Stanley (2022). The location of silicic vents of the Little Butte Volcanic Series as mapped by Peck et al. (1964) are shown by a yellow "X". Other abbreviations are as follows: PLL – Puget Lowland, Mtn – mountain, HS – high school, Crk – Creek, LOVF – Lake Owyhee Volcanic Field, R – Roose Comb Caldera, MVF – McDermitt Volcanic Field, WSRP – western Snake River Plain, ESRP – eastern Snake River Plain, BJ – Bruneau-Jarbidge Volcanic Field, TF – Twin Falls Volcanic Field.

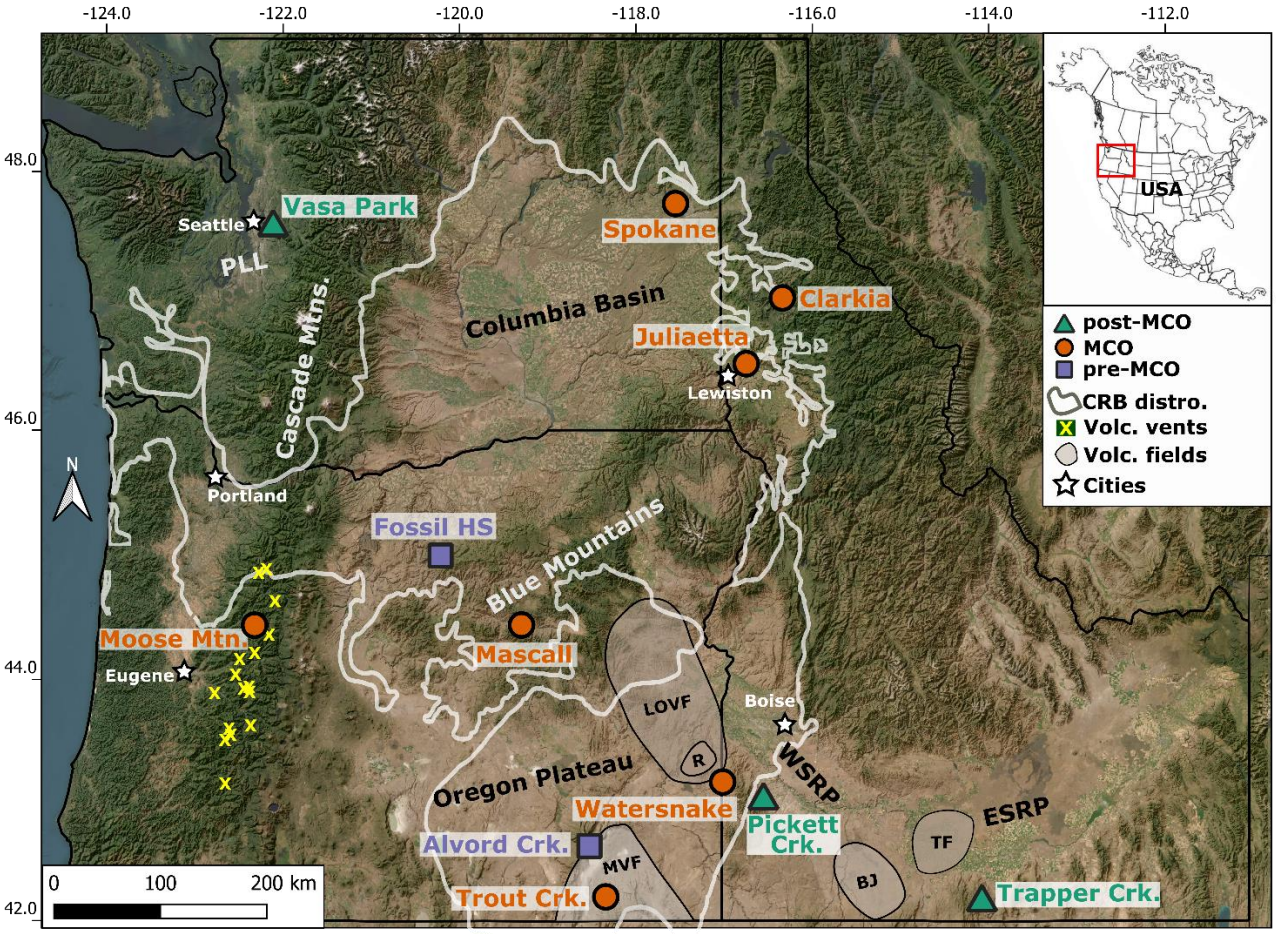

Figure 2. Non-metric multidimensional scaling analysis of floral composition before, during, and after the Miocene Climatic Optimum (MCO). Note, axes values are meaningless so are not labelled. A-C, Analysis of foliar morphotypes in terms of (A) presence-absence, (B) relative abundance (C) the relative abundance of woody non-monocot angiosperms (WNMA) only. D-E, Analysis of pollen taxa in terms of (D) presence absence and (E) relative abundance. Note sites in two cases (C, E) were excluded because very large dissimilarity made interpretations of other sites difficult. Site abbreviations follow Table 1.

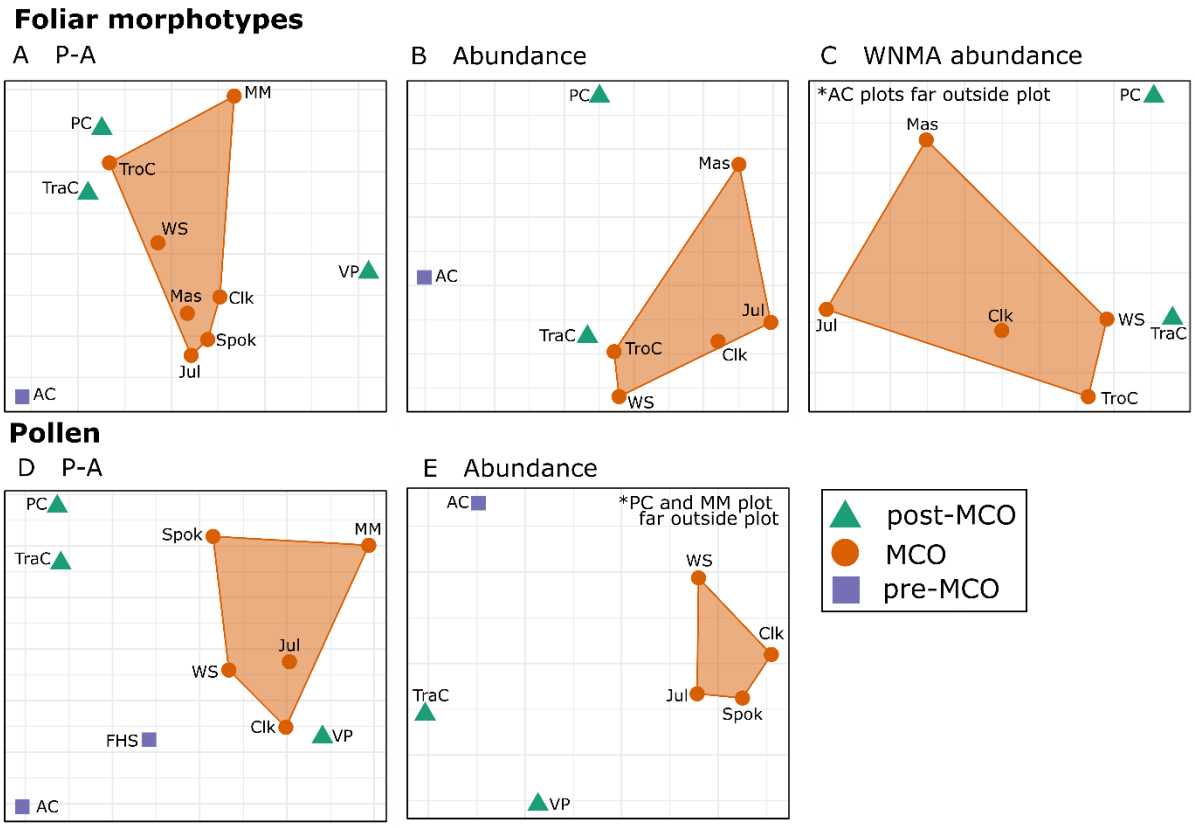

Figure 3. Temporal occurrences and range-through plots in relation to the Miocene Climatic Optimum (MCO; marked by the dashed line) and Middle Miocene Climatic Transition (MMCT) as shown by trends in benthic foraminifera $\delta^{18}O$, modified from Westerhold et al. (2020). Unique taxa or morphotypes are arranged along the x axis and are organized by broad functional and taxonomic groups. Occurrences of (A) foliar morphotypes, (B) genera in the macrofossil record, and (C) pollen taxa are reported. Vasa Park is shown as a separate color to highlight divergent trends across the MMCT.

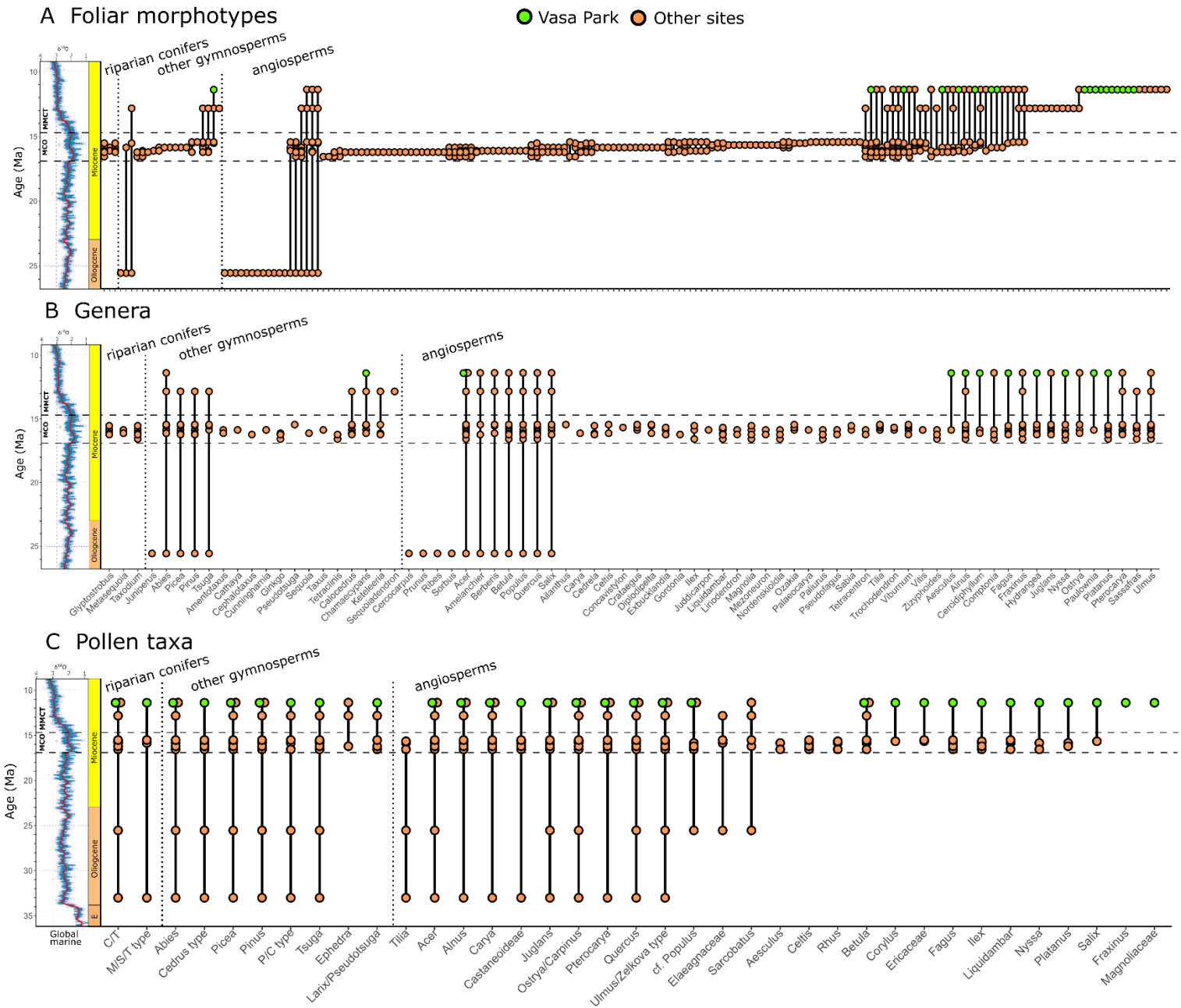
A Foliar morphotypes
Vasa Park
Other sites
riparian conifers
other gymnosperms
angiosperms
Age (Ma)
MCO
MMCT
Miocene
Oligocene
B Genera
Glyptostrobus
Metasequoia
Taxodium
Juniperus
Abies
Picea
Pinus
Tsuga
Amentotaxus
Cathaya
Cephalotaxus
Cunninghamia
Ginkgo
Pseudotsuga
Sequoia
Taxus
Tetracentron
Calocedrus
Chamaecyparis
Keteleeria
Sequoiadendron
Cercocarpus
Prunus
Ribes
Sorbus
Acer
Ameianchier
Berberis
Betula
Populus
Quercus
Salix
Allanthus
Carya
Cedrela
Celtis
Concavistylon
Craigia
Craibiodendron
Diplodiploetia
Exbucklandia
Gordonia
Ilex
Juddicarpon
Liquidambar
Lmiodendron
Magnolia
Mezoneuron
Nordenskioldia
Ozakia
Palaeocarya
Palliurus
Pseudofagus
Sabia
Tetracentron
Tilia
Trochodendron
Viburnum
Vitis
Zizyphoides
Aesculus
Alnus
Cercidiphyllum
Comptonia
Fagus
Fraxinus
Hydrangea
Juglans
Nyssa
Ostrya
Paulownia
Platanus
Pterocarya
Sassafras
Ulmus
C Pollen taxa
Global marine
C/T
M/S/T type
Abies
Cedrus type
Picea
Pinus
P/C type
Tsuga
Ephedra
Larix/Pseudotsuga
Tilia
Acer
Alnus
Carya
Castaneoideae
Juglans
Ostrya/Carpinus
Pterocarya
Quercus
Ulmus/Zelkova type
cf. Populus
Elaeagnaceae
Sarcobatus
Aesculus
Celtis
Rhus
Betula
Corylus
Ericaceae
Fagus
Ilex
Liquidambar
Nyssa
Platanus
Salix
Fraxinus
Magnoliaceae

Figure 4. Biodiversity patterns in relation to the Miocene Climatic Optimum (MCO; marked by the dashed line) and Middle Miocene Climatic Transition (MMCT) as shown by trends in benthic foraminifera $\delta^{18}O$, modified from Westerhold et al. (2020). Analyses include (A) the percentage of exotic taxa and (B-C) evenness as measured by the Simpson's Index, considering the relative abundance of (B) all foliar morphotypes, and (C) woody non-monocot angiosperm foliage only. Black squares and solid lines mark time bin average values.

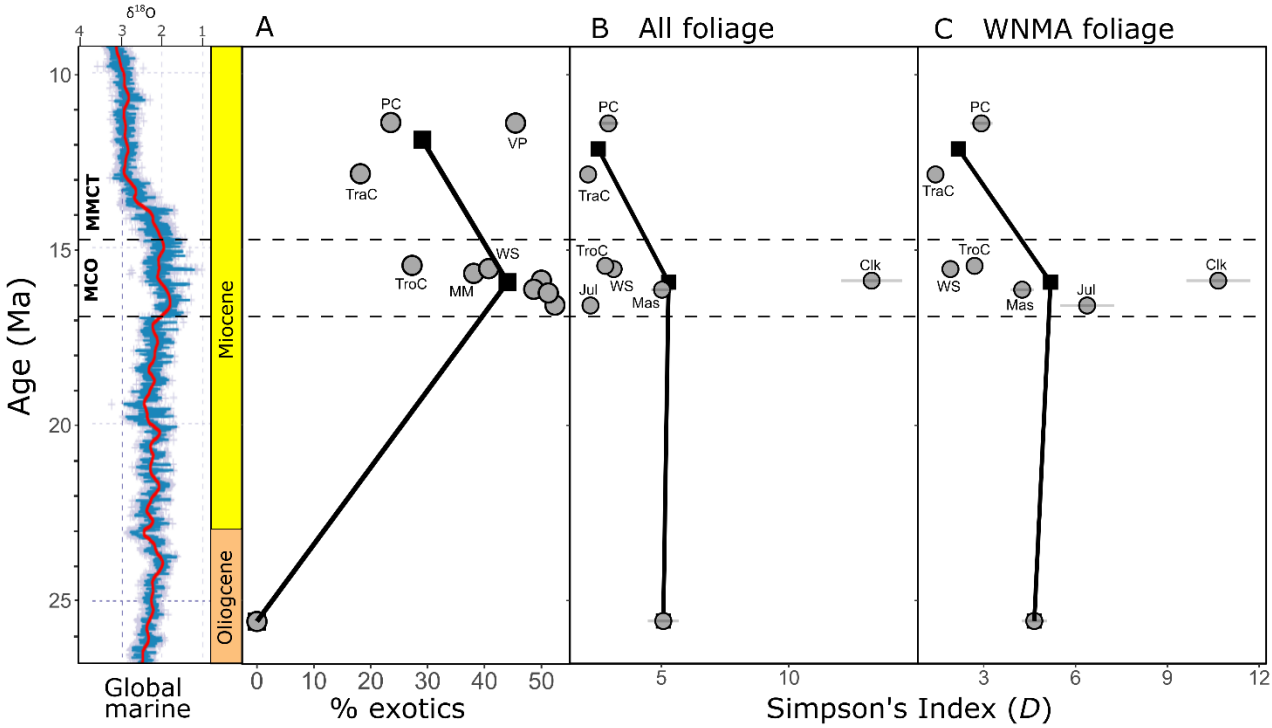

Figure 5. Mean climate variables for (A, C, E) extant members of taxa ascribed as either exotic (no longer native to the US west coast) or Remnant (still native), compared to (B, D, F) the range of modern lowland climates of the Pacific Northwest (PNW) both east and west of the Cascade Mountains.

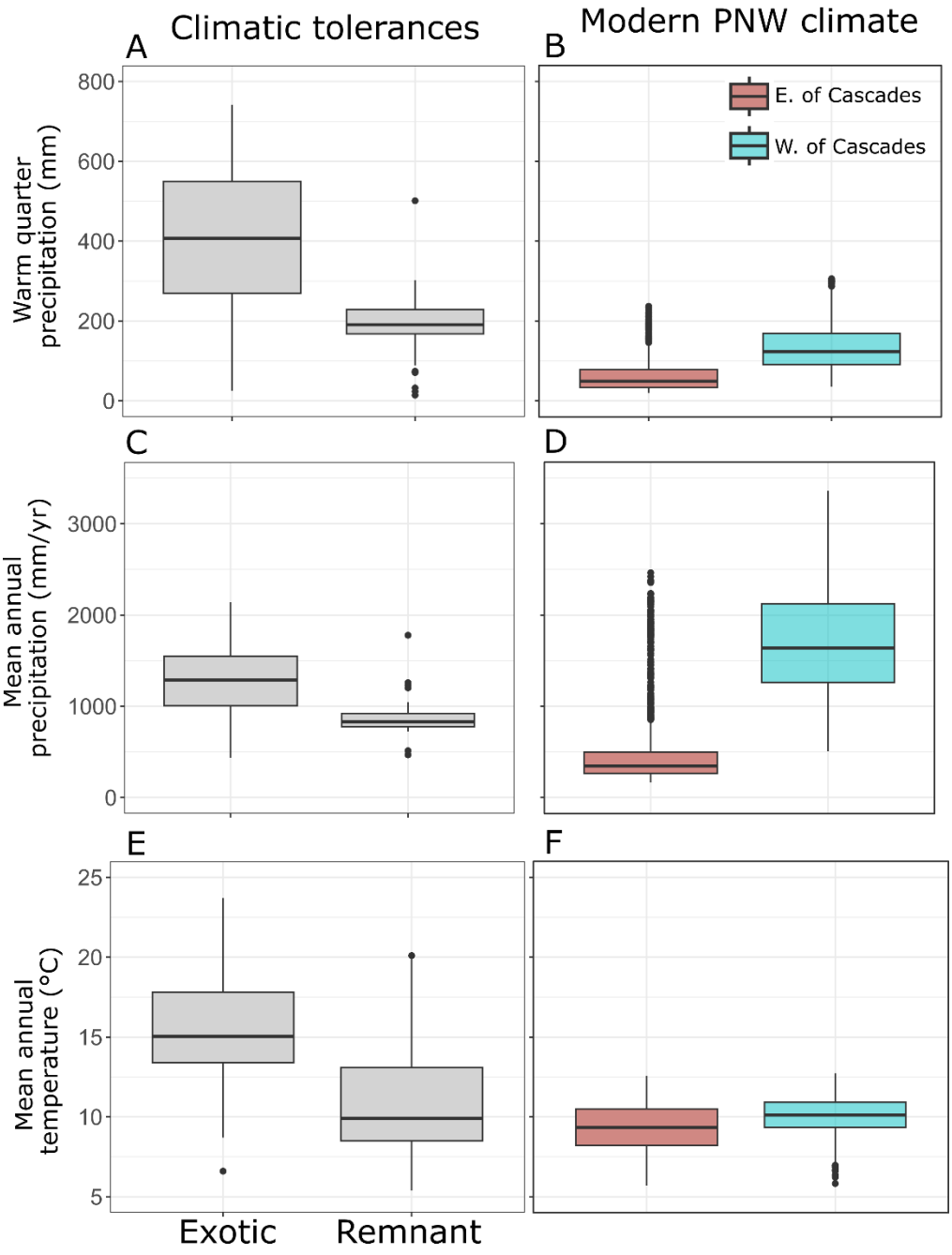

Figure 6. Reconstructed ecological measures compared to values from modern plant communities in various climate types (box plots above, data from Lowe et al. In Review), and in relation to the Miocene Climatic Optimum (MCO; marked by the dashed line) and Middle Miocene Climatic Transition (MMCT) as shown by trends in benthic foraminifera $\delta^{18}O$, modified from Westerhold et al. (2020). A, Probability-based reconstructions of the percentage of evergreen, relative to deciduous, non-monocot angiosperms, based on NLRs. Error bars are ±1 SD of bootstrap resampled values. B, Reconstructed site mean leaf mass per area (M_A). C, The correspondence between reconstructed % evergreen and mean LMA across sites of this study. Point colors represent average mean annual precipitation estimates from this study. Black squares and solid lines mark time bin average values.

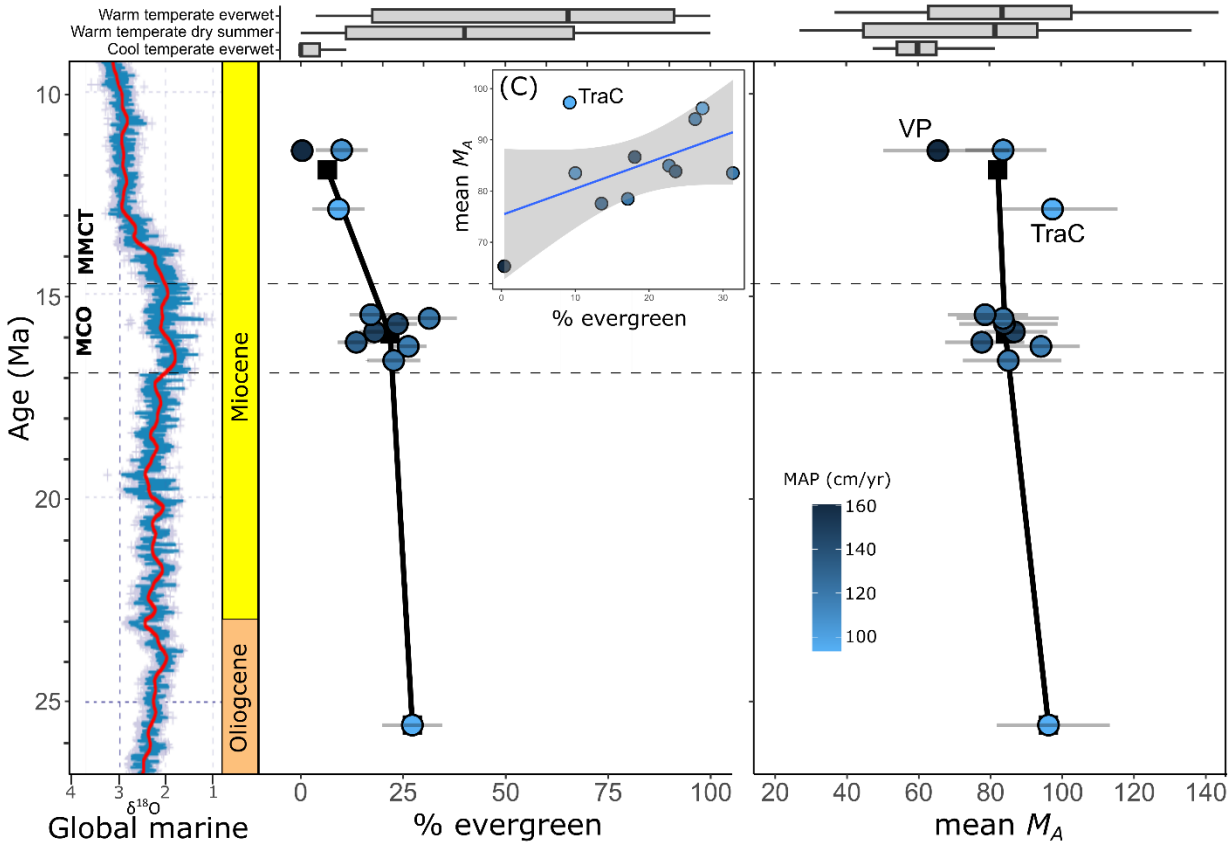

Figure 7. Relative abundance and diversity of plant functional groups. The dashed lines delimit sites within the Miocene Climatic Optimum (MCO). A, The relative richness of macrofossil morphotypes within groups, and (B) their relative abundance. C, The relative richness of pollen taxa within similarly defined groups, and (D) their abundance. E, The relative abundance of phytoliths identified to various functional groups, with individual samples from a site plotted separately. WNM = woody non-monocot, Cup./Tax. = Cupressaceae/Taxaceae.

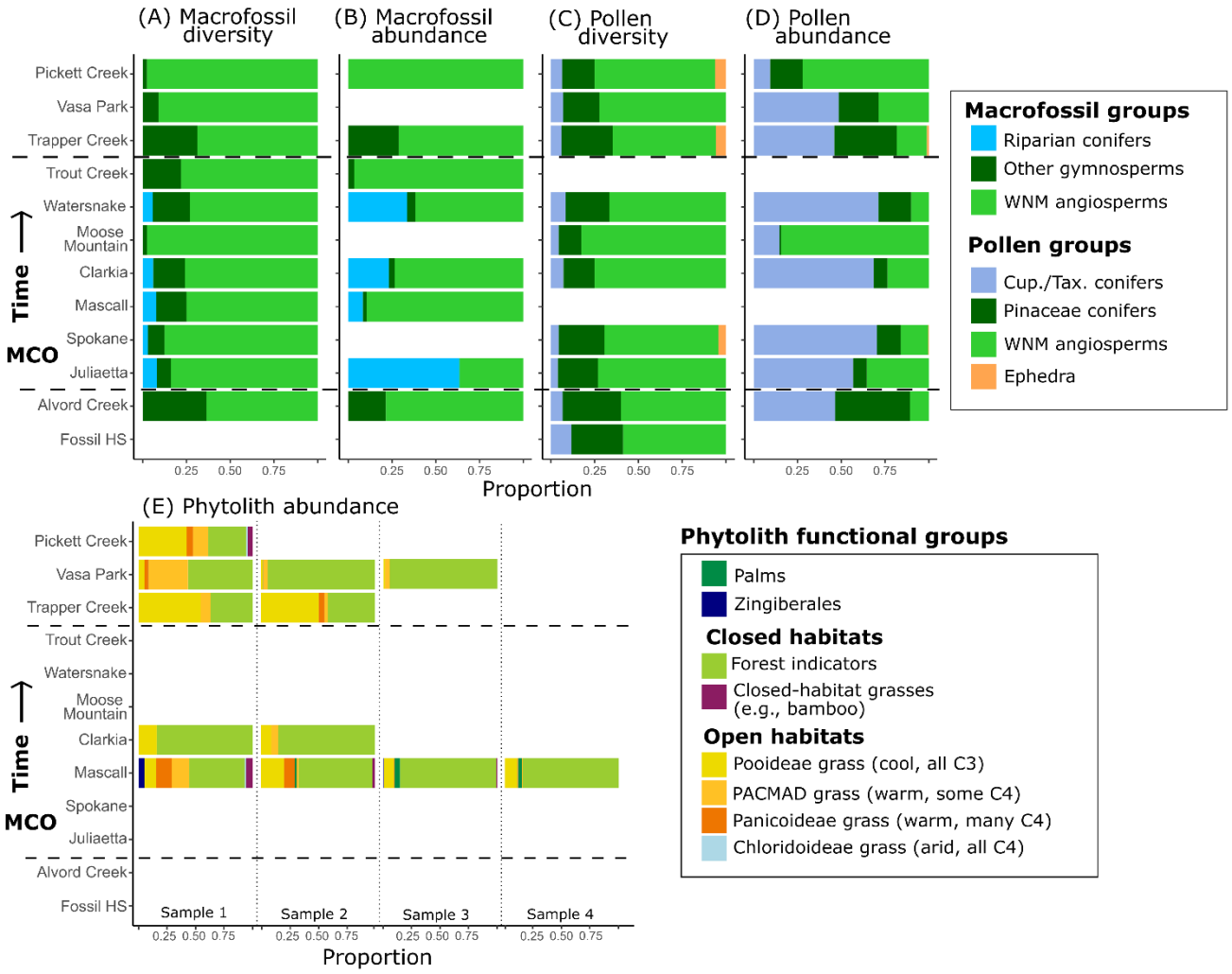

Figure 8. Temperature reconstructions compared to the range of modern Pacific Northwest climate values east and west of the Cascade Mountains (kernel density functions above), and in relation to the Miocene Climatic Optimum (MCO; marked by the dashed line) and Middle Miocene Climatic Transition (MMCT) as shown by trends in benthic foraminifera $\delta^{18}O$, modified from Westerhold et al. (2020). A-B, Mean annual temperature reconstructions from leaf physiognomy proxies, including (A) equations reported in Peppe et al. (2011), including multiple- (i.e., digital leaf physiognomy [DiLP]) and single (i.e., leaf margin analysis [LMA]) regression models reported in Peppe et al. (2011), and (B) LMA equation reported in Wing and Greenwood (1993), incorporating a published margin percentage from Fossil HS reported in Meyer and Manchester (1997) as the oldest point. C-D, Temperature reconstructions from the Bioclimatic Analysis (BA) proxy, for (C) mean annual temperature, and (D) cold quarter temperature. Site abbreviations follow Table 1.

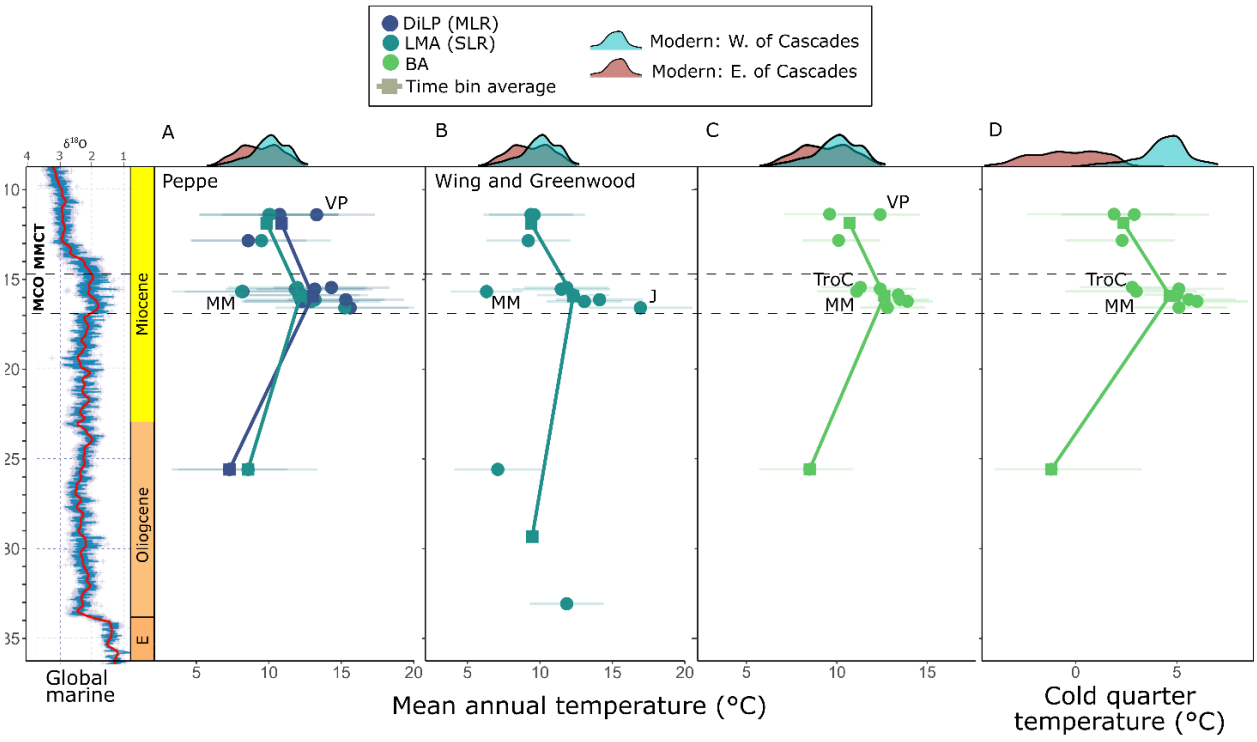

Figure 9. Precipitation reconstructions compared to the range of modern Pacific Northwest values east and west of the Cascade Mountains (kernel density functions above), and in relation to the Miocene Climatic Optimum (MCO; marked by the dashed line) and Middle Miocene Climatic Transition (MMCT) as shown by trends in benthic foraminifera $\delta^{18}O$, modified from Westerhold et al. (2020). A-B, Mean annual precipitation reconstructions from leaf physiognomy proxies, including (A) equations reported in Peppe et al. (2011), including multiple- (i.e., digital leaf physiognomy [DiLP]) and single (i.e., leaf area analysis [LAA]) regression models reported in Peppe et al. (2011), and (B) LAA equation reported in Wilf et al. (1998). C, Mean annual precipitations reconstructions from the Bioclimatic Analysis (BA) proxy. Site abbreviations follow Table 1.

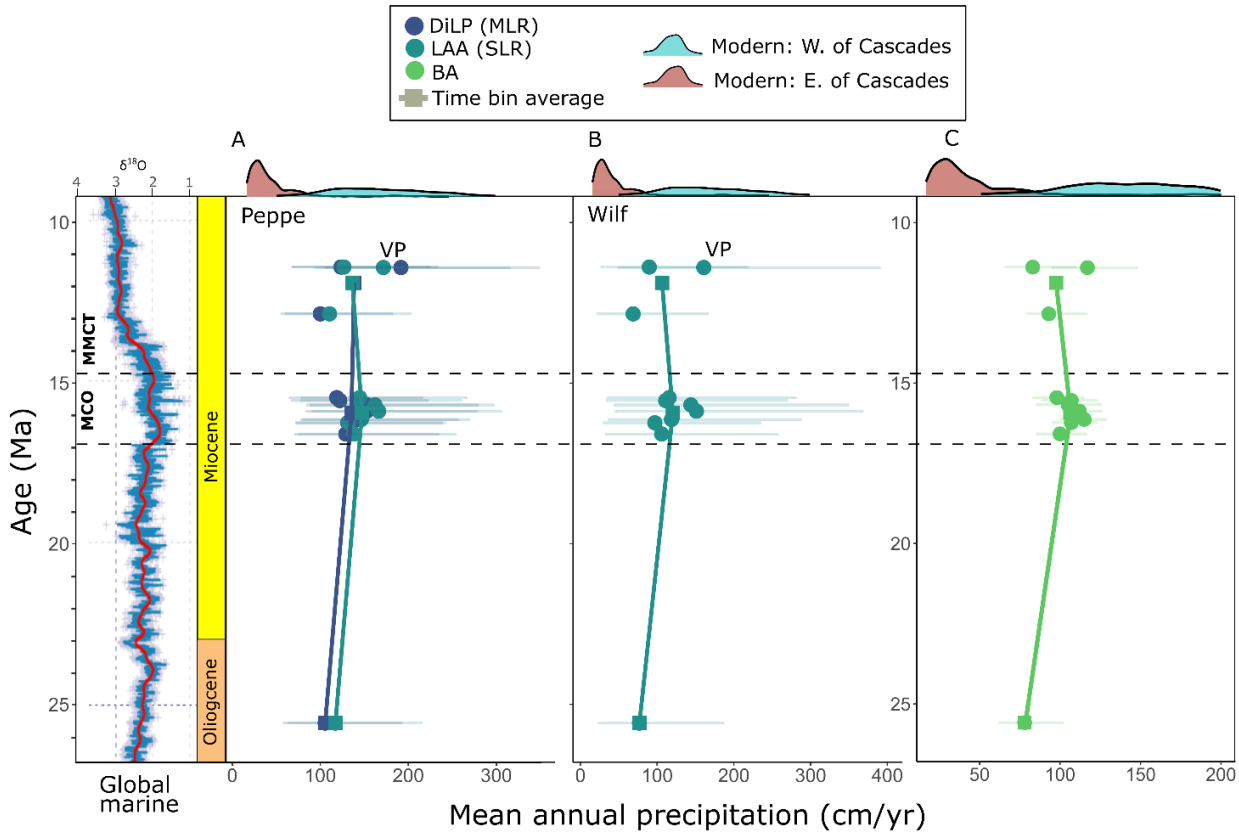

Conclusions and Outstanding Questions

Naturally, results and conclusions from studies of this dissertation have identified several additional knowledge gaps and spurred additional research questions. This section summarizes these outstanding questions and in many cases proposes potential ways to address them.

Petiole Metric and Leaf Mass per Area

First, there is still much to be understood regarding the petiole metric (PM) and leaf mass per area relationship (LMA). For example, in Chapter 2, we found weak correlation between PM and LMA among species, and an in-significant relationship among deciduous species only. In a quick analysis isolating sites included in Chapter 1, I find that PM and LMA do not correlate at the species-scale within ~25% of sites. This raises important questions about the scalability of PM-LMA relationships, and in what contexts the relationship is strongest and most reliably applied. For example, I wonder the extent to which low- and high-end outliers are responsible for influencing the significance of PM-LMA relationships. In considering high LMA and PM outliers, we have found they are often characterized by very small leaves. This could very well be an ecological and meaningful co-variance but petiole diameter may respond non-linearly to leaf mass and this low end of the spectrum. I think tests of relationships within taxonomic groups, plant functional types, and plants living in various climate and vegetation types, would help clarify this issue. In addition, biomechanical models are now much more sophisticated than those originally cited by Royer et al. (2007), and applying these models would help resolve the biomechanical significance of the LMA-PM relationship.

For PM measurements on fossil leaves, leaf area is often reconstructed on incomplete leaves, as completely preserved fossil leaves are often rare. To my knowledge, the sensitivity of PM measurements and LMA reconstructions to error introduced to leaf area measurements

during reconstruction has not been quantified, leaving some uncertainty inherent to the method unconstrained. This could be addressed through a study creating artificial damage to modern leaves through digital manipulation and having a paleobotanist digitally reconstruct that damage as they would a fossil leaf, and then compare subsequent PM measurements and LMA reconstructions to those where the leaf was not altered. Another consideration is the applicability of PM-LMA relationships in leaves having a pulvinus (e.g., leaflets of Fabaceae), which are often swollen relative to standard petiole types. LMA has been reconstructed from Fabaceae leaflets by several previous paleobotanical publications (e.g., Currano et al. 2010), including in our Chapter 3, but the reliability of such reconstructions needs to be quantitatively demonstrated.

Chapter 1 and 2 studied leaves sampled from standing vegetation, accounting for potential taphonomic influence only through the targeted sampling of sun leaves. Taphonomic biases, including those related to differential production, transportability (in air, overland, and in water), susceptibility to physical, biological, and chemical degradation, and fossil sampling are missing from the samples (e.g., Greenwood 1991). Although our studies represent an important perspective for the starting point of fossil assemblages, minimal representation of taphonomic biases raises an important question—once these taphonomic biases are imparted, do results of our studies still apply? Leaf litter collections incorporate production and some transport and degradation biases and have often been used as a fossil analog given their ease of collection and study (e.g., Burnham et al. 1992; Greenwood 1992). For Chapter 2, we collected leaf litter at all stands (except the 4 yo stand), which are currently being studied by members of Dr. Ellen Currano's lab (University of Wyoming) and will offer important perspective. In addition, brueid "leaf pack" assemblages sampled from stream banks or lake bottoms represent additional steps in transport, degradation, and burial, and offer an even closer analog to fossil leaf assemblages

(e.g., Spicer and Wolfe 1987; Azevedo-Schmidt et al. 2022). Future work studying patterns in LMA and PM from these assemblages, in relation to the forest they were sourced from, will offer critical insight into the question of how well these traits measured in fossil assemblages reflect the measurements made from standing vegetation in our Chapter 1 and 2 studies. An additional taphonomic bias worth considering is how either leaf shrinkage during drying (e.g., Blonder et al. 2012) or petiole flattening during burial and fossilization, skew petiole metric measurements. The influence of petiole flattening would be difficult to test but could potentially be done through experimental studies placing leaves into a hydraulic press and applying reasonable ranges of burial pressure.

Lastly, in preliminary analyses of data included in Chapter 1, we found that (although not included in the publication), in warm temperate dry-summer climates (i.e., Mediterranean climates), woody non-monocot angiosperms (WNMAs) that occur in conifer-dominated forest types had lower LMA and those occurring in WNMA-dominated forest types. This preliminary result is consistent with niche partitioning as conifers typically represent "slower" resource acquisition strategies (e.g., Brodribb et al. 2012), and thus low LMA angiosperms fill "faster" resource acquisition niches. This would suggest that site-level reconstructions of LMA using WNMAs may offer a biased perspective for whole communities in these conifer-dominated forest types, and largely preclude the ability to scale to ecosystem-level inference. This question could be addressed through a global study of LMA in warm temperate sites classified as angiosperm- or conifer-dominated.

Leaf Traits Across Succession

Results from Chapter 2 showed that the leaf economic spectrum may apply in deciduous-dominated temperate forests among WNMAs, with lower LMA trees more prevalent in early,

compared to late, succession. This result conflicts with several previous studies showing shade tolerant species (typical of late succession) often have lower LMA than shade intolerant species (typical or early to middle succession) (Niinemets and Kull 1994; Niinemets et al. 1998; Aranda et al. 2004; Hallik et al. 2009). In this chapter, we provided some reservation to this interpretation given our limited sample size and suggested further work at the community-scale to determine how universal our results were for deciduous-dominated temperate forests. This may be accomplished more broad characterizations of forests into old growth and disturbed/secondary rather than a continuous chronosequence design as in our study. Regardless, I feel in situ measurements of entire tree communities are critical in obtaining the most reliably interpretable results.

We found that the presence/absence of high LMA and evergreen WNMA outliers drove both LMA and PM patterns across succession, and the correlation between the two. This suggests that, more generally, LMA and PM patterns among WNMAs in humid temperate forests may be primarily driven by patterns in the % of evergreen species present. Thus, an understanding on the controls on the diversity of evergreen WNMAs across this forest type is critical to interpretations of reconstructed LMA in the fossil record. As there is little intraspecific variability of leaf habit (deciduous vs. evergreen) in temperate forests, such a study could be conducted from plot vegetation census data, without the need for in situ leaf measurements.

In Chapter 2, we also found that tree species more often had toothed leaves in early, compared to late, succession. This same pattern was found in a tropical rainforest (Kappelle and Leal 1996). The applicability of these results to interpretations of the fossil record requires a strong functional tie between leaf teeth, fitness, and ecology. Despite much previous work, the primary function of leaf teeth (and leaf lobes) is debated (e.g., Edwards et al. 2016; Givnish and

Kriebel 2017), and additional insight would strengthen the confidence in applying leaf teeth as a paleoecological (and paleoclimatological) tool. Previous authors have questioned whether enhanced carbon gain in the early growing season, as afforded by enhanced photosynthetic and transpiration rates, would contribute meaningfully to the plants annual carbon budget (e.g., Edwards et al. 2016; Givnish and Kriebel 2017). I find this question critical to the leaf gas exchange hypothesis for leaf teeth function (e.g., Royer and Wilf 2006) and the question could be reasonably tested through photosynthesis and carbon budget modeling. The functional significance of leaf shape characteristics beyond teeth, including leaf circularity and lobiness is of additional interest to both modern- and paleobotanists and are easily measurable on fossil leaves. Although these traits showed less meaningful patterns in our Chapter 2 study, they have been shown to vary significantly with climate (Peppe et al. 2011), and are known to effect leaf boundary layer thickness and thermoregulation (e.g., Leigh et al. 2017) and vary across climate types (Peppe et al. 2011). State-of-the-art physical and thermodynamic models of leaf surfaces, combined with a resolved understanding of leaf shape variation in various climate and environment types, may provide critical insights to the ecophysiology of leaf shape and permit the greater use of leaf morphology as a paleoecological tool. Environmental controls on measures of leaf morphological diversity have been explored by only a few recent studies (e.g., Roth-Nebelsick and Traiser 2024), and even fewer calculate morphological diversity using quantitative (rather than categorical) traits—offering an additional and interesting avenue of research.

In Chapter 2, we found that leaf morphology patterns among trees (DBH $\geq$ 10 cm) vs. the entire community (trees + species restricted to the understory) were divergent across succession. This result forced us to consider which data analysis method was more applicable to the fossil

record. We suggested that patterns among trees are likely most applicable to ancient forested vegetation given the relationship between leaf litter abundance and stem basal area, reflecting the greater number of leaves produced by trees (Burnham et al. 1992; Steart et al. 2005). However, fossils allied to shrubs from ancient forested vegetation have been reported by several previous authors and may turn up in well sampled assemblages (e.g., Chaney and Axelrod 1959; Wolfe and Wehr 1987). Leaf litter collections from Chapter 2 stands, currently in study by Dr. Ellen Currano's lab, can be used to partially test this question by determining if leaves from those species occurring only in the understory are represented.

Paleoecology and the Pacific Northwest Neogene

Many important questions remain regarding our work in the Neogene of the Pacific Northwest (PNW; Chapter 3). First, there are a plethora of taxonomic investigations and nomenclatural revisions still needed. These are in most cases acknowledged in supporting documents not included in this dissertation, but which we plan to upload to a publicly available database in the near future. The number of sites included in our study was limited by time, and a bolstering of this sample set would improve temporal and spatial resolution. For example, while the MCO is well represented in sites of this study, pre-MCO conditions are poorly resolved and leaves outstanding questions regarding the MCO onset. Early Miocene rocks in eastern Washington and Oregon are rare, although a collection of fossil sites in the western Cascades of Oregon occur in a region of complicated geology, but are thought to be roughly early Miocene in age (Peck et al. 1964; Wolfe 1969). These floras would benefit from more reliable radiometric dating and further investigation, and exploration of potentially early Miocene rock exposures in the PNW may reveal new fossil floras. In addition, we have yet only incorporated three post-MCO sites. Our preliminary results reveal a coastal-interior gradient of continentality in several

paleoclimate and paleovegetation metrics. Understanding this gradient will benefit by inclusion of several more late Miocene sites, spanning a more continuous east-west gradient—for example, the late Miocene floras of the western Columbia Basin (Smiley 1963; Mustoe and Leopold 2014).

In our Chapter 3 discussion, we consider whether differences found in the Snake River Plain floras result from global climatic change, regional uplift associated with the Yellowstone hotspot, or taphonomic biases. While we find a global climatic driver most likely, it is difficult rule the other potential influences with certainty. The inclusion of additional late Miocene sites in the interior PNW outside the Snake River Plain, and late Miocene coastal lacustrine sites (Vasa Park is fluvial) would help clarify these issues. In addition, quantification of continental gradients of climate in analogous modern environments would help evaluate the feasibility of a global climatic driver acting alone. Lastly, a strong spatial sampling of late Miocene conditions will also help understand potential heterogeneity occurring between the PNW, Rocky Mountain region, and the northern Great Plains (e.g., Strömberg 2005; Harris et al. 2017; Kukla et al. 2022).

Several improvements and questions remain regarding methodology. For example, the method used to reconstruct the percentage of WNMA species in Chapter 3 requires improvement. For many of the genera, we only have included leaf habit information for a limited number of species as only those species were represented in the TRY database. This dataset can be bolstered by referencing regional floras for assignment of leaf habit and, for our purposes, potentially filtering to only include species living in temperate Northern Hemisphere climates. Ancestral state reconstructions may also be useful for considering if modern percent evergreen

calculations are biased by anonymously cool global temperatures characterizing the last ~3 million years.

Weighting site level calculations by abundance is well practiced in modern ecology to better reflect to community at large and for more reliable scaling to ecosystem processes (e.g., Enquist et al. 2015). Such practice would benefit calculations of site mean in paleobotanical studies as well, but there is limited understanding for how fossil census counts reflect numerical abundance in the source forest. While the number of leaves in forest floor litter best reflect stem basal area (the measure also most commonly used by modern ecologists for abundance weighting) the correspondence is not perfect and the uncertainty introduced through such a practice is not well constrained (Burnham et al. 1992; Steart et al. 2005). Additional insight may be gained through application to a specific morphological variable. For example, one could compare the reconstructed LMA mean of a leaf litter or leaf pack assemblage weighted by leaf counts, to the reconstructed LMA mean of standing vegetation weighted by stem basal area. Is the correspondence between the two any better than if LMA mean of the leaf litter/pack assemblage is not weighted at all?

Paleobotanical and stable isotope geochemical evidence are in conflict regarding the timing of the uplift of the Cascade Mountains, and reconciling these two types of evidence is needed. Stable isotopic studies usually show a rainout effect thought to be caused by significant Cascade topography occurring since the Oligocene, and certainly in place during the middle Miocene (e.g., Kohn et al. 2002; Takeuchi and Larson 2005; Bershaw et al. 2019; Pesek et al. 2020; McLean and Bershaw 2021). In contrast, paleobotanical records show no evidence for strong differences in floras on the east vs. west side of the Cascades, revealing little impact to terrestrial ecosystems until the latest Miocene or Pliocene (Smiley 1963; Leopold and Denton

1987; Mustoe and Leopold 2014). Geochemical studies have argued that because fossil plants are biased to flood plain environments where water availability is high, they are less sensitive recorders of regional hydroclimate beyond the flood plains. For example, Kukla et al. (2022) suggests that an open habitat transition occurred in the PNW during the late Oligocene - middle Miocene and paleobotanical evidence of forests reflect flood plains environments, not drier and more open habitats beyond the flood plain. I think this question of the sensitivity of plant fossil records to regional hydroclimate is of critical importance and needs to be explicitly addressed. One potential way to assess this is by considering biodiversity—can such diverse forests, as those reconstructed from MCO plant records, be restricted to only the flood plain? One could quantify the richness of woody plants in flood plains of grasslands or consider what traits or conditions characterize those flood plain forests, and if they can be assessed from the fossil record.

Similarity, stable isotope geochemical evidence has suggested summer-dry conditions that characterize the PNW today were in place as far back as the Oligocene (Kukla et al. 2022), in contrast with palaeobotanical evidence suggesting summer-wet or ever-wet conditions until late Miocene or Pliocene. A change in forest type and reduction in exotic species (including riparian conifers) in the Snake River Plain, as reconstructed in Chapter 3, likely results from a reduction in rainfall, but provide no reliable evidence to discern if the reduction was in annual rainfall or just summer rain fall. The summer-dry precipitation regime today is driven by the Northeast Pacific High, just west of California, and the Aleutian Low. In summer, low pressure systems are typically centered on land due to colder continents, the Aleutian Low is then very weak, while the Northeast Pacific High is centered more north and is much stronger. As a result, westerly winds are deflected northward around the cell into Canada. In winter, low pressure

centers typically develop over colder oceans and the Aleutian Low becomes much stronger, while the Northeast Pacific High weakens and migrates farther south. As a result, westerly winds track storms sourced from the tropical Pacific and precipitation into the Pacific Northwest of the U.S. (Lyle et al. 2008). Thus, the questions of when and why a PNW summer-dry climate type established would benefit from collaboration with paleoclimatologists and paleo-oceanographers, and by considering how decreased latitudinal temperature gradients in the Miocene may have impacted the presence and location of these pressure centers. In addition, as stated above, providing addition empirical evidence demonstrating that fossil plant records can reliably inform the presence or absence of a summer-dry precipitation regime is critical for providing paleobotanical evidence on the issue.

Literature cited

Azevedo-Schmidt, L., E. K. Meineke, and E. D. Currano. 2022: Insect herbivory within modern forests is greater than fossil localities. Proceedings of the National Academy of Sciences 119:e2202852119.

Bershaw, J., E. J. Cassel, T. B. Carlson, A. R. Streig, and M. J. Streck. 2019: Volcanic glass as a proxy for Cenozoic elevation and climate in the Cascade Mountains, Oregon, USA. Journal of Volcanology and Geothermal Research 381:157–167.

Blonder, B., V. Buzzard, I. Simova, L. Sloat, B. Boyle, R. Lipson, B. Aguilar-Beaucage, A. Andrade, B. Barber, C. Barnes, D. Bushey, P. Cartagena, M. Chaney, K. Contreras, M. Cox, M. Cueto, C. Curtis, M. Fisher, L. Furst, J. Gallegos, R. Hall, A. Hauschild, A. Jerez, N. Jones, A. Klucas, A. Kono, M. Lamb, J. D. R. Matthai, C. McIntyre, J. McKenna, N. Mosier, M. Navabi, A. Ochoa, L. Pace, R. Plassmann, R. Richter, B. Russakoff, H. St. Aubyn, R. Stagg, M. Sterner, E. Stewart, T. T. Thompson, J. Thornton, P. J. Trujillo, T. J. Volpe, and B. J. Enquist. 2012: The leaf-area shrinkage effect can bias paleoclimate and ecology research. American Journal of Botany 99:1756–1763.

Brodribb, T. J., J. Pittermann, and D. A. Coomes. 2012: Elegance versus Speed: Examining the Competition between Conifer and Angiosperm Trees. International Journal of Plant Sciences 173:673–694.

Burnham, R. J., S. L. Wing, and G. G. Parker. 1992: The reflection of deciduous forest communities in leaf litter: implications for autochthonous litter assemblages from the fossil record. Paleobiology 18:30–49.

Chaney, R. W., and D. I. Axelrod. 1959: Miocene floras of the Columbia Plateau. Publication 617. Carnegie Institution of Washington.

Currano, E. D., C. C. Labandeira, and W. Peter. 2010: Fossil insect folivory tracks paleotemperature for six million years. Ecological Monographs 80:547–567.

Edwards, E. J., E. L. Spriggs, D. S. Chatelet, and M. J. Donoghue. 2016: Unpacking a century-old mystery: Winter buds and the latitudinal gradient in leaf form. American Journal of Botany 103:975–978.

Enquist, B. J., J. Norberg, S. P. Bonser, C. Violle, C. T. Webb, A. Henderson, L. L. Sloat, and V. M. Savage. 2015: Scaling from Traits to Ecosystems: Developing a General Trait Driver Theory via Integrating Trait-Based and Metabolic Scaling Theories. Pp.249–318 *in* S. Pawar, G. Woodward, and A. I. Dell, eds. Advances in Ecological Research. Vol. 52. Academic Press.

Givnish, T. J., and R. Kriebel. 2017: Causes of ecological gradients in leaf margin entirety: Evaluating the roles of biomechanics, hydraulics, vein geometry, and bud packing. American Journal of Botany 104:354–366.

Greenwood, D. R. 1991: The taphonomy of plant macrofossils. The processes of fossilization:141–169.

———. 1992: Taphonomic constraints on foliar physiognomic interpretations of Late Cretaceous and Tertiary palaeoeclimates. Review of palaeobotany and palynology 71:149–190.

Harris, E. B., C. A. E. Strömberg, N. D. Sheldon, S. Y. Smith, and D. A. Vilhena. 2017: Vegetation response during the lead-up to the middle Miocene warming event in the Northern Rocky Mountains, USA. Palaeogeography, Palaeoclimatology, Palaeoecology 485:401–415.

Kappelle, M., and M. E. Leal. 1996: Changes in leaf morphology and foliar nutrient status along a successional gradient in a Costa Rican upper montane Quercus forest. Biotropica:331–344.

Kohn, M. J., J. L. Miselis, and T. J. Fremd. 2002: Oxygen isotope evidence for progressive uplift of the Cascade Range, Oregon. Earth and Planetary Science Letters 204:151–165.

Kukla, T., J. K. C. Rugenstein, D. E. Ibarra, M. J. Winnick, C. A. E. Strömberg, and C. P. Chamberlain. 2022: Drier Winters Drove Cenozoic Open Habitat Expansion in North America. AGU Advances 3:e2021AV000566.

Leigh, A., S. Sevanto, J. D. Close, and A. B. Nicotra. 2017: The influence of leaf size and shape on leaf thermal dynamics: does theory hold up under natural conditions? Plant, Cell & Environment 40:237–248.

Leopold, E. B., and M. F. Denton. 1987: Comparative age of grassland and steppe east and west of the northern rocky mountain. Annals of the Missouri Botanical Garden:841–867.

McLean, A., and J. Bershaw. 2021: Molecules to mountains: A multi-proxy investigation into ancient climate and topography of the Pacific Northwest, USA. Frontiers in Earth Science 9:624961.

Mustoe, G. E., and E. B. Leopold. 2014: Paleobotanical evidence for the post-Miocene uplift of the Cascade Range. Canadian Journal of Earth Sciences 51:809–824.

Peck, D. L., A. B. Griggs, H. G. Schlicker, F. G. Wells, and H. M. Dole. 1964: Geology of the central and northern parts of the western Cascade Range in Oregon. Geological Survey Professional Paper 449.

Peppe, D. J., D. L. Royer, B. Cariglino, S. Y. Oliver, S. Newman, E. Leight, G. Enikolopov, M. Fernandez-Burgos, F. Herrera, J. M. Adams, E. Correa, E. D. Currano, J. M. Erickson, L. F. Hinojosa, J. W. Hoganson, A. Iglesias, C. A. Jaramillo, K. R. Johnson, G. J. Jordan, N. J. B. Kraft, E. C. Lovelock, C. H. Lusk, Ü. Niinemets, J. Peñuelas, G. Rapson, S. L. Wing, and I. J. Wright. 2011: Sensitivity of leaf size and shape to climate: global patterns and paleoclimatic applications. New Phytologist 190:724–739.

Pesek, M. E., N. D. Perez, A. Meigs, C. C. Rowden, and S. M. Giles. 2020: Exhumation Timing in the Oregon Cascade Range Decoupled From Deformation, Magmatic, and Climate Patterns. Tectonics 39:e2020TC006078.

Roth-Nebelsick, A., and C. Traiser. 2024: Diversity of leaf architecture and its relationships with climate in extant and fossil plants. Palaeogeography, Palaeoclimatology, Palaeoecology 634:111932.

Royer, D. L., and P. Wilf. 2006: Why do toothed leaves correlate with cold climates? Gas exchange at leaf margins provides new insights into a classic paleotemperature proxy. International journal of plant sciences 167:11–18.

Royer, D. L., L. Sack, P. Wilf, C. H. Lusk, G. J. Jordan, Ü. Niinemets, I. J. Wright, M. Westoby, P. D. Coley, A. D. Cutter, K. R. Johnson, C. C. Labandeira, A. T. Moles, and F. Valladares. 2007: Fossil Leaf Economics Quantified: Calibration, Eocene Case Study, and Implications. Paleobiology 33:574–589.

Smiley, C. J. 1963: The Ellensburg flora of Washington. Publications in Geological Sciences, University of California Press.

Spicer, R. A., and J. A. Wolfe. 1987: Plant taphonomy of late Holocene deposits in Trinity (Clair Engle) Lake, northern California. Paleobiology 13:227–245.

Steart, D. C., D. R. Greenwood, and P. I. Boon. 2005: Paleoecological implications of differential biomass and litter production in canopy trees in Australian *Nothofagus* and *Eucalyptus* forests. PALAIOS 20:452–462.

Strömberg, C. A. E. 2005: Decoupled taxonomic radiation and ecological expansion of open-habitat grasses in the Cenozoic of North America. Proceedings of the National Academy of Sciences 102:11980–11984.

Takeuchi, A., and P. B. Larson. 2005: Oxygen isotope evidence for the late Cenozoic development of an orographic rain shadow in eastern Washington, USA. Geology 33:313.

Wolfe, J. A. 1969: Neogene floristic and vegetational history of the Pacific Northwest. Madroño 20:83–110.

Wolfe, J. A., and W. Wehr. 1987: Middle Eocene dicotyledonous plants from Republic, northeastern Washington. USGS Geological Survey Bulletin 1597, 1–25 p.